Splitting Steam via Eutectic Molten Hydroxide Assisted Electrolysis for Hydrogen Gas Production

Nawar Kader Al-Shara, MSc.

THESIS SUBMITTED TO THE UNIVERSITY OF NOTTINGHAM
FOR THE DEGREE OF DOCTOR OF PHILOSOPHY

DEPARTMENT OF CHEMICAL AND ENVIRONMENTAL ENGINEERING

FEBRUARY 2018

ABSTRACT

In recent years, the development of hydrogen gas production from renewable energy sources has become a major area of focus to cover the shortfalls in demands of global energy. The development of water electrolysis can be considered as a promising technique in this regard for increasing the production of hydrogen fuel to meet energy requirements.

In this research, the splitting steam via eutectic molten hydroxide (NaOH-KOH; 49-51 mol%) electrolysis for hydrogen gas production has been electrochemically investigated. A new reference electrode for eutectic molten hydroxide has been fabricated by covering $Ni/Ni(OH)_2$ with an ionic membrane of alumina or mullite tube. It was found that the $Ni/Ni(OH)_2$ covered with a mullite membrane was stable and reusable over a range of temperatures (225-300^{o}C) without any deterioration. The $Ni/Ni(OH)_2$ covered by a mullite tube reference electrode has been compared with silver and platinum quasi–reference electrodes. The results have shown the designed reference electrode had a more stable and effective performance towards controlling the platinum working electrode as compared to the other quasi-reference electrodes.

In addition, this work carried out a cyclic voltammetry investigation of different working electrodes such as Ni, Pt, Ag, Mo, and stainless steel (SS) using eutectic molten hydroxide at different operating temperatures to examine the occurring reaction on each electrode. The comparison of cyclic voltammetry for examined working electrodes found that the reduction potential for hydrogen evolution was in order of (more positive potential to negative): Ni>Pt>Ag>SS>Ag>Mo. This finding has been additionally confirmed by chronoamperometry.

Finally, the high-temperature eutectic molten hydroxide domain has been electrochemically investigated to split steam into hydrogen fuel. The electrolysis investigations were carried out using nickel, platinum, and stainless steel as the cathode while for the anode, stainless steel and graphite was used. Electrolysis was explored at a temperature range between 225 to 300^{o}C and at different applied voltages of 1.5 to 2.5 V. The current efficiency achieved using stainless steel as an anode and using nickel, stainless steel and platinum as a cathode at 300^{o}C were 90.5%, 80.0% and 68.6% respectively. The current efficiency using graphite anode for an individual cathode material was lower than that for stainless steel anode. Consequently, splitting steam via molten hydroxides for hydrogen was shown a promising alternative to current technology for hydrogen production, with beneficial implications to integrate with renewable energy sources to generate the process.

CONFERENCE PRESENTATION

- Nawar Al-Shara and George Z. Chen., Water electrolysis in molten hydroxide for hydrogen production. Molten Salt Group (MSDG): 2014 Christmas Research Meeting, Royal Society of Chemistry, London.

- Nawar Al-Shara, Li Guan, Ossama Al-Juboori, Happiness Ijije and George Z. Chen., Steam electrolysis in molten hydroxide for hydrogen gas production. The Midlands Electrochemistry Group (MEG): 2015 ISE Satellite Student Regional Symposium on Electrochemistry, Warwick.

- Nawar Al-Shara, Li Guan, Happiness Ijije, Cheng-gong Sun and George Z. Chen., Water Electrolysis in Eutectic NaOH−KOH for Hydrogen Gas Production. Molten Salt Group (MSDG): 2015 Christmas Research Meeting, UCL, London.

ACKNOWLEDGEMENT

Firstly, I am grateful to God almighty for his divine love strength during the course of this research. It was not always easy, but 'Verily in remembrance of Allah do hearts find peace'. Special thanks to my supervisors Professor George Z. Chen and Dr. Cheng-gong Sun for their supervision, guidance and encouragement throughout this project.

My deepest gratitude goes to Dr. Happiness Ijije, Dr. Grace Guan, Ossama Al-Juboori, Dr. Anthony Stevenson, Dr. Hu Di, Dr. Linpo Yu and Li Junfu from the electrochemical research group for their invaluable contribution and assistance during the period of this research. Special thanks to Dr. Wang Xu research visitor from China for his great contribution to this research.

Special thanks are given to the University of Nottingham / Faculty of Engineering for their assistance. I would also like to extend my appreciation to the staff in the Department of Chemical and Environmental Engineering including, but not limit to Bryce Marion, Dave Mee, Mike Fletcher, Fred Anderton, Phil Bennett and all L3 technicians for their assistance.

Finally, to my husband HABEEB HABEEB and my beloved daughters (FATIMA and LANA) for their patience, encouragement and support during my studies. My sincere gratitude also goes to my mother and Father, my parents-in-law, my brothers and my sister for their emotional support and encouragement during this PhD project.

My sincere gratitude also going to Alnahrain University in Iraq and to the minister of higher education in Iraq to offer me this scholarship to complete my PhD degree and for all their financial support.

TABLE OF CONTENT

LIST OF FIGURES

LIST OF TABLES

NOMENCLATURE

▪ Symbols:

Symbol	Meaning	Units
ΔE	Potential difference	V
ΔG	Gibbs free energy	kJ mol^{-1}
ΔH	Enthalpy Change	kJ mol^{-1}
ΔS	Entropy Change	kJ mol^{-1} K^{-1}
A	Cross-sectional area	cm^2
A_o	Frequency factor	
C_o	Concentration of the reactant	mol l^{-1}
C_R	Concentration of the product	mol l^{-1}
E	Potential	V
E_A	Activation energy	kJ mol^{-1}
E^o_{cell}	Equilibrium potential	V
E_{pa}	Anodic peak potential	V
F	Faraday number	C mol^{-1}
I	Current	A
J	Current density	A cm^{-2}
K	Rate constant	
K_{eq}	Reversible constant	
K^o	Standard rate constant	

L	Length	Cm
N	Number of moles	mole
pH	Potential of hydrogen	
Q	Charge transfer	Coulomb
QE	Thermal Energy	kJ mol^{-1}
R	Gas constant	
R'_1	External electric resistance at cathode	Ω
R^2	Statistical correlation	
R_{anode}, $R_{cathode}$	Resistance of the electrodes	Ω
$R_{bubble,H2}$	Resistance of hydrogen bubbles	Ω
$R_{bubble,O2}$	Resistance of oxygen bubbles	Ω
R_{ions}	Resistance of electrolyte	Ω
$R_{membrane}$	Resistance of membrane	Ω
T	Temperature	°C
Z	Number of electrons	
A	Transfer coefficient	
H	Overpotential of the reaction	V
K	Electrical conductivity	Ω^{-1} cm^{-1}
M	Viscosity	centipoises
P	Density	g cm^{-1}

▪ Abbreviations

Abbreviation	Meaning
Ag	Silver
CE	Counter electrode
CV	Cyclic voltammetry
HER	Hydrogen Evolution Reaction
IHL	Inner Helmholtz layer
LH_2	Liquid hydrogen
Mo	molybdenum
Ni	Nickel
OHL	Outer Helmholtz layer
PPM	Part per million
Pt	Platinum
PTFE	Polytetrafluoroethylene
RE	Reference electrode
SS	Stainless steel
SWV	Square wave
WE	Working electrode

CHAPTER 1

INTRODUCTION

1.1 Research Motivation

The widespread use of fossil fuels has rapidly contributed to industrial development in the last century. In the present times however, there is increasing concern regarding the adverse effect of greenhouse gas pollutants (such as CO_2, N_2O, SO_2 etc) from burning fossil fuels, on the atmosphere. In recent years, there has been an increasing interest in the production of hydrogen gas. It is considered to be one of the most promising and vital fuels for the future because of its remarkable capability of reducing air pollution in comparison to the continuous use of fossil fuels. Hydrogen is a high-efficiency energy carrier and has technically shown that it can be used for transportation, heating and power generation. It has the potential to replace current fuels in all present applications. However, there are challenges and barriers to production of hydrogen gas such as storage and safe transportation (Kumar, 2015).

Despite these challenges which occur both during and after the production process of hydrogen fuel, but it can be used to overcome the problem of greenhouse gas emissions which are unsafe to the environment. Therefore it can be stated that hydrogen gas will play an important role in the future of the energy industry to provide for the rapidly increasing demand of the world (Kumar, 2015).

Hydrogen gas can be produced from either non-renewable, conventional energy sources such as hydrocarbon, natural gas and coal; or from renewable energy sources such as hydropower, solar, wind and biomass. Gupta (2008) states that a large reduction in the release of harmful emissions will occur if hydrogen is produced from renewable energy resources. Electrolysis is the most common method that is used to produce hydrogen gas using water as a clean and renewable energy resource. This process has high end-product purity that can reach 99.9 vol%, and can be achieved on both small and large-scale productions. The only setback is that electrolysis can be also be responsible for the emission of CO_2 gas if power plants use a non-renewable energy resource to generate the needed electricity (Kothari et al., 2008). The materials used to construct the electrolysis cell must also withstand certain tough operating conditions and need further development in order to commercialise this clean energy method for producing hydrogen gas as fuel.

1.2 Hydrogen Fuel

An important mitigation tool to counter global warming involves finding an ideal, alternative fuel that should be inexpensive, convenient to use, clean and cause lower greenhouse gas emissions. Hydrogen has received focus from among several alternative fuel sources because it provided the highest potential benefits and fulfils most of the criteria required for an ideal fuel (Kumar, 2015). Hydrogen fuel is similar to electricity in terms of being a high-efficiency energy carrier and when it is used, it can lead to zero or near-zero emissions. For this reason, recently, many researchers and organisations have recently propagated hydrogen fuel as the solution to global warming. As hydrogen is a potentially emissions-free alternative to fossil fuels, it has a very high specific energy content of about 140 MJ kg^{-1} in comparison to gasoline which has a value of 48.6 MJ kg^{-1} (Gupta, 2008). Figure 1.1 is a schematic diagram of the hydrogen fuel production cycle. It has been conceived as an ideal cycle which can potentially be the solution to the depletion of conventional fuels and global environmental problems.

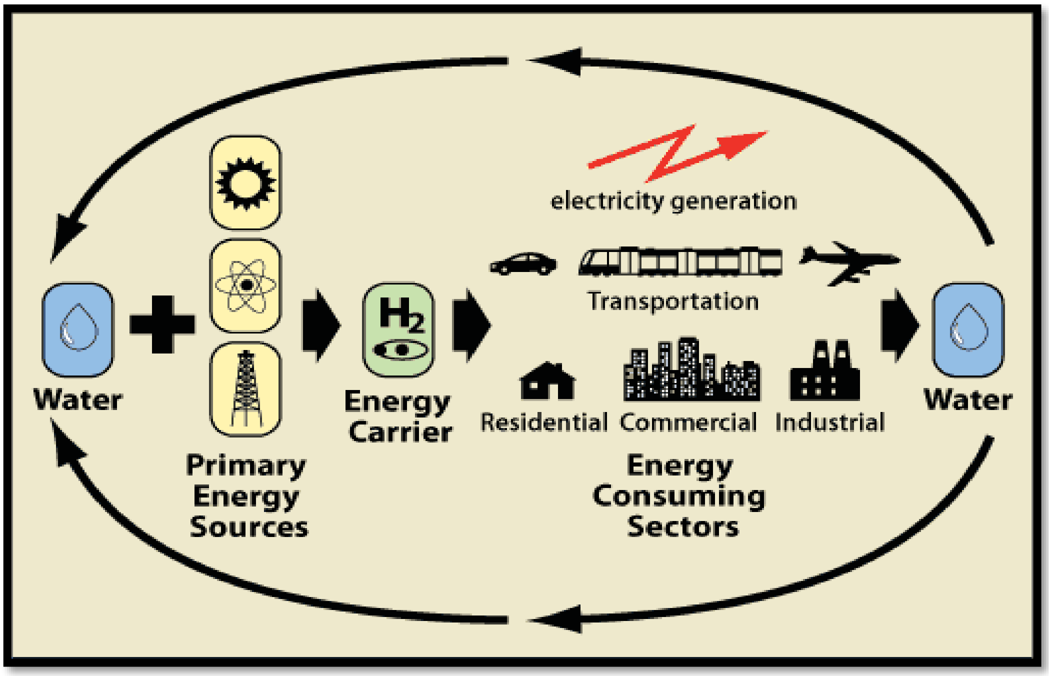

Figure 1.1 – A sustainable hydrogen fuel cycle (Gönderen B zaman, 2013).

Hydrogen fuel is highly flammable over a wide range of temperatures and concentration values. Even though its combustion efficiency is very high for use as a future fuel, there are technological challenges that need to be overcome such as safety in production, storage and transportation. In a fuel cell, hydrogen reacts with oxygen releasing energy to produce water as its only by-product. Hydrogen is not available on earth in its fundamental form, in contrast to coal and hydrocarbons that occur as ready-to-use fuels. It is available as a compound in water, fossil hydrocarbons such as coal, petroleum, natural gas; and biomass products such as carbohydrate, protein, and cellulose (Gupta, 2008).

One of the key issues of plaguing the economic aspects of the hydrogen fuel industry is efficient and affordable storage, and distribution of hydrogen gas that has been produced in small-scale, local plants or in large-scale, central plants. The hydrogen gas can be stored and transport in the form of gaseous hydrogen, liquid hydrogen or metal hydrides.

Hydrogen gas can be stored or transported through three major routes in order to reach a selling market. The first route involves using a pipeline. Hydrogen can be transported through pipelines similar to those used for natural gas. Hydrogen is convenient for being delivered through pipelines made of low-carbon steel, aluminium or brass. Secondly, it can be stored using large-scale storage tanks such as those used for storing natural gas. Gaseous hydrogen can also be stored and transported using a gas cylinder for small-scale operations. The gas stored in such cylinders is at substantially high pressure. Industrial user of hydrogen often use cylinders at pressures ranging from 20 Mpa to 80 Mpa (Dell and Rand, 2004).

Liquid hydrogen (LH_2) has a low density of 70.8 kg cm^{-3} and boils at a very low temperature of -252.3^{o}C (Dell and Rand, 2008). The problem with storing hydrogen as a liquid is that it requires extremely low temperatures. A cryostat can be used for this purpose. The disadvantage of liquefied hydrogen is the requirement of a high cost for the conversion process and subsequently for running and maintaining a cryostat. In this form, it is used more frequently for aircraft rather than road vehicles.

Finally, hydrogen gas can also be stored using certain metal alloys. These metal alloys absorb hydrogen gas reversibly to form metal hydrides. This is considered as an alternative method to store hydrogen (Klebanoff and Keller, 2012).

1.3 Hydrogen Production Methods

All primary energy resources can be used in the hydrogen gas production (Balat, 2008). Hydrogen gas can be produced through several avenues such as fossil fuels, biomass and electrochemical processes.

From several methods of hydrogen production, reforming fossil fuels such as natural gas and oil, is currently still the major method in practice. However, the main by-product from this method is carbon dioxide which is considered as the main cause of the global greenhouse effect. Considering the global environment and people's health, the world needs to turn eventually to renewable energy resources. Hydrogen production without carbon emissions i.e. through renewable energy sources, will be needed in the future.

1.3.1 Hydrogen production from fossil fuels

At present, hydrogen production mainly relies on processes that extract hydrogen from fossil fuel feedstock as shown in Figure 1.2. Most of the commercial hydrogen is thus produced by steam reforming of natural gas (which is essentially methane) (Kothari et al., 2008).

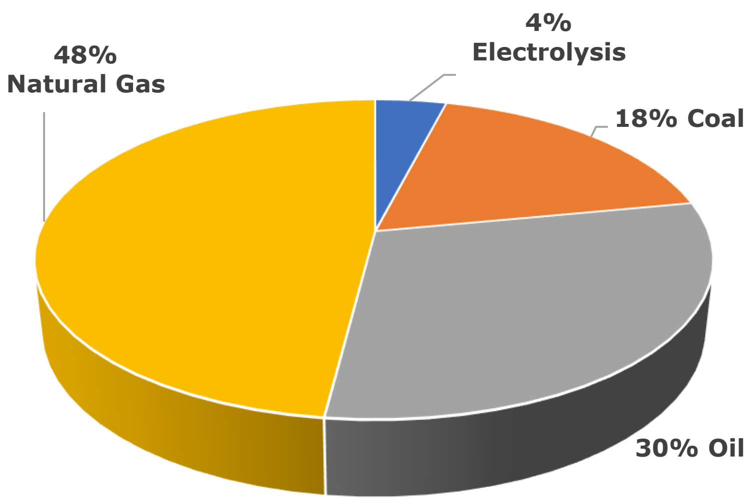

Figure 1.2 – Feedstock used for production of hydrogen (Kothari et al., 2008).

There are three major methods of hydrogen production from fossil fuels: steam reforming of natural gas, partial oxidation of hydrocarbons and coal gasification (Kothari et al., 2008).

The basic reactions of these methods can be generalised as follows (Geissler et al., 2001, Sørensen, 2005a):

Steam reforming of natural gas,

$$C_nH_m + nH_2O \rightarrow nCO + \left(\frac{n+m}{2}\right)H_2 \qquad \textbf{(1.1)}$$

$$CO + H_2O \rightarrow CO_2 + H_2 \qquad \textbf{(1.2)}$$

Partial oxidation of heavier hydrocarbons,

$$2C_nH_m + H_2O + \frac{23}{2}O_2 \rightarrow nCO + nCO_2 + (m+1)H_2 \qquad \textbf{(1.3)}$$

Coal gasification,

$$CH_{0.8} + 0.6O_2 + 0.7H_2O \rightarrow CO_2 + H_2 \qquad \textbf{(1.4)}$$

All three methods have the disadvantage of emitting a large amount of carbon monoxide and require one or more water-gas-shift reactors during the process to reduce carbon monoxide to an acceptable level. Figure 2.1 shows a simple diagram of the steam methane reforming method for hydrogen production (Pant and Gupta, 2009).

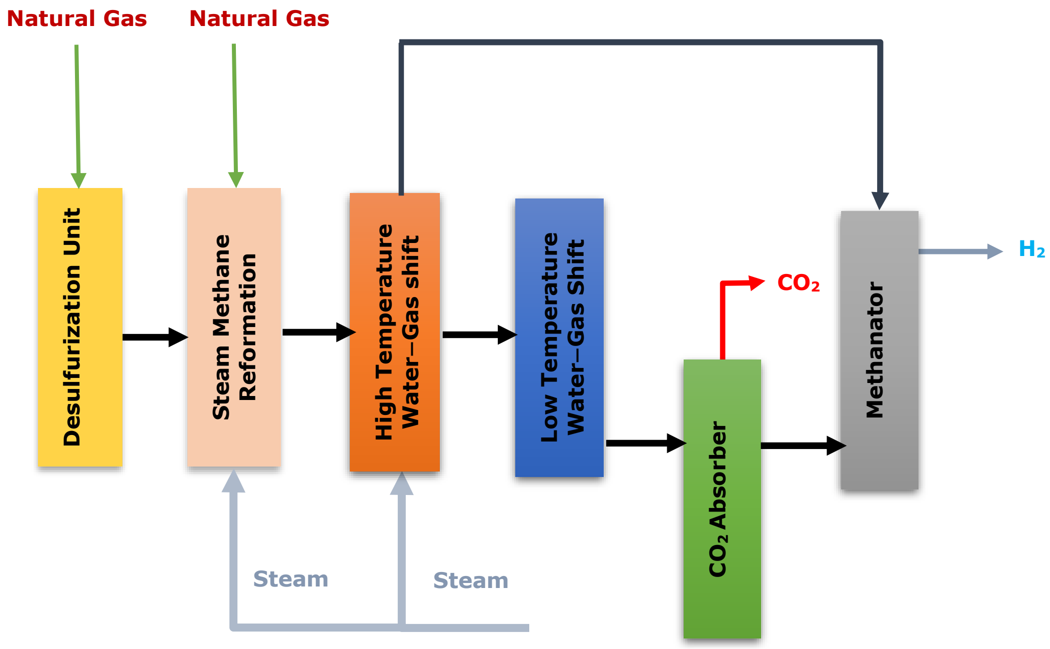

Figure 1.3 – A schematic of hydrogen production by steam methane reforming (SMR) (Pant and Gupta, 2009).

Momirlan and Veziroğlu (1999) list CO, CO_2, C_nH_m, SO_x, NO_x, radioactivity, heavy metals and ashes as some of the pollutants that can be generated in a larger amount when hydrogen is produced from fossil fuels in comparison to renewable energy sources.

1.3.2 Hydrogen production from biomass

Biomass is a carbon-containing fuel but it can also be counted as a renewable fuel energy source. It is formed by fixing carbon dioxide in the atmosphere by photosynthesis. It is available from a wide range of resources such as agricultural crops and waste, animal waste, municipal waste etc. (Ni et al., 2006). There are currently several technologies in place for hydrogen production from biomass:

1.3.2.1 Steam gasification of biomass

Hydrogen can be produced by the thermal gasification of biomass. Solid biomass can be produced from a variety of sources: pellets derived from dedicated energy crops, forestry waste products, straw and even solid organic waste. In the first stage, known as pyrolysis, the solid biomass is heated and broken down into coke, condensates and gases. In the second stage, the products are combined with oxygen and steam. The resulting gas consists mainly of H_2, CO and CH_4. Steam is then applied to reform the methane into hydrogen and CO. The resulting CO is then recycled back into the process to increase the yield of hydrogen (Czernik et al., 2002).

1.3.2.2 Fermentation of biomass

This process uses the high moisture content of biomass or liquid manure. A gas known as biogas is produced via methane fermentation. Biogas is composed primarily of CO and CH_4, and a small amount of H_2 is produced during the fermentation of the latter. The biogas can then be processed further, via steam reforming, to extract the H_2 or be used directly in fuel cells that allow internal reforming, such as molten carbonate or solid oxide fuel cells (Ni et al., 2006).

1.3.2.3 Biological production

Blue-green algae, green algae, and some types of bacteria can be used to produce hydrogen through this method. Biological electrolysis is the first step in photosynthesis. This is where enzymes use sunlight to break water down into hydrogen and oxygen. In most plants, the hydrogen is then combined with carbon dioxide to form carbohydrates. Certain microorganisms, however, release hydrogen instead of carbohydrate during photosynthesis. The yield and efficiency for biological production is low, but further genetic research is currently being conducted towards improving the process (Levin et al., 2004, Kapdan and Kargi, 2006).

1.3.3 Hydrogen production from water

Hydrogen can be produced from directly splitting water using different techniques. These techniques include photoelectrochemical hydrogen production (photoelectrolysis), thermochemical water splitting and water electrolysis. This study focuses on using electrolysis to split water into its core components of hydrogen and oxygen in the gaseous forms respectively.

1.3.3.1 Photoelectrolysis

Photoelectrolysis of water uses sunlight to directly split water into hydrogen and oxygen. The process requires a photosensitive semiconductor device, similar to a photovoltaic solar cell, in conjunction with water-splitting catalysts. The wet semiconductor surface absorbs solar energy and acts as an electrode for dissociation of water. This technique eliminates the need for separate power generation and the electrolysis system in general; however, the yield and efficiency are both quite low (Fujishima and Honda, 1972, Rocheleau et al., 1998).

1.3.3.2 Thermochemical water splitting

Thermochemical water splitting is the conversion of water into hydrogen and oxygen by a series of chemical reactions. Energy, as heat, is the input to a thermochemical cycle via one or more high-temperature endothermic reactions. Excess heat is given off via one or more low-temperature exothermic reactions. Water must be injected to maintain the reactions while all other reactants are regenerated and recycled. The sulphur-iodine system is an example of a thermochemical cycle. It consists of three chemical reactions (1.5), (1.6) and (1.7), with the net reaction (1.8) showing the dissociation of water (Funk, 2001, Holladay et al., 2009).

$I_2 + SO_2 + H_2O \rightarrow 2HI + H_2SO_4$ 120°C exothermic **(1.5)**

$H_2SO_4 \rightarrow SO_2 + H_2O + \frac{1}{2}\ O_2$ 850°C endothermic **(1.6)**

$2HI \rightarrow I_2 + H_2$ 350°C endothermic **(1.7)**

$H_2O \rightarrow \frac{1}{2}\ O_2 + H_2$ Net reaction **(1.8)**

Sulphuric acid and hydrogen iodide are formed during the exothermic reaction of H_2O, SO_2 and I_2 (1.5). The sulphuric acid is dissociated in reaction (1.6), consuming the greatest amount of heat input. The hydrogen is generated through the decomposition of hydrogen iodide (1.7). Since hydrogen and oxygen are derived in different steps, the need for high-temperature gas separation is eliminated (Kubo et al., 2004).

1.3.3.3 Electrolysis

Even though water electrolysis is not currently a mainstream technology for hydrogen production, from a long-term perspective, producing hydrogen through water electrolysis is simple, reliable and clean; thereby producing high purity hydrogen. In the year 1800, Nicholson and Carlisle first explored the ability of electrolytic water to decompose. By 1902, more than 400 industrial water electrolysis units were in operation. In the 1930s, electrolysers were developed from filter press operations to function as large tank-type electrolysers. By the 1950s, pressurised electrolysers had also been developed (Zeng and Zhang, 2010). The next major progress in this field had been the development of new solid electrode materials such as polymers and solid oxides (Zoulias et al., 2004).

Three main methods are currently under consideration for production of hydrogen via water electrolysis: alkaline electrolysis, proton exchange membrane (PEM) electrolysis and solid oxide cell electrolysis (SOCE).

I. Proton exchange membrane electrolysis (PEM)

A proton exchange membrane electrolyser typically involves using a Nafion membrane which is proton-conducting in nature and has the ability to separate hydrogen from oxygen at two different electrodes. Water is split into protons and oxygen at the anode, and produced protons are transported to the cathode via the Nafion membrane. The protons at the cathode combine with electrons to form hydrogen gas. Proton exchange membrane electrolysers can achieve efficiencies of 50-70% (Holladay et al., 2009). The general reaction follows this method at the anode and cathode as in reactions (1.9) and (1.10) respectively. The overall reaction is seen in (1.11) (Sørensen, 2005b, Holladay et al., 2009):

Anode: $2H_2O \rightarrow O_2 + 4H^+ + 4\,e^-$ **(1.9)**

Cathode: $4H^+ + 4e^- \rightarrow 2H_2$ **(1.10)**

Overall reaction: $2H_2O \rightarrow O_2 + 2H_2$ **(1.11)**

II. Solid oxide electrolysis cells (SOECs)

Solid oxide electrolysers are solid–state devices without sensitive electrode electrochemistry and well suited to operate at elevated pressures. These devices use steam and do not undertake the otherwise expensive cation removal method from water or carbon dioxide. Solid oxide cells operate at temperatures ranging from 750-1000^{o}C and thus at a lower thermodynamic potential than a system operating at Lower temperatures. The elevated operating temperature enables the use of non-precious metal electrodes which has faster reaction kinetics at these elevated conditions (Quandt and Streicher, 1986). The process of solid oxide high-temperature electrolysis of steam follows the exact reverse reaction of a solid oxide fuel cell (SOFC). The heat discharged from the system can be utilised. The efficiencies of a solid oxide electrolyser depend on the temperature and subsequent thermal sources (Holladay et al., 2009).

The typical reactions involved at the anode, cathode and the overall reaction in the solid oxide electrolysis cell are seen in reaction (1.12), (1.13) and (1.14) respectively (Borup et al., 2007):

Anode: $O^{2-} \rightarrow \frac{1}{2} O_2(g) + 2e^-$ **(1.12)**

Cathode: $H_2O(g) + 2e^- \rightarrow H_2(g) + O^{2-}$ **(1.13)**

Overall reaction: $H_2O \rightarrow H_2 + \frac{1}{2}O_2$ **(1.14)**

III. Alkaline electrolysis

An alkaline electrolysis cell usually contains two electrodes, an aqueous alkaline electrolyte and a microporous ion-conduction separator. The OH^- ions produced at the cathode are transported to the anode and the H^+ ions remaining at the cathode combine with electrons to form hydrogen gas. The cathode is typically a metal with good catalytic activity and the anode is usually a metal with a layer of oxide coating. As an electrolyte, KOH or NaOH are commonly employed as solutions. The microporous ion-conducting separator allows the transit of OH^- and prevents the mixing of produced hydrogen and oxygen. The efficiency of alkaline electrolysis can reach 70% (Balat, 2008).

The composition of alkaline water electrolysis cell will be further explained in Chapter 2, section 2.1.

1.4 Water Splitting and Solar Energy

There are basically three ways (along with their respective combinations) for producing hydrogen through solar energy: electrochemical, photoelectrolysis, and thermochemical (Steinfeld, 2005). Some basic water splitting technologies for hydrogen production utilise electric power from solar energy (Zoulias et al., 2004). Photoelectrolysis however, uses solar energy to directly split water into hydrogen and oxygen. The photovoltaic (PV) cell device is used to convert solar energy into electricity. The integration of solar energy with water splitting technologies is considered as a direct way for storing energy as hydrogen fuel. This stored energy in the form of chemical bonds can directly or indirectly react with oxygen to release energy (Lewerenz et al., 2013).

1.5 The Advantage of Splitting Water via Molten Hydroxide Electrolysis

Water splitting via molten hydroxide electrolysis has several advantages. The main advantage is that a significant part of the energy needed for electrolysis is added as heat, which is cheaper than electricity. The conductivity of a hydroxide electrolyte at high temperatures is very good and increases with increasing temperature. This electrolyte specification is important for accelerating reaction kinetics, reducing energy loss due to electrode overpotential and therefore increasing the overall system efficiency (Zoulias et al., 2004). In addition, this technology has no need for precious catalytic metal and requires the use of base metals instead to produce hydrogen gas. This is because the molten hydroxide itself acts as a catalyst during the process (Licht et al., 2016, Zoulias et al., 2004). The required decomposition potential of water is also reduced because the operating temperature of molten salt is high. For long-term use, if the electrolysis system is well isolated, energy consumed is consistently reduced. Furthermore, molten salt does not need any additional heat because it maintains the required heat from the current passing through during electrolysis if the system well isolated. This process can also utilise waste heat from other systems to do the work (Zoulias et al., 2004).

The main disadvantage of this process due to which it is not utilised as an industrial process, is a working temperature of less than 300^{o}C. This according to the Carnot cycle for thermodynamic expenditure, results in the wastage of heat (Zoulias et al., 2004).

1.6 Research Aims and Objectives

The aim of this research is to investigate, demonstrate and understand the electrochemical process for splitting steam for hydrogen gas production via eutectic molten hydroxide (NaOH-KOH; 51-49 mol%) electrolysis. This includes characterisation of produced hydrogen gas electrochemically, analytically and also measuring the rate of hydrogen gas production. To achieve the above aims, the research was carried out with the following objectives:

- Designing and fabrication of high-temperature molten salt reactors and electrodes to perform electrolysis.
- Fabricating and investigating suitable reference electrodes (Fast Kinetics) for use in the eutectic molten hydroxide.
- Investigation of steam electro-splitting using cyclic voltammetry (CV), Chronoamperometry and conventional two-electrode electrolysis in eutectic molten hydroxide (NaOH-KOH; 49-51 mol%) under an argon atmosphere.
- Understanding the thermodynamics of the electrochemical reaction process using both phase diagrams and HSC chemistry software.

- Studying the effect of different process variables such as applied voltage, electrode material, and molten salt temperature on the electrochemical process.
- Analytical characterization of the hydrogen gas produced using a hydrogen gas sensor (ProGASBADGE) and a hydrogen gas tube detector (GASTEC).
- Physical measurement of hydrogen gas production using the water displacement technique.
- Theoretically calculate of the actual hydrogen gas volume using Dalton low for gases.

1.7 Scope of Thesis

This project studies the electrochemical kinetics of splitting steam via a eutectic molten hydroxide for hydrogen gas production. This thesis, which consists of eight chapters, investigates different metals to determine a novel, stable and proper reference-electrode for use inside eutectic molten hydroxide. It also examines different working electrodes that are more efficient for increasing hydrogen gas production while decreasing the energy consumed. It is divided into the following chapters:

Chapter 1 outlines the research motivation and lists a clear background about hydrogen fuel, transportation and the methods used for hydrogen gas production. The main advantages of the water electrolysis process via molten hydroxide are also provided. It also outlines the research aims and objectives and includes the scope of the thesis. A comprehensive literature review of the topic is provided in Chapter 2. This is achieved through reviewing the fundamental and relevant literature on alkaline water splitting, molten hydroxide and process conditions.

Chapter 3 begins by introducing the equipment and chemicals used to carry out the experimental aspects of this PhD research. The design and fabrication of the molten salt reactor used to carry out the research are outlined. The chapter also gives details of the various electrochemical, analytical and physical methods employed. For better appreciation and understanding of the experimental results, fundamentals of the underlying principles behind the different methods are also discussed.

In Chapter 4, ionic membranes for the nickel reference electrode in eutectic molten hydroxide are discussed. Cyclic voltammetry is used for analysing the stability, productivity, and reusability for the fabricated nickel reference electrode in eutectic molten hydroxide. Chapter 5 uses cyclic voltammetry to compare different reference electrodes such as quasi-platinum, quasi-silver and fabricated nickel in eutectic molten hydroxide. This comparison is based on their effect on reaction kinetics and the stability to control the working electrode at the same operating process conditions.

Cyclic voltammetry and chronoamperometry investigations of different working electrodes in eutectic molten hydroxide are discussed in Chapter 6. The investigations are based on studying the effect of changing different process variables on eutectic molten hydroxide such as scan rate, operating temperature and the effect of the presence of steam under an argon gas atmosphere. Different working electrodes were employed in this study such as Ni, Pt, Ag, Mo, and SS.

The two-electrode electrolysis process was conducted in Chapter 7 to study the rate of hydrogen gas production and cell efficiency. This investigation is based on studying the effect of different process variables such as cathode and anode metals, applied voltages and varying eutectic molten hydroxide temperature, on the hydrogen gas production process and current efficiency. Chapter 8 concludes the main findings of this work and provides recommendations for future work.

CHAPTER 2

LITERATURE REVIEW

2.1 An Alkaline Water Electrolysis Cell

The most popular technique for producing hydrogen gas from water is through the electrolysis of aqueous alkaline hydroxide solutions. Notably, recent studies concerned with the development of alkaline electrolysis processes have focused on the use of advanced anode materials in electrolysers to reduce electrode polarisation, thus improving the overall electrical efficiency (Dabo et al., 1997, Marshall et al., 2007). Some of the most promising published process modifications have involved increasing the electrolysis cell operating temperature (Miles et al., 1976, Ferreira et al., 1988). Miles et al. (1976) first discovered that increasing the operating temperature of an alkaline electrolysis cell with nickel-based electrodes allowed for increased electrolyte ionic conductivity and enhanced electrode surface kinetics. However, they also found that the main disadvantage of increasing the cell temperature was the reduced durability of cell materials which came into contact with the corrosive electrolyte.

Several decades later, Ganley (2008) demonstrated the effectiveness of a molten hydroxide eutectic solution in a direct ammonia fuel cell system; which was constructed using housing and electrode materials that were stable up to a temperature of 450°C. Ganley (2009)'s subsequent study focused specifically on high-temperature and pressure alkaline electrolysis which increased the ionic conductivity of an electrolyte and enhanced the rates of electrochemical reactions at the electrode surfaces. On the other hand, Zecevic et al. (2004) demonstrated that in the case of direct carbon fuel cells, the continuous existence of high water content in a similar electrolytic hydroxide, enhanced the characteristics of high ionic conductivity.

2.1.1 General fundamentals of alkaline water electrolysis

The general fundamentals of alkaline water electrolysis are based on the passage of a direct current through water to separate it into its core molecules of hydrogen and oxygen gas respectively (Bockris et al., 1980). Water electrolysis essentially requires two metal electrodes and an electrolyte to generate this separation. A direct current must flow between the two electrodes (anode and cathode). The connectivity between the two electrodes (anode and cathode) happens through the electrolyte and as a result, this can raise the ionic conductivity. Furthermore, the electrodes have to be resistant to corrosion, have good electric connectivity, exhibit good catalytic properties and maintain a reliable structure during the process. The electrolyte’s composition must not change during the process, as well as it must remain inert in terms of reacting with the electrodes (Ursua et al., 2012).

Hydrogen and oxygen gas generated at the electrodes from water electrolysis, is required to be separated by a membrane in order to avoid synthesis into water. This membrane must exhibit high ionic conductivity and high stability in both its physical and chemical properties.

The main components of the electrochemical cell are the electrodes, the membrane and the electrolyte. The overall water electrolysis reaction can be summarised as:

$$H_2O \rightarrow H_2(g) + \tfrac{1}{2}O_2(g) \qquad \textbf{(2.1)}$$

During electrolysis, electrons are given or taken by the ion at the respective electrode surface, generating a multiphase, gas-liquid-solid system. At the cathode of the half-cell, reduction occurs while the oxidation of water occurs at the anode. At the cathode, the half-cell polarises the electrode negatively, and the electrons flow from the outside circuit, generating hydrogen. However, at the anode half-cell, the electron leaves the anode for the outside circuit. The electrode is polarised in a positive direction, generating oxygen gas.

The electrolysis process of water converts electric and thermal energy to chemical energy which is stored in the form of hydrogen fuel. This process can be described according to the fundamentals of thermodynamics (Leroy et al., 1980, Onda et al., 2004). When this reaction takes place at constant pressure and temperature, the required energy for water splitting is determined by the process enthalpy change (ΔH). For this reaction to occur, part of the electric energy must be used which is represented by the Gibbs free energy change (ΔG). The rest of the energy is the thermal energy (Q_E) which equals the temperature of the system (T) and the entropy change (ΔS). The following expression shows the relationship between these thermodynamics properties (Zoulias et al., 2004):

$$\Delta G = \Delta H - Q_E = \Delta H - T\Delta S \qquad \textbf{(2.2)}$$

Therefore, the minimum cell voltages (E°_{cell}) for electrolysis under a certain value of pressure and temperature can be expressed as follows (Zoulias et al., 2004):

$$\Delta E^{o}_{cell} = \frac{-\Delta G^{o}}{z\,F} \qquad \textbf{(2.3)}$$

Where ΔG° is the change in the Gibbs free energy under standard conditions and z is the number of electron moles transferred per hydrogen mole (z=2). F is the Faraday Number, a constant which represents the charge of one mole of electrons (96485 C mol^{-1}). The difference between ΔG^{o} and ΔG is that the former represents the minimum theoretical amount of the electrical energy required for a reaction to occur. Conversely, ΔG is the actual electrical energy consumed during the reaction (Zeng and Zhang, 2010). In an ideal electrolysis process, the minimum voltage that needs to cause the reaction is known as the thermo-neutral voltage ΔE° which is equal to the enthalpy change potential $\Delta E_{\Delta H}$. Meanwhile, the enthalpy change potential is equal to the total energy required. Therefore, the following expression can be used to find ΔE_{cell} and $\Delta E_{\Delta H}$ (Zoulias et al., 2004).

$$\Delta E_{\Delta H} = \Delta E_{cell} = \frac{\Delta H}{z\,F} \qquad \textbf{(2.4)}$$

For an actual electrolysis process, ΔE_{cell} must be greater than $\Delta E_{\Delta H}$. This additional energy in terms of electrical and thermal, is caused by thermodynamic irreversibility that is mainly related to water vapour contained in the hydrogen and oxygen streams. The thermal losses in the system take place even though water flow occurs at low temperature and pressure because of convection and radiation (Diéguez et al., 2008). The thermodynamic properties of water electrolysis at standard conditions (1atm and 25°C) can be illustrated in Table 2.1.

Table 2.1 – The standard thermodynamic properties of a water electrolysis cell (Zoulias et al., 2004).

	ΔH° (kJ mol^{-1})	ΔG° (kJ mol^{-1})	ΔS° (kJ mol^{-1} K)	E°cell (V)
H_2O	285.8	237.2	0.16	1.23
H_2	–	–	0.13	–
O_2	–	–	0.21	–

2.1.2 The working principle of an alkaline water electrolysis cell

A simple alkaline water electrolysis unit consists of an anode, a cathode, a power supply unit and an electrolyte, as shown in Figure 2.1. A direct-current (DC) is applied to maintain the electricity balance whereby electrons flow from the negative compartment of the DC source to the cathode. It is at the cathode where the electrons are consumed by hydrogen ions to form hydrogen gas. The electric charge is kept in balance as hydroxide ions transfer through the electrolyte solution to the anode electrode. At the anode, the hydroxide ions give away electrons and these electrons return to the positive terminal of the DC source. In order to enhance the connectivity of the solution, electrolytes which generally consist of ions with high mobility are used in the electrolyser (Oldham and Myland, 1993).

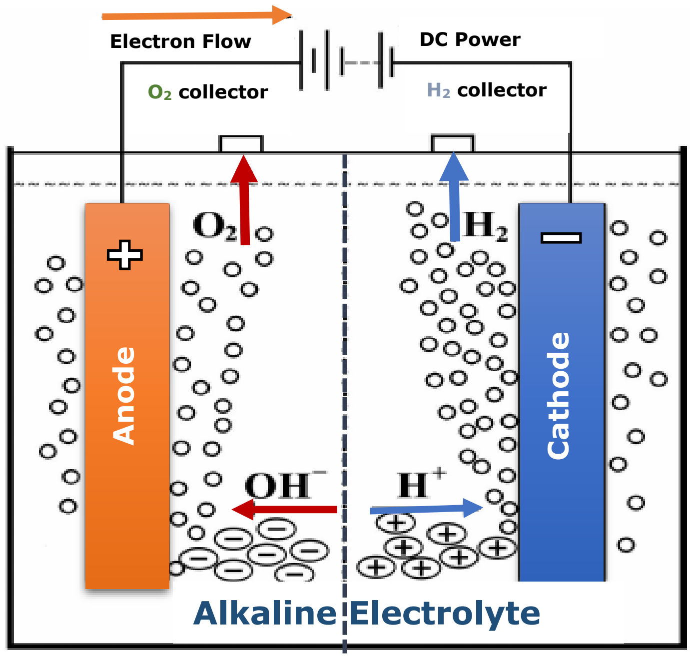

Figure 2.1 – A schematic illustration of a basic water electrolysis system (Zeng and Zhang, 2010).

Potassium hydroxide is the most commonly used electrolyte in water electrolysis because it avoids the vast corrosion loss caused by acid electrolytes (LeRoy, 1983). The most popular electrode material in use is nickel due to its high activity, widespread availability as well as low cost (Janjua and Le Roy, 1985). Therefore, during the process of water electrolysis, hydrogen ions move towards the cathode and hydroxide ions move towards the anode. By the use of a membrane, gas receivers can collect hydrogen and oxygen which form on and depart from the cathode and the anode, respectively (Zeng and Zhang, 2010).

The half reactions taking place at the cathode and anode compartment, are given by equation (2.5) and (2.6) respectively (Zeng and Zhang, 2010):

$$\text{Cathode: } 2H_2O + 2e^- \rightarrow H_2 + 2OH^- \; (E^o = -0.83\text{ V}) \qquad \mathbf{(2.5)}$$

$$\text{Anode: } 2OH^- \rightarrow \tfrac{1}{2}O_2 + H_2O + 2e^- \quad (E^o = 0.40\text{ V}) \qquad \mathbf{(2.6)}$$

The overall chemical reaction of water electrolysis is as follows (Zeng and Zhang, 2010):

$$\text{Overall reaction: } \mathrm{H_2O} \rightarrow \mathrm{H_2} + \tfrac{1}{2}\mathrm{O_2} \quad (\mathrm{E^o} = -1.23\ \mathrm{V}) \qquad \textbf{(2.7)}$$

The sum potential of equation (2.5) and (2.6) is -1.23 V, which is taken as the value of the theoretical cell voltage required for this process. In order for the above reactions to occur, there are a number of barriers to be overcome which are dependent upon several electrolytic cell components: the boundary layers at an electrode surface, electrode phase, electrolyte phase, separator and electrical resistance of the circuit (Santos et al., 2013). These barriers also include the electrical resistance of the circuit, activation energies of the electrochemical reactions occurring on the surfaces of the electrodes, availability of electrode surfaces due to partial coverage by gas bubbles formed and the resistance to the ionic transfer within the electrolyte solution. These barriers are significant for analysing this process in the context of thermodynamics, kinetics as well as transport process principles (Zeng and Zhang, 2010).

Figure 2.2 shows the resistances presented in a simple water electrolysis system. The first resistance that starts from the left-hand side is the external electrical circuit resistance R_1 including the wiring and connections at the anode. R_{anode} is created from the overpotential characteristics of the oxygen evolution reaction on the surface of the anode. R_{bubble} of O_2 is the resistance due to partial coverage of the anode by the oxygen bubbles, which hinder the contact between the anode and the electrolyte. There are also resistances that arise from the electrolyte and the membrane and are denoted as R_{ions} and $R_{membrane}$ respectively. In the same way, R_{bubble} of H_2

arises from the blockage of the cathode by hydrogen bubbles; $R_{cathode}$ is the resistance caused by the overpotential for the hydrogen evolution reaction, whereas $R`_1$ is the electrical resistance of the wiring and connections at the cathode (Zeng and Zhang, 2010). Consequently, the total resistance can be expressed as in equation (2.8).

$$R_{total} =$$

$$R_1 + R_{anode} + R_{bubble,O_2} + R_{ions} + R_{membrane} + R_{bubble,H_2} + R_{cathode} + R'_1 \quad \textbf{(2.8)}$$

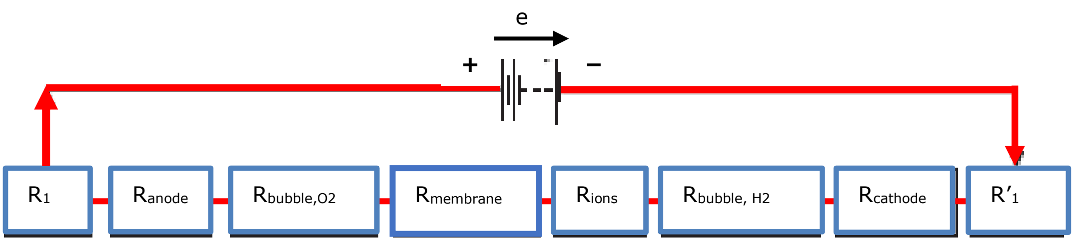

Figure 2.2 – An electrical circuit analogy of resistance in the water electrolysis system (Zeng and Zhang, 2010).

These resistances in the electrolysis systems can be classified into three categories: the first category includes all the electrical resistances, the second includes the reaction resistances and the third includes the transport resistances. The electrical resistance can be calculated using Ohm's law as in equation (2.9) (Oldham and Myland, 1993):

$$R = \frac{E}{i} \quad \textbf{(2.9)}$$

Where E is the applied voltage and i is the current passing through the circuit when the voltage is applied (Oldham and Myland, 1993). Furthermore, the electrical resistance can be calculated using equation (2.10):

$$R = \frac{L}{k\,A} \qquad \textbf{(2.10)}$$

Where L, *k* and A are the length, electrical connectivity and cross-sectional area of the conductor, respectively. This category belongs to R_1 and R'_1 in the equation (2.8).

The reaction resistances exist due to the over-potential required to overcome the activation energies of the hydrogen and oxygen formation reactions on the cathode and anode surfaces. These reactions result in a direct increase in the overall cell potential. These are the intrinsic energy barriers of the reactions which determine the kinetics of the electrochemical reactions (Bard and Faulkner, 2001). The reaction resistances are inherent resistances of the electrochemical reactions depending on the surface activities of the electrode employed (Zeng and Zhang, 2010). R_{anode} and $R_{cathode}$ are reaction resistances in this context.

The transport related resistances are the physical resistances experienced in the electrolysis process such as gas bubbles present in the electrolyte solution and covering the electrode surfaces; resistance to the ionic transfer in the electrolyte and lastly due to the membrane used for separating the hydrogen and oxygen gas. R_{bubble,O_2}, R_{ions}, $R_{membrane}$, and R_{bubble,H_2} are considered as transport resistances. Both electrical and transport resistances cause heat generation according to Joule's law (Oldham and Myland, 1993) and transport phenomena (Bird et al., 2007), thereby increasing inefficiency in the electrolysis system. The loss in energy due to this resistance is known as Ohmic loss (Belmont and Girault, 1994).

Thereby, in order to improve the energy efficiency of water electrolysis and thus the overall performance of the system, an understanding of these resistances must be pursued in order to minimise them (Zeng and Zhang, 2010).

2.1.3 Thermodynamics of an alkaline electrolysis cell

In general, literature regarding thermodynamics of an electrochemical cell can be found in physical chemistry and electrochemical books. The equilibrium potential can be obtained by subtracting the equilibrium potential of the cathode electrode from the equilibrium potential of the anode electrode (Wendt and Kreysa, 1999) as in equation (2.11):

$$E^{o}_{cell} = E^{o}_{cathode} - E^{o}_{anode} \qquad \textbf{(2.11)}$$

The equilibrium cell potential is related to the Gibbs free energy change of the overall cell reaction as expressed in equation (2.12) (Wendt and Kreysa, 1999):

$$\Delta G_{Cell} = -nFE^{o}_{cell} \qquad \textbf{(2.12)}$$

where n is the number of moles of transferred electrons. ΔG_{Cell} is the electrochemical cell reaction and can be calculated from the difference between the summation of free energy values for products and reactants (Wendt and Kreysa, 1999):

$$\Delta G_{cell} = \sum \Delta G_{product} - \sum \Delta G_{reactant} \qquad \textbf{(2.13)}$$

For a spontaneous cell reaction, the driving force has a negative value of ΔG_{Cell}, (Wendt and Kreysa, 1999) which can be expressed as:

$$\Delta G_{cell} = \Delta H_{cell} - T\,\Delta S_{cell} \qquad \textbf{(2.14)}$$

Where ΔH_{Cell} and ΔS_{Cell} are respectively the enthalpy change and entropy change associated with the cell reaction, and T is the temperature of the reaction. It should be mentioned in this regard that for spontaneous cell reactions, T ΔS_{Cell} > ΔH_{Cell}, resulting in ΔG_{Cell} < 0.0. The equilibrium cell potential for water electrolysis is -1.23V, and the free Gibbs energy is 238kJmol^{-1} of hydrogen (Kim et al., 2006). Even though electrolysis of water converts the liquid into two gases, hydrogen and oxygen; this process causes a large increase in the entropy of the system accompanied by an extraordinary high enthalpy value 286 kJ mol^{-1} at 25^{o}C. It should also be mentioned that the conversion of water to hydrogen and oxygen is thermodynamically unfavourable and can be achieved only when there is enough electrical energy supplied. Therefore, thermodynamically this overall cell reaction will take place and the current will flow when an external electrical circuit interconnects the two electrodes of the cell. The cell reaction has either a negative ΔG_{cell} or a positive ΔG_{cell} value, but the cell potential should be larger than the applied potential between the two electrodes to drive the chemical reaction. Some reactions are essentially fast and give reasonable current density values, even close to the equilibrium potential E^{o}. In contrast, others are essentially slow, requiring an overpotential, η, to obtain a necessary current density (Bard and Faulkner, 2001, Rossmeisl et al., 2005). The kinetics of the electrode reactions were discussed in the previous section, where η can be seen to increase with current density. The requirement of the extra energy causes a potential drop, IR_{cell}. This potential drop is a function of the electrolyte properties, the shape of the electrodes and cell design. The cell potential as it is expressed in equation (2.15), is always between 1.8-2.0V, with a current density value between 0.001-0.003 A cm^{-2} for an industrial water electrolysis system (Kinoshita, 1992).

$$E^{o}_{cell} = E^{o}_{cathode} - E^{o}_{anode} - \sum \eta + i\,R_{cell} \qquad \textbf{(2.15)}$$

Where $\sum\eta$, is the sum of overpotentials from the differences in the electrolyte concentration, obstruction at the electrode surface because of bubble formation; and from the bubble formation itself. The current density increases with the increase in both η and $i\,R_{cell}$, causing inefficiencies during electrolysis.

Many researchers mention that the relationship between the electrolytic cell potential and operating temperature can be expressed through Figure 2.3 (Bockris et al., 1981, Viswanath, 2004). The cell potential-temperature for the electrolysis system as in Figure 2.3, is divided into three regions which are separated by two lines: equilibrium voltage line and thermoneutral voltage line. The equilibrium voltage line represents the minimum potential required to dissociate water by electrolysis and thus below this line, the electrolysis of water cannot proceed. It should be mentioned here that the equilibrium voltage decreases with increasing temperature. The thermo-neutral voltage is the actual minimum voltage that has to be applied to the electrolysis cell and thus below this line, electrolysis is endothermic in nature. In an alternate scenario, above this line, electrolysis is exothermic in nature. The thermo-neutral voltage actually includes the over-potential of the electrodes, which are only weakly dependent on temperature. Therefore, the thermos-neutral voltage simply displays a slight increase in the potential with temperature (Zeng and Zhang, 2010).

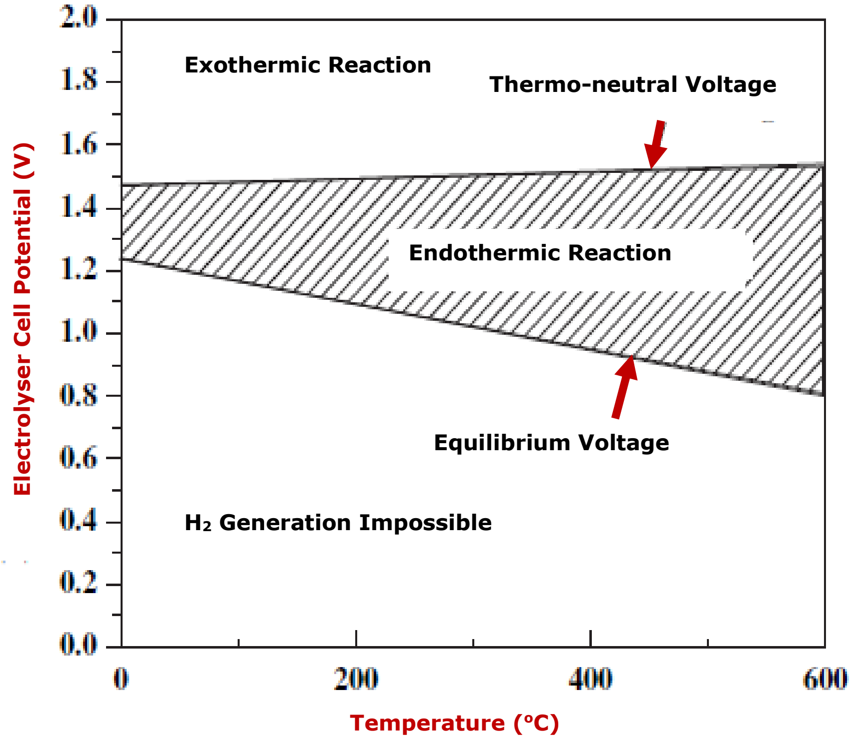

Figure 2.3 – Cell potential for hydrogen gas production by water electrolysis process as a function of temperature (Bockris et al., 1981, Viswanath, 2004).

Electrolytic efficiency can be expressed in many ways. The voltage efficiency of an electrolyser is the proportion of effective voltage used to split water against the total voltage applied to the cell voltage (Bloom and Gutmann, 1977, White et al., 1984). This efficiency can be expressed in equation (2.16):

$$\text{Voltage Efficiency } \% = \frac{E^{o}_{cell}}{E_{cell}} \qquad \textbf{(2.16)}$$

The thermal efficiency in equation (2.17) is based on the energy changes of the water electrolysis reaction and can be expressed as (Bloom and Gutmann, 1977, White et al., 1984):

$$\text{Faradaic Efficiency} = \frac{\Delta H_{cell}}{\Delta G_{cell}} \qquad \textbf{(2.17)}$$

This thermal efficiency takes the whole thermal balance into account. Furthermore, the efficiency can also be calculated from the rate of hydrogen gas production against the total electrical energy applied to the electrolysis system (Santos et al., 2013) as in equation (2.18):

$$\text{Efficiency of } H_2 \text{ production rate} = \frac{r_{H_2} \text{ of production rate}}{\Delta W}$$

$$= \frac{-V_{H_2}}{i \;\; E_{cell} \;\; t} \qquad \textbf{(2.18)}$$

Where t is the time of electrolysis and V_{H_2} is the hydrogen production rate per unit volume of the cell. Obviously, using the above efficiency expressions, an improvement to the electrolytic process can be made by reducing the energy required to split water. This can be achieved by increasing the temperature or pressure and by reducing the energy loss through minimisation of system resistance. Therefore, as this research is focused on increasing the efficiency of the electrolysis system and the efficiency of the rate of hydrogen gas production, it focuses on high-temperature steam electrolysis (Zeng and Zhang, 2010).

2.1.4 Electrode kinetics

The rate of the electrode reaction that is characterised by the current density firstly depends on the nature and pre-treatment of the electrode surfaces. Furthermore, the rate of reaction depends on the composition of the electrolytic solution adjacent to the electrodes. These ions in the solution close to and under the effect of the respective electrodes, form a layer known as a double layer (Oldham and Myland, 1993). An example of this is the charge layer that forms near the cathode due to hydroxyl ions and potassium ions due to the charge of the electrodes during electrolysis. Finally, the rate of the reaction depends on the electrode potential which is itself characterised by the reaction overpotential. Therefore, the investigation of electrode kinetics seeks to establish the macroscopic relationship between the current density, the surface overpotential and the composition of the electrolytic solution adjacent to the electrode surface (Newman, 1991).

Figure 2.4 a shows the double layer. There are accumulated ions forming two mobile layers of solvent molecules and adsorbed species. The layer near the electrode surface is relatively ordered and is termed as the Inner Helmholtz Layer (IHL). Another layer with less organisation is called the Outer Helmholtz layer (OHL) (Pickett, 1979). The electrical charges on the surface of the electrodes are balanced by ionic counter-charges in the surrounding area of the electrodes. The potential distribution is also plotted against the distance from the electrode surface as in Figure 2.4 b.

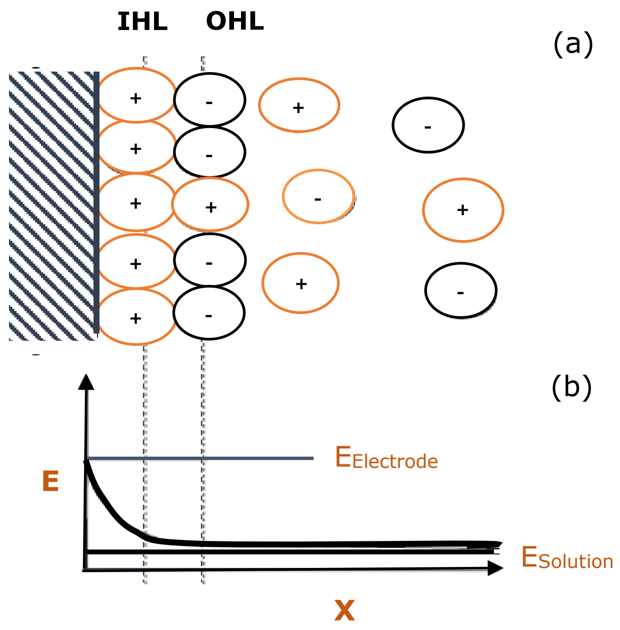

Figure 2.4 – An electrical double layer near a negatively charged electrode surface (a) A simplified schematic of its structure and (b) Potential vs distance profile (Zeng and Zhang, 2010).

It can be noted here that an interfacial potential difference exists between the electrode surface and the electrolyte due to the existence of this double layer (Wendt and Kreysa, 1999). The double layer formation phenomenon is a non-faradic process (Wendt and Kreysa, 1999). It leads to the capacitive behaviour of the electrode reactions and needs to be considered in the electrode kinetics.

The number of moles of the electrolyzed species (H^+ or O^{2-}) is given by Faraday's law (Bard and Faulkner, 2001) as follows:

$$n = \frac{Q}{z\ F} \qquad \textbf{(2.19)}$$

Where Q is the total charge in Coulombs transferred during the reactions, z is the stoichiometric number of electrons consumed in the electrode reaction (equal to 2 in both equations (2.18) and (2.19)) and F is the

Faraday constant (Bard and Faulkner, 2001). The rate of electrolysis can be expressed as:

$$\text{Rate} = \frac{\text{dn}}{\text{dt}} \qquad \textbf{(2.20)}$$

Where the Faradic current i (Bard and Faulkner, 2001) can be expressed as:

$$\text{i} = \frac{\text{dQ}}{\text{dt}} \qquad \textbf{(2.21)}$$

Furthermore, the surface area at which the reaction takes place must be taken into account (Zeng and Zhang, 2010). Therefore, the electrolysis rate can be expressed as follows:

$$\text{Rate} = \frac{\text{i}}{\text{z F A}} = \frac{\text{j}}{\text{z}} \qquad \textbf{(2.22)}$$

Where J is the current density (Zeng and Zhang, 2010). The Arrhenius equation can be expressed as the rate constant of a chemical reaction.

$$\text{k} = \text{A}_\text{o}\text{e}^{-\text{E}_\text{A}/\text{RT}} \qquad \textbf{(2.23)}$$

Where E_A is the activation energy in kJ mol^{-1}, A_o is the frequency factor, R is the gas constant and T is the reaction temperature. This equation quantifies the relationship between the activation energy and the rate constant.

The Butler-Volmer equation gives the dependence of the current density on the surface potential and the composition of the electrolytic solution adjacent to the electrode surface. This can be written as a one-electron reaction that relates the current to the rate of the reaction (Bard and Faulkner, 2001) as in equation (2.24):

$$i = i_{cathodic} - i_{anodic}$$

$$= FAK^{o}\left(C_{o}(0,t)e^{-\alpha f(E-E^{o})} - C_{R}(0,t)e^{(1-\alpha)f(E-E^{o})}\right) \qquad \textbf{(2.24)}$$

Where A is the electrode surface area through which the current passes, K^0 is the standard rate constant, $\propto$ is referred to as the transfer coefficient (its value lies between 0 and 1 for this one−electron reaction) and *f* is the F/RT ratio. The t and 0 in the bracket are the specific time at which this current occurs and the distance from the electrode. For the cathode reaction, as in equation (2.23), $C_0(0,t)$ stands for the concentration of the reactant species at the cathode in the oxidised state of the hydrogen ions (H^+). Consequently, $C_R(0,t)$ is the concentration of the reaction product hydrogen (1/2) H_2, which is in the reduced state. The Butler-Volmer equation is derived using the transition-state theory (Bard and Faulkner, 2001). This theory describes a set of curvilinear coordinates in the reactions paths as in Figure 2.5a. The potential energy is a function of the independent positions of the coordinates in the system. When a potential increase in ΔE is encountered, it will cause the relative energy of the electron to decrease by $F(E-E^o)$ as shown in Figure 2.5 a. The decrease, in turn, reduces the Gibbs free energy of the hydrogen ions in the hydrogen production reaction by $(1-\propto)(E-E^o)$ and, in contrast, increases the Gibbs free energy of hydrogen by $\propto(E-E^o)$, respectively. Thus, this behaviour provides no limitation for mass transfer; and subsequently, the Bulter-Volmer equation can be derived from equations (2.22) and (2.23) using Gibbs free energy change in Figure 2.5.

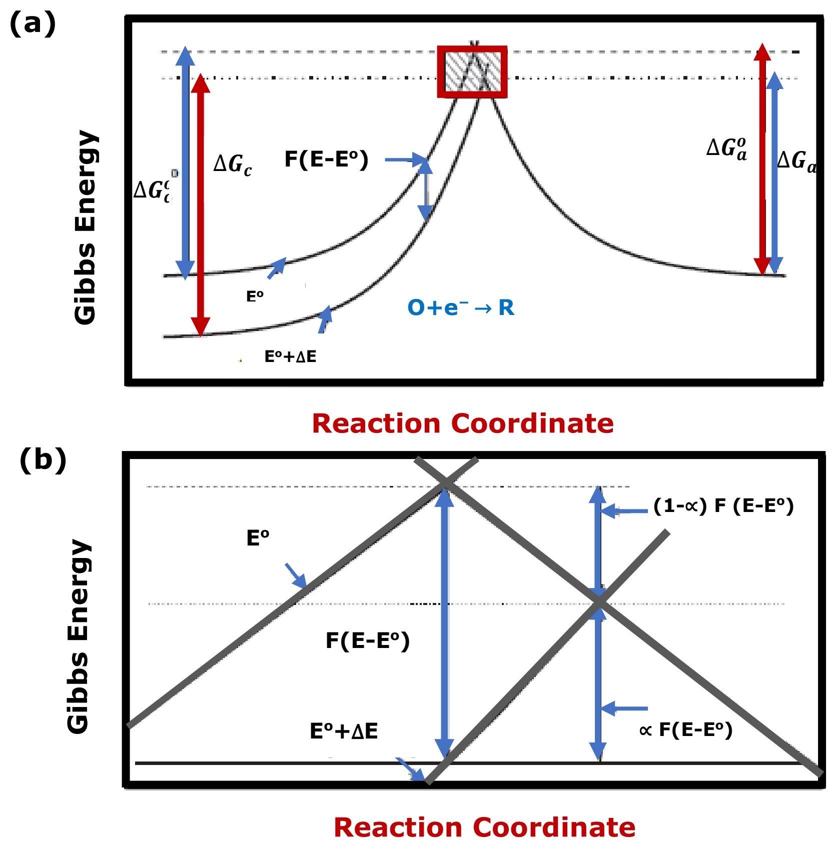

Figure 2.5 – Effect of potential change in Gibbs energy: (a) The overall relationship between energy change and state of reaction and (b) Magnified picture of the shaded area in (a) (Zeng and Zhang, 2010).

The Butler-Volmer equation can be simplified as (Zeng and Zhang, 2010) :

$$i = i_o \left(e^{-\alpha f \eta} - e^{-(1-\alpha) f \eta}\right) \quad \textbf{(2.25)}$$

Where i_0 is known as the current exchange density that is defined as the current of the reversible water splitting reaction (Rieger, 1987). The overpotential at each electrode can be derived from the above-simplified equation. In the absence of the influence of mass transfer and at large overpotentials >118 mV at 25°C, one of the terms in the equation of total resistance can be neglected i.e. when $e^{-\alpha f \eta} > e^{-(1-\alpha) f \eta}$. The relation between i and $\eta(E-E^o)$ can be written in terms of the Tafel equation (Abouatallah et al., 2001).

$$\eta = a + b \log i \quad \textbf{(2.26)}$$

Where a $=(2.3\ RT)/(\alpha F)\log i_o$ and $b=(-2.3\ RT)/(\alpha F)$. Therefore the linear relationship between the overpotential and the logarithm of current density is characterised by the slope (b) and a is the exchange current density i_o. The slope is also known as the Tafel slope. These parameters are generally used as Kinetic data to compare electrodes in electrochemistry.

It can be concluded from the above analysis that the rate of electrolysis can be expressed by the current or current density. The rate of the reaction is directly determined by the overpotential, which depends on a number of factors. One of the significant factors is the activation energy, E_A, which is strongly influenced by the electrode material. Thus a vast majority of the research is focused on reducing the activation energy of the electrode reactions and also optimising the influence of the electrode materials and surface configurations.

2.1.5 Hydrogen evolution reaction

The mechanism of the hydrogen evolution reaction from water electrolysis is generally accepted to be a step involving the formation of absorbed hydrogen (Bockris et al., 1981) as expressed in equation (2.27):

$$H^+ + e^- \rightarrow H_{ads} \quad \textbf{(2.27)}$$

This reaction is followed by either chemical desorption (Bockris et al., 1981) as in equation (2.28):

$$2H_{ads} \rightarrow H_2 \quad \textbf{(2.28)}$$

Or by electrochemical desorption (Bockris et al., 1981) as expressed in equation (2.29):

$$H^+ + e^- + H_{ads} \rightarrow H_2 \quad \textbf{(2.29)}$$

Where the subscript 'ads' represents the absorbed status. The over-potential of hydrogen evolution is commonly measured by the Tafel equation as expressed in equation (2.30) (Zeng and Zhang, 2010):

$$\eta_{cathode} = 2.3\frac{R\,T}{\alpha\,F}\log\frac{i}{i_o} \quad \textbf{(2.30)}$$

From the above equation, i_o represents the current density of the reaction which can be identified as the rate constant of the reaction and it is affected by the nature of the cathode material (Newman, 1991). The over-potential of hydrogen gas production results in the prevalence of more energy barriers during the process of hydrogen formation.

The over-potential on the cathode is directly related to the formation of hydrogen in the region surrounding the electrode. The formation of hydrogen is basically determined by the bond between hydrogen and the electrode surface. Nickel has the highest heat adsorption of hydrogen of 105kJmol^{-1} as compared to 83.5kJmol^{-1} for palladium (Trasatti, 1971). However, the formation of hydrogen is also influenced by the electrolyte type and concentration, the electrode properties and the reaction temperature.

2.1.6 Oxygen evolution reaction

The mechanism of oxygen evolution from water electrolysis is more complex as compared to the hydrogen evolution reaction. The most general mechanism involving the oxygen evolution reaction is expressed as reactions (2.31), (2.32) and (2.33) (Bockris et al., 1981):

$$OH^-_{ads} \leftrightarrow OH_{ads} + e^- \qquad \textbf{(2.31)}$$

$$OH^- + OH^-_{ads} \leftrightarrow O_{ads} + H_2O + e^- \qquad \textbf{(2.32)}$$

$$O_{ads} + O_{ads} \leftrightarrow O_2 \qquad \textbf{(2.33)}$$

The over-potential of the oxygen evolution reaction is basically measured by the Tafel equation as expressed in equation (2.34) (Zeng and Zhang, 2010):

$$\eta_{anode} = 2.3\frac{RT}{(1-\alpha)F}\log\frac{i}{i_o} \qquad \textbf{(2.34)}$$

The reaction rate decreases with an increase in activation energy. Therefore, reducing activation energy is always favoured for more efficient water electrolysis. In addition, the activation energy increases with an increase in the current density; and it can be lowered by using an electro-catalytic electrode. Potvin and Brossard (1992) found that the oxygen over-potential reduced when an alloy of Fe-Ni was used as an anode.

2.2 Process Condition

In this section, the effect of the process conditions on the anodic and cathodic reactions is considered in order to clearly explain the principal reactions. However, the reactions that occur in a molten hydroxide electrolysis cell are significantly influenced by the process conditions, such as salt compositions, pressure, atmosphere, temperature and electrode materials. Hydrogen gas can also be produced from the electrolysis of hydroxide salt at different production rates under certain process conditions. This section provides an overview of the effects of such process conditions.

Table 2.2 shows the conditions under which authors in the literature have used hydroxide salts as an electrolyte in their electrochemical studies. Different conditions such as room temperature versus high-temperature; and through an aqueous hydroxide salt or molten hydroxide salt, have been included for comparison. It is obvious from Table 2.2 that the atmosphere employed for a low-temperature electrolysis process using ionic liquid is almost air while for high-temperature electrolysis, argon, ammonia or nitrogen gas are the most commonly used choices.

Table 2.2 – Experimental conditions from the literature which have used hydroxide salts and its mixtures at different operating conditions and compositions during the electrochemical process.

Composition of Electrolyte	Temperature (°C)	Atmosphere	Reference Electrode	Working Electrode	Crucible material	Anode	Cathode	Applied voltage(V)	References
NaOH	25	Air	SCE	Cu rod					(Zaafarany and Boller, 2009)
NaOH (8.0 M)	90		Hg/HgO/ 1M NaOH	Co-Mo alloy					(Zabinski et al., 2003)
KOH (10 wt%)	20, 40, 60	Air			Vinyl chloride	Ni-Cr-Fe alloy	Ni-Cr-Fe alloy	6	(Nagai et al., 2003)
NaOH–NaHS (50:50)	80	Air	Hg/HgO (1M NaOH)		Glass	Graphite, Ni, Ni-Cr alloy	Ni, graphite		(Anani et al., 1990)
NaOH	320-400	Argon				Ni	Ni		(Divisek et al., 1980)
Aqueous KOH **NaOH** **LiOH-NaOH**	110-140 350 300-400	Argon				Activated Ni	Activated Ni	1.55 1.3 1.45	(Divisek et al., 1982)
KOH (1.0 M)	25	Air	Ag/AgCl	C-felt supported Ni, Co, Ni-Co					(Döner et al., 2012)
NaOH (0.1-5.0 M)	25		Ag/AgCl	Ni-Mo-Fe coated stainless steel					(Jayalakshmi et al., 2008)

Composition of Electrolyte	Temperature (°C)	Atmosphere	Reference Electrode	Working Electrode	Crucible material	Anode	Cathode	Applied voltage(V)	References
NaOH	550	Ar	Ni rod	Pt wire, Ni wire, and Ni pallet	Ni				(Ge et al., 2015)
NaOH-KOH	200	Ar	Pt wire	Pt, Au, Fe rod	Platinum				(Híveš et al., 2006)
NaOH-KOH (50:50)	347	N_2	Cu plated Platinum sheet	Pt	Vitreous carbon crucible				(Schiavon et al., 1972)
LiOH-NaOH, LiOH-KOH, NaOH-KOH	250-300		Ag/AgCl	Pt, Pd, Ni, Ag, Al	Nickel Crucible				(Miles, 2003)
KOH	110-160		Fe	Fe, FeSi, and FeC	PTFE				(Lucia H. et al., 2013)
KOH	35-400	Steam			Ni 400	Ni, Ni400, Co plated Ni	Ni 400		(Ganley, 2009)
KOH, NaOH, $Ba(OH)_2$, LiOH	200-700 ℃	Ar			Alumina	Ni, Pt and lithiated Ni	Ni	1.1-2.3 V	(Licht et al., 2016)

Composition of Electrolyte	Temperature (°C)	Atmosphere	Reference Electrode	Working Electrode	Crucible material	Anode	Cathode	Applied voltage(V)	References
NaOH-KOH (57:43)	200-220	Ar or NH_3	Ag wire	Pt plate	Ni-400 (commercial Monel® alloy				(Yang et al., 2014)
NaOH	530	Ar			Ni-covered by Alumina	Ni	FeO	1.7	(Cox and Fray, 2008)
KOH (50 wt%)	80, 150, 208, 264		(DHE)	Ni					(Miles et al., 1976)
NaOH-KOH (51:49)	200-450	NH_3		Ni tube	Ni-400 (commercial Monel® alloy				(Ganley, 2008)
NaOH-KOH (50:50)	200	N2 and steam				Planar Ni	Mesh Ni monel	1.2	(Licht et al., 2014)
NaOH	550	O_2+Air	Ag wire	Ni alloy	Alumina				(Guo et al., 2013)
NaOH-KOH (54:46)	400	O_2+Air	Ag wire	Ni alloy	Alumina				(Guo et al., 2013)
NaOH (8.0 M)	70	Air	Hg/HgO	Ni	plastic				(Abouatallah et al., 2002)

The influence of molten hydroxide temperature on the electrode kinetics for hydrogen and oxygen evolution was first explored in an alkaline solution by Miles et al. (1976). A solution of 50 wt% of KOH was used as an electrolyte at temperatures of 80, 150, 208 and 264°C respectively. Nickel was used both as the anode and cathode for hydrogen and oxygen evolution, while a dynamic hydrogen electrode was used as the reference electrode. Miles et al. (1976) found that the influence of increasing temperature was more significant for the oxygen evolution reaction than for the hydrogen evolution reaction. The authors further mentioned that it is possible to achieve 100% energy efficiency at a temperature of about 150°C using the water electrolysis method.

Miles (2003) explored electrochemically different eutectic molten hydroxides (NaOH-KOH, LiOH-NaOH, LiOH-KOH) using palladium, nickel, silver and aluminium working electrodes. The study of Miles (2003) suggested the use of Ag/AgCl as a reference electrode because of its faster reaction kinetics in molten hydroxides. The researcher revealed that molten hydroxides can be used in thermal battery applications and found that the minimisation of H_2O and O_2^- were the key to using lithium or sodium anodes in these melts.

Further studies conducted focused on how to enhance the output of the hydrogen evolution reaction by supporting a cathode made from different materials such as Ni, Co, and Ni-Co alloy with C-felt coating (Döner et al., 2012). A 1.0M KOH aqueous solution was used in this study as an electrolyte at room temperature. For testing the supported cathode materials with C-felt, a platinum sheet was used as a counter electrode and an Ag/AgCl electrode was used as a reference electrode. Figure 2.6 shows the cyclic voltammograms for a C-felt, C-felt/Ni, C-felt/Co and C-felt/Ni-Co. Döner et al. (2012) found that the current densities of the C-felt, C-felt/Ni, C-felt/Co and C-felt/Ni-Co electrodes increased considerably in comparison to the C-felt electrode type. The C-felt/Ni-Co recorded the highest current density at a specified over-potential among the other tested electrodes.

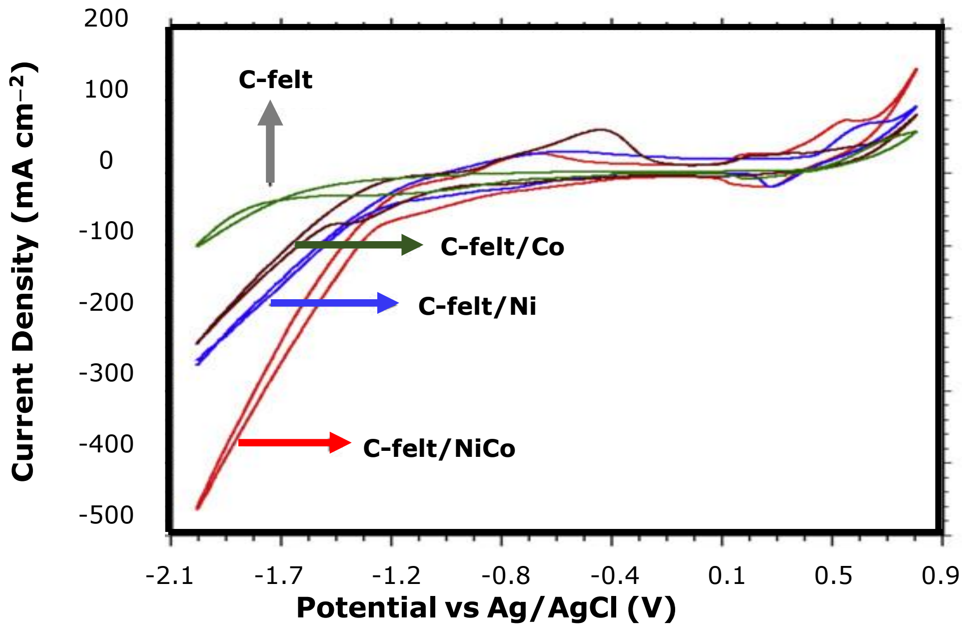

Figure 2.6 – Cyclic voltammograms of C-felt, C-felt/Co, C-felt/Ni and C-felt/Ni-Co working electrodes in 1.0 M KOH at 25°C and at a scan rate of 100 mV s^{-1}. Platinum sheet counter electrode; Ag/AgCl reference electrode (Döner et al., 2012).

The study of Nagai et al. (2003) focused on the effect of formation of bubbles between the electrodes, on the efficiency of hydrogen production by water electrolysis. This study was conducted using 10wt% of KOH aqueous solution under atmospheric pressure and using Ni-Cr-Mo alloy as electrodes. This study determined that the void fraction between electrodes was increased by decreasing the space between electrodes brought to decrease the electrolysis efficiency.

The electrodeposited Co-Mo alloy cathode was supported by adding carbon to enhance the electrolytic hydrogen evolution activity as investigated by (Zabinski et al., 2003). This study was performed using 8M of NaOH at 90^{o}C. Furthermore, the addition of carbon to the Co-Mo alloy cathode was also done to prevent the dissolution of molybdenum during immersion in the hot alkaline (Zabinski et al., 2003). However, this was not attained during this study even though the activity of hydrogen evolution increased. Jayalakshmi et al. (2008) investigated electrochemically the catalytic activity of a stainless steel substrate working electrode coated with a composite film of Ni-Mo-Fe in alkali solutions for hydrogen evolution. The composite film of the Ni-Mo-Fe coated stainless steel substrate was tested in 0.1-5.0M NaOH solutions at 25^{o}C. It was found that the composite material that coated the stainless steel substrate also enhanced the catalytic activity of hydrogen evolution in dilute alkali solutions (Jayalakshmi et al., 2008)

Divisek et al. (1980) studied the electrolysis of water in molten NaOH for hydrogen gas production at a temperature ranges between 320 and 400^{o}C. The electrodes used in this instance were made from Ni covered by Al_2O_3. An argon-water vapour atmosphere was used and directed into the melt. Divisek et al. (1980) found that the overall efficiency of hydrogen production was roughly between 38-39% using a primary energy source. Later, Divisek et al. (1982) investigated the electrochemical splitting of water in an aqueous KOH solution at a temperature range between 110-140^{o}C; and in molten hydroxides such as NaOH and LiOH-NaOH at a temperature range between 300-400^{o}C. The study used activated nickel as both the anode and cathode respectively. An aqueous solution of KOH was used to improve the activated nickel electrode. The achieved current efficiency using a NaOH melt at 350°C and 1.3 V applied voltage, was 90%. This observed current efficiency was not for hydrogen production, but for the side reaction of peroxides production (Divisek et al., 1982). This peroxide formation was significantly reduced in a LiOH-NaOH melt. Divisek et al. (1982) found that can be achieved current efficiency of 100% at a cell voltage of 1.45 V and current density of 500 mA cm^{-2}. The author also mentioned that the formed hydrogen and oxygen gas were separated by a nickel-diaphragm which is cathodically protected.

The study of Licht et al. (2016) explored a high-temperature molten hydroxide to electrochemically split water into hydrogen gas. Licht et al. (2016) examined a wide range of pure and mixed hydroxide electrolytes such as LiOH, KOH, NaOH, $Ba(OH)_2$ and NaOH-KOH at temperatures ranging from 200 to 700°C. The study used nickel, Platinum and lithiated nickel as an anode but only nickel as the cathode. The electrolyte was contained within a pure alumina crucible. Steam and an argon gas stream was directed inside the electrolyte.

Licht et al. (2016) found in their study that increasing the temperature of molten NaOH or KOH beyond the maximum of 400°C decreased the quantity of water available for hydrogen generation, instead resulting in the formation of oxides. This increase in temperature also decreased the coulombic efficiency of hydrogen gas. For the combined hydroxide electrolyte (NaOH-KOH; 50-50 mol%), as temperature increased from 200 to 600°C, the efficiency of hydrogen gas evolution decreased from 96% to 13.4%, as shown in Figure 2.7.

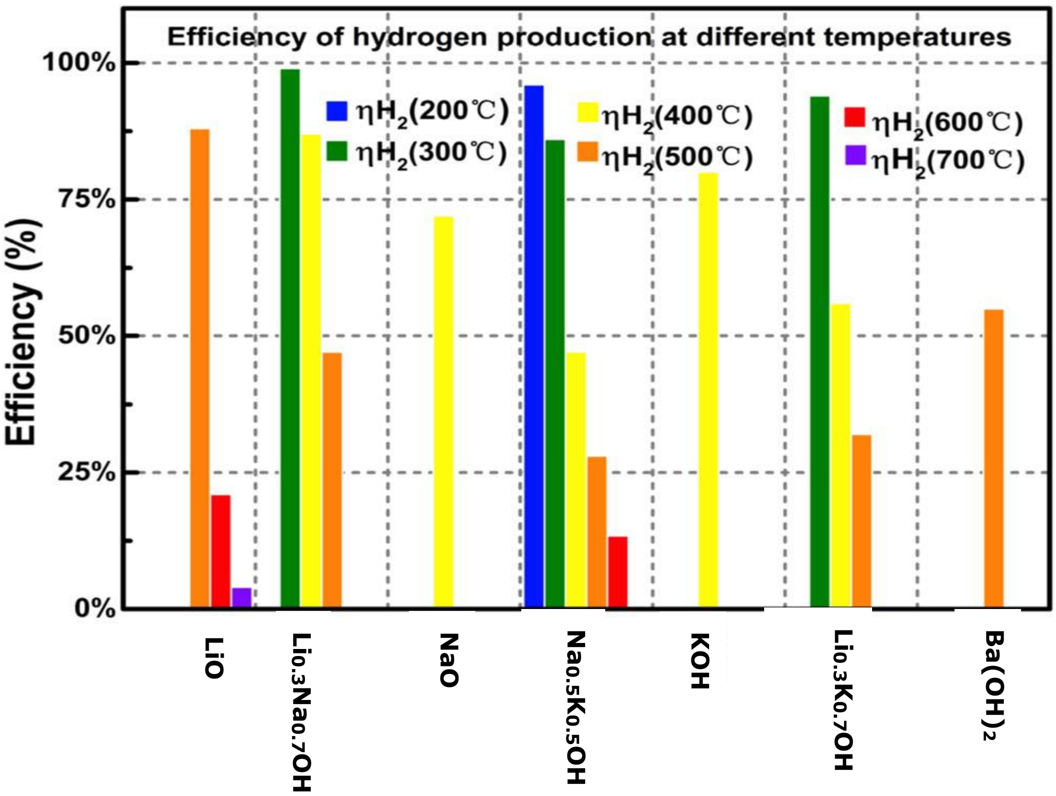

Figure 2.7 – The efficiency of hydrogen generated as a function of temperature and the chosen hydroxide electrolyte under atmospheric pressure as measured at 1 A between two planar nickel electrodes (Licht et al., 2016).

Furthermore, there is scope for producing hydrogen by electrolysis of sulphur hydrogen at 80^{o}C in an equimolar, aqueous solution of NaOH as shown by (Anani et al., 1990).

Ge et al. (2015) investigated the electro-deoxidation of nickel oxide to prepare nickel powder in molten sodium hydroxide at 550^{o}C. Furthermore, the study also examined the electrochemical behaviour of pure nickel wire in molten NaOH to discern the effect on corresponding reactions that take place. Ge et al. (2015) found that the reduction of nickel oxide to nickel can be achieved in a one-step reaction and was followed by a side reaction of hydrogen evolution.

The study of Abouatallah et al. (2002) investigated the effect of the addition of soluble V_2O_5 to 8 M of KOH aqueous solution at 70^oC to reactivate a nickel cathode during hydrogen evolution. Abouatallah et al. (2002) found that the V_2O_5 additive was an effective activating agent; however, the electro-catalytic activity of vanadium-modified nickel was not higher in comparison to a fresh nickel electrode.

On the other hand, Ganley (2008) tested and developed a direct ammonia fuel cell that utilised eutectic molten hydroxides (NaOH-KOH) at a temperature range between 200 to 450^oC, achieving a maximum power density of 40 mW cm^{-2} at 450^oC. The researcher clearly explained that the reason for using a molten hydroxide in the fuel cell was because of its high conductivity and very low cost. Yang et al. (2014) also developed a direct ammonia fuel cell using a platinum electrode and a eutectic electrolytic solution of NaOH-KOH. The cell was operated between 200 and 220^oC and achieved a maximum power of approximately 16 mW cm^{-2}. However, Licht et al. (2014) used eutectic molten hydroxide of NaOH-KOH at a 50:50 molar ratio but only for the production ammonia. The used eutectic molten hydroxide has a suspension of nanoscale Fe_2O_3 in it and a nickel plate was used as both the cathode and anode in this process. Nitrogen and steam was bubbled inside the electrolyte at a temperature of 200^oC. The researchers found that it was possible to produce ammonia at an applied voltage of 1.2 V and at a coulombic efficiency of 35% alongside the excess cogeneration of hydrogen. Furthermore, the molten hydroxide was also used to develop a direct carbon fuel cell at a low temperature. Guo et al. (2013) presented the performance and characterisation of a carbon fuel cell using molten hydroxides of NaOH at 550^oC, and NaOH-KOH (54:46 mol%) at 400^oC. The study found that the performance of the carbon fuel cell improved with a decrease in temperature up to 400°C using the eutectic mixture as an electrolyte.

Ganley (2009) focused on the study of the effect of high temperature and pressure for alkaline electrolysis. The electrolyte employed for direct-current electrolysis was high concentration KOH at a temperature of 400°C under various pressures. The study used nickel Monel as a cathode, while several different anode materials were tested in this study including nickel, Monel alloy, lithiated nickel and cobalt-plated nickel. Ganley (2009) found that the best cell performance was obtained when using a cobalt-plated nickel anode at a temperature of 400°C and under steam partial pressure of 8.7 Mpa.

Zaafarany and Boller (2009) investigated the behaviour of a copper electrode in 5 M of NaOH solution electrochemically. The researchers found that the behaviour of the copper electrode in NaOH solution was quite complicated. No simple relations were found between the voltage scan rate and both peak of current and peak of potential (Zaafarany and Boller, 2009).

However, there were several other studies used a molten hydroxide for electrochemical formation of iron and iron oxide (VI). Híveš et al. (2006) investigated for the first time, the production of ferrate (VI) electrochemically in eutectic molten hydroxide NaOH-KOH at 200°C. Ferrate (VI) FeO_4^{2-} formation in the eutectic molten hydroxide was observed at the inert electrode in contact with ferrate (III) ions and at an iron electrode as mentioned by (Híveš et al., 2006). The researchers found that ferrate (VI) was produced at the potential where the evolution of oxygen begins. Further investigation was also carried out on the formation of ferrate (VI) by Híveš et al. (2008) using a NaOH-KOH eutectic hydroxide at a temperature range between 170-200^{o}C when employing a stationary iron electrode. The formation of ferrate (VI) at the anodic oxidation of the iron electrode was confirmed by visible means and spectroscopy, achieving a current efficiency of Fe (VI) formation up to 72%. Lucia H. et al. (2013) studied the influence of the anode composition on the electrochemical production of ferrate (VI) using molten KOH. The study examined the influence of three different anode materials in molten KOH: pure iron (Fe), white cast iron (FeC) and silicon-rich steel (FeSi) electrodes. Lucia H. et al. (2013) found that the formation of ferrate (VI) together with a massive oxygen evolution occurs. On the other hand, Cox and Fray (2008) investigated the formation of iron from iron (III) oxide in molten sodium hydroxide at 530^{o}C and recovered to produce iron with 2 wt% oxygen that was suitable for re-melting. The operating cell voltage was 1.7 V and nickel was used as the anode material. Fe_2O_3 was successfully reduced to iron using the electro-deoxidation method. Hydrogen generation and sodium formation were controlled by a precondition of adding sodium oxide. The achieved current efficiency from this process was approximately 90%.

2.3 Cyclic Voltammetry of Hydroxide Molten Salts

Many of the reactions that can occur in molten salt electrolytes have been deduced using cyclic voltammetry. In this section, cyclic voltammetry of hydroxide electrolytes is discussed for various working electrode materials. This section focuses on only hydroxide molten salts due to the fact that they were used as electrolyte in the experimental studies of the present work.

2.3.1 Cyclic voltammetry of a nickel electrode in a molten hydroxide

The study of Miles (2003) examined a nickel working electrode in molten NaOH-KOH at 280°C. The cyclic voltammetry result was visually observed in the form of a black film on the surface of the nickel electrode. This was attributed to the oxidation of NiO to NiO_2, as expressed in equation (2.35):

$$\mathrm{NiO} + 2\mathrm{OH}^- \rightarrow \mathrm{NiO_2} + \mathrm{H_2O} + 2\mathrm{e}^- \qquad \textbf{(2.35)}$$

In the work of Ge et al. (2015), nickel was also oxidised to nickel oxide in a one-step reaction using molten NaOH at 550°C, followed by a side reaction of hydrogen evolution. Figure 2.8 shows the cyclic voltammogram of a nickel wire working electrode in molten NaOH at 550°C. From this plot, a couple of redox peaks can be observed.

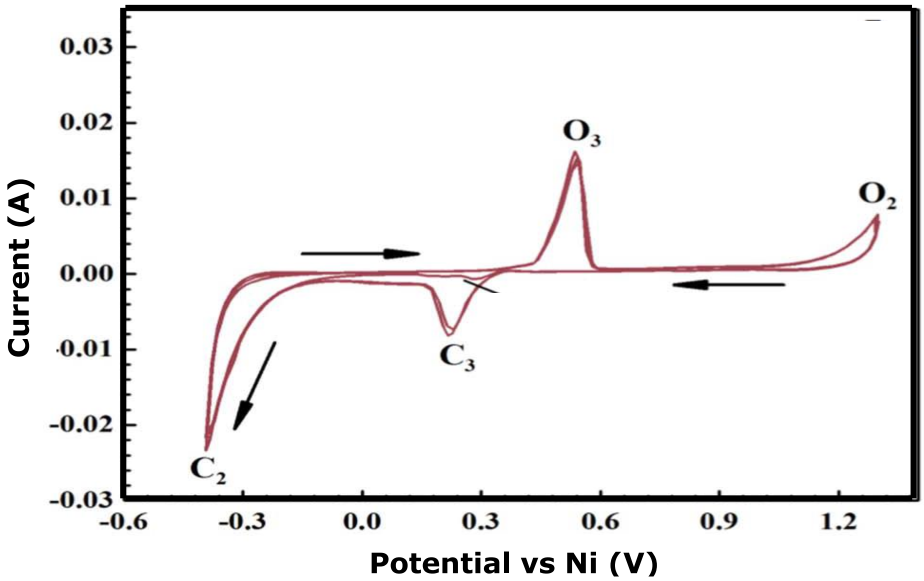

Figure 2.8 – Cyclic voltammogram of a nickel wire electrode in the NaOH melt at 550°C and at a scan rate of 100 mV s^{-1}. Reference electrode Nickel wire; potential limited between -0.4 V and 1.3 V (Ge et al., 2015).

The oxidation peak O_3 corresponds to the oxidation of Ni wire in NaOH, leading to the formation of a thin oxide film on the Ni surface. The peak C_3 is the reduction of the oxide C_3. However, the increased current at the cathode in C_2 and at the anode O_2 corresponds to the evolution of hydrogen and oxygen gas respectively (Ge et al., 2015), as expressed in reaction (2.36) and (2.37):

$$2H_2O + 2e^- \rightarrow H_2(g) + 2OH^- \qquad \textbf{(2.36)}$$

$$2OH^- \rightarrow \frac{1}{2}O_2(g) + H_2O + 2e^- \qquad \textbf{(2.37)}$$

2.3.2 Cyclic voltammetry of a platinum electrode in a molten hydroxide

Ge et al. (2015) were the first to conduct cyclic voltammetry on a platinum electrode using molten NaOH at 550°C. The researchers chose this material before investigating any other electrodes because of its relatively high chemical stability. Figure 2.9 shows the cyclic voltammograms that were presented by (Ge et al., 2015) during their study using platinum as a working electrode. The cathodic peak C_1 is attributed to the reduction of a thin oxide film formed on the surface of the platinum wire. The anodic current O_1 is due to oxidation. The increasing current at cathodic limit C_2 can be attributed to the hydrogen evolution reaction. This reaction is expressed in equation (2.36). The peak O_2 is attributed to the oxygen evolution reaction as expressed in equation (2.37). Miles (2003) also studied the effect of using platinum wire as working electrode in three different eutectic molten hydroxides: NaOH-KOH at 280°C, LiOH-NaOH and LiOH-KOH at 270°C. From the performed cyclic voltammograms of platinum wire in NaOH-KOH as shown in Figure 2.10 and as observed by (Miles, 2003), a large cathodic peak at -0.32 V was noted. This cathodic peak can be attributed to the reduction of superoxide ions O_2^- in the NaOH-KOH melt

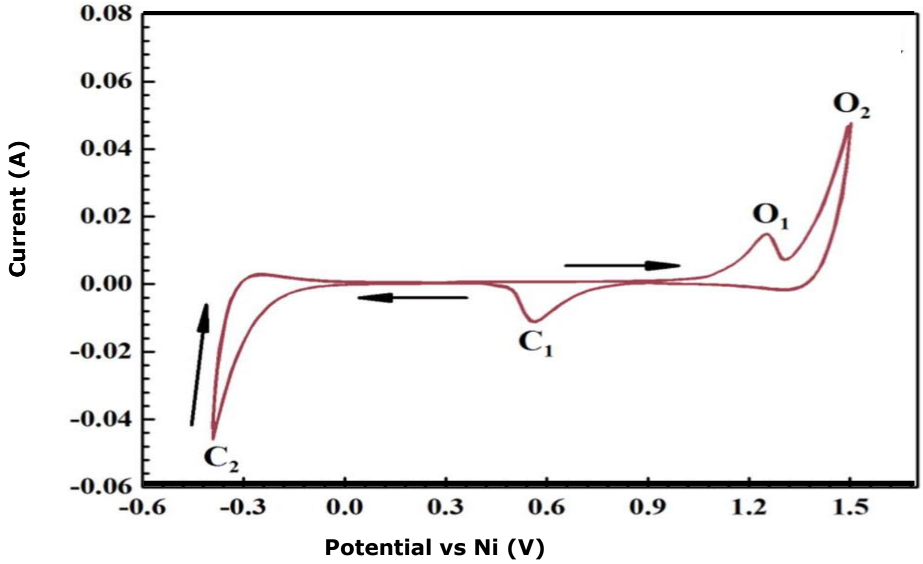

Figure 2.9 – Cyclic voltammogram of a platinum wire electrode in the NaOH melt at 550°C and a scan rate of 100 mV s^{-1}. Reference electrode Nickel wire; potential limited between -0.4 V and 1.3 V (Ge et al., 2015).

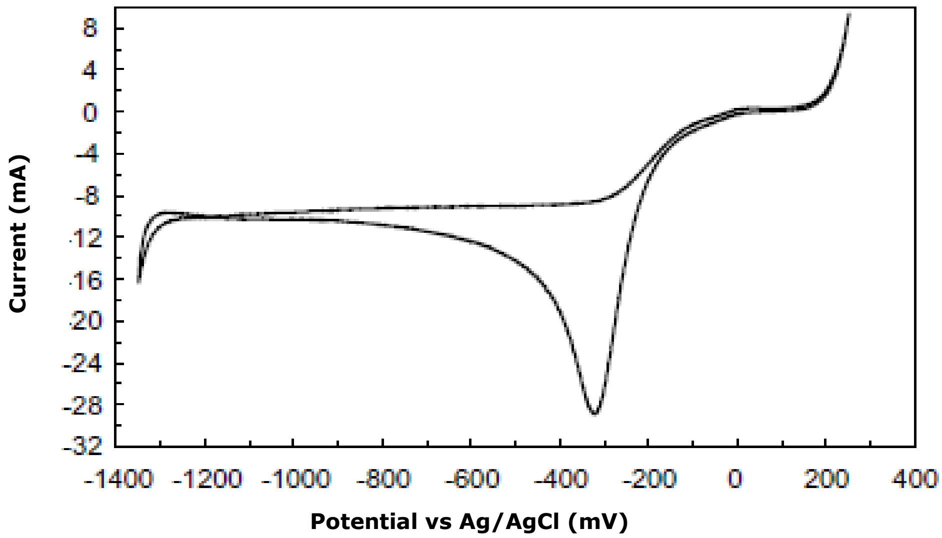

Figure 2.10 – Cyclic voltammogram of a platinum wire electrode in the NaOH-KOH melt at 280°C and a scan rate of 200 mV s^{-1}. Reference electrode Ag/AgCl; potential limited between -1300 mV and 300 mV,(Miles, 2003).

Yang et al. (2014) examined the electrochemical oxidation of ammonia on a platinum electrode using molten NaOH-KOH as an electrolyte. Figure 2.11 shows the performed cyclic voltammetry of the platinum electrode with a supply of argon gas or ammonia at 200°C. Ag was used as a reference electrode throughout the study of (Yang et al., 2014).

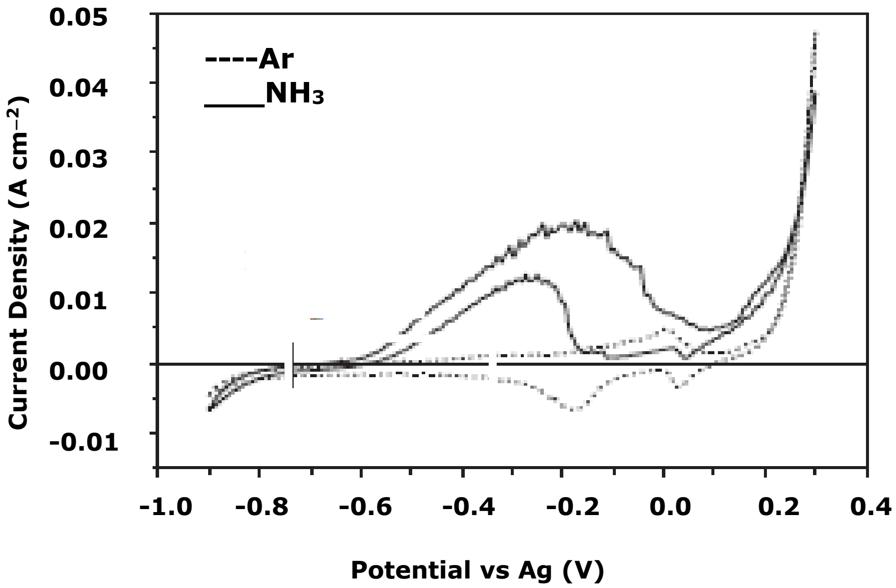

Figure 2.11 – Cyclic voltammograms of a platinum electrode in NaOH–KOH at 200°C and a scan rate of 20 mV s^{-1}; with argon gas or ammonia as atmosphere and a Ag reference electrode, (Yang et al., 2014).

Yang et al. (2014) mentioned that the dash line in the above figure represents the cyclic voltammogram of a Pt electrode with argon which is considered as a blank profile for the platinum electrode in the molten hydroxide electrolyte. The observed redox reaction peaks for oxidation and reduction as seen in the profile with argon gas and was assumed by (Yang et al., 2014) to be due to the redox effect of Pt. The solid line in Figure 2.11 represents the cyclic voltammograms of the Pt electrode with ammonia. Yang et al. (2014) found that ammonia can be oxidised to N_2 on the platinum electrode using eutectic molten hydroxides.

2.3.3 Cyclic voltammetry on other metals in molten hydroxides

Miles (2003) extended his study to investigate other electrode materials in molten hydroxides including Al, Mg, Zn and Li-Fe electrodes. The electrochemical study of Al in LiOH-NaOH at 270^{o}C found that Al completely passivated in the eutectic molten hydroxide during the anodic scan; perhaps extending the electro-stability window up to 3 V. However, the investigation of Mg in LiOH-NaOH was passivated with an anodic current, even yielding an open circuit potential of -0.95 V in the eutectic molten hydroxides (Miles, 2003). When Li-Fe was investigated in molten NaOH-KOH and molten LiOH-NaOH, Miles (2003) found that the Li-Fe anode material was reactivated for all electrochemical studies.

A cyclic voltammetry investigation was also performed for Fe, FeSi and FeC in a molten KOH electrolyte at temperatures of 110, 130 and 160^{o}C, as shown in Figure 2.12. Lucia H. et al. (2013) mentioned that the cathodic limit of the cyclic voltammetry is represented by the evolution of the hydrogen reaction. Subsequently, the anodic limit is represented by the evolution of the oxygen reaction and the anodic peak is represented the melt decomposition. Lucia H. et al. (2013) observed several anodic and cathodic current peaks as shown in Figure 2.12. The development of these peaks is dependent upon the operating temperature and the electrode materials used.

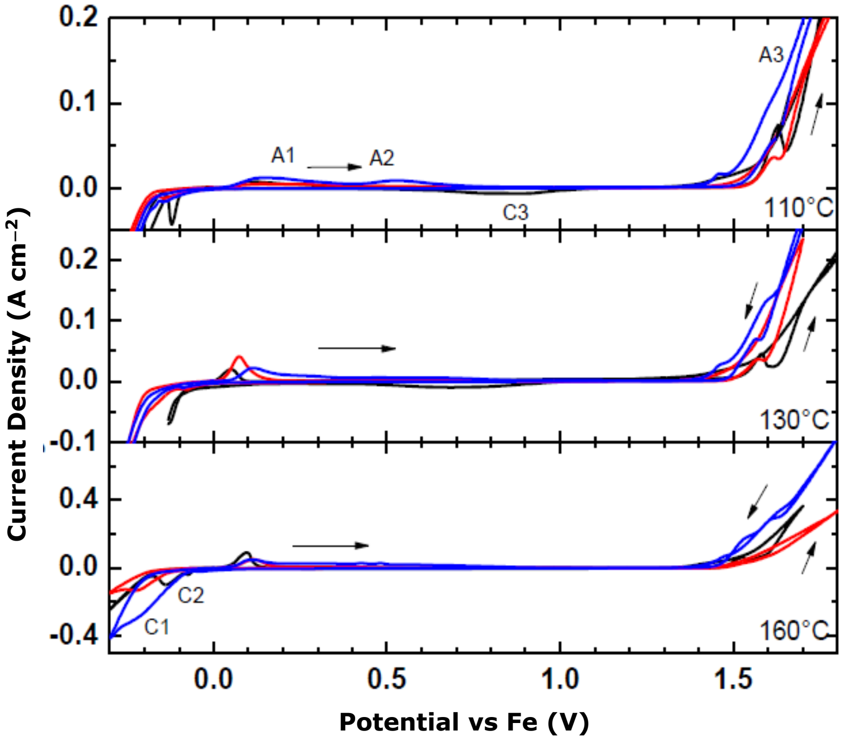

Figure 2.12 – Cyclic voltammograms of working electrodes, i.e. pure iron (black line), FeSi (red line) and FeC (blue line) at different temperatures in molten KOH and at a scan rate of 20 mV s^{-1}. Fe was used as a reference electrode and mild steel as a counter electrode (Lucia H. et al., 2013).

At 110^{o}C, Lucia H. et al. (2013) observed two separate anodic peaks at A1 and A2 using a FeC electrode. It was however more difficult to clearly notice these peaks using the Fe or FeSi electrodes. Peak A1 as mentioned before by (Híveš et al., 2008), corresponds to Fe(II) formation as expressed in equation (2.38):

$$\mathrm{Fe} + 3\mathrm{OH}^- \rightarrow \mathrm{Fe(OH)_3} + 3\mathrm{e}^- \quad \textbf{(2.38)}$$

Therefore, the most negative anodic peaks were assigned by (Lucia H. et al., 2013) to Fe(0)→Fe(II)→Fe(III) reactions and subsequent layer reconstruction. After these oxidation reactions, ferrate (VI) formed alongside a massive oxygen evolution.

In all of the studies reviewed here, an alkaline hydroxide salt was mainly used as an electrolyte to construct the electrolysis cell and be used at both low and high temperatures. Furthermore, these studies reviewed were used to understand different application aspects such as synthesising new cathode materials for increasing hydrogen and oxygen evolution, the formation of new metal oxides or the development of the process for producing hydrogen fuel or ammonia as fuels. There is no direct study as yet which focuses on developing steam electrolysis via eutectic molten hydroxide for hydrogen production through the use of base metals. Therefore, this study mainly contributes to filling this gap and working to increase the efficiency of hydrogen gas using base metals. In addition, this research contributes towards constructing a new suitable reference electrode for molten hydroxides. This is highly important since the present researcher encountered difficulty in finding a suitable reference electrode to use in molten hydroxides alongside the use of a quasi-metal as reference electrode.

CHAPTER 3

METHODOLOGIES

3.1 Introduction

This chapter comprises the procedure followed to collect data in this research while also providing a brief description of the equipment used.

3.2 General Scope of Research Methodologies

The work carried out in this PhD project can be split into two categories: theoretical studies and experimental studies. Various theoretical studies were carried out. Phase diagrams were studied in order to determine the eutectic compositions and temperatures of the molten hydroxide mixtures used as electrolytes. The theoretical standard Gibbs free energies of reaction and standard potentials of possible electrochemical reactions were calculated using HSC chemistry software (Version 6.12; Outokumpu research).

The second half of the chapter describes the empirical methodologies employed. Firstly, the electrochemical molten salt reactor used for three-electrode and two-electrode experimentation is described, along with the materials, electrodes, and electrolytes used in the reactor. Finally, methods used to analyse and quantify the hydrogen gas sample considered in this chapter. Figure 3.1 shows a schematic diagram of that described used methodologies throughout this research.

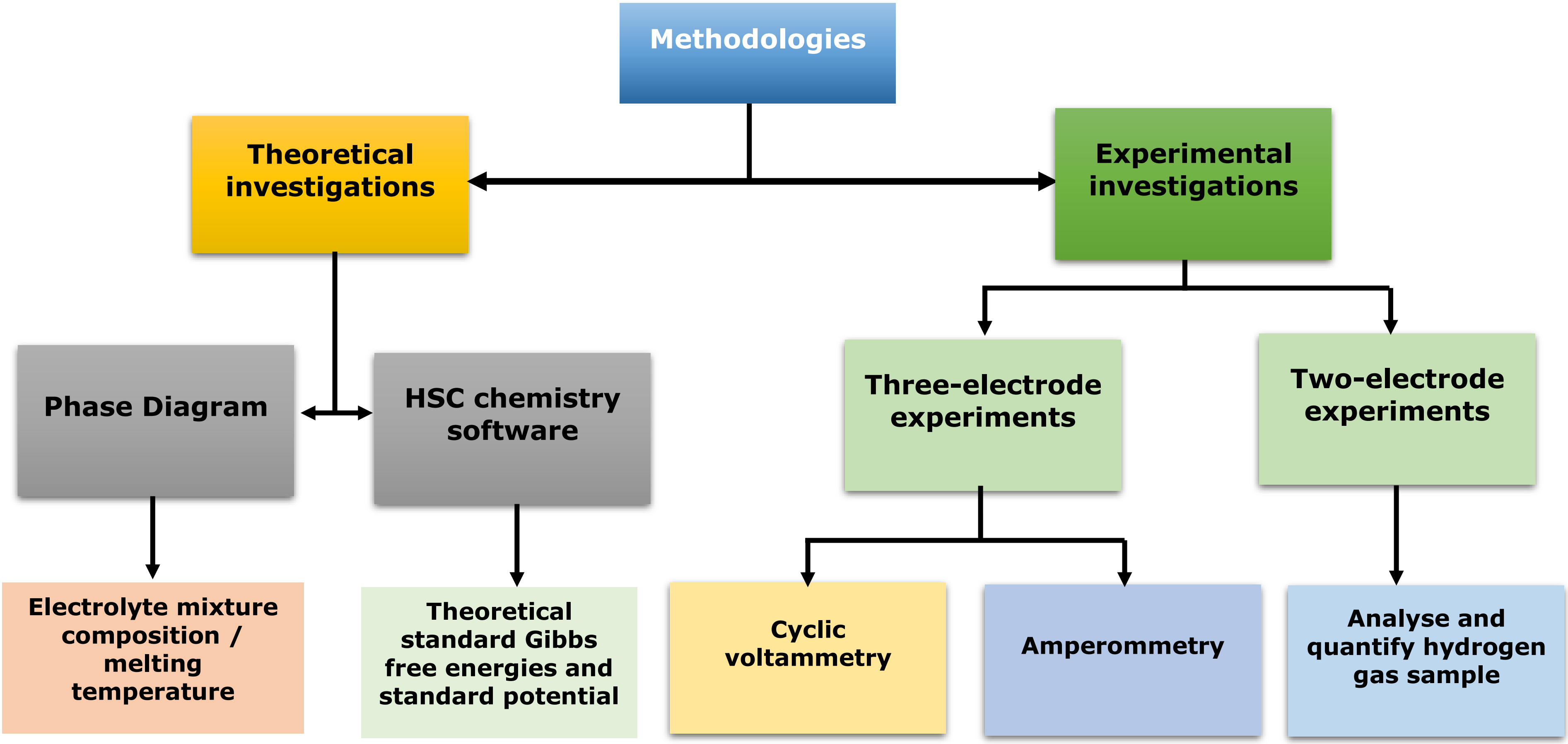

Figure 3.1 – A Schematic diagram of the methodologies used in this research.

3.3 Electrochemical Molten Hydroxides Reactor Setup

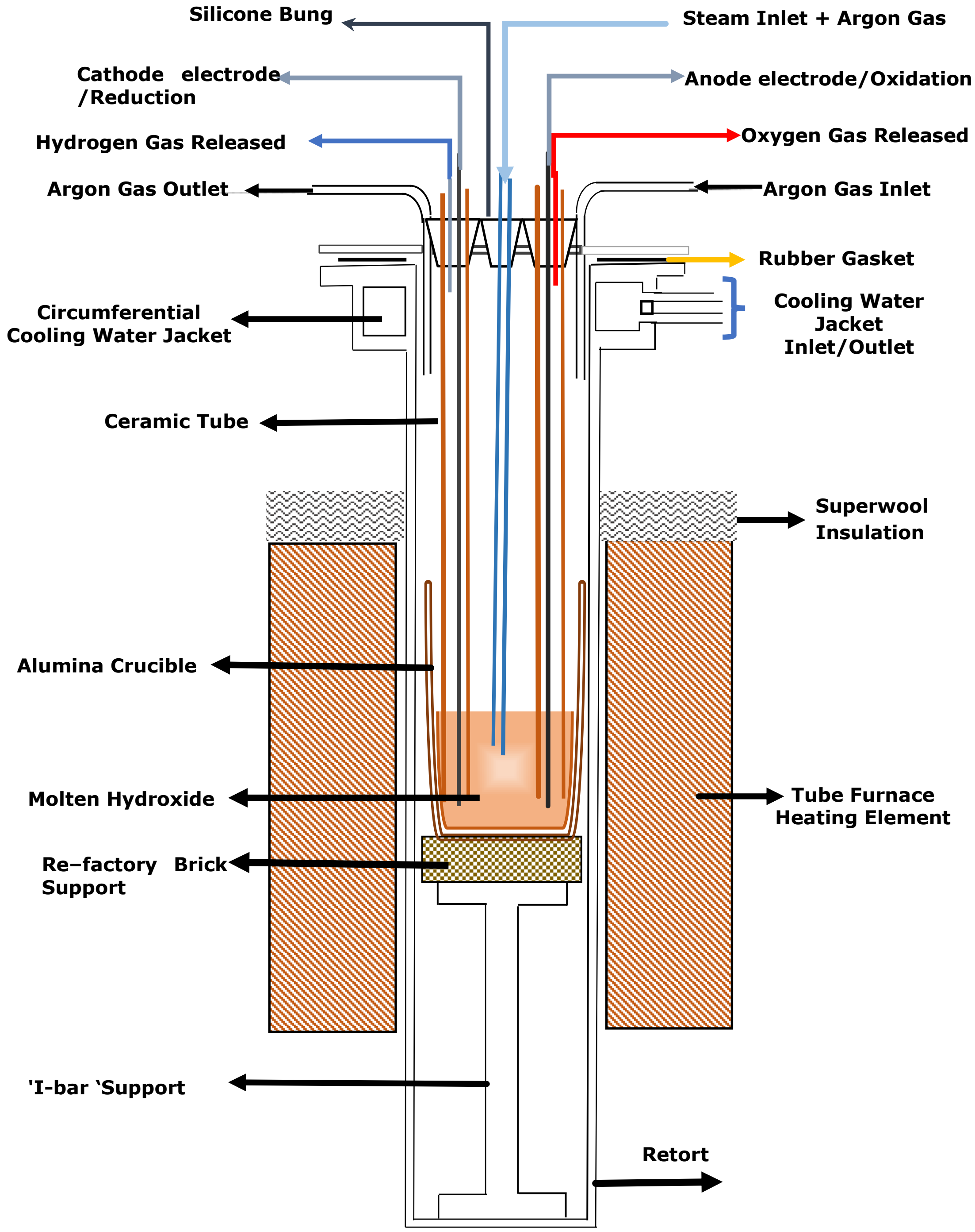

Figure 3.2 – Schematic representation of the electrochemical cell used in this study, set up in a two-electrode arrangement (anode and cathode).

Figure 3.2 shows the general experimental setup used for electrochemical experiments in this study. The setup of the molten salt reactor was fabricated in-house using 316-grade stainless steel (17 % Ni, 12 %, Cr, and 2 % Mo) to construct both the cylindrical retort and the flange type cover. The cylindrical retort was placed through the bore of a vertical tube furnace. The molten salt mixture was held in a crucible placed in the hottest zone of the retort. The furnace was designed by Vecstar Furnace Ltd. and consisted of two shells, allowing it to be opened. The bore of the furnace has an internal diameter of 160 mm and a tube length of 500 mm. A 2416CG Eurotherm PID 8 segment programmable controller was used to the control the furnace, which has a maximum achievable temperature of 1200^{o}C. The controller has an accuracy of ±1^{o}C and also has a power consumption meter for monitoring the energy consumption of the furnace.

Figure 3.3a shows a schematic diagram of the retort. Superwool 607 fibre was used as thermal insulation to bridge the gap between the retort and the furnace in order to reduce heat loss. The retort was hermetically sealed using a rubber gasket and a flange-type stainless steel cover (also made from 316-grade stainless steel), which had holes drilled for insertion of electrodes as well as for observation purposes. Figure 3.3b shows a schematic diagram of the retort lid. Silicone rubber bungs (Fisher Scientific Ltd. and Cole-Parmer Instrumental Co. Ltd.) were used to hold the electrodes in place and to seal the observation holes. A cooling water jacket was utilised to prevent the bungs from melting through overheating and also to allow safe handling.

(a)

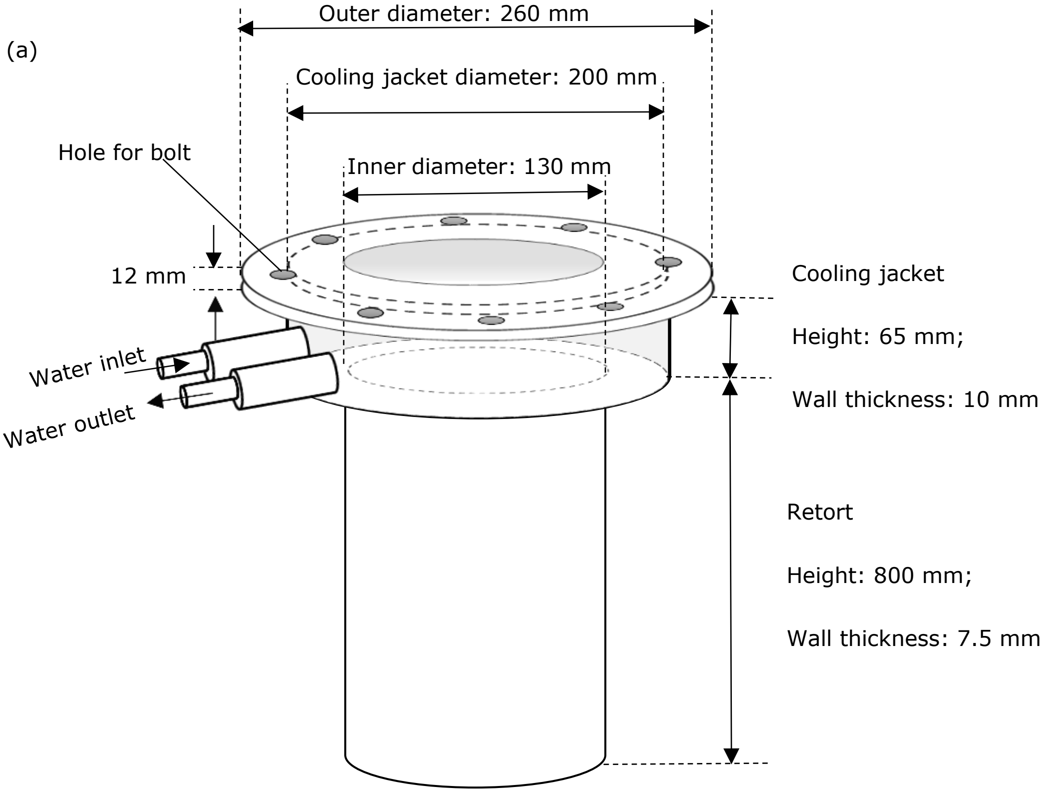

(b)

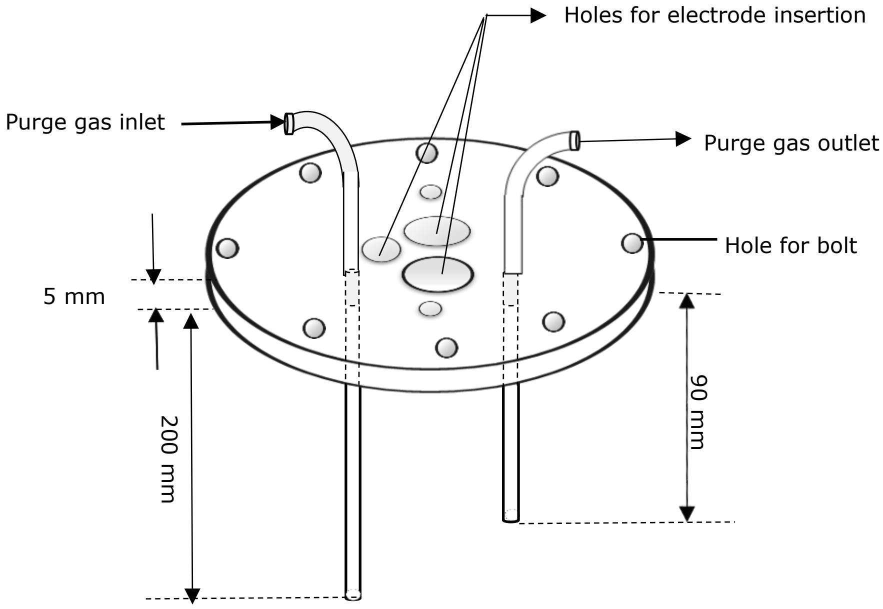

Figure 3.3 – Schematic representation of (a) The retort and (b) The retort lid, showing dimensions and important features. NB. These diagrams are not to scale.

Metal pipes were welded to the retort lid to allow argon purge gas (99.99% pure; Air Products Ltd.) to be supplied to the retort from a gas cylinder. The argon cylinder was fitted with a two-stage argon regulator (GIS Leengate), whose outlet pressure was set at 0.5 bar during the experimental process. To ensure that purge gas reaches the surface of the molten salt with a high velocity, the inlet pipe was constructed longer and narrower than the outlet. The gas outlet pipe was constructed shorter and wider than the inlet and therefore boosted flow from the bottom of the retort to the top. The wide diameter of the outlet also prevented it from becoming blocked with condensed salt (Lawrence, 2013). A calibrated rotameter (Roxapur Measurement and Control) was used to control the purge gas flow rate, which was typically in this study kept at 40 cm^3 min^{-1} at atmospheric temperature and pressure (ATP). The operating range of the rotameter was kept between 20–200 ml min^{-1} at ATP. A dreschel bottle containing 'Labovac 10' mineral oil (Jencons) was used as the gas outlet to prevent the entry of air into the system. The molten salt electrolyte was enclosed in an alumina crucible and placed in the hottest area of the furnace. The crucible was supported on a refractory brick, which was itself supported on a stainless steel stand (manufactured in-house). Cup-shaped alumina crucibles (Almath Crucibles Ltd.) were used, with dimensions of 92mm outer diameter and a height of 100mm. The crucible has a wall thickness of 3.5mm. The purity of the alumina was 99%, and the total volume of the crucible is approximately 567cm^3.

Prior to starting the actual experiment, after the purge gas flow was initiated, the furnace temperature was raised above the electrolyte melting temperature and maintained at that temperature for the duration of the experiment. The temperature inside the crucible was taken using a

YCT-727D thermometer (TC Ltd.) with an attached 3mm diameter 1m long mineral insulated thermocouple (310-grade stainless steel K). The thermocouple was placed within the molten salt for up to a minute in order to obtain an accurate temperature reading but also to minimise electrolyte contamination.

3.4 Electrolyte

In this work, a eutectic molten hydroxide salt of NaOH and KOH was employed as the electrolyte. This eutectic molten hydroxide NaOH-KOH was used at 49-51 mol%. For the salt mixture, the eutectic composition was chosen from thermodynamic phase diagrams shown in Figure 3.4 (Thermochemistry, 2016). Table 3.1 lists the electrolyte components used, along with their purities and manufacturers. Note that all of the salts were purchased in anhydrous form. Table 3.2 gives the electrolyte composition used in this study, as well as their melting/eutectic temperatures at this composition.

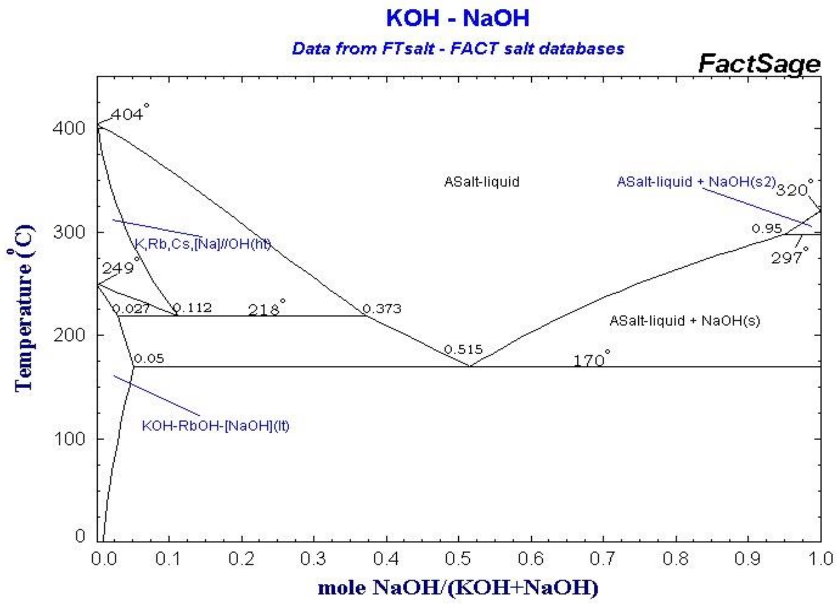

Figure 3.4 – Phase diagram in mole percentage for binary hydroxide salts (NaOH-KOH) (Thermochemistry, 2016).

Table 3.1 – Electrolyte components used in this study, with supplier and purity of each chemical. All of the salts were purchased in anhydrous form.

Substance	Supplier	Specification
NaOH	Sigma-Aldrich, VWR chemicals	Reagent grade, ≥98% pure, Reagent grade, 98.5-99.5 % pure
KOH	Sigma-Aldrich, Fisher	Reagent grade, 90% pure, Reagent grade, ≥85% pure

Table 3.2 – Electrolyte used in this study; the composition and melting/eutectic temperature of electrolyte. References *Rossini et al. (1952); † Powers and Blabock (1954); ‡ Otto and Seward (1964).

Electrolyte	Composition (mol%)		Melting /Eutectic Temperature (°C)
	NaOH	KOH	
NaOH	100	0	318 *†
KOH	0	100	400 †
NaOH-KOH	49	51	170 ‡

It should be mentioned here that temperature has a significant effect on molten hydroxides and hence this was monitored closely to avoid thermal dissociation of the salt as stated by Goret and Tremillon (1966). This study used the eutectic composition of a binary salt of NaOH-KOH (49-51 mol%) due to the fact that this combination has the lowest individual temperatures on the liquidus line of their respective phase diagrams as in Figure 3.4.

3.5 Electrodes

3.5.1 Working, cathode, anode and counter electrode

Table 3.3 lists the materials used as working, cathode, anode or counter electrodes in this study. For anode materials, stainless steel and graphite rods were used during two-electrode electrolysis. Alternately, for the cathode material, nickel, platinum and stainless steel electrode were used for two-electrode electrolysis. The anode and cathode were firmly held in place using silicone bungs and then inserted into the alumina tube (99% pure) with an inner diameter of 20 mm and outer diameter of 26 mm (Almath Crucible Ltd.). The length of the tube is 500 mm. This tube was inserted inside a bung to hold the ceramic and fitted into the electrode hole on the retort lid. The reason for inserting electrodes inside the alumina tube was to manage the collection of hydrogen gas and oxygen gas produced around the cathode and anode electrode respectively during electrolysis. This also prevents mixing of the gases with the internal reactor environment. Furthermore, this design makes it easy to separately collect the hydrogen and the oxygen gases which are produced on the surface of the anode and the cathode respectively. Figure 3.5a, b, and c shows a photograph of ceramic tubes and an internal picture of the ceramic tubes respectively.

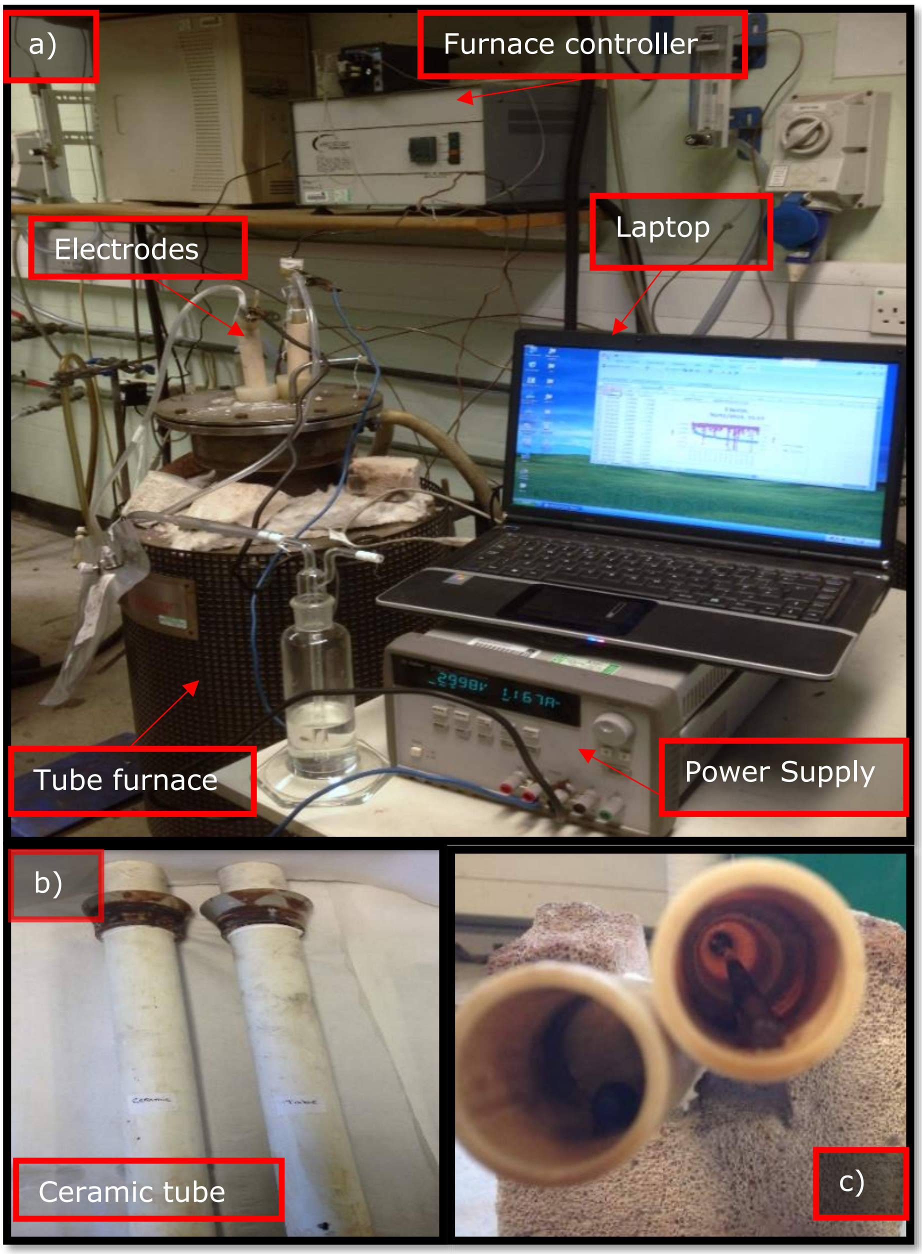

Figure 3.5 – Photograph of (a) The complete two electrode cell during the electrolysis, (b) The ceramic tube that was used to cover the anode and cathode electrodes and (c) The cross-sectional picture from the bottom part of the anode and cathode electrodes.

Table 3.3 – Electrode materials used, with the supplier and type of each material included.

Material	Manufacturer	Type/Grade
Stainless Steel Rod (5 mm diameter)	Unicorn Metals	304
Molybdenum Rod (4 mm diameter)	Advent Research Materials	99.95 % pure Temper Annealed
Nickel Rod (5 mm diameter)	Advent Research Materials	99.0 % pure Temper Annealed
Stainless Steel Wire (0.25 mm diameter)	Advent Research Materials	AISI302 Fe/Cr18/Ni8v Temper hard
Nickel Wire (0.5 mm diameter)	Advent Research Materials	99.98% pure Temper Annealed
Platinum Wire (0. 5 mm diameter)	Advent Research Materials	99.95 % pure Temper Annealed
Copper Wire (1 mm diameter)	Advent Research Materials	99.998% pure Temper Annealed
Molybdenum Wire (1 mm diameter)	Advent Research Materials	99.95 % pure Temper Annealed
Silver wire (0.25 mm diameter)	Advent Research Material	99.99 % pure Temper Annealed
Graphite (10 mm)	_____	_______

Nickel, platinum, silver, molybdenum and stainless steel wires were used as working electrodes (at an approximate length of 25 mm), and attached to the ends of long and clean stainless steel metal rods in order to use them as working electrodes in the three electrode experiments. It must be noted here that a stainless steel rod was used for the attachment. The stainless steel rod with the attached desire wires was then held using a silicone bung and placed inside the retort from the drilled holes at the retort lid as shown in Figure 3.6.

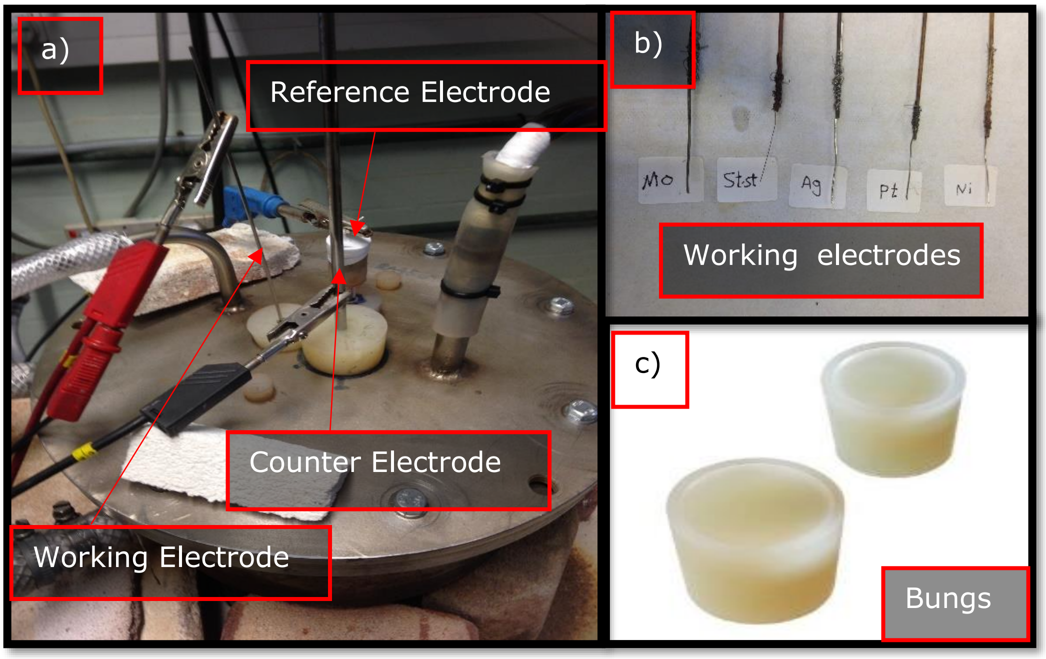

Figure 3.6 – The photograph of (a) Three-electrode cell, (b) The metal working electrode and (c) Silicone bungs.

A variety of combinations of these electrodes were used in electrochemical experiments. This aspect will be explored in Sections 3.6 and 3.7. In this study, stainless steel was most often chosen as the counter electrode material due to its inherent stability and good electrical conductivity.

3.5.2 Reference electrode

To achieve the successful reduction, it is crucial to have a sufficiently accurate potential controlling, mechanically robust and electrochemically stable reference electrode. In this study, various types of reference electrodes such as a high-temperature mullite and alumina membrane $Ni/Ni(OH)_2$, quasi-silver and quasi-platinum types were used. The reason for using these different types of reference electrodes was to find a suitable, stable, reproducible and reusable reference electrode. The primary purpose of this electrode investigation is to understand the electrochemical reactions involved during electrolysis in a molten hydroxide electrolyte. When the silver and platinum quasi-reference electrodes were used in this study, these electrodes consisted simply of metal wires with diameters of 1 mm and 0.5 mm respectively. The wires were individually attached to a stainless steel rod 1.5 mm in diameter.

As one of the objectives of this study was to find a suitable reference electrode, a high-temperature mullite and alumina membrane $Ni/Ni(OH)_2$ reference electrode was individually fabricated, respectively. It should be mentioned that this study followed a modified description laid out by (Wang et al., 2012) to fabricate these reference electrodes. The author described how to make a used Ag/AgCl alumina membrane reference electrode. This study, on the other hand, used the same method to design both an alumina and mullite membrane $Ni/Ni(OH)_2$ reference electrode. The Ag/Agcl alumina membrane reference electrode fabricated by (Wang et al., 2012) was tested in different molten salts such as $CaCl_2$, $CaCl_2$-LiCl, $CaCl_2$-NaCl, $CaCl_2$-LiCl-KCl, Li_2CO_3-K_2CO_3. The investigation carried out in this research is considered novel as it aims to design a suitable reference electrode for molten hydroxides. The study of (Ge et al., 2015) used nickel rod in this regard as a quasi-reference electrode to conduct electrolysis of a NaOH melt at 550^{o}C. Characterisation of the designed reference electrodes is explored in Chapter 4 and Chapter 5.

Figure 3.7 shows a schematic diagram of the $Ni/Ni(OH)_2$ reference electrode used. The $Ni/Ni(OH)_2$ reference electrode consisted of a 50 cm long mullite tube (Multilab Ltd.) or an alumina tube (Multilab Ltd.), sealed at one end with inner and outer diameters of 3 mm and 5 mm respectively. In order to allow ionic conduction with the main electrolyte, the mullite or alumina membrane tube was filled with 1.16 g of salt having the same composition as the main electrolyte (i.e. NaOH-KOH; 49-51 mol%). The electrolyte in the tube also contained 1 mol% of $Ni(OH)_2$ (Arcos Organics).

The end of this tube containing the salt was submerged in the bulk molten electrolyte. Once the salt inside the tube had melted, nickel wire (99.0 % pure; Advent Research Materials Ltd.) was submerged in the salt inside the tube. The reference electrode was then hermetically sealed with a silicone bung as shown in Figure 3.7.

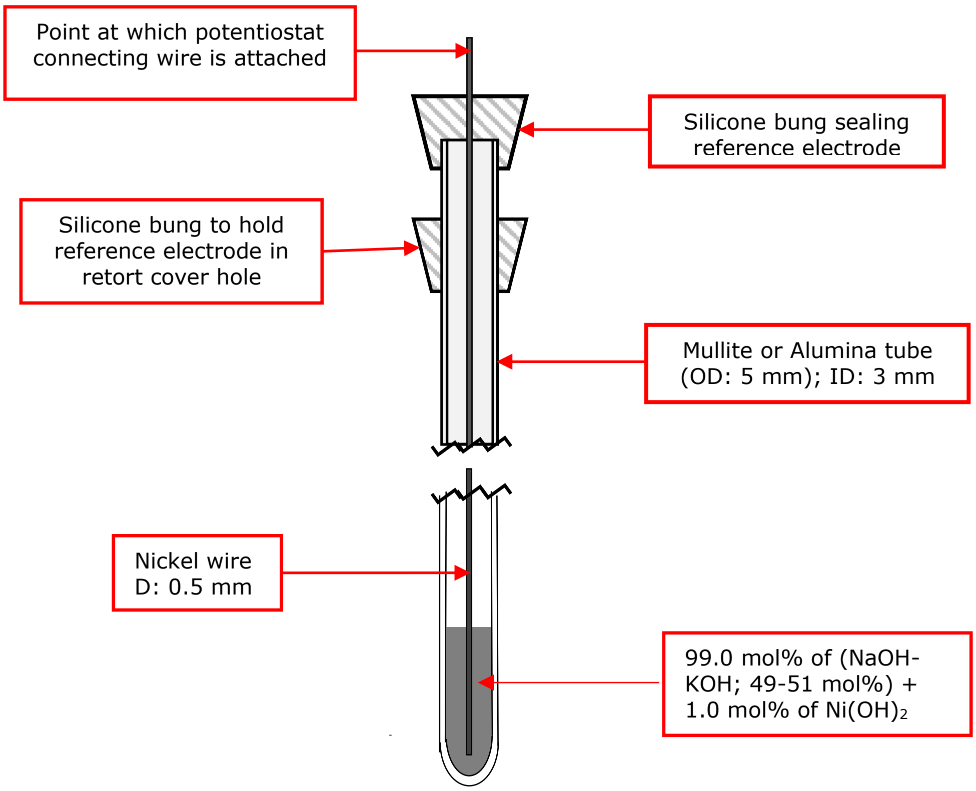

Figure 3.7 – Schematic diagram of the high-temperature $Ni/Ni(OH)_2$ reference electrode cover with a mullite or alumina tube membrane as used in this study. N.B. this diagram is not to scale.

The use of a reference electrode in a three-electrode system allows issues with an (iR) drop to be addressed in a controlled manner. Considering that the actual potential of a working electrode is smaller than the applied potential because of the ohmic losses (Heinze, 1984):

$$E_{actual} = E_{applied} - i\,R \qquad \textbf{(3.1)}$$

Where E_{actual} is the working electrode potential, $E_{applied}$ is the set cell voltage, i is the current and R is the internal resistance of the electrolyte.

The electrical resistance across the cell can cause a drop in the actual potential. Moreover, the current flow during electrolysis may vary which could affect the resistance value, in turn altering the actual electrode potential.

During three-electrode electrolysis, the potential of the working electrode is thus measured with respect to the constant potential of the reference electrode. A very low current reading also means that any iR drop between the working and reference electrodes is reduced.

3.6 Three-Electrode Experiments

Two main types of three-electrode experiments were carried out in this study: cyclic voltammetry, and chronoamperometry. In all of the three-electrode experiments, control and data logging were carried out using an Iviumnstat multichannel electrochemical analyser controlled by a computer using Iviumsoft software (developed by Ivium Technologies). For potential controlled experiments, the voltage across the working and counter electrodes was adjusted to maintain the potential difference between working and reference electrodes respectively. This arrangement is described in Figure 3.8. The current limit for the multichannel analyser ranges from 10 nA to 10 A. For convenience, the abbreviations WE, CE, and RE are frequently used in figure captions throughout this thesis to refer to the working, counter, and reference electrodes respectively. Various electrochemical techniques used for the three electrode studies are discussed below.

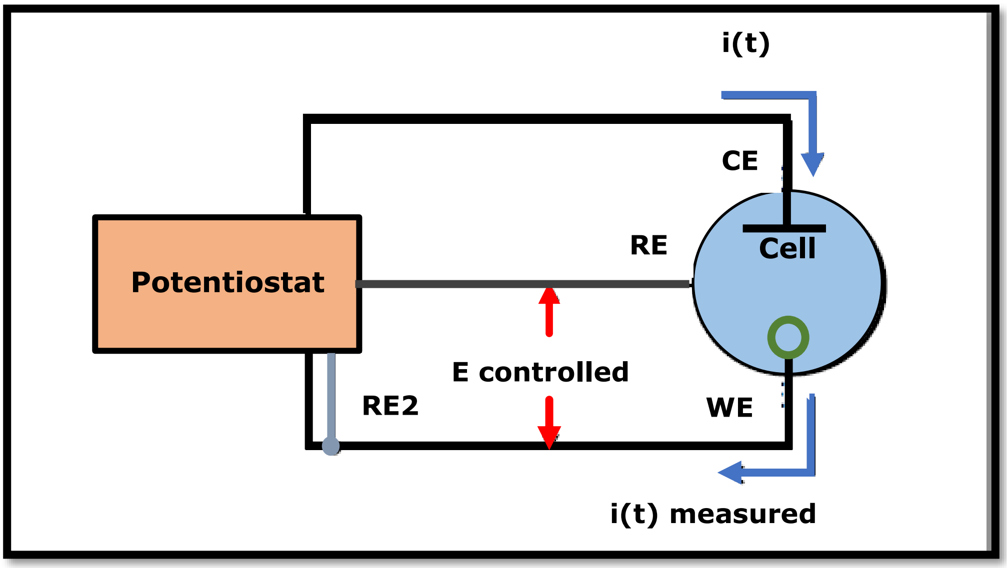

Figure 3.8 – Schematic arrangement for potential controlled experiments (Stevenson, 2017).

3.6.1 Cyclic voltammetry (CV)

For cyclic voltammetry (CV), various metal wires (nickel, platinum, silver, molybdenum and stainless steel) were used as the working electrode and these different electrodes were submerged to a depth of 14 mm inside the eutectic molten hydroxide. A stainless steel rod was used as the counter electrode having a diameter of 5.0 mm. In every experiment, the counter electrode was immersed to such a depth as to provide a significantly larger surface area in contact with the electrolyte, in comparison to the working electrode. The working electrode area was typically between 0.1 to 0.4 cm^2, while the counter electrode surface area typically exceeded 2.5 cm^2. Thus the effect of any reactions occurring at the counter electrode was minimised in each experiment. The reference electrodes used were quasi-silver, quasi-platinum and the high-temperature $Ni/Ni(OH)_2$ types described above.

Cyclic voltammetry was used for qualitative and quantitative analyses of the electrochemical reactions in molten hydroxide electrolyte. In this type of experiment, the potential was linearly varied at a constant, user-defined scan rate; while the direction of potential variation can also be reversed and the cycle repeated. For studying cathodic reactions, the potential was made more negative than the starting potential until it reached the cathodic limit. Upon reaching the cathodic limit potential, the potential direction was reversed to the positive direction up to the anodic limit.

Once the potential scan or cyclic voltammetry was completed; the starting potential was re-achieved again. In this regard, a number of cycles can also be performed to examine the stability response of the system. Figure 3.9 shows an example of a reversible cyclic voltammetry technique that exhibits the magnitude of important parameters of cyclic voltammetry. These parameters are the anodic current peak ($I_{pa,ox}$), the anodic potential peak ($E_{pa,ox}$), the cathodic current peak ($I_{pa,red}$) and the cathodic potential peak ($E_{pa,red}$). The current peak is usually observed when the chemical reaction occurs during the cycles and at this point, the current gradually becomes independent of the potential difference (Kissinger and Heineman, 1983). If there is a chemical reaction happening, then a peak will form and simply an increase in current will be observed.

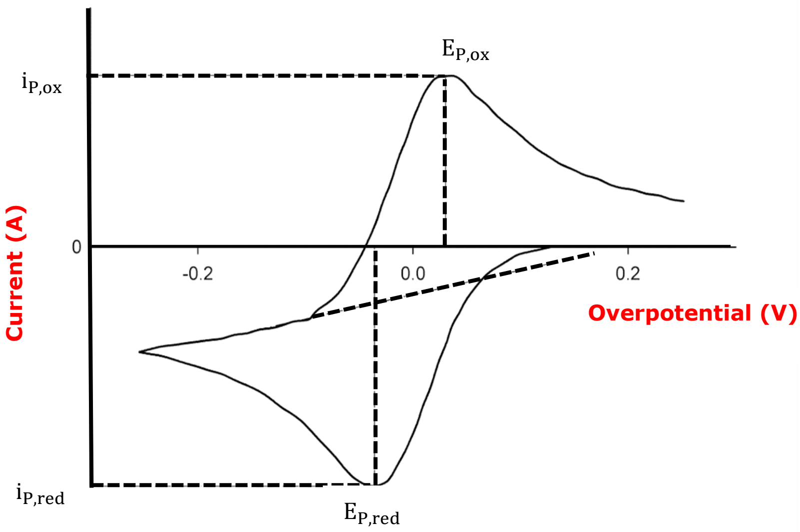

Figure 3.9 – An example of a reversible cyclic voltammogram technique. Modified from (Fischer, 1996).

In order to further understand the electrochemical reactions occurring on the working electrode, the scan rate was also varied because for a reversible mass transfer-limited reaction, the peak height is proportional to the square root of the scan rate (Kissinger and Heineman, 1983).

3.6.2 Chronoamperometry

For chronoamperometry, a stainless steel rod was used as the counter electrode; while the reference electrode used was the same high-temperature $Ni/Ni(OH)_2$ type as described in Section 3.5.2. Different working electrodes used for the chronoamperometry studies include nickel, platinum, silver, molybdenum, or stainless steel wires respectively.

In chronoamperometry, the potential of the working electrode is set at a constant value for a specific period of time and the variation of current with time is recorded. Iviumsoft was used to record the current and hence the value of the overall charge passing through the cell during the reaction process. Chronoamperometry was mainly used to compare the behaviour of different working electrodes in the eutectic molten hydroxide salt with regards to hydrogen gas production at certain cathodic peak potentials observed during cyclic voltammetry studies.

3.7 Two-Electrode Electrolysis

Two−electrode electrolysis was carried out using an Agilent E3633A 20A/10V auto ranging DC power supply and a laptop with an EXCEL add-on to collect data from the instrument as shown in Figure 3.5a. The cathode materials used were platinum wire, nickel, and stainless steel rods. Stainless steel and graphite rods were used as anode materials. The applied voltages during two electrode electrolysis ranged from 1.5 to 2.5 V in this study. The reason for applying this range of voltages is to allow sufficient electrical energy for water to split into hydrogen and oxygen gas (i.e higher than the minimum theoretical electrical energy of 1.23 V (Zeng and Zhang, 2010)).

As stated in section 3.4.2, one major disadvantage of the two-electrode technique is that cathode potential is not controlled with respect to the potential of the reference electrode. Therefore, the potential of the cathode may vary during electrolysis depending on the change of the anode potential and the IR drop. This, therefore, makes the electrochemical reaction occurring at the cathode more difficult to control.

However, there are advantages in using two-electrode electrolysis instead of three-electrode electrolysis, especially from an industrial perspective. The first advantage considers the fact that when the reference electrode is in a molten salt, it is impractical for industrial application because it can only be used for a limited time (Jewell, 2009). Furthermore, in the industry, the current range is very high which can be extremely costly if a three-electrode system were to be used (Wu et al., 2008).

3.8 Steam Generation

Before any electrochemical process was performed, a mixture of steam and argon gas was introduced to the eutectic molten hydroxide. In this study, steam was generated by placing a 500 ml dreschel bottle filled with 300 ml of distilling water, on a hot plate heater. The temperature of the hotplate can be varied from the insert temperature button. The argon gas inlet stream was connected to the inlet of the dreschel bottle head which was directly dipped into hot, distilled water. Then, the argon gas left the dreschel bottle from the outlet head. The stream of argon gas loaded with steam was connected to a ceramic tube which was then submerged in molten hydroxide as shown in Figure 3.10.

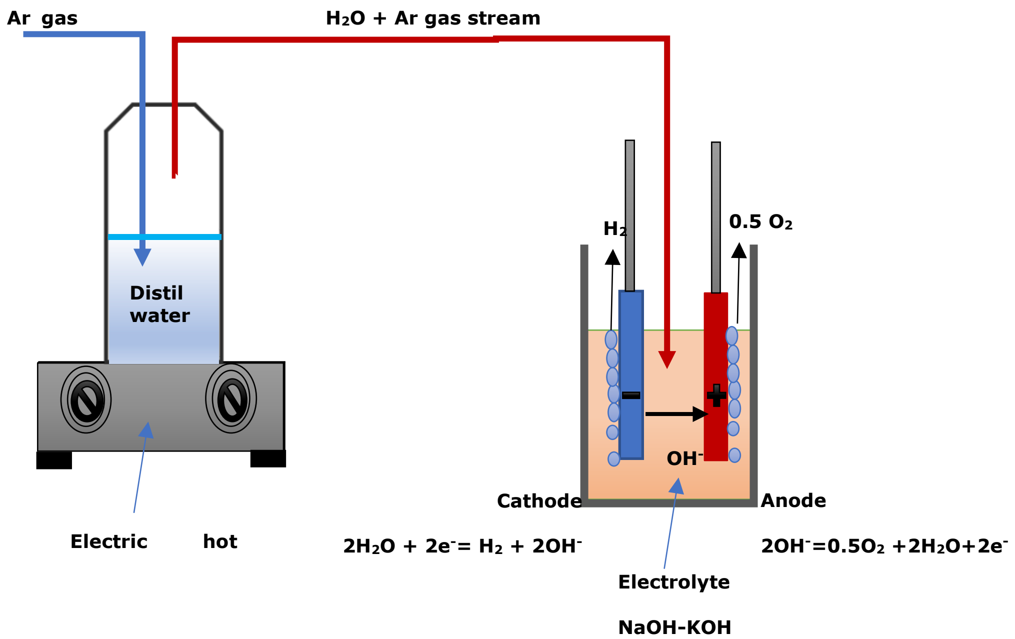

Figure 3.10 – Schematic process of generating steam for the electrolysis process.

In this study, distilled water was heated up to 70^{o}C. The argon gas stream bubbled through the hot water and left the bottle loaded with water vapour. This was then introduced directly to the molten hydroxide. The humidity of the argon gas when it left the dreschel bottle at a temperature of 70^{o}C and an argon flow rate of 40 cm^3min^{-1}, was about 50%. The steam flow rate was about 7.28 cm^3min^{-1} and was calculated using Dalton's law for gases (i.e. the Dalton law calculation method has been discussed in Chapter 3 Section 3.9.3).

The residence time required to achieve saturation between the eutectic molten hydroxide and the humid mixture of argon gas was influenced by the salt volume in the crucible. In this study, the residence time needed to achieve the saturation between eutectic molten hydroxide and a humid argon gas flow rate was between 2-6 min.

3.9 Hydrogen Gas Analysis

There are different types of methods that can be used to analyse hydrogen gas production. This study focused on using simple methods to detect hydrogen gas and quantify it. Methods used for detection include a hydrogen gas detector and hydrogen gas sensor. For quantifying purposes, the displacement of water cylindrical method has been utilised.

3.9.1 Hydrogen gas detector

A Gastec Hydrogen gas tube detector was used in this study to detect hydrogen gas generated from a two-electrode experiment. The gas detector can detect hydrogen gas between 0.5-2.0 vol%. The Gastec tubes are thin glass tubes with calibration scales printed on them which allow the concentration of the substance (gases and vapours) to be measured directly. Each tube contains detecting reagents that are especially sensitive to the target substance and quickly produces a distinct layer colour change upon detection. The tubes are hermetically sealed and the GASTEC detector tube's inner diameters are tightly controlled with detecting reagents, thereby providing long-term stability. All tubes undergo stringent quality control with each production percentage independently tested and calibrated (Corporation., 2016). It should be mentioned here that the GASTEC gas detector tube is considered as the state-of-art technology for accurately analysing not just hydrogen gas, but also a wide variety of other substances including gases, vapours and ground substance.

For sampling the gas in this study, a gas pump GASTEC model having a handle with two clearly defined positions allowing for accurate and consistent sampling of volumes of either 50 or 100 ml, was used. The end of the sampling tube was broken in the tip beaker of the gas pump. This tube end was cut by inserting it into the breaker tip which has a diamond cutter. The detector tube was rotated so that the diamond cutter of the tube tip breaker scratched the surface of the tube end. After that, the detector gas tube was held firmly near the tube tip breaker and the tube was bent to break the tube tip. It should be confirmed prior to the experiment that the pump handle is fully pushed in. Subsequently, the detector tube was inserted into the rubber inlet of the pump with the arrow on the tube pointing towards the pump. After the detector tube was inserted inside the pump, the handle of the pump pulled out to 50 ml, providing at least 3 min of sampling to allow the gas flow inside the tube or until a colour change which indicates the gas sample concentration. Figure 3.11a shows the gas tube detector before and after usage, while Figure 3.11b shows the GASTEC sampling pump attached to the hydrogen gas tube that was used in this study.

Figure 3.11 – Hydrogen gas detector (a) Hydrogen gas tube detector, (b) GASTEC sampling pump.

The gas tube detector works by reducing hydrogen via sodium palla-disulphide to liberate metallic palladium as in equation (3.2):

$$H_2 + Na_2Pd(SO_3)_2 \leftrightarrow Pd + Na_2SO_3 + H_2SO_3 \qquad \textbf{(3.2)}$$

The above reaction results in the change of colour inside the detector tube from yellow to yellowish brown. In addition, the concentration of the gas is not directly gauged from the tube, but it is read from the concentration chart that is attached to the hydrogen gas tube as shown in Figure 3.11a.

3.9.2 Hydrogen gas sensor

A hydrogen gas sensor PRO-GASBADGE was used in this study to detect hydrogen gas produced from the electrolysis process. This type of sensor was used to detect hydrogen gas up to 2000 PPM. This sensor has an interchangeable "smart" sensors monitor for hydrogen gas. The sensor communicates directly via an infrared interface to optional accessories such as Docking Station, Datalink and/or an infrared printer to simplify further and automate calibration, bump testing and data downloading. Standard Short Term Exposure Limit (STEL) and Time Weighted Average (TWA) readings, and data logging of up to one of survey data are featured along with an event-logger that records the past 15 alarm events. The monitor of the sensor is water resistant and extremely durable. It has a four button navigation system that allows easy access for setup, operation and calibration functions. Figure 3.12 shows the photograph of the hydrogen gas sensor used throughout this study.

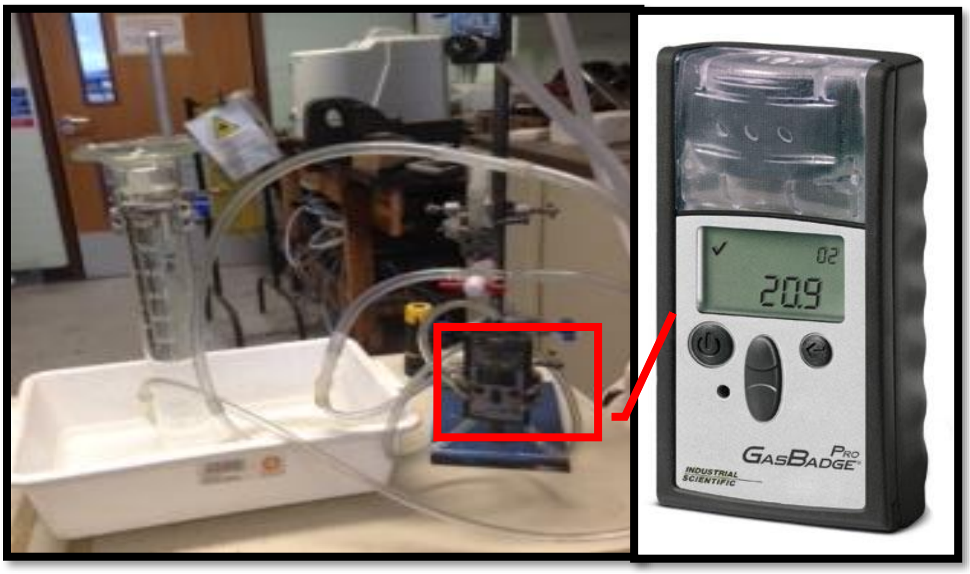

Figure 3.12 – The hydrogen gas sensor as assembled in this study.

The detect the presence of hydrogen gas by the sensor, the first step includes pressing the button of the sensor until the reading is calibrated at 0 PPM as displayed on the monitor. The plastic tube stream exit from the sensor is then connected to the hydrogen gas stream produced from the electrolysis process. For an accurate reading, the reading from the sensor is obtained after 2 minutes of constant gas flow. This sensor is used to confirm the existence of hydrogen gas but not to quantify the amount of hydrogen gas production. This limitation of using these hydrogen gas analyser was overcome by using a physical analysis method as will described in the next section.

3.9.3 Water displacing method (Pneumatic trough)

The water displacing method or a pneumatic trough is widely used in chemistry to collect and quantify the gas produced from either a chemical or an electrochemical reaction. The reason for using this method to quantify the gas is because the density of the gas is very small and it can be difficult to measure its mass. Particularly, for this study, the main product that was produced from the electrochemical process was hydrogen gas at the cathode and oxygen gas at anode. Therefore, the hydrogen gas stream was connected directly to the inverted cylinder that was filled with water at room temperature and immersed in a trough of water, as shown in Figure 3.13. As the hydrogen gas produce enters the cylinder, it displaces the water and becomes trapped in the closed, upper part of the cylinder. However, it should be mentioned that the collected gas in the cylinder is not only hydrogen gas. It is a mixture of hydrogen gas and water vapour. This water vapour comes from liquid water which is always in equilibrium with its vapour phase.

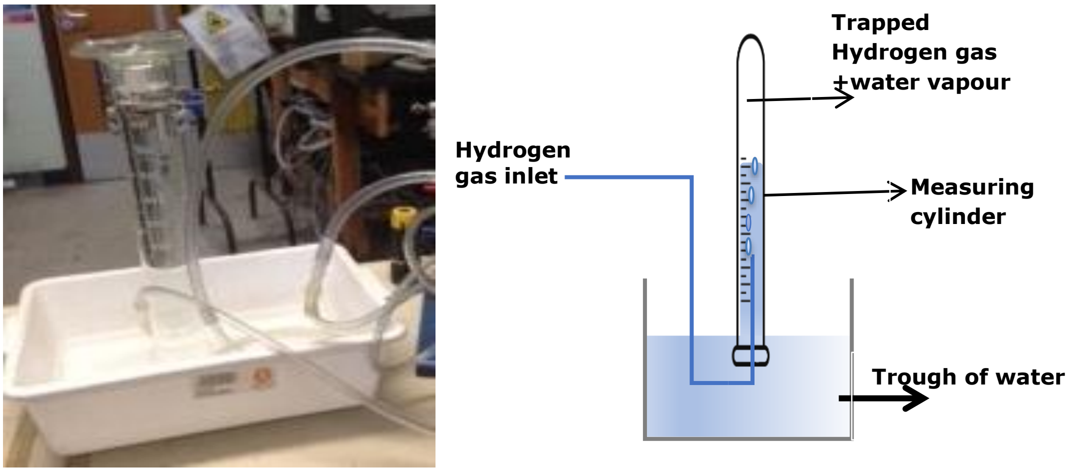

Figure 3.13 – A simple diagram and photograph of the water displacing method (Pneumatic trough).

Therefore, in order to find the actual quantity of hydrogen gas collected, it is important to find its partial pressure. The partial pressure of the hydrogen gas can be obtained by using Dalton's law as in equation (3.3).

$$P_{total} = P^{*}_{W} + P^{*}_{H_2} \quad \textbf{(3.3)}$$

Where P_{total} is the total vapour pressure of the mixture, P^{*}_{W} is water vapour pressure and $P^{*}_{H_2}$ is the partial pressure of the hydrogen gas produced. Therefore, by subtracting the water vapour pressure (calculated from the steam table at room temperature) from the total vapour pressure of the mixture, we obtain the value of partial pressure of hydrogen gas. In this study, the measured room temperature was about 25^{o}C for collecting the gas mixture. The water vapour pressure at this temperature is 0.0313 atm. Therefore, the partial pressure of hydrogen gas equals 0.968 atm and the mole fraction of hydrogen is 0.968.

Furthermore, the number of moles of hydrogen gas produced is calculated by using the equation of state for an ideal gas as follows:

$$P^*_{H_2} V_{H_2} = n_{H_2} RT \quad \textbf{(3.4)}$$

Where $P^*_{H_2}$ is the calculated partial pressure of the hydrogen gas, V_{H_2} is the actual volume of the trapped hydrogen gas in the cylinder, n_{H_2} is the number of hydrogen gas moles, R is the gas constant which equals 8.314 J mol^{-1} K and T is the room temperature of 298 K.

The number of moles of hydrogen gas was directly influenced by the rate of hydrogen gas produced. Therefore the increase in the volume of hydrogen gas collected is proportional to the increase in the number of moles achieved from the equation of the state.

3.10 Experimental Setup for Preparation of a $Ni/Ni(OH)_2$ Reference Electrode

Preparation of the $Ni/Ni(OH)_2$ reference electrode. The two types of membrane used to manufacture reference electrodes were alumina and mullite respectively. The commercial alumina tube (99.7% Al_2O_3, 500mm length, 5.0mm external diameter and 1.0mm wall thickness, Multi-Lab Ltd.) had a minimum bulk density of 3.92 g cm^{-3} with a water absorption capacity of 0.01 vol% as reported by the supplier. On the other hand, the mullite tube (62% Al_2O_3, 36% SiO_2, 500 mm length, 5.0 mm diameter, and 1.0mm thickness, Multi-Lab Ltd.) had a minimum bulk density of 2.7 g cm^{-3} with water absorption capacity of 0.02vol%. 1mol% $Ni(OH)_2$ (Arcos Organics) was mixed with the eutectic molten hydroxide (NaOH-KOH; 49-51 mol%) (Internal electrolyte, Aldrich) and inserted into the tube (alumina or mullite) forming the internal electrolyte of the reference electrode. The total amount of salt placed in the tube was 1.16g. The tube was initially placed inside the retort but once outside the crucible, it was filled quickly with the prepared mixture of salt to avoid the hydroxides absorbing any moisture from air. Note that the internal composition of eutectic hydroxides is the same as that of the external electrolyte composition (i.e. the bulk electrolyte used for electrolysis). The temperature of the furnace was immediately raised above the working temperature of 300^oC to completely melt the mixed salts in the tube. It should be mentioned here that the mixture was filled into the tube up to a length longer than the uniform heating zone (ca. 12 cm) of the furnace. A nickel (Ni) wire (99.98% pure temper annealed, 0.5mm diameter, Advent Ltd.) was then inserted into the bottom of the tube as the salt began to melt. Subsequently, the tube was sealed and left for 24 h to complete the melting of the salt mixture. Following this, the furnace was cooled to the working temperature so that the upper part of the molten mixture in the tube solidified to seal the tube. A schematic diagram of the $Ni/Ni(OH)_2$ reference electrode is shown in Figure 3.14.

Performance tests of the nickel reference electrode were conducted in a cylindrical alumina crucible (>99%, 60 mm outer diameter, 120 mm height, 280ml volume, Almath Crucibles) under an argon atmosphere, using an Iviumnstat multichannel electrochemical analyser. In all of the experiments, 250g of the eutectic molten hydroxide (NaOH-KOH;49-51mol%) were left under 40cm^3min^{-1} of argon gas at 300^oC for 24 h before use.

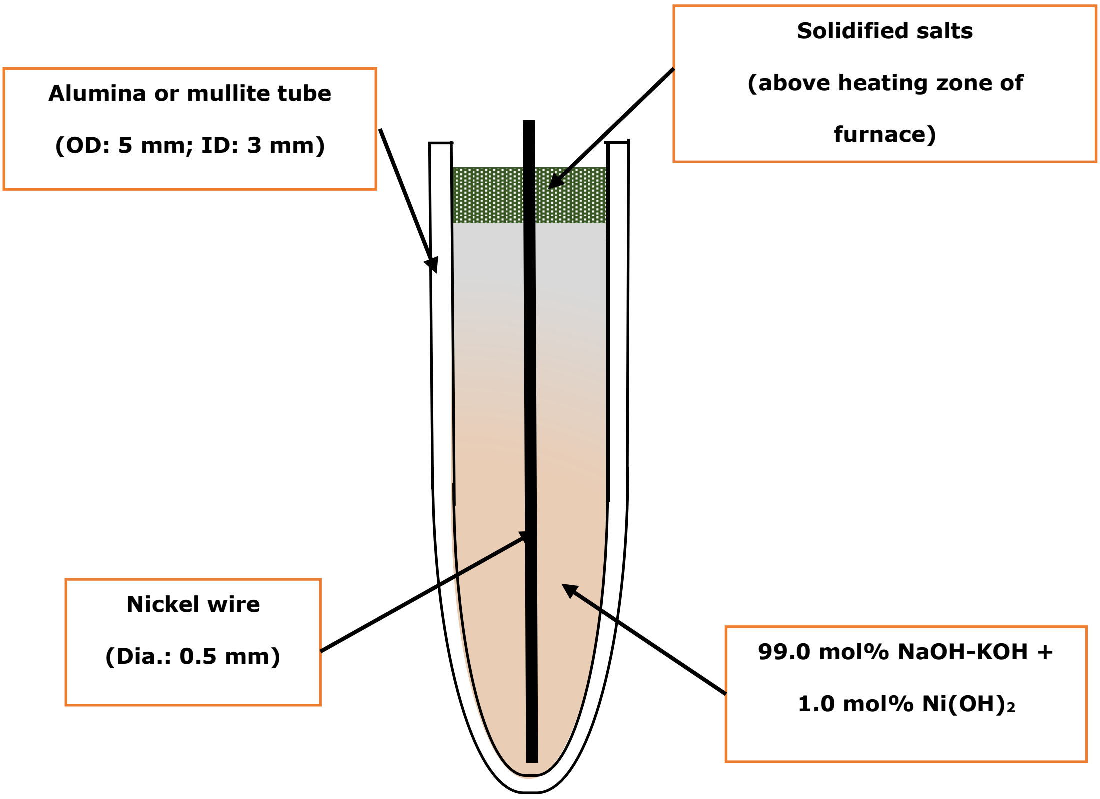

Figure 3.14 – A schematic of the $Ni/Ni(OH)_2$ reference electrode in a tube membrane.

The cyclic voltammetry technique was used to examine the stability and repeatability of the prepared nickel reference electrode. The measurement was taken using the nickel wire as a working electrode and the prepared nickel reference electrode enclosed within either an alumina or mullite tube. A stainless steel rod (5 mm in diameter) acted as the counter electrode and the immersion depth of the working electrode was ~14 mm. The reason for using the prepared reference electrode is to control any issues with the *iR* drop. During measurement, the scan started at an open circuit potential progressing in the negative direction before reversing in the positive direction. Cyclic voltammetry was employed to scan and check the nickel working electrode potential stability together with the two different types of prepared nickel reference electrodes. Different scan rates were employed during the cyclic voltammetry investigations. Cyclic voltammogram plots in this research are expressed in terms of current rather than current density because the nickel working electrode is used at a fixed depth inside the eutectic molten hydroxide for all cases.

3.11 Experimental Setup for Determining a Suitable Reference Electrode

Three types of reference electrodes were used in this investigation. Silver wire (99.99% pure temper annealed, 1.0mm diameter, Advent Research Materials), and platinum wire (99.95% pure temper annealed, 0.5mm diameter, Advent Research Materials) as quasi-electrode and the mullite membrane $Ni/Ni(OH)_2$ reference electrode. Platinum wire was used as the working electrode, while a stainless steel rod (304 Grade, 5mm diameter, Unicorn Metals) was used as the counter electrode.

The performance tests were conducted in a cylindrical alumina crucible (>99 %, 60 mm of outer diameter, 120 mm in height, 280 ml in volume, Almath Crucibles) under an argon atmosphere; using an Iviumnstat multichannel electrochemical analyser. In all experiments, 250 g of the eutectic hydroxide (NaOH-KOH; 49-51 mol%) was left under $40cm^3min^{-1}$ of argon gas at 300°C for 24 h before beginning the electrochemical analysis. The furnace was then set to the required experimental temperature.

Subsequently, the working temperature was reduced to the temperature that needs to be examined. However, it was difficult in practice to obtain the exact temperature required because the electrolyte temperature can only be adjusted by changing the furnace set temperature. The furnace temperature controller in turn only has an accuracy of $\pm$1°C. The electrolyte temperature was also influenced by additional factors such as the effectiveness of the furnace insulation and the ambient temperature. These factors proved difficult to maintain constant throughout all experiments.

The cyclic voltammetry technique was used to examine these reference electrodes in terms of stability and reliability in the eutectic molten hydroxide. The measurement was made using a platinum wire as a working electrode and one of the reference electrodes (silver wire, platinum wire or the prepared nickel reference electrode). The immersion depth of the working electrode was ~14 mm. During measurement, the scan started at an open circuit potential, progressing in the negative direction before reversing in the positive direction. Cyclic voltammetry was employed to scan and check the platinum working electrode potential stability and reliability with the three different types of reference electrodes. The scan rate was varied during the tests and the effect of molten salt temperature was also considered. The effect of introducing water to the eutectic molten hydroxide via the Ar gas stream was also considered. The flow of the water stream was maintained at 7.28 cm^3min^{-1} and it was mixed with argon gas at 40 cm^3min^{-1}. This steam and argon gas mixture was bubbled inside the eutectic molten hydroxide. Cyclic voltammetry plots are expressed in current instead of current density because the platinum working electrode was used at a fixed depth inside the eutectic molten hydroxide through this study.

3.12 Experimental Setup For Studying Different Working Electrodes

The reference electrode used is the Ni/Ni(OH)$_2$ reference electrode will be discussed in Chapter 4 and Chapter 5 of this thesis; with the preparatory technique details in Section 3.5.2 (Chapter 3). A stainless steel rod (304 Grade, 5 mm diameter, Unicorn Metals) was used as the counter electrode. Five different types of working electrodes were used: Ni (99.98% pure Temper Annealed, 0.5 mm diameter, Advent Research Materials), Pt (99.95% pure Temper Annealed, 0.5 mm diameter, Advent Research Material), Ag (99.99% pure Temper Annealed, 1.0 mm diameter, Advent Research Material), Mo (99.95% pure Temper Annealed, 1.0 mm diameter, Advent Research Material), and SS (99.99% pure Temper Annealed, 0.25mm diameter, Advent Research Material). Figure 3.15 shows the different types of working electrodes.

Figure 3.15 – The working electrodes used in this study.

The performance tests were conducted in a cylindrical alumina crucible (>99 %, 60 mm of outside diameter, 120 mm in height, 280 mL in volume, Almath Crucibles) under an argon atmosphere, using an Iviumnstat multichannel electrochemical analyser. In all of the experiments, 250 g of the eutectic molten hydroxide (NaOH-KOH; 49-51 mol%) were left inside the reactor under 40 cm^3 min^{-1} of argon gas at 300^oC for 24 hours before use. Subsequently, the working temperature was reduced to the required temperature. However, it was difficult in practice to obtain the exact temperature required because the electrolyte temperature can only be altered by changing the furnace set temperature. The furnace temperature controller had an accuracy of $\pm 1^oC$, where the electrolyte temperature was also influenced by factors such as the effectiveness of the furnace insulation and the ambient temperature, which was difficult to keep constant for all experiments.

The electrochemical techniques used in this investigation were cyclic voltammetry and amperometry. These techniques were used to study the behaviour of the working electrodes in the eutectic molten hydroxide at different operating conditions. The measurements were made between one of the working electrodes (e.g. Ni, Pt, Ag, Mo, SS) and the prepared nickel reference electrode. The immersion depth of the working electrodes inside the electrolyte was ~14 mm. During the cyclic voltammetry measurement, the scan started at an open circuit potential progressing in the negative direction before reversing in the positive direction. Cyclic voltammetry investigations were conducted at different scan rates, different operating temperatures as well as with and without the presence of steam inside the eutectic molten hydroxide. In the case of the presence of steam, the steam flow rate was fixed at 7.28 cm^3 min^{-1}, mixing with argon gas that itself flows at 40 cm^3 min^{-1}. The steam and argon gas mixture was bubbled inside the eutectic molten hydroxide. The cyclic voltammetry plots are expressed as current density versus potential. The reason for this is because each working electrode has a different diameter although they have the same immersion depth inside the eutectic molten hydroxide. Expressing these plots in current density becomes easier to discern the comparison between the obtained results from the various working electrodes. Table 6.1 shows the working electrodes used in this study, their diameters and calculated surface area respectively.

Table 3.4 – The surface area of the different working electrodes immersed inside the eutectic molten hydroxide with an immersion depth: 14 mm.

Working electrode	Diameter (cm)	Surface area (cm^2)
Nickel	0.05	0.22
Platinum	0.05	0.22
Silver	0.10	0.44
Molybdenum	0.10	0.44
Stainless steel	0.025	0.11

The surface area of the working electrodes can be calculated using equation (3.5).

$$A = \pi \times D \times h + \frac{1}{4} \times \pi \times D^2 \quad \textbf{(3.5)}$$

where A: the surface area of the immersion part inside the melt (cm^2), π: mathematical constant (3.141), D: Diameter of working electrode (cm), and h: the immersion depth of the wire inside the eutectic molten hydroxide (cm).

3.13 Hydrogen Gas Production via Two-electrode Electrolysis

Hydrogen gas production was carried out using a two-electrode electrochemical cell, and the methodology of this type of experiment is described in Section 3.8 of this thesis. A mixture of 300 g of NaOH-KOH (49-51 mol%) was used as the electrolyte and placed inside the retort, before being heated to a temperature of 300^{o}C for 24 h. It must be noted here that the retort has already been placed inside the pore of the vertical tube furnace as described in Section 3.3 (Chapter 3). A pure alumina crucible was used to hold the mixture of hydroxide salt. Nickel, platinum and stainless steel were used as the cathode; whereas stainless steel and graphite were used as the anode during the experiments, respectively. Prior to immersing the cathode and anode inside the eutectic molten hydroxide to begin electrolysis, each electrode was placed inside an alumina tube with 20mm inside diameter. The reason for covering the electrodes with an alumina tube was to prevent the hydrogen gas formed at the cathode from mixing with the oxygen gas formed at the anode. This compartment should be tightly sealed to avoid any gas leakage. The diameter of the different electrodes used in this study and the calculated areas are listed in Table3.5. Figure 3.16 shows a photo of the used electrodes.

Table 3.5 – Different materials used as electrodes (anode and cathode) and their respective dimensions.

Electrode material	Diameter (cm)	Depth (cm)	Surface area (cm^2)
Nickel	0.5	1.5	2.55
Platinum wire	0.05	1.5×15	2.55
Stainless steel	0.5	1.5	2.55
Graphite	1	1.5	5.50

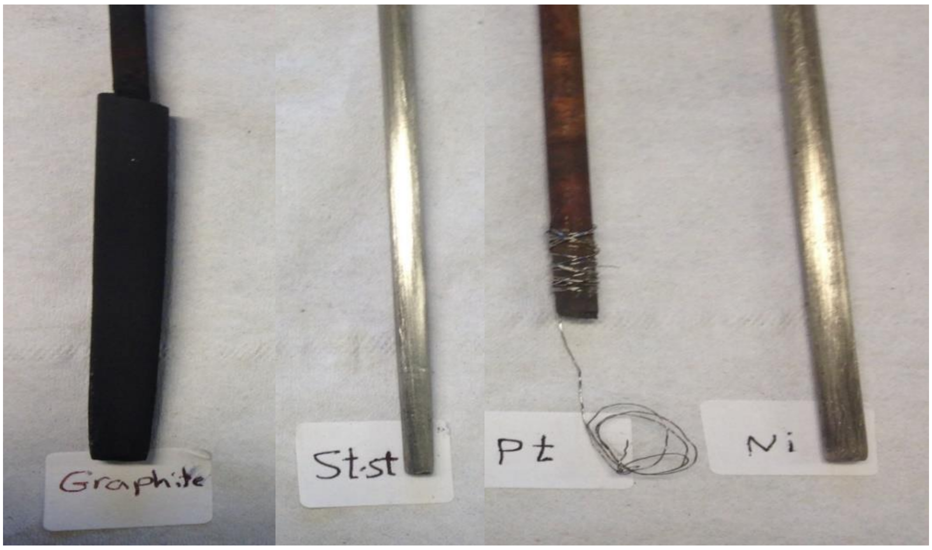

Figure 3.16 – A photograph of the different cathode and anode electrodes used in the study.

The total duration of the steam electrolysis process was approximately 1800s after which hydrogen gas was collected. A voltage was applied to both electrodes using a direct current power supply. This applied voltage was altered between 1.5 V and 2.5 V. It is worth mentioning that although the voltage is listed as being positive, the negative terminal of the power supply was actually connected to the cathode which is the electrode of interest. Therefore the polarity of this electrode, in reality, is negative.

Steam and argon were both introduced in-situ into the electrochemical cell as described in Section 3.8 (Chapter 3). It must be ensured that the stream of steam and argon gas, bubbles inside the eutectic molten hydroxide. This process decreases the loss in steam used in the electrolysis process and results in the maintenance of equilibrium hydration of the molten hydroxide as steam occurs. Generally, the flow rate of argon gas was controlled by a flow meter at $40cm^3min^{-1}$, and mixed with distilled water that was heated up to 70^oC using an electric hotplate. The output stream of humid argon left the water bottle as the humidity reached 50%. The humidity was measured using a water vapour detector tube. The flow rate of the steam entering the system was calculated using Dalton's law for gases as explained in Section 3.9 (Chapter 3). The flow rate of the heated water during the electrochemical process was kept at 7.23 cm^3 min^{-1}.

The start of production of hydrogen gas at the cathode was detected by using a gastec gas detector tube. This gas tube detector is capable of measuring up to 2 vol% of hydrogen gas; the use of which is explained in Section 3.9.1 (Chapter 3). A hydrogen gas sensor pro-gasbadge was also used to detect hydrogen gas produced up to 2000 ppm; the use of which is seen in Section 3.9.2 (Chapter 3). As the gas produced at the cathode was confirmed as hydrogen gas, the production rate of the hydrogen gas was measured using the water displacing method (Pneumatic Trough) and calculated as an actual gas rate using Dalton's law for gases. This method is described in Section 3.9.3 (Chapter 3).

A schematic diagram of the electrolysis process to split steam through eutectic mixture of NaOH-KOH while detecting the hydrogen gas produced and subsequently quantified, is illustrated in Figure 3.17.

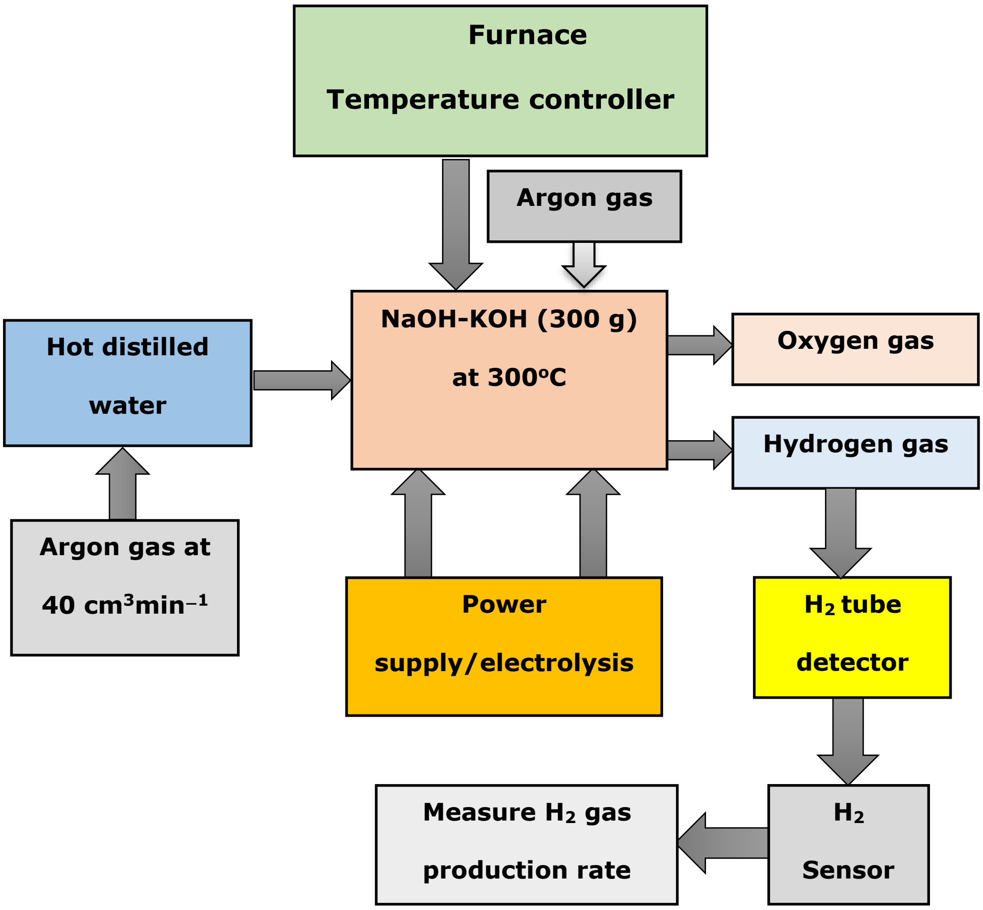

Figure 3.17 – A schematic diagram of the splitting steam via molten hydroxide for hydrogen gas production.

The hydrogen gas production rate due to steam splitting via the electrolysis of eutectic molten hydroxide, was calculated using the following equation:

$$\text{Production Rate} = \frac{\text{Mass of } \mathrm{H_2} \text{ produced}}{\text{Immersed area of cathode} \times \text{Duration of } \mathrm{H_2} \text{ production}} \times 100 \quad \textbf{(3.6)}$$

The values that were inserted into this equation were determined as follows. The mass of hydrogen gas production was found from the multiplication of the actual number of moles of hydrogen gas by the molecular weight of hydrogen gas. The actual number of moles of hydrogen gas can be calculated using the equation of state of gases at a temperature of 25°C, partial pressure of hydrogen gas and the actual volume of hydrogen. The partial pressure of hydrogen was calculated using Dalton's law for gases at 25^{o}C and 1 atm. The actual volume of hydrogen gas was calculated by multiplying the mole fraction of hydrogen gas by the total volume of the collected gas during the electrolysis process from the cathode compartment using water displacement method. It must be noted here that the gas collected using the water displacement method, was a mixture of water vapour and hydrogen gas as explained in Section 3.9.3 (Chapter 3).

As for the current efficiency of hydrogen gas production, this was calculated using the following equation:

$$\text{Current Efficiency} = \frac{\text{Charge needed to produce hydrogen in theory}}{\text{Charge passed during electrolysis}} \times 100 \qquad \textbf{(3.7)}$$

The values that were inserted into this equation were determined as follows. The amount of electric charge (Q) passing through the electrolytic mixture during hydrogen gas production can be obtained by integrating the current-time plots. To calculate the charge needed to produce hydrogen gas, in theory, the number of electrons involved to split steam to hydrogen gas was multiplied by the Faraday constant (96485 C/mol) and the number of moles of hydrogen gas produced. Thus, higher electric charge flow will indicate more hydrogen gas produced at the cathode.

CHAPTER 4

INVESTIGATION OF AN IONIC MEMBRANE FOR A NICKEL REFERENCE ELECTRODE

4.1 Introduction

Prior to studying different reference electrodes for electrolysis resulting in hydrogen gas production, selecting a suitable membrane material is necessary. The reference electrode designed in this study contains a membrane, the electrolyte and a nickel wire. Selecting the right ionic membrane is important in designing the reference electrode and these membranes must have good chemical and electrochemical stability, reproducibility and reusability.

There is a lack of literature regarding choosing suitable membrane materials an adequate reference electrode in the case of molten hydroxides. Miles (2003) stated that no single reference electrode has been established for a molten hydroxide system. Different reference electrodes such as PTFE membrane-enclosed Cu^{+}/Cu in NaOH-KOH (Schiavon et al., 1972), quartz, Pyrex, porcelain, mullite membrane-enclosed Ag/AgCl (Labrie and Lamb, 1959, Sakamura, 2004, Gao et al., 2005), Graphite-protected silica tube Ag/AgCl (Pal et al., 2011) and alumina membrane tube Ag/AgCl (Martin et al., 2010, Wang et al., 2012) have been reported as options for high-temperature molten salt. The study of Wang et al. (2012) examined a Ag/AgCl reference electrode in an alumina tube membrane using different types of molten salts such as $CaCl_2$, $CaCl_2$-LiCl, $CaCl_2$-NaCl, $CaCl_2$-LiCl-KCl,

Li_2CO_3-K_2CO_3. Another study conducted by Ge et al. (2015) used a nickel rod quasi-reference electrode to test in molten NaOH. All of these previous studies did not use a proper, specifically prepared reference electrode in the molten hydroxide. Hence this study has focused on investigating the best prepared nickel reference electrode for eutectic molten hydroxide.

Another key point to focus on is the solubility of $Ni(OH)_2$ in molten hydroxides. It was reported by Gayer and Garrett (1949) that the solubility of Nickel hydroxide in an alkaline solution of NaOH at 25^oC was low, while it was high in any high acidic solution medium. Alternatively, the solubility product of $Ni(OH)_2$ of 6.5×10^{-18} was unchanged when observed from the reaction of nickel hydroxide with either base or acid. A low concentration of 1.0 mol% of $Ni(OH)_2$ in this work was therefore used to make an internal electrolyte mixture of the reference electrode.

Therefore this chapter attempts to fill the gap in knowledge with regards to finding suitable, stable and reusable reference electrodes for molten hydroxides. In this study, two types of membrane have been investigated: alumina membrane (Al_2O_3) and mullite membrane ($3Al_2O_3.2SiO_2$).

The cyclic voltammetry electrochemical technique was used to study stability and reusability of the prepared reference electrode covered with an ionic membrane.

4.2 $Ni/Ni(OH)_2$ Reference Electrode with an Alumina Membrane

Cyclic voltammetry (CV) of a nickel working electrode in a molten hydroxide (NaOH-KOH;49-51mol%) at 300°C was carried out. The reference electrode used in the CV study contained a nickel wire inserted inside an alumina tube comprising of a salt mixture ($Ni(OH)_2$-(NaOH-KOH);1-99mol%). Figure 4.1 shows the cyclic voltammetry obtained at a scan rate of 100 mV s^{-1}.

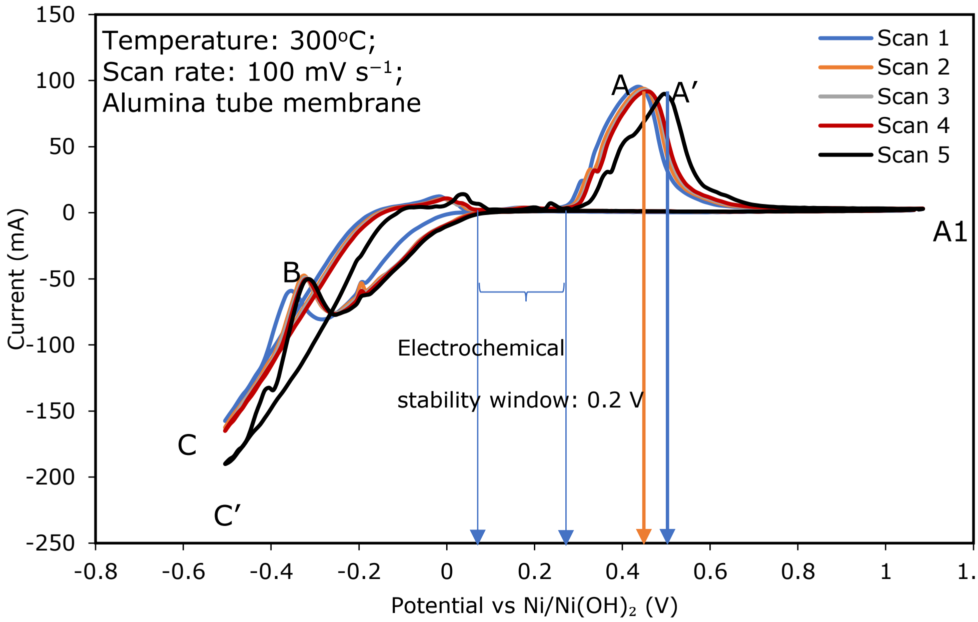

Figure 4.1 – Cyclic voltammograms of a 0.5 mm Ni wire working electrode (WE) in eutectic molten hydroxide and scanned negatively from -0.5 to 1.0 V vs $Ni/Ni(OH)_2$ at 300°C. Counter electrode (CE): 5 mm diameter stainless steel rod; reference electrode (RE): $Ni/Ni(OH)_2$ in the alumina tube membrane; immersion depth: 14 mm; an Ar gas atmosphere: 40 cm^3 min^{-1}.

The electrochemical stability window observed from Figure 4.1 for a nickel working electrode in the eutectic molten hydroxides at 300°C is about 0.20V vs $Ni/Ni(OH)_2$. From the literature, the electrochemical stability window of the nickel electrode in molten NaOH-KOH at 280°C is 0.35 V vs Ag/AgCl

(Miles, 2003). This main reaction of the cathodic (C or C′) and anodic limits (A1) are expressed in equations (4.1) and (4.2):

Cathode limit: $2H_2O + 2e^- \rightarrow H_2(g) + 2OH^-$ **(4.1)**

Anodic limit: $2OH^- \rightarrow \frac{1}{2}O_2(g) + H_2O + 2e^-$ **(4.2)**

From the CVs in Figure 4.1, the cathodic limit (C or C′) near -0.5 V is likely due to the reduction of water to generate hydrogen gas as expressed in reaction 4.1. While the anodic limit (A1) near 1.2 V appears due to the main oxidation reaction in the eutectic molten hydroxide (reaction (4.2)) because the molten salt reaction contains an OH^- ion. These results agree with Miles (2003) who reported gas evolution at both the anodic and cathodic limits. There is a strong possibility that these could be hydrogen and oxygen gases formed from both the cathodic and anodic reactions (Miles, 2003).

Miles (2003) stated that the oxidation peak encountered during electrolysis of molten NaOH−KOH at 280°C using a nickel working electrode, was due to the oxidation of NiO to NiO_2 according to the following reaction (4.3):

$NiO + 2OH^- \rightarrow NiO_2 + H_2O + 2e^-$ **(4.3)**

Therefore, nickel oxide (NiO_2) forms when the nickel surface is in touch with the molten hydroxide and peak (A) at 0.46 V Figure 4.1 is attributed to the oxidation of NiO to NiO_2. Furthermore, Miles (2003) also found that when a nickel crucible was used for heating LiOH-KOH at 500°C, it became evenly blackened. Llopis et al. (1976) also reported that nickel crucibles containing molten NaOH form a protective black oxide layer.

4.2.1 Stability of the Ni/Ni(OH)$_2$ reference electrode with an alumina membrane

After understanding the main reactions at anodic and cathodic limits, it is imperative to study the change in behaviour of the nickel working electrode during the CV test. From the CVs in Figure 4.1, there is a shift in the oxidation potential noted for the formation of NiO_2 at peak A′. The CVs were scanned 5 times; scan 1 to 4 has a similar oxidation potential of 0.42 V while for scan 5, the potential peak has shifted to a more positive potential value of 0.53 V. The shift in the oxidation peak is also accompanied by slight shifts in the cathodic limit potential. This shift in the oxidation peak is likely due to the fact that the hydroxide ions are unable to penetrate easily through the alumina membrane after a certain amount of time. This thus leads to higher ionic resistance which in turn prevents a stable ionic channel with the internal reference electrolyte mixture.

In addition to understanding the main reactions of a nickel working electrode and the behaviour of the electrode during the test, an investigation of the electrode kinetics at different scan rates was also carried out. The reason for carrying out this investigation was to determine the accuracy of the reference electrode potentials and understand how a change in the scan rate can affect the kinetics of the electrolytic process. Figure 4.2 shows cyclic voltammetry results obtained at different scan rates and a temperature of 300^{o}C.

The change and shift of the NiO_2 oxidation peak (as the arrow indicates in Figure 4.2) is close to 230 mV and varies from 0.36 to 0.53 V as the scan increases from 50 to 150 mV s^{-1}. The cathodic limit which is assigned to the generation of hydrogen gas, also shifts positively from 0.05 to 0.15 V (i.e. a 100 mV increase) as the scan rate increases from 50 to 150 mV s^{-1}. The oxidation peak at C, C2 and C3 are however a complex reaction area. The oxidation reaction of NiO to NiO_2 is an irreversible reaction and there is also an increase in the oxidation peak current with the increase in scan rate from 50 to 150 mV s^{-1}. Therefore, these scan rate variations likely indicate poor stability of the reference electrode in the eutectic molten hydroxide. The reason for this poor stability is the fact the alumina membrane has a high resistance, making it difficult to build a stable ion channel between the electrolyte and the internal reference electrolyte mixture.

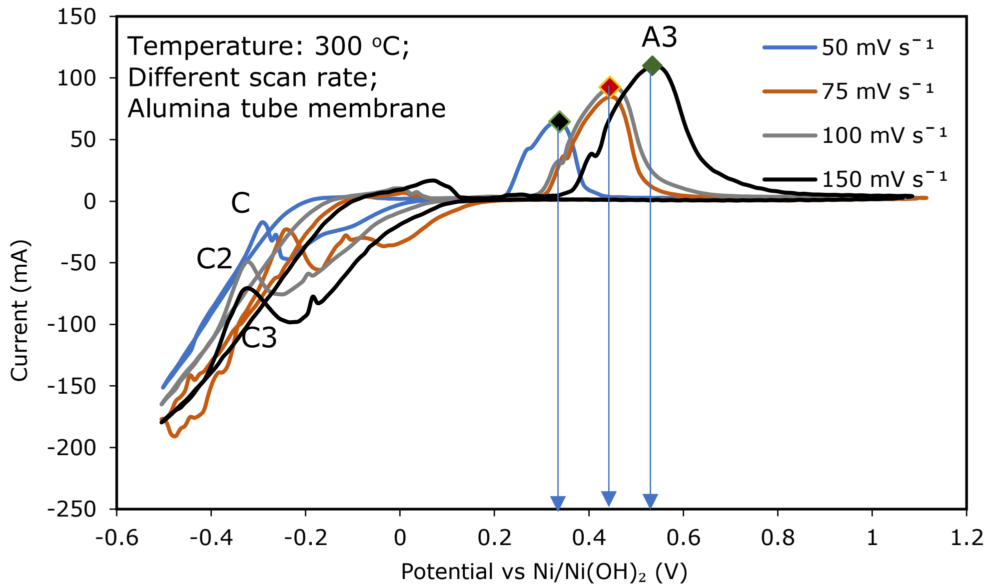

Figure 4.2 – Cyclic voltammograms of a 0.5mm nickel wire in eutectic molten hydroxide at different scan rates at 300°C. RE: $Ni/Ni(OH)_2$ in the alumina tube membrane; CE: 5 mm stainless steel rod; immersion depth: 14mm; an Ar gas atmosphere: 40cm^3min^{-1}.

4.2.2 Reusability of the $Ni/Ni(OH)_2$ reference electrode with an alumina membrane

In order to further check the stability, reusability and lifetime of the prepared nickel reference electrode covered with an alumina membrane tube, the CV examination was repeated at the same operating conditions as the previous test (Section 4.2) after 24 h. Figure 4.3 shows the cyclic voltammetry of the nickel working electrode in the eutectic molten hydroxide at 300°C using the same nickel reference electrode covered with an alumina membrane tube.

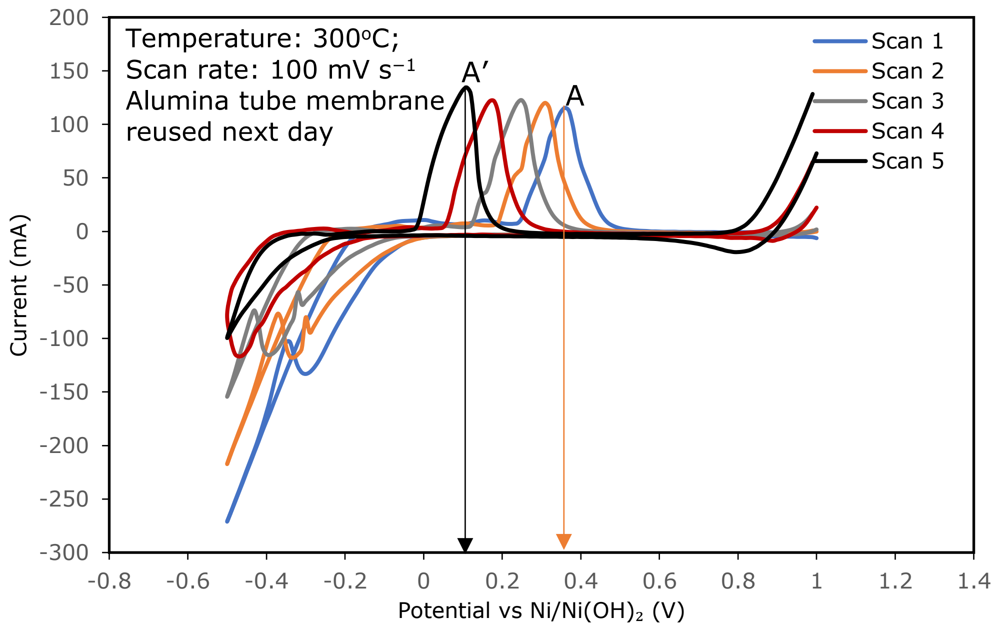

Figure 4.3 – Cyclic voltammograms of a 0.5 mm Ni wire working electrode in the eutectic molten hydroxide repeated after 24 h (Figure 4.2). The potential scan negatively from -0.6 to 1.0 V at 300°C. RE: $Ni/Ni(OH)_2$ in the alumina tube membrane; CE: 5 mm stainless steel rod; immersion depth: 14 mm; an Ar gas atmosphere: 40cm^3 min^{-1}.

From Figure 4.3, it is obvious that the oxidation peak of NiO_2 shifts negatively from scan 1 to 5. This shift in the oxidation peak between A and

A′ is about 280 mV and lies between 0.38 and 0.1 V. Meanwhile, there is also a negative shift for the cathodic limit from scan 1 to 5 as shown in Figure 4.3. This shift is about 200 mV and lies between -0.02 and -0.22 V. The current of the cathodic limit also decreases from 271.1 mA in scan 1 to 99.4 mA in scan 5. This decrease in the current value between scan 1 and 5 in Figure 4.3 likely indicates that there was a decrease in the yield of hydrogen gas during the actual experiment.

The results observed from the cyclic voltammetry test to check the stability and reusability of the nickel reference electrode covered by an alumina membrane tube, were compared. Scan 3 from both Figure 4.1 and Figure4.3 was merged into one figure to clarify the difference in the reference electrode behaviour with time, as shown in Figure 4.4.

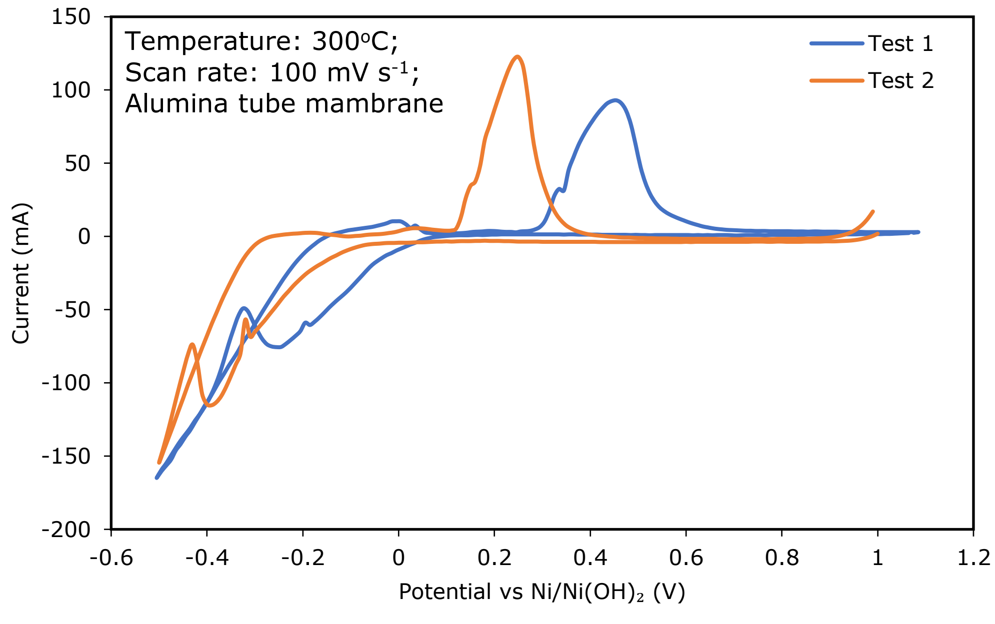

Figure 4.4 – Cyclic voltammograms of a 0.5 mm nickel wire in eutectic molten hydroxide at 300°C to compare the reusability of the nickel reference electrode in the alumina tube membrane. CE: 5mm stainless steel rod; immersion depth: 14mm; an Ar gas atmosphere: 40 cm^3 min^{-1}.

Figure 4.4 clearly indicates the unstable behaviour of the nickel working electrode in the eutectic molten hydroxide during the cyclic voltammetry test. This unstable performance is due to the difficulty exhibited by the prepared nickel reference electrode in terms of controlling the nickel working electrode. Therefore, the nickel reference electrode covered with an alumina membrane tube, in terms of stability, is not a desirable option for a reference electrode. The compared scan in Figure 4.4 shows that there is a negative shift in the oxidation peak of about 200 mV when Test 1 was repeated after 24 h (Test2).

In terms of the reusability, the nickel reference electrode covered with an alumina membrane tube, was also tested after 36 h at the same operating conditions as in Figure 4.3. During the cyclic voltammetry study, the open circuit potential was very unstable and hence abnormal CV scans were obtained. These unstable CV tests for stability and reusability were repeated three times with unchanged results obtained. The main reason for the poor stability of the nickel reference electrode coupled with the alumina tube membrane is that the eutectic molten hydroxide cannot permeate through the alumina membrane which is made from inert $\propto$-Al_2O_3 with high resistance. Since the mixture does not form a stable ion channel with the internal reference electrode-electrolyte mixture, instability abounds. In addition to this instability, this reference electrode cannot be used for more than 2 consecutive days to function as a part of a reliable electrochemical test because the alumina membrane ($\propto$-Al_2O_3) becomes very high resistance material in the eutectic molten hydroxide. It can thus be concluded that the prepared nickel reference electrode covered by an alumina membrane tube has a very short usable lifespan.

4.3 Ni/$Ni(OH)_2$ Reference Electrode with a Mullite Membrane

In order to overcome the shortcomings of an alumina membrane, a commercial mullite membrane was used to fabricate the reference electrode. A mixture ($Ni(OH)_2$-(NaOH-KOH); 1-99 mol%) was used as an internal electrolyte and a nickel wire was inserted into the tube containing the electrolyte mixture. The mullite tube was sintered by $\propto$-Al_2O_3 and SiO_2.

4.3.1 Stability of the Ni/$Ni(OH)_2$ reference electrode with a mullite membrane

The cyclic voltammetry result is shown in Figure 4.5. CV tests were also carried out using a nickel wire as working electrode and a prepared nickel wire covered with a mullite membrane tube as reference electrode in the eutectic molten hydroxide at 300^{o}C with a scan rate of 75 mV s^{-1}.

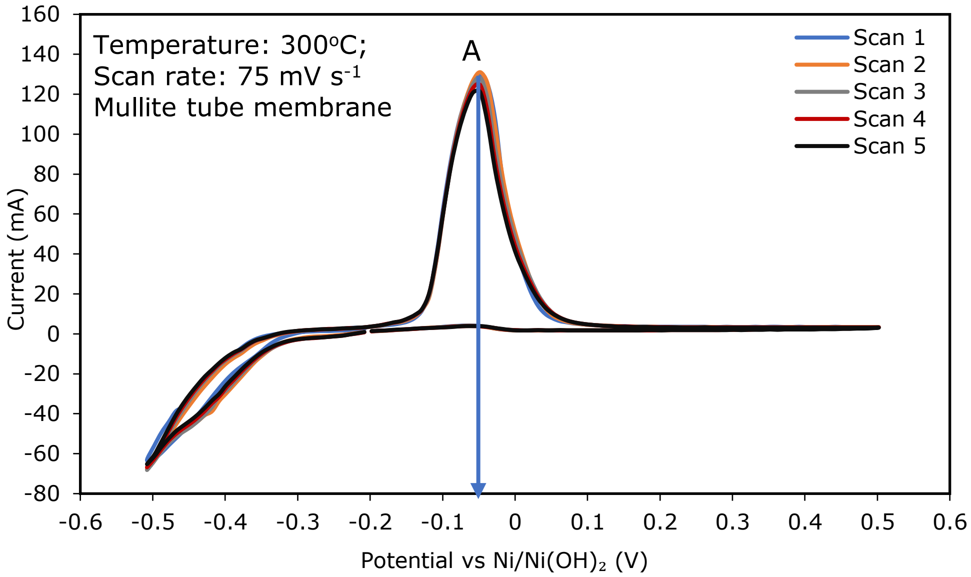

Figure 4.5 – Cyclic voltammograms of a 0.5 mm Ni wire working electrode in eutectic molten hydroxide; the scan is altered negatively from -0.5 to 1.0 V at 300°C; CE: 5 mm diameter stainless steel rod; RE: Ni/Ni(OH)$_2$ in the mullite tube membrane; immersion depth: 14 mm; an Ar gas atmosphere: 40 cm^3 min^{-1}.

The potential of the oxidation peak A for scan 1 to 5 was about -0.068 V. Consequently, the reduction potential of the cathodic limit for hydrogen gas formation for all scans is about -0.34 V. This preliminary result obtained using the prepared reference electrode in eutectic molten hydroxide confirms its stability and reliability. This stability and reliability of the nickel reference electrode covered by a mullite membrane tube, can be attributed to the eutectic molten hydroxide penetrating through the membrane and reacting with SiO_2. The latter is one of the substances that is used to construct the mullite tube membrane. Consequently, this membrane forms a stable ion channel through it, acting between the internal reference mixture and outside melt. This observed result in terms of stability due to the freshly prepared nickel reference electrode covered by a mullite tube is different from the result obtained from the freshly prepared nickel reference electrode covered by an alumina tube.

In order to understand the behaviour of the nickel working electrode during the eutectic molten hydroxide reaction, the scan rate for cyclic voltammetry observations were changed from slow to fast. The result was obtained by changing the scan rate in cyclic voltammetry between 50-150 mV s^{-1} at 300^{o}C using a nickel reference electrode covered with a mullite membrane tube, as shown in Figure 4.6.

The potential of the oxidation peak as shown in Figure 4.6 is very stable with the increase in scanning rate from 50-150 mV. Not only is there no shift in the potential of the oxidation peaks for the formation of NiO_2, but also the value of the oxidation potential is close to -0.03 V. These results further show the reliability and stability of the nickel reference electrode covered by the mullite membrane. As mentioned before, this stability and reliability of a mullite membrane covering $Ni/Ni(OH)_2$ is attributed to the eutectic molten hydroxide being able to penetrate through and react with the SiO_2; thus forming a stable ion channel between the internal electrolyte ($Ni(OH)_2$-(NaOH-KOH)) and external electrolyte of the eutectic molten hydroxide.

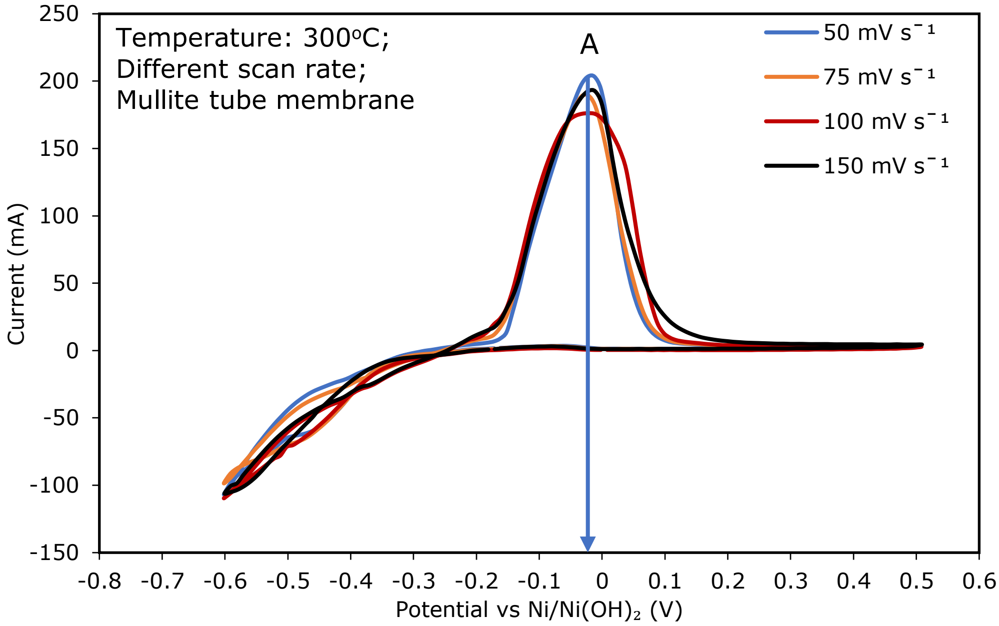

Figure 4.6 – Cyclic voltammograms of a 0.5 mm nickel wire in eutectic molten hydroxide with different scan rates at 300°C. RE: $Ni/Ni(OH)_2$ in the mullite tube membrane; CE: 5 mm stainless steel rod; immersion depth: 14mm; an Ar gas atmosphere: 40cm^{3}min^{-1}.

4.3.2 Reusability of the $Ni/Ni(OH)_2$ reference electrode with a mullite membrane

In order to check the reusability of the prepared reference electrode in eutectic molten hydroxide, the CV test was repeated after 24 h and Figure4.7 shows the obtained results at a temperature of 300°C and scan rate of 75 mV s^{-1}.

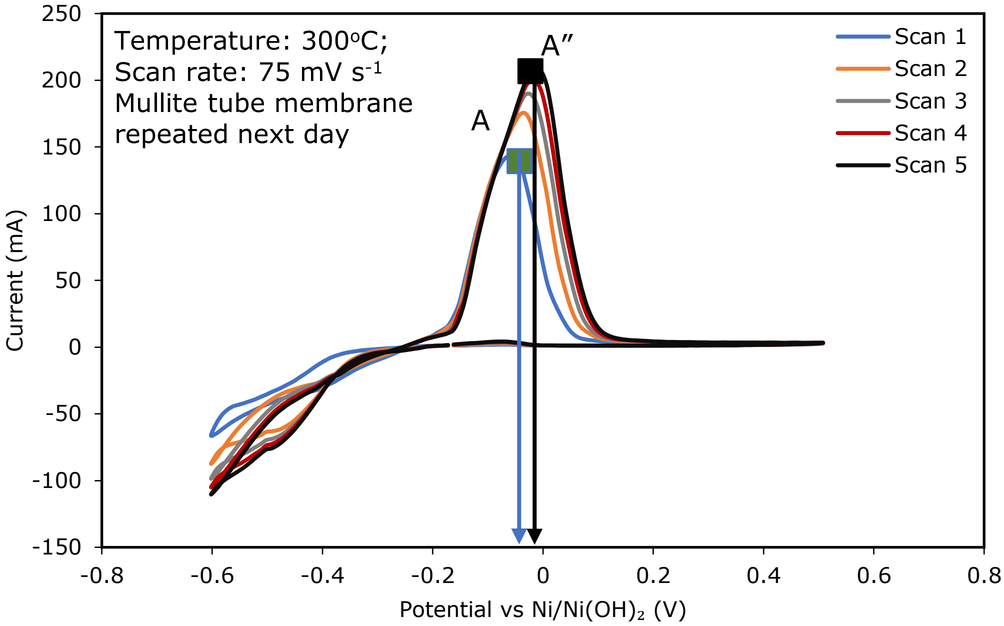

Figure 4.7 – Cyclic voltammograms of a 0.5 mm Ni wire working electrode in eutectic molten hydroxide repeated after 24 h (Figure4.5). The potential is negatively scanned from -0.6 to 1.0 V at 300°C. RE: Ni/$Ni(OH)_2$ in the mullite tube membrane; CE: 5 mm stainless steel rod; immersion depth: 14mm; an Ar gas atmosphere: 40cm^{3}min^{-1}.

The observed scans show a slight positive shift in the oxidation peak. This result was obtained by reusing the reference electrode after 24 h as shown in Figure 4.7. This shift in the scans is about 64 mV between scan 1 and 5; thus it can be considered negligible. The reduction potential also stays the same during the test at -0.34 V. This stable behaviour of the nickel reference electrode covered by a mullite tube confirms the ability to reuse it and get reliable results. In contrast, the nickel reference electrode covered by an alumina tube was unstable during the test and shifted negatively by about 280 mV.

The CV scan of a freshly prepared nickel reference electrode covered by a mullite membrane tube was compared with the CV scan of the same reference electrode after 24 h and at the same operating conditions. The reason for comparing these scans is to gauge the durability and the stability of the reference electrode that controls the working electrode potential inside the eutectic molten hydroxide during electrochemical analysis. Figure4.8 shows the comparison between CV scans obtained from both days.

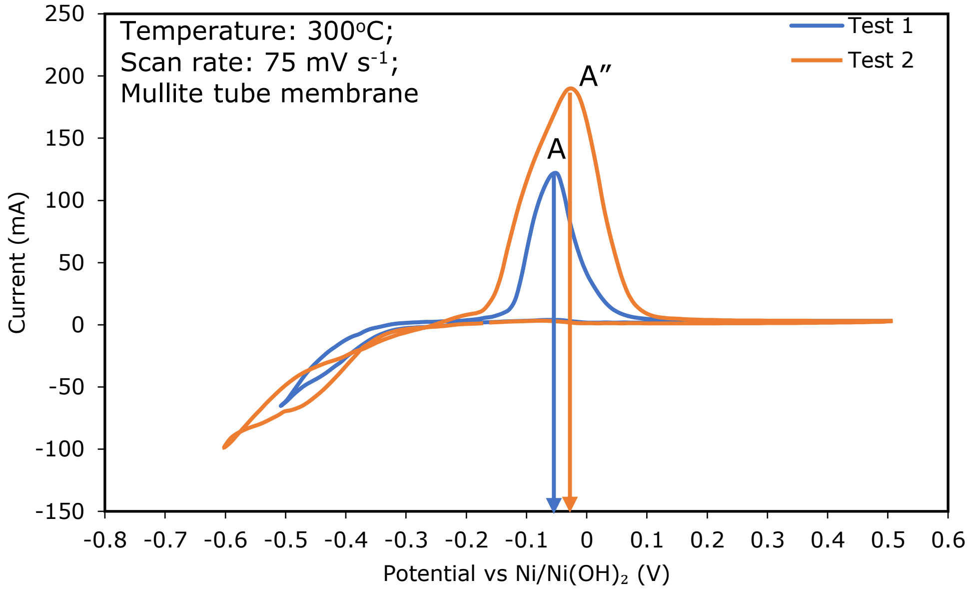

Figure 4.8 – Comparison of cyclic voltammograms of the repeatable use of the nickel reference electrode in the mullite tube membrane (Figure 4.7 and Figure 4.5). The 0.5 mm nickel wire in eutectic molten hydroxide at 300ºC has been used for comparison. CE:5 mm stainless steel rod; immersion depth: 14mm; an Ar gas atmosphere: 40 cm^{3}min^{-1}.

The potential of the oxidation peak of NiO_2 on Test 1 is about -0.07 V and on Test 2 is about -0.04 V. This can be considered as equal and shown via an arrow in Figure 4.8. Even though there is no change in the potential, the current of the oxidation peak for forming NiO_2 increases from Test 1 to Test2. The current increases from 121 mA at point A to 190 mA at point A″, this being about 68 mA higher for the Test 2 after 24 h. The increase in the current of the oxidation peak A″ is also followed by an increase in the current of the reduction potential. There is, however, no change in the reduction potential assigned to hydrogen gas generation which further demonstrates the stability of the reference electrode.

Subsequently, it is significant to further test the stability and reusability of the reference electrode in the bulk molten hydroxides. CV tests were carried out using the same electrode for 10 days. Figure 4.9 shows the photos of the immersed part of the mullite membrane reference electrode in the bulk eutectic molten hydroxide. These photos were taken for the mullite reference electrode after the first, third and tenth day of use in the test.

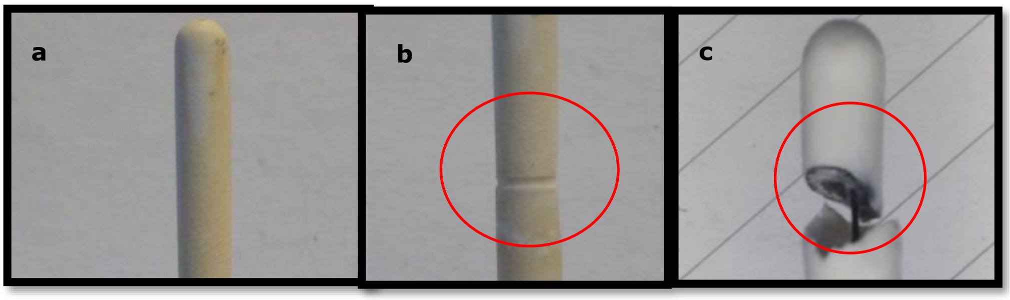

Figure 4.9 – The change in the nickel reference electrode coupled with a mullite tube membrane inside eutectic molten hydroxide (a) 1st day, (b) 3rd day and (c) 10th day.

It obvious from the photo in Figure 4.9a, which was taken for the mullite membrane after the first test of the reference electrode, that there is no drastic change in the external appearance of the mullite membrane. There is a slight corrosion line on the outside surface of the membrane surface after it was used on the third day as seen in Figure 4.9b. This change in the reference electrode surface does not affect the stability of the scans. Using the reference electrode to carry out CV studies and hence examining its stability and lifetime was continued until cracks were observed on the tenth day as shown in Figure 4.9c. It can be concluded from the above observations that the lifetime of using the reference electrode is at least up to 9 days to avoid any contamination of the outside electrolyte with the internal mixture. The examination of the lifetime of the reference electrode was repeated thrice and it was found that the lifetime of the reference electrode was between 7-9 days in the chosen eutectic molten hydroxide. Hence, the ideal ionic membrane to use to construct a reference electrode for the eutectic molten hydroxide is mullite because of its stability, reusability and longer lifetime as compared to an alumina membrane. The latter failed to provide a stable ionic channel between the electrolyte and the internal mixture.

4.4 Summary

The findings of this chapter can be summarised as follows:

- Firstly, the main oxidation peak reaction of the nickel working electrode in the eutectic molten hydroxide (NaOH-KOH; 49-51 mol%) is NiO_2, probably via the following reaction:

$$\mathrm{NiO + 2OH^- \rightarrow NiO_2 + H_2O + 2e^-} \qquad \textbf{(4.4)}$$

This agrees well with the published literature on nickel electrode behaviour in eutectic molten hydroxides (Miles, 2003).

- However, this study determined the basic anodic and cathodic limit reactions in the eutectic molten hydroxide to be oxygen and hydrogen gases production respectively, as expressed in the below equations:

$$\text{Cathode limit: } \mathrm{H_2O + 2e^- \rightarrow H_2(g) + 2OH^-} \qquad \textbf{(4.5)}$$

$$\text{Anodic limit: } \mathrm{OH^- \rightarrow \tfrac{1}{2}O_2(g) + H_2O + 2e^-} \qquad \textbf{(4.6)}$$

- The Ni/Ni(OH)$_2$ alumina membrane reference electrode in the eutectic molten hydroxide generated unreliable and inconsistent results. The performed cyclic voltammograms for a freshly prepared reference electrode was unable to produce stable scans, resulted in the scan shifting in the positive direction. Changing the CV scan rate also resulted in significant shifts of the potential of the oxidation peak. For example, the oxidation peak shifts positively by a difference of 230 mV when the scan rate is changed from 50 to 150 mV s^{-1}.
- In addition, when the Ni/Ni(OH)$_2$ alumina membrane reference electrode was reused after 24 hours, a significant negative shift difference (280 mV) in the oxidation peak potential is observed from scan 1 to 5. No CV was produced on the third day as this was not possible because of the failure of the reference electrode. This nickel reference electrode covered by an alumina membrane was prepared and tested thrice after which it was confirmed that it was not efficient enough to obtain reliable results.
- The reason for the poor stability of the nickel reference electrode covered by an alumina membrane is because of the high resistance of the alumina membrane that leads to issues with creating a stable ion channel between the electrolyte and the internal reference electrode mixture (Ni(OH)$_2$-(NaOH-KOH); 1-99 mol%).
- When a mullite membrane of the Ni/Ni(OH)$_2$ reference electrode was used and tested, only a slight positive shift in the oxidation peak is observed (64mV from scan 1 to 5). This was considered negligible. The stability of the reference electrode was also tested by changing the scan rate between 50-150 mV s^{-1} and the peak potentials were also confirmed to be stable.
- The same mullite reference electrode was reused after 24 hours and there was only a small, negligible change in the oxidation peak potential.

- Good mullite membrane reference electrode stability was noted in contrast to the alumina membrane in the eutectic molten hydroxide. This is because of the ability of salts to penetrate through and react with the SiO_2 which is one of the substances that is a part of the structure of the mullite membrane. Conversely, the $\propto$-Al_2O_3 membrane formed a stable ion channel between the internal reference mixture ($Ni(OH)_2$-NaOH-KOH; 1-99 mol%) and the external electrolyte.
- The stability and reusability of the prepared nickel reference electrode covered with mullite tube membrane were also checked in the eutectic molten hydroxide. The results indicate that the mullite membrane reference electrode can be used to carry out electrochemical investigations for up to 9 days.

CHAPTER 5

INVESTIGATION INTO DETERMINING A SUITABLE REFERENCE ELECTRODE

5.1 Introduction

Chapter 4 discussed finding a suitable membrane to fabricate a $Ni/Ni(OH)_2$ reference electrode. This chapter, on the other hand, aims to discuss suitable reference electrodes that can be used to carry out electrolysis in molten hydroxide. In other words, it compares the fabricated mullite membrane $Ni/Ni(OH)_2$ reference electrode with other types of reference electrodes. Two different types of inert quasi-reference electrodes were employed in this study for comparison: silver and platinum wire respectively.

As mentioned previously in this thesis, there are limited reference electrodes that have been deemed suitable for a molten hydroxide (Divisek et al., 1982, Bard and Faulkner, 2001). Many studies have used an Ag/AgCl reference electrode at low temperatures to investigate the electrochemical behaviour of different base or alloy metals in an aqueous solution of hydroxide salt (Jayalakshmi et al., 2008, Döner et al., 2012). Miles (2003) also used an Ag/AgCl reference electrode in eutectic molten hydroxides at high-temperature. A silver quasi-reference electrode was also investigated in molten hydroxides by (Guo et al., 2013, Yang et al., 2014). There were further studies on molten hydroxides that used platinum wire (Híveš et al.,

2006) or copper plated platinum (Schiavon et al., 1972) as a quasi-reference electrode respectively. A nickel rod quasi-reference electrode was also used in a molten hydroxide to prepare nickel powder from nickel oxide (Ge et al., 2015).

Cyclic voltammetry was used to characterise the electrode and also ascertain its stability. Finding a reliable reference electrode allows proper understanding of various working electrode materials as will be discussed later on in Chapter 6.

5.2 Standard Reaction

Before studying any electrochemical reaction in an alkali hydroxide with or without the presence of water, it is imperative to study the possible reactions that can occur. Additionally, a calculation of the standard reaction potential associated with these reactions must also be made. The possible general reactions in an alkali hydroxide electrochemical process include H_2 and O_2 formation at the cathode and anode respectively (reactions 5.1-5.3). The general reaction of an alkali hydroxide which is in equilibrium with water and metal oxide is shown in reaction 5.4 (Licht et al., 2016).

$$\text{General reaction: } \mathrm{H_2O \rightarrow H_2 + \tfrac{1}{2}O_2} \quad \textbf{(5.1)}$$

$$\text{Cathode: } \mathrm{2\,H_2O + 2\,e^- \rightarrow H_2 + 2\,OH^-} \quad \textbf{(5.2)}$$

$$\text{Anode: } \mathrm{2\,OH^- \rightarrow \tfrac{1}{2}O_2 + H_2O + 2\,e^-} \quad \textbf{(5.3)}$$

$$\mathrm{2\,MOH \leftrightarrow H_2O + M_2O\ \ (M: Na, K)} \quad \textbf{(5.4)}$$

When the general reaction of water (5.1) is added to the reaction of hydroxide salt (5.4), the product of this combination generates equivalent yields of hydrogen gas as in reaction (5.5):

$$2\,\mathrm{MOH} \rightarrow \mathrm{H_2} + \tfrac{1}{2}\mathrm{O_2} + \mathrm{M_2O} \qquad \textbf{(5.5)}$$

From the reaction (5.5), it was clear that hydroxide salt, was dehydrated and produced a metal oxide, hydrogen and oxygen. For this reason, steam was continuously bubbled inside the eutectic molten hydroxide in order to maintain equilibration hydration of molten hydroxide as steam splitting occurs (Licht et al., 2016).

The corresponding standard reaction potential of reaction (5.4) was calculated using HSC chemistry software (version 6.1; outotec) for the dissociation of the alkali hydroxide NaOH, KOH and the eutectic mixture (NaOH-KOH; 49-51 mol%) as a function of temperature. This is shown in Figure 5.1.

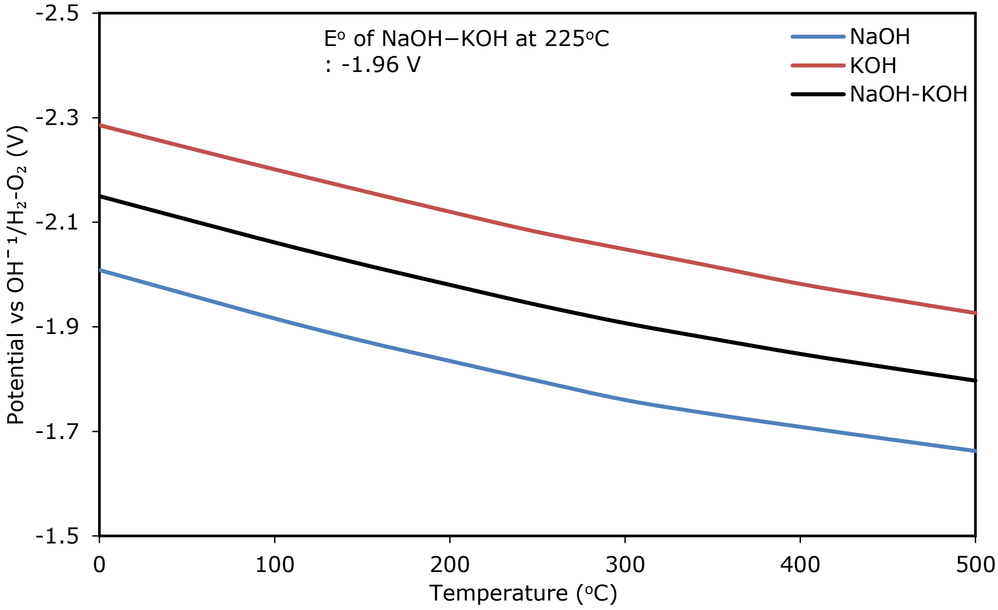

Figure 5.1 – Standard potential against temperature for the decomposition of molten hydroxides NaOH and KOH; and the eutectic molten hydroxide (NaOH-KOH; 49-51 mol%) into their metal oxides (Na_2O and K_2O), hydrogen gas (H_2) and oxygen gas (O_2). The potential was calculated using HSC chemistry software (version 6.1; outotec) and is reported versus the OH^{-1}/H_2-O_2 reference reaction.

It is obvious from Figure 5.1 that the standard reaction potential required for splitting an alkali hydroxide decreases with increasing temperature. In addition, the standard reaction potential for equation (5.1) (splitting H_2O to H_2 and O_2) is also calculated using the same software. Figure 5.2 shows the comparison between the standard reaction potential of equation (5.1) and the standard reaction potential of a binary mixture of hydroxides at a different temperature. This standard reaction potential gives good information about the minimum energy required to carry out the reaction. The standard potential for the formation of hydrogen gas as observed from Figure 5.2 for the decomposition of the eutectic molten hydroxide at 225°C is -1.96 V. However, it is -1.06 V from splitting water at the same temperature.

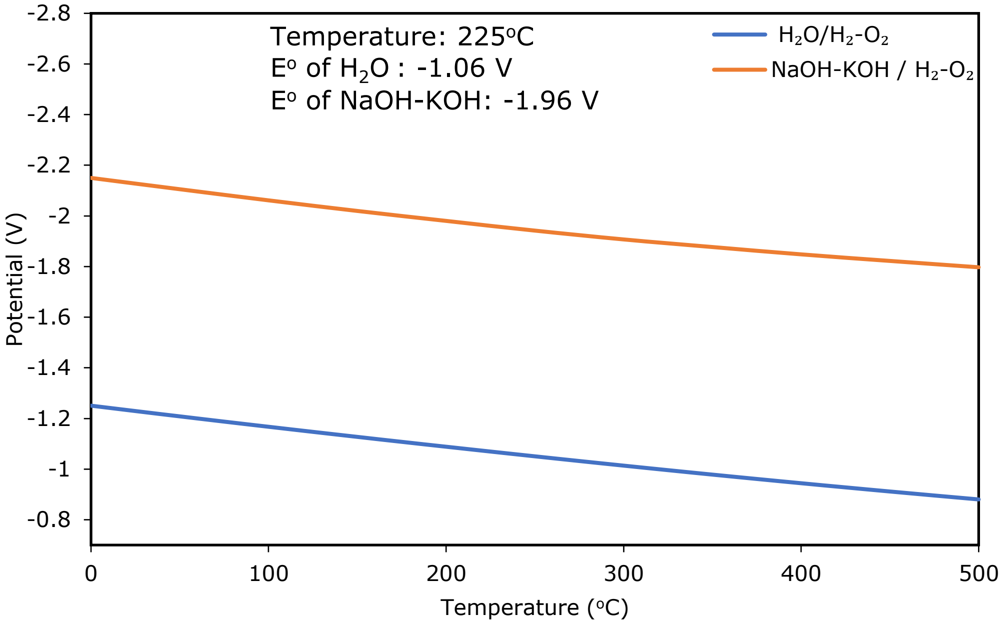

Figure 5.2 – Comparison between the standard potential of the splitting water (H_2O) into Hydrogen gas (H_2) and oxygen gas (O_2) using the standard potential of decomposition of the eutectic molten hydroxide to their metal oxide (Na_2O and K_2O), hydrogen gas (H_2) and Oxygen gas (O_2) respectively. The potential is calculated using HSC chemistry software (version 6.1; outotec).

5.3 Blank Cyclic Voltammetry Tests using Ag, Pt, and Ni/Ni(OH)$_2$ Reference Electrodes

Cyclic voltammetry of a platinum working electrode in the eutectic molten hydroxide at 225°C was carried out. The first examination used a silver wire as the quasi-reference electrode. Figure 5.3 shows the cyclic voltammetry data obtained at a scan rate of 100 mV s^{-1}.

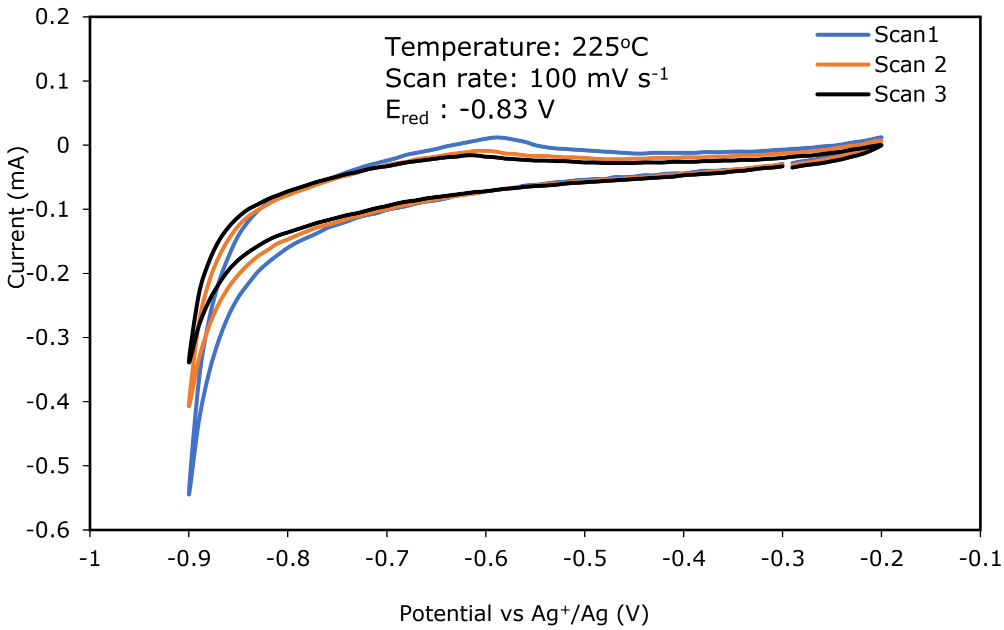

Figure 5.3 – Cyclic voltammograms of a 0.5 mm Pt wire in the eutectic molten hydroxide; scan rate: 100 mV s^{-1}; CE: 5mm diameter stainless steel rod; an Ar gas atmosphere: 40 cm^3 min^{-1}. For negative scan limits of -0.9 V RE: 1.0 mm Ag wire; immersion depth: 14 mm.

In Figure 5.3, the potential range for cyclic voltammetry scans in this section to test the platinum wire working electrode is set from -0.9 to -0.2V against the silver reference electrode. This is down for the following reasons. Miles (2003) reported that the reduction of water at the cathodic limit was -1.3 V vs a silver reference electrode,

$$2H_2O + 2e^- \rightarrow H_2 + 2\,OH^- \quad \textbf{(5.6)}$$

Yang et al. (2014) however determined that the cathodic limit was -0.9 V vs a silver reference electrode for a setup similar to this study. Therefore, the lower potential limit of -0.9 V vs Ag in this study was used to avoid the negative influence of hydrogen gas. At the beginning of the forward scan from -0.9 V vs Ag, the reduction current begins at a potential lower than

-0.83 V and the current lesser than -0.5 mA. The potential window is kept between -0.83 and -0.2 V which is roughly 0.6 V.

Figure 5.4 shows the preformed cyclic voltammetry of the platinum working electrode in the eutectic molten hydroxide using a platinum quasi-reference electrode at a temperature of 225°C and a scan rate of 100 mV s^{-1}.

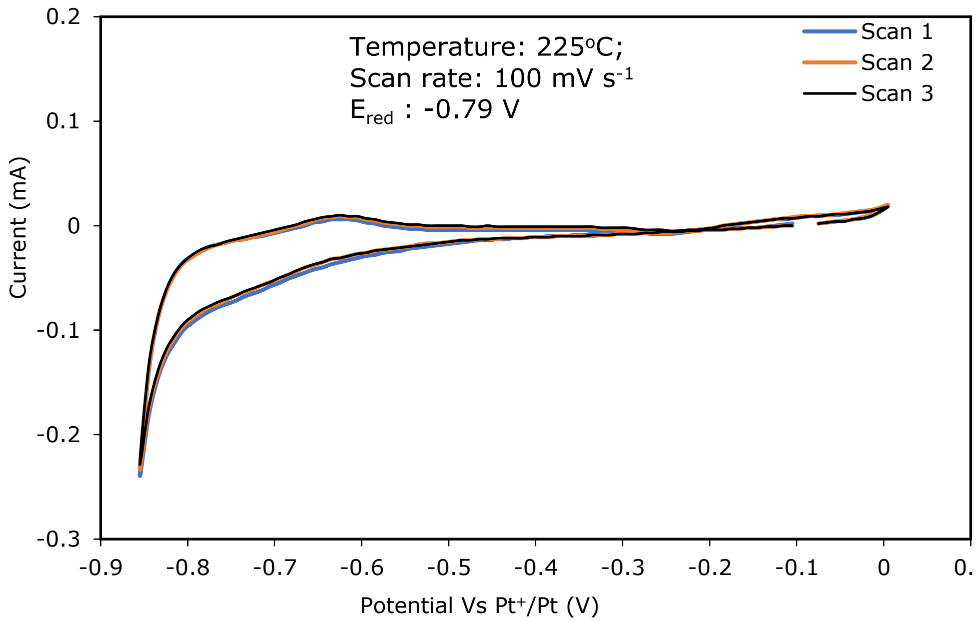

Figure 5.4 – Cyclic voltammograms of a 0.5 mm Pt wire in the eutectic molten hydroxide; scan rate: 100 mV s^{-1}; CE: 5mm diameter stainless steel rod; an Ar gas atmosphere: 40 cm^3 min^{-1}. For negative scan limits of -0.85 V RE: 0.5 mm Pt wire; immersion depth: 14 mm.

CV is scanned negatively from -0.85 to 0.0 V as presented in Figure 5.4. The cathodic limit reaction from the above figure is influenced by reaction (5.6) showing water decomposition ($2H_2O + 2e^- \rightarrow H_2 + 2OH^-$). This water is already formed at the anodic limits as reported by Híveš et al. (2006) who found that the reduction potential limit was about -0.81 V vs Pt. This is in agreement with findings observed from Figure 5.4 which exhibit a value of -0.8 V. The potential window of the general reaction (5.5) ranges between -0.83 and -0.025 V, which is approximately 0.8 V.

A prepared nickel reference electrode was also used during the CV investigation on a platinum working electrode at a temperature of 225°C and a scan rate of 100 mV s^{-1}. The CV results obtained are displayed in Figure 5.5.

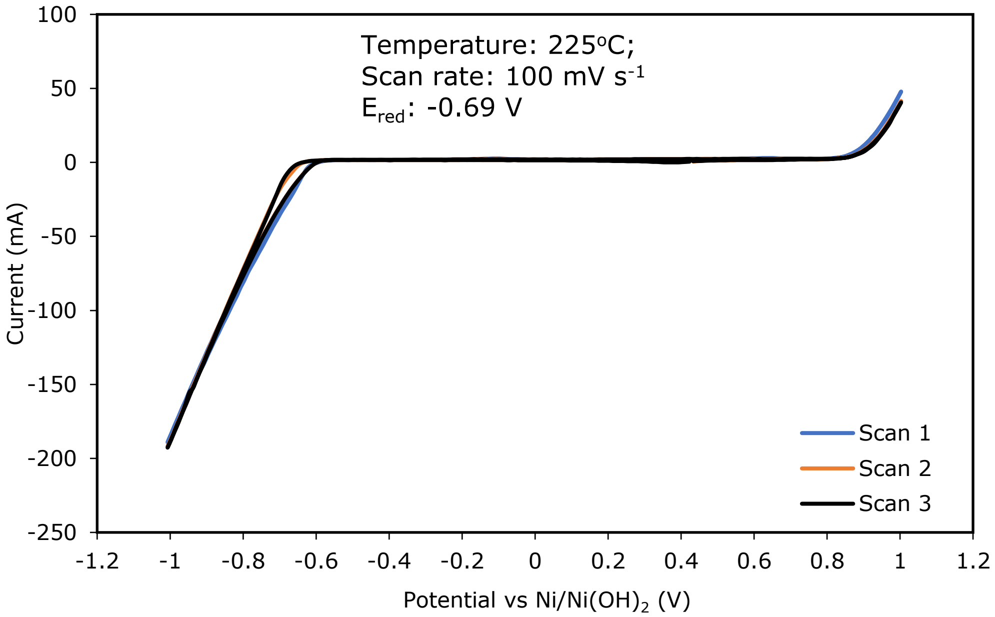

Figure 5.5 – Cyclic voltammograms of a 0.5 mm Pt wire in the eutectic molten hydroxide; scan rate: 100 mV s^{-1}; CE: 5 mm diameter stainless steel rod; an Ar gas atmosphere: 40 cm^3 min^{-1}. For negative scan limits of -1.0 V Ni/Ni(OH)$_2$ in a mullite tube; immersion depth: 14 mm.

In Figure 5.5, cyclic voltammetry CV is scanned negatively from -1.0 to 1.0V vs Ni/Ni(OH)$_2$. The potential for water reduction to hydrogen gas is initiated at -0.69V versus Ni/Ni(OH)$_2$. This water originates from the oxidation of hydroxide ions at the anodic limits as expressed in ($2OH^- \rightarrow \frac{1}{2}O_2+H_2O+2e^-$) of reaction (5.3). The electro-stability window of reaction (5.5) ($2MOH \rightarrow H_2+\frac{1}{2}O_2+M_2O$) is 1.68V. This result somewhat agrees with the findings of Ge et al. (2015) in terms of electro stability windows. In the case of the authors, this was reported to be about 1.4 V even though the reduction and the oxidation potential were different from the current study. This difference in the potential can be attributed to a variation in the reference electrode used. Ge et al. (2015) used a nickel rod as a quasi-reference electrode while this study used a prepared mullite membrane $Ni/Ni(OH)_2$ reference electrode to control the working electrode potential.

General features that can be concluded from Figure 5.3, 5.4 and 5.5 irrespective of the reference electrode used are discussed. No cathodic peak or oxidation peak is visible prior to the start of the current wave around the cathodic and anodic limit respectively when the platinum wire was used as a working electrode. This observation indicates that the platinum working electrode was inert in the eutectic molten hydroxide at least within the relatively short experimental time scale considered in this study. From Figure 5.2, the general standard potential for the reduction of hydroxide ions to the hydrogen gas, oxygen gas and oxides of the reaction (5.5) ($2MOH \rightarrow H_2 + \frac{1}{2} O_2 + M_2O$) is -1.96 V at 225 ^{o}C. This standard potential is close to -1.68 V vs $Ni/Ni(OH)_2$ as obtained from Figure 5.5. The comparison between the reference electrodes used shows that the prepared nickel has more stability in comparison to silver and platinum quasi-reference electrodes.

5.4 Effect of Changing Potential Scan Rate

Cyclic voltammetry investigations at different potential scan rates were carried out for the platinum working electrode in the eutectic molten hydroxide. This investigation was also carried out using the above-mentioned reference electrodes (silver and platinum quasi-reference electrode, and $Ni/Ni(OH)_2$) to control the working electrode potential. Figure5.6 shows the obtained cyclic voltammetry in the eutectic molten hydroxide at 225°C and at the scan rates ranging between 25 and 150mV s^{-1}. Silver wire was used as the reference electrode.

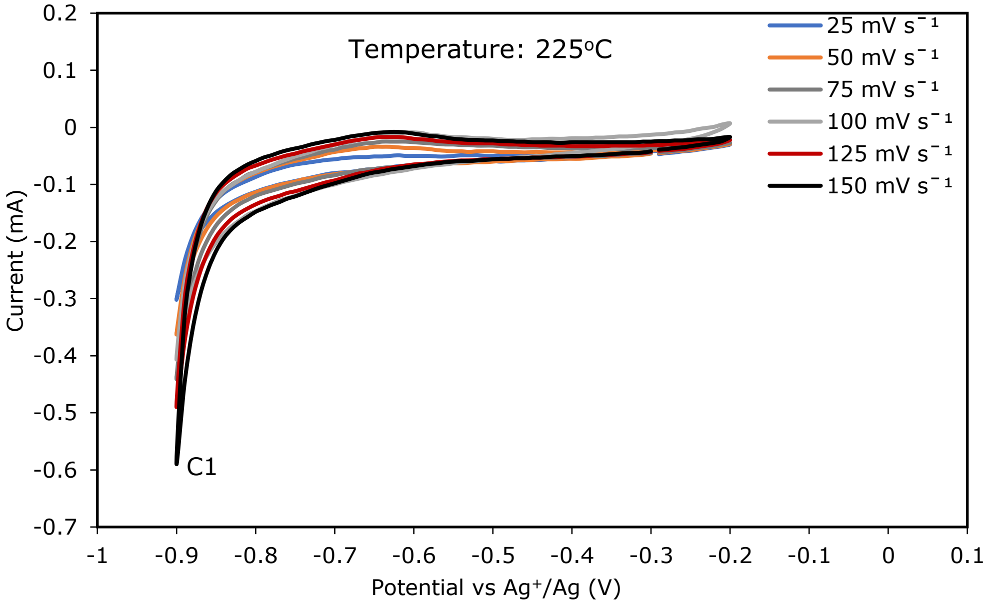

Figure 5.6 – Cyclic voltammograms of a 0.5 mm Pt wire working electrode in the eutectic molten hydroxide at 225°C. For the indicated scan rates; CE: 5 mm diameter stainless steel rod; immersion depth: 14 mm; an Ar gas atmosphere: 40 cm^3 min^{-1}; for negative scan limit of -0.9 V, RE: 1.0 mm Ag wire.

The height of the cathodic current at the reduction limit C1 increases with an increase in the speed of the potential scan rate as shown in Figure 5.6. The various, recorded reduction currents are summarised in Table 5.1.

Using these, obtained results showcase a relationship between the reduction current and the square root of the potential scan rate, demonstrating that mass transport can occur under semi-infinite linear diffusion conditions as in (5.6):

$$I_R = -0.0998 - 0.0347\ v^{\frac{1}{2}} \quad (R^2 = 0.7849;\ \text{Ag wire}) \qquad \textbf{(5.6)}$$

Varying the rate at which the Pt working electrode was scanned using a Pt reference electrode, gave similar CVs in Figure 5.7 as those obtained for Ag reference electrode.

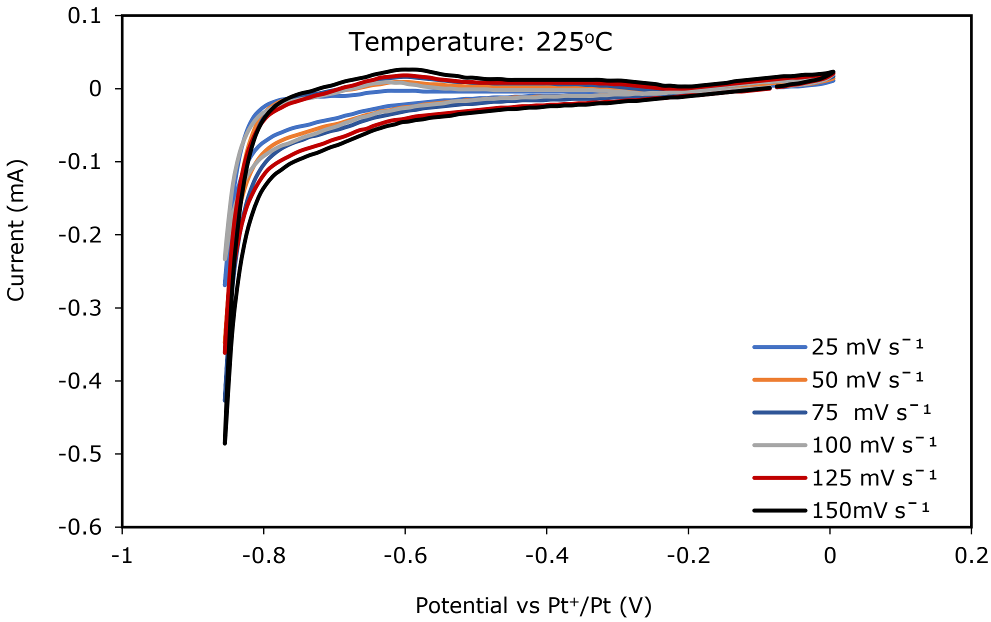

Figure 5.7 – Cyclic voltammograms of a 0.5 mm Pt wire working electrode in the eutectic molten hydroxide at 225°C. For the indicated scan rates; CE: 5 mm diameter stainless steel rod; immersion depth: 14 mm; an Ar gas atmosphere: 40 cm^3 min^{-1}; for negative scan limit of -0.85 V, RE: 0.5 mm Pt wire.

The reduction current of the cathodic limit also increased with an increase in the speed of the scan rate. Equation (5.7) provides the linear relationship between the reduction current and the square root of the scan rate, demonstrating that mass transport can occur under semi-infinite diffusion conditions:

$$I_R = -0.1645 - 0.0211\, v^{\frac{1}{2}} \quad (R^2 = 0.677;\ \text{Pt wire}) \qquad \textbf{(5.7)}$$

The prepared nickel reference electrode was also used to control the platinum working electrode at the same operating conditions. Hence its stability was compared with the silver and the platinum reference electrodes at different scan rates as shown in Figure 5.8.

Table 5.1 – The current limits of a 0.5 mm Pt wire working electrode in the eutectic molten hydroxide at 225°C. For the indicated scan rates; CE: 5mm diameter stainless steel rod; immersion depth: 14mm; an Ar gas atmosphere: 40 cm³ min⁻¹.

Scan rate ($mV\ s^{-1}$)	Ag wire	Pt wire	$Ni/Ni(OH)_2$
	cathodic current limit (mA)	cathodic current limit (mA)	cathodic current limit (mA)
25	-0.31	-0.27	-197.50
50	-0.36	-0.34	-198.57
75	-0.33	-0.48	-199.39
100	-0.41	-0.23	-199.41
125	-0.48	-0.36	-199.66
150	-0.58	-0.48	-198.70

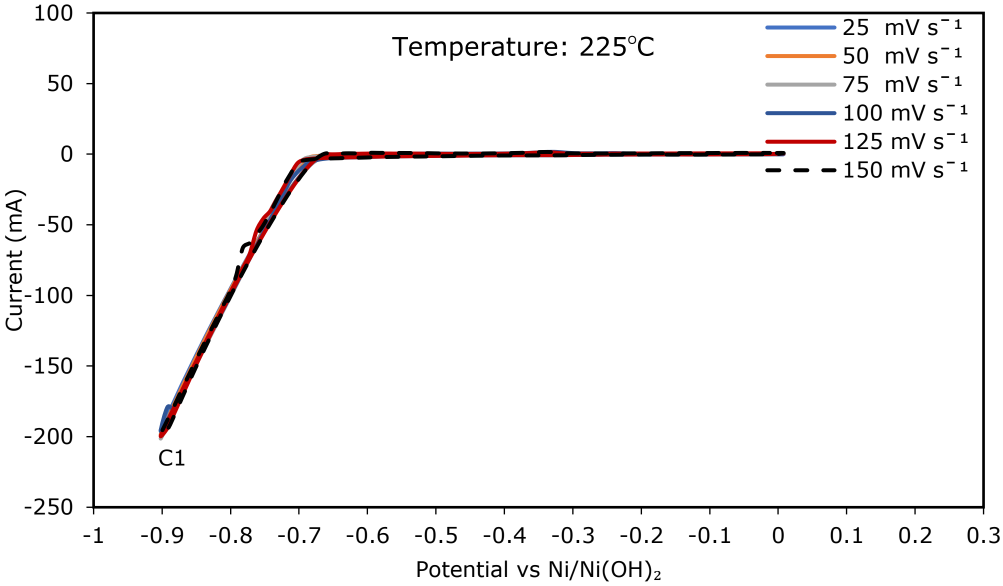

Figure 5.8 – Cyclic voltammograms of a 0.5 mm Pt wire working electrode in the eutectic molten hydroxide at 225°C. For the indicated scan rates; CE: 5 mm diameter stainless steel rod; Immersion Depth: 14 mm; an Ar gas atmosphere: 40 cm^3 min^{-1}; for negative scan limit of -0.9 V RE: $Ni/Ni(OH)_2$ in a mullite tube.

The comparison between the reference electrodes was based on checking the stability of the reduction current at different potential scan rates. It is obvious from Figure 5.8 with the $Ni/Ni(OH)_2$ reference electrode that the reduction current for the platinum wire working electrode at different scan rates did not change as the scan rate increased. Furthermore, it can be determined that the mass transport reaction between water and the electrode occurs under semi-infinite linear diffusion conditions as in equation (5.8):

$$I_R = -193.38 - 0.2992\, v^{\frac{1}{2}} \quad (R^2 = 0.8799;\ Ni/Ni(OH)_2) \qquad \textbf{(5.8)}$$

In contrast, there is an increase noted in the reduction current as the scan rate increased when either silver or platinum electrodes were used as a reference electrode. This result further provides evidence regarding the stability of the prepared nickel reference electrode.

5.5 Effect of Changing the Eutectic Molten Hydroxide Operating Temperature

The effect of the eutectic molten hydroxide operating temperature on the cyclic voltammetry studies and hence reference electrode stability was also investigated. A platinum wire was also used as the working electrode in the eutectic molten hydroxide while the reference electrodes were silver, platinum (both wires) and the mullite membrane $Ni/Ni(OH)_2$ discussed earlier. Figure 5.9 shows cyclic voltammograms obtained at temperatures of 250 and 300^oC and a scan rate of 100 mV s^{-1} using silver wire as a reference electrode to control the working electrode potential.

From the CVs displayed in Figure 5.9, the cathodic limit shifts positively (~0.13 V) between (C2 and C1) as the operating temperature of the eutectic molten hydroxide increases from 250 to 300^oC. This positive increase in the reduction potential is due to the increase in the operating temperature which in turn affects directly the electrode kinetics. A similar observation was obtained when the platinum wire was used as the reference electrode as shown in Figure 5.10. The recorded reduction potentials for the reference electrodes used are tabulated in Table 5.2. The results clearly indicate a positive shift in the working electrode potential with a molten salt temperature variation of 50^oC for the Ag and Pt electrodes respectively.

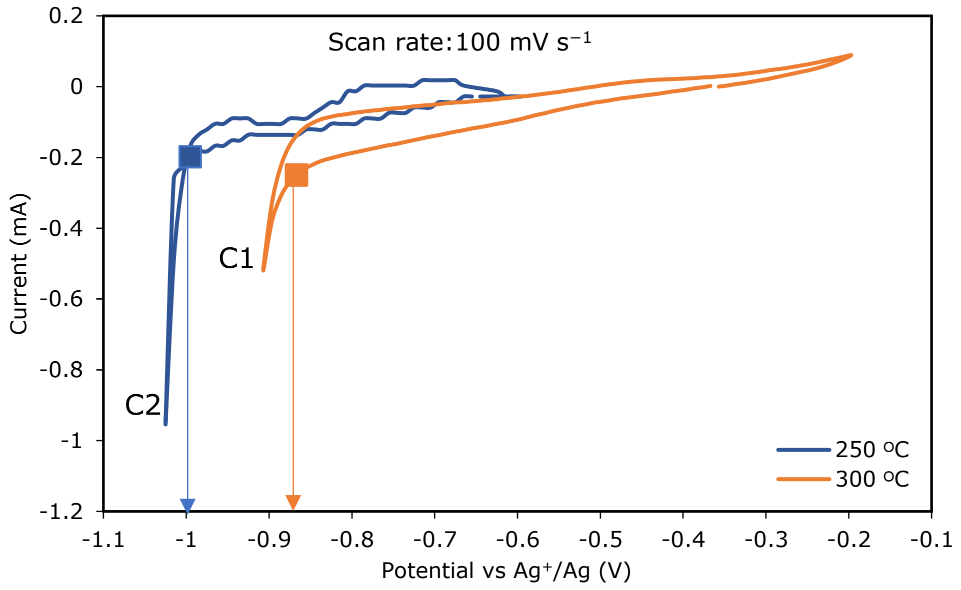

Figure 5.9 – Cyclic voltammograms of a 0.5 mm Pt wire working electrode in the eutectic molten hydroxide at different operating temperatures and a scan rate of 100 mV s^{-1}; CE: 5 mm diameter stainless steel rod; immersion depth: 14 mm; an Ar gas atmosphere: $40 cm^3 min^{-1}$. RE: 1.0 mm Ag wire.

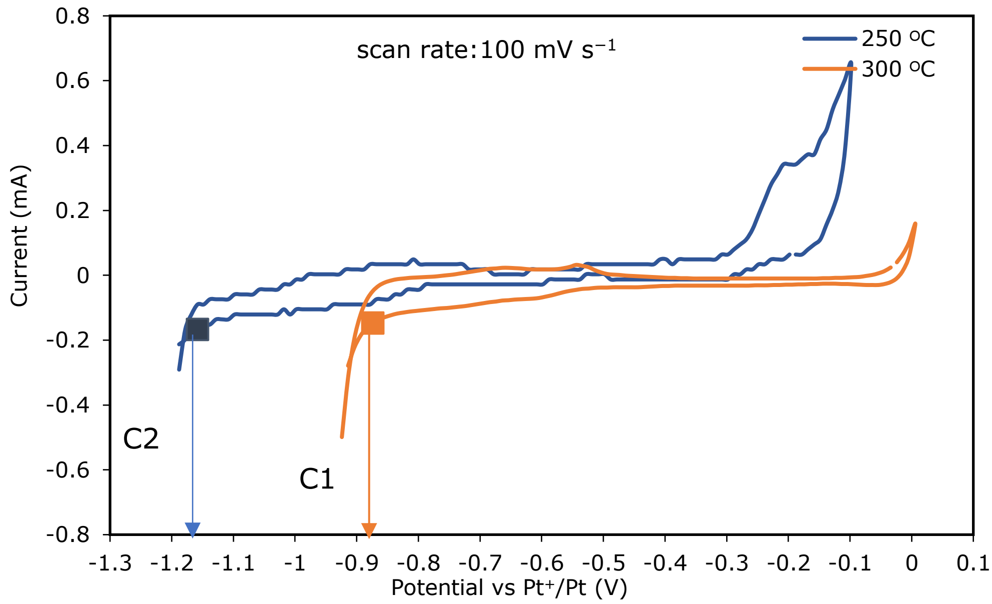

Figure 5.10 – Cyclic voltammograms of a 0.5 mm Pt wire working electrode in the eutectic molten hydroxide at different temperatures and a scan rate of 100 mV s^{-1}; CE: 5 mm diameter stainless steel rod; immersion depth: 14 mm; an Ar gas atmosphere: $40 cm^3 min^{-1}$. RE: 0.5 mm Pt wire.

In the case of the platinum reference electrode, a positive shift of 0.22 V is observed between (C2 and C1) which is 0.1 V higher than when using the silver wire reference electrode at different operating temperature. The reduction potential limit shifts positively by approximately 0.3 V with an increase in temperature as shown in Figure 5.10. The recorded reduction potential is illustrated in Table 5.2. The recorded results clearly show that the reduction potential shifts positively with an increase in the temperature of the eutectic molten hydroxide of approximately 50^{o}C. The recorded reduction potentials for the reference electrodes used are tabulated in Table5.2. The results clearly show a positive shift in the working electrode potential with a molten salt temperature variation of 50^{o}C for the Ag and Pt electrodes.

Table 5.2 – The reduction potential and current of a 0.5mm platinum wire working electrode in the eutectic molten hydroxide at various temperatures; with 100 mV s^{-1} scan rate; CE: 5 mm diameter stainless steel rod; immersion depth: 14mm; an Ar gas atmosphere: 40cm^{3}min^{-1} (a) Ag wire; (b) RE: 0.5 mm Pt wire; (c) RE: Ni/Ni(OH)$_2$ in a mullite tube.

Reference electrode	**250^{o}C**		**300^{o}C**	
	Reduction potential (V)	Current limit (mA)	Reduction potential (V)	Current limit (mA)
Ag wire	-0.99	-0.95	-0.85	-0.52
Pt wire	-1.17	-0.29	-0.87	-0.49
Ni/Ni(OH)$_2$	-0.63	-117.37	-0.63	-224.50

Using the Ni/Ni(OH)$_2$ covered with the mullite membrane reference electrode on the other hand, shows only a slight positive shift in the reduction potential as displayed in Figure 5.11 at different operating temperatures and a scan rate of 100 mV s^{-1}.

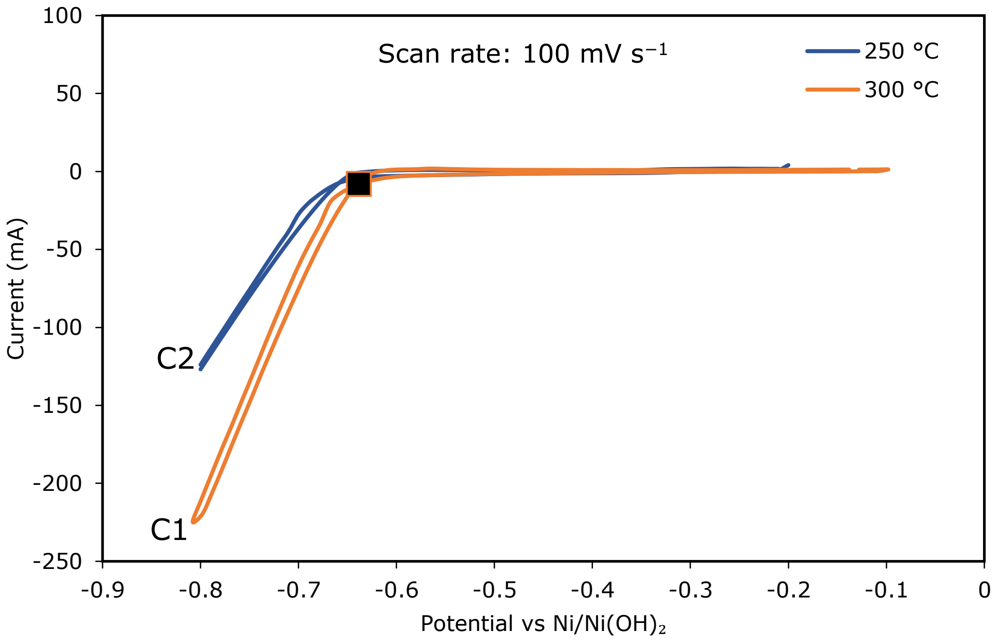

Figure 5.11 – Cyclic voltammograms of a 0.5 mm Pt wire working electrode in the eutectic molten hydroxide at different temperatures and a scan rate of 100 mV s^{-1}; CE: 5 mm diameter stainless steel rod; immersion depth: 14 mm; an Ar gas atmosphere: 40cm^{3}min^{-1}. RE: Ni/Ni(OH)$_2$ in a mullite tube.

The shift in the potential is positive but less than 0.02 V approximately. However, the cathodic limit current increased with an increase in the operating temperature of the eutectic molten hydroxide from -117.37 mA at 250^{o}C (point C2) to -224.62 mA at 300^{o}C (point C1). It can be noted here that the increase in the current of the cathodic limit slightly increased with an increase in the operating temperature. This significant increase in the current of cathodic limit is recorded in Table 5.2 and compared with the current of the cathodic limit of other reference electrodes (Ag and Pt). The results discussed further highlight the stability of the Ni/Ni(OH)$_2$ covered with mullite membrane reference electrode in the eutectic molten hydroxide. Chapter 6 of this thesis will thus study the behaviour of various working electrode materials using this reference electrode.

5.6 Presence of Steam in Eutectic Molten Hydroxide

All the cyclic voltammetry investigations discussed so far in this chapter were carried out in the eutectic molten hydroxide under a dry Ar atmosphere. Cyclic voltammetry investigations were hence carried out with the presence of steam to study this effect in the eutectic molten hydroxide on the kinetic activity of the working electrode potential. Firstly, argon gas was bubbled through hot H_2O at 70^oC. Subsequently, argon left the bottle loaded with H_2O. Then, this wet gas stream entered the retort which was already at a temperature >225^oC to convert the H_2O in the wet argon to steam, as described in Section 3.8, Chapter 3. The working electrode used was a platinum wire while the reference electrode used were Ag and Pt wires, and $Ni/Ni(OH)_2$ covered with a mullite membrane. The molten eutectic hydroxide operating temperature was 225^oC and the cyclic voltammetry CV scan rate was 100 mV s^{-1}. Figure 5.12 shows the cyclic voltammetry CV of the platinum working electrode obtained with the silver reference electrode with and without the presence steam.

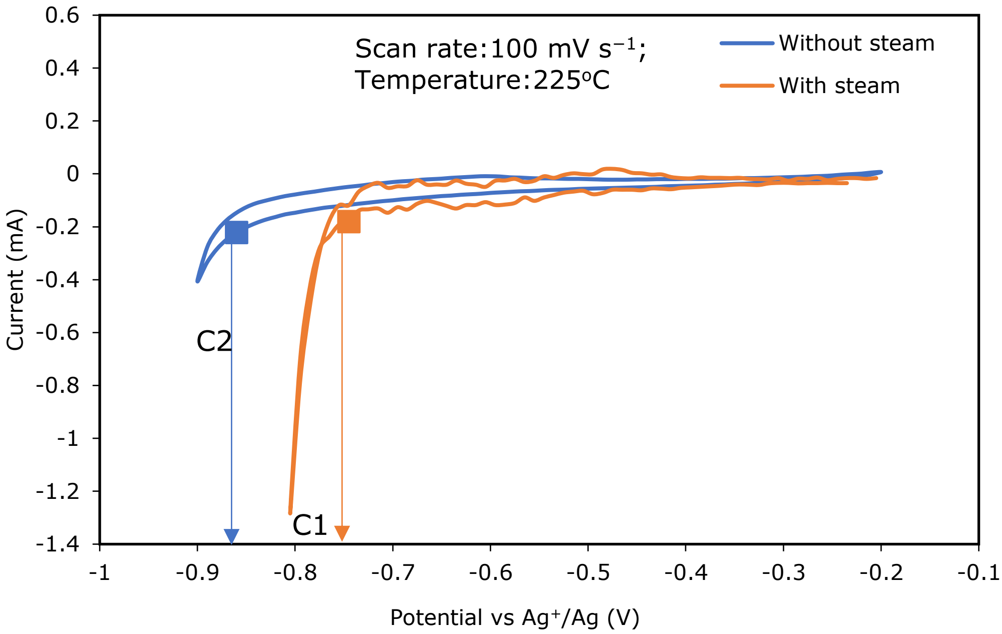

Figure 5.12 – Cyclic voltammograms of a 0.5 mm Pt wire working electrode in the eutectic molten hydroxide with and without steam at 225°C; CE: 5 mm diameter stainless steel rod; RE: 1.0 mm diameter Ag wire; immersion depth: 14 mm; an Ar gas atmosphere: 40cm^3 min^{-1}.

It is obvious from Figure 5.12 that the cathodic limit shifts positively with the presence of steam inside the eutectic molten hydroxide. The reduction potential without the presence of steam is -0.88 V and it shifts positively to -0.75 V with the presence of steam. As can be seen from the figure, a higher reduction current is also observed with the presence of steam inside the eutectic molten hydroxide. Table 5.3 summarises the reduction potential and the current at the cathodic limit achieved with and without the presence of steam insides the eutectic molten hydroxide. The current at the cathodic limit increases from -0.41 mA at C2 to -1.26 mA at C1 with the presence of steam. This increase in the current suggests that the presence of steam contributes to the reduction process and hence increases the production rate of hydrogen gas formed at the working electrode (cathode).

Figure 5.13 shows the platinum working electrode cyclic voltammetry with and without steam at the eutectic molten hydroxide operating temperature of 300°C using platinum wire as the quasi-reference electrode.

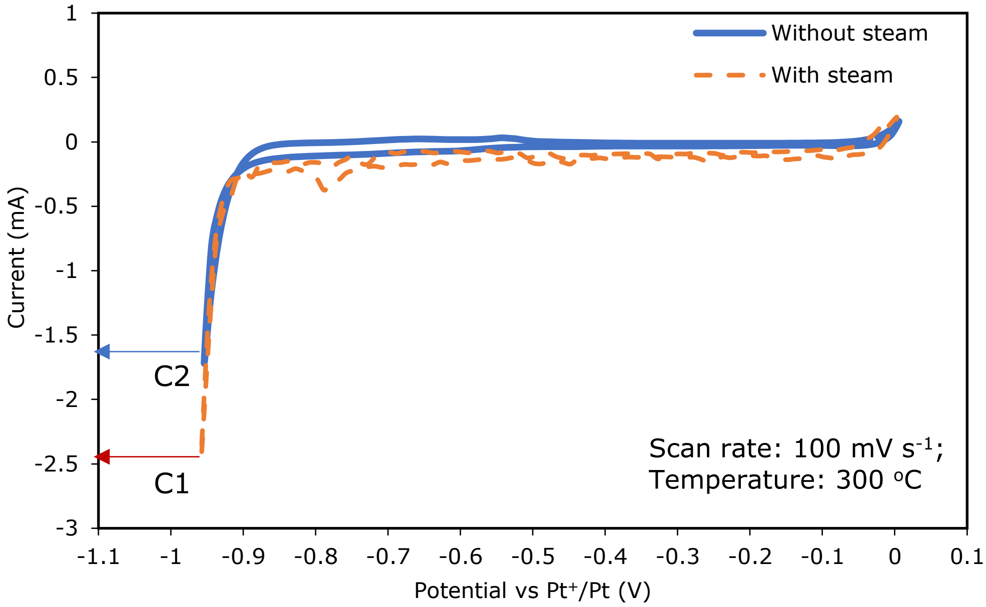

Figure 5.13 – Cyclic voltammograms of a 0.5 mm Pt wire working electrode in the eutectic molten hydroxide with and without steam at 300°C; CE: 5 mm diameter stainless steel rod; RE: 0.5 mm Pt wire; immersion depth: 14 mm; an Ar gas atmosphere: 40 cm^3 min^{-1}.

Unlike the silver electrode, the platinum reference electrode showed no obvious difference in the reduction potential with and without the presence of steam inside the eutectic molten hydroxide. In the presence of steam, however, the production rate of hydrogen gas likely increased as noticed by the increase in current at the cathodic limit C1 (see Figure 5.13). In this case, the current increases from -1.75mA (without steam at C2) to -2.5mA (with steam at C1) as reported also in Table 5.3.

Table 5.3 – The reduction potential and the current limit produced with and without the presence of steam in the eutectic molten hydroxide. WE: 0.5 mm Pt wire; CE: 5 mm Stainless steel rod; and RE:1mm Ag wire at 225°C, 0.5 mm Pt wire at 300°C and Ni/Ni(OH)$_2$ at 225°C; immersion depth: 14mm; an Ar gas atmosphere at 40cm^{3}min^{-1}.

Reference electrode	Without steam		With steam	
	Reduction potential (V)	Current limit (mA)	Reduction potential (V)	Current limit (mA)
Ag wire	-0.86	-0.41	-0.76	-1.28
Pt wire	-0.88	-1.57	-0.88	-2.45
Ni/Ni(OH)$_2$	-0.67	-196.01	-0.66	-217.50

Cyclic voltammetry scans using Ni/Ni(OH)$_2$ reference electrode are displayed in Figure 5.14. The operating temperature during the test was 225°C, the working electrode was Pt wire and the scan rate was maintained at 100 mV s^{-1}. The electrochemical behaviour of the working electrode was the same with and without presence steam as shown in Figure 5.14. The reduction potential for hydrogen gas formation in the two cases is still the same at -0.67 V. Therefore, the platinum working electrode controlled by the prepared Ni/Ni(OH)$_2$ reference electrode produces stable cyclic voltammetry results even when water is found in the eutectic molten hydroxide. In general, the presence of steam inside the eutectic molten hydroxide increases slightly the value of the cathodic limit current implying an increase in the yield of hydrogen gas. This stable reduction potential behaviour is also similar to that obtained using the platinum reference electrode. In terms of gas produced however, the cathodic current obtained when the Pt reference electrode was used is only -2.5 mA while that for the

$Ni/Ni(OH)_2$ electrode is -217.3 mA. This observed current indicates that the latter has a higher evolution of the hydrogen gas reaction than without the presence of steam. In other words, the $Ni/Ni(OH)_2$ covered with a mullite membrane reference electrode designed in this research has proven to be very stable in effectively controlling the potential of the Platinum working electrode. This leads to the high cathodic product (hydrogen gas).

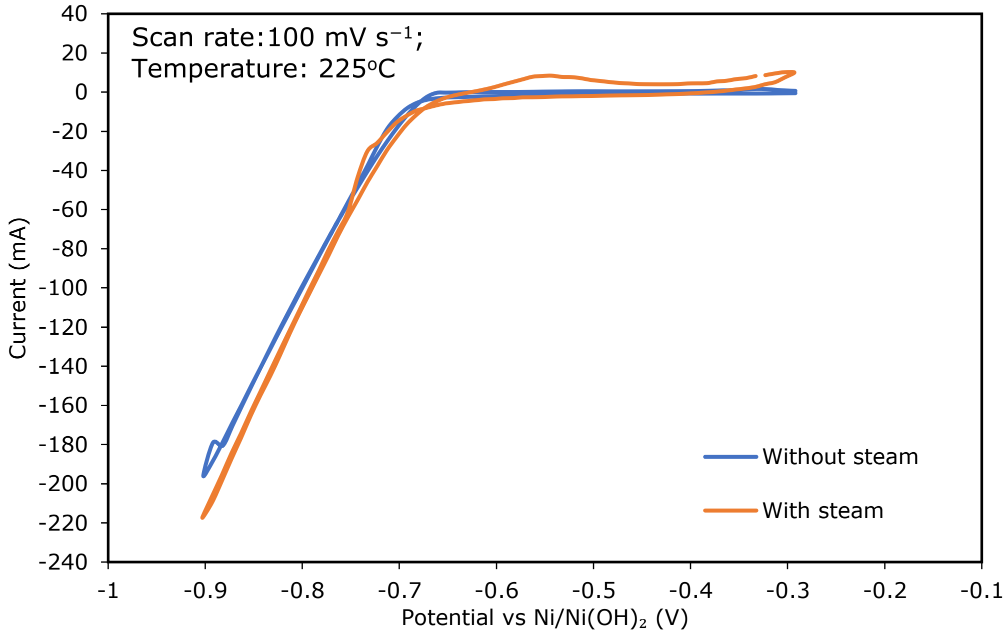

Figure 5.14 – Cyclic voltammograms of a 0.5 mm Pt wire working electrode in the eutectic molten hydroxide with and without steam at an operating temperature of 225°C and a scan rate of 100 mVs^{-1}; CE: 5mm diameter stainless steel rod; RE: $Ni/Ni(OH)_2$ in a mullite tube; Immersion Depth: 14mm; an Ar gas atmosphere: 40cm^{3}min^{-1}.

5.7 Summary

The findings of this chapter can be summarised as follows:

- Eutectic molten hydroxide (NaOH-KOH; 49-51 mol%) at 225°C is -1.96 V and this was calculated using HSC chemistry software (version6.1; outotec).
- The cyclic voltammetry investigation of the platinum working electrode using three different types of reference electrodes: Ag, Pt, $Ni/Ni(OH)_2$, showed that the platinum working electrode kinetics was more positive when it was controlled by the prepared nickel electrode under the same operating conditions.
- When the potential scan rate was changed, the current limit changed and this change in current confirmed that mass transport can occur under semi-infinite linear diffusion conditions at the cathodic limit of the platinum working electrode.
- One of the more significant findings to emerge from this study is that increasing the operating temperature of molten hydroxides by about 50°C influences the cyclic voltammetry results obtained using both silver and platinum reference electrodes. The reduction potential of the platinum working electrode using either silver or platinum reference electrode shifted positively. It was shifted about 0.13 V against the silver reference electrode and about 0.22 V against the platinum reference electrode. When the prepared $Ni/Ni(OH)_2$ covered with a mullite membrane was used as reference electrode however, only a slight positive shift of 0.02 V was observed. This suggests that it has good stability as temperature varies.
- The results also indicate that the prepared nickel and platinum reference electrode can be used to control the platinum working electrode, thereby

producing stable and reliable cyclic voltammetry results with and without the presence of steam in the eutectic molten hydroxide. The silver reference electrode, on the other hand, showed positive shifts of up to 0.1V in the reduction potential.

- The $Ni/Ni(OH)_2$ covered with a mullite membrane reference electrode designed in this research, has shown to be very stable in effectively controlling the potential of the Platinum working electrode. This subsequently leads to a high cathodic product yield (hydrogen gas). Therefore, effective control of the working electrode by the stable reference electrode directly contributes to increasing the hydrogen gas evolution reaction through constructing a stable ion channel.

CHAPTER 6

AN ELECTROCHEMICAL INVESTIGATION OF DIFFERENT WORKING ELECTRODES

6.1 Introduction

After the successful investigation into finding a suitable reference electrode for eutectic molten hydroxide (NaOH-KOH; 49-51 mol%) as explored in Chapter 5, it is imperative to extend the scope of the study through presenting a comparative study on different types of working electrodes. These working electrodes should possess the ability to conduct adequate catalytic activity for splitting water in eutectic molten hydroxide; resulting in the enhancement of reaction kinetics and a subsequent increase in the yield of hydrogen gas. The various working electrodes studied here are Ni, Pt, Ag, Mo and stainless steel wires.

Several studies have previously investigated the use of different working electrodes such as Ni, Pt, Ag, Mo or stainless steel. These metals were either investigated in molten hydroxide or in an aqueous solution of a hydroxide at low temperature. Even though these studies used a hydroxide in their investigation, the results generated were under different operating conditions and also used a different type of reference electrode to control the working electrode. For instance, Miles (2003) studied the electrochemistry of molten NaOH-KOH salt at 280^{o}C using platinum, nickel and silver as working electrodes and Ag^{+}/Ag as a reference electrode. The study of Ge et al. (2015) involved a cyclic voltammetry investigation using platinum wire, nickel wire and nickel oxide pellet as the working electrode in molten NaOH at 250^oC. A nickel rod was used as the reference electrode in this instance to study the electrochemical reaction mechanism of the reduction of NiO in the melt. Zabinski et al. (2003) employed a Co-Mo-C alloy to enhance the cathodic activity for electrolytic hydrogen evolution reaction (HER) in a hot alkaline solution 8 M of NaOH at 90^oC. This was also done to prevent the dissolution of molybdenum during open circuit immersion in the solution. Furthermore, the investigation of (Jayalakshmi et al., 2008) consisted of coating the stainless steel electrode with a Ni-Mo-Fe film to enhance catalytic activity for hydrogen evolution in the dilute alkali solution. When Ni, Co and NiCo were used as coatings to support a carbon felt electrode, this also resulted in enhanced catalytic activity for the hydrogen evolution reaction (HER) (Döner et al., 2012). However, the study of (Abouatallah et al., 2002) found that the nickel cathode deactivated during hydrogen evolution in alkaline water electrolysis and to reactivate it, vanadium oxide V_2O_5 was added to the alkaline solution. Even though vanadium is an effective activation agent, the resultant electrocatalytic activity of the modified nickel electrode was not higher than fresh nickel (Abouatallah et al., 2002). On the other hand, Yang et al. (2014) conducted a cyclic voltammetry investigation of the platinum working electrode regarding the presence of ammonia in the eutectic molten hydroxide.

Cyclic voltammetry and amperometry techniques were the two techniques used to investigate the electrocatalytic activity of the working electrodes in this study. This chapter aims to find cheaper, electrocatalytic working electrodes that can be used to increase the feasibility of hydrogen gas production in eutectic molten hydroxide.

6.2 Investigation of Different Working Electrodes by Cyclic Voltammetry

In this section cyclic voltammetry scans were performed for different working electrodes (e.g. Ni, Pt, Ag, Mo and SS) in eutectic molten hydroxide as explored below:

6.2.1 Cyclic voltammetry investigation of a nickel working electrode

Cyclic voltammetry was conducted on the blank nickel working electrode in the eutectic molten hydroxide at a temperature of 300^{o}C and a potential scan rate of 100 mV s^{-1} using the prepared nickel reference electrode. Figure 6.1a displays the obtained cyclic voltammetry full scan. Figure 6.2b shows cyclic voltammetry scanned from -0.8 V to -0.1 V vs Ni/Ni$(OH)_2$. The latter only focuses on the reduction limit.

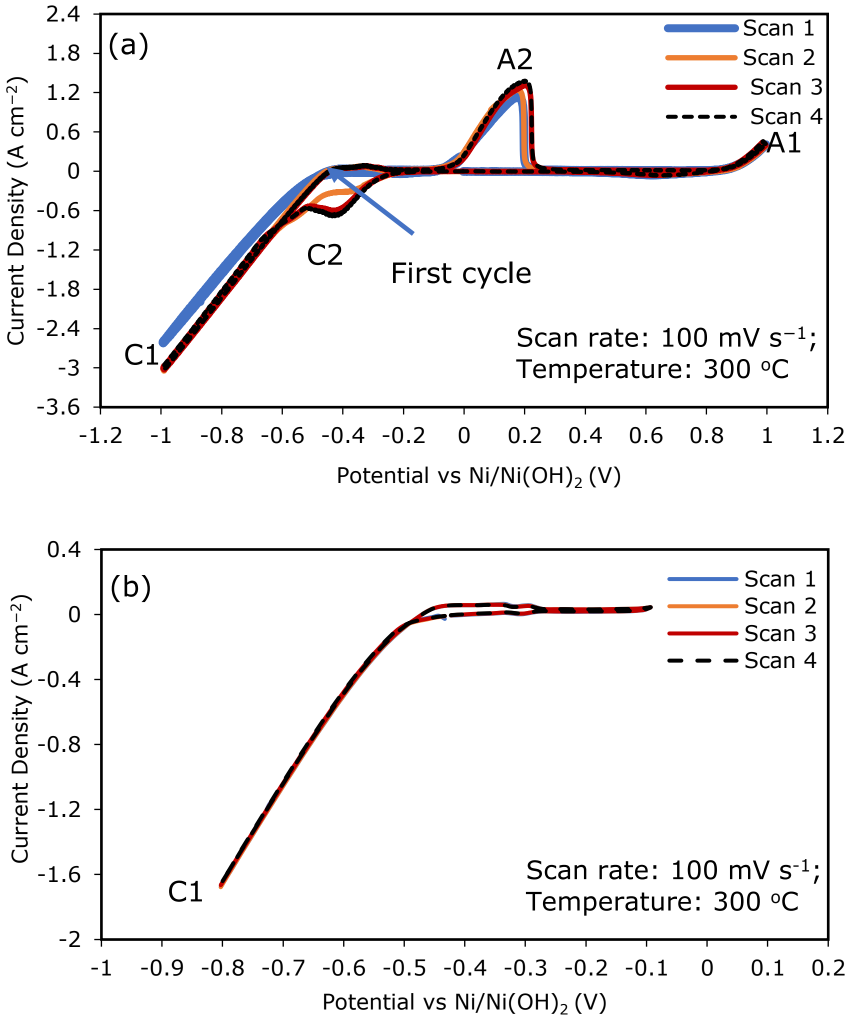

Figure 6.1 – Cyclic voltammograms of a 0.5 mm nickel working electrode in the eutectic molten hydroxide at a temperature of 300°C. RE: Ni/Ni(OH)$_2$; CE: 5 mm stainless steel rod; atmosphere of Ar gas at 40 cm^{3}min^{-1}; the immersion depth : 14 mm; scan rate: 100mVs^{-1}, (a) Scan negatively between -1.0 and 1.0 V, (b) Limiting the scan between -0.8 and -0.1 V.

A couple of redox peaks can be easily observed as shown in Figure 6.1a. The cathodic current peak C2 is attributed to the reduction of the thin oxide film formed on the surface of the Ni wire, and the anodic current peak of A2 is due to its oxidation. In addition, the reduction potential started at -0.465V likely corresponds to the evolution of hydrogen gas (Cox and Fray, 2008, Ge et al., 2015) and the corresponding reaction is shown in Figure6.1a and expressed as reaction (6.1). The peak A1 is assigned to the generation of oxygen gas as seen in Figure6.1a and represented as reaction (6.2).

$$2\ H_2O + 2e^- \rightarrow H_2(g) + 2\ OH^- \qquad \textbf{(6.1)}$$

$$2\ OH^- \rightarrow \tfrac{1}{2} O_2(g) + H_2O + 2\ e^- \qquad \textbf{(6.2)}$$

The peak C2 (Figure 6.1a) has a potential of -0.37 V which is barely visible compared to peak A2 during the first potential cycle (Figure 6.1a). This phenomenon can be attributed to the redox reactions of the Ni electrode in the eutectic molten hydroxides (Ge et al., 2015). The peak A2 represents the oxidation of Ni wire in the eutectic molten hydroxide, which may lead to the accumulation of a thin oxide film on the nickel surface. Consequently, the peak C2 should show the reduction of the oxide film. When the potential range is limited between -0.8 V and -0.1 V, the peak C2 disappears as in Figure 6.1b due to the lack of oxidation of the nickel wire.

The disappearance of the reduction peak C2 as shown in Figure 6.1a, reveals that no distinct reduction peak during the potential scan was confirmed when the scan was limited as shown in Figure 6.1b. In order to understand this phenomenon, the decomposition potential of water and nickel oxide at a temperature of 300^{o}C was calculated using HSC 6.0 software following the reactions (6.3 and 6.4). The calculated results reveal that the two decomposition potentials of the reactions are very close, indicating that those reactions may take place simultaneously during the cathodic sweep. This finding agrees with (Ge et al., 2015) who stated that the decomposition potentials of water and nickel oxide at 550^{o}C were very close.

$$H_2O \rightarrow H_2(g) + \frac{1}{2}O_2(g) \quad (E = -1.013\ V) \tag{6.3}$$

$$2\ NiO \rightarrow 2\ Ni + O_2(g) \quad (E = -0.965\ V) \tag{6.4}$$

6.2.1.1 Effect of changing potential scan rate

Further understanding of the reaction activity of the nickel wire in the eutectic molten hydroxide can be conducted by changing the potential scan rate of the cyclic voltammetry test. It was changed from 50 to 150 mV s^{-1} at a temperature of 300°C as shown in Figure 6.2a. It can be observed from the figure that the current reduction peak C2 decreased with slowing potential scan rates. This phenomenon also influenced the oxidation current of peak A2 which decreased with a slowing of the potential scan rate. The current density of the reduction peak C2 decreased from 0.915 to 0.49Acm^{-2}, while the current density of the oxidation peak A2 decreased from 1.95 to 1.46 A cm^{-2} with slowing scan rate from 150 to 50 mV s^{-1}. These decreases in the current densities at C2 and A2 with a slower scan rate was favourable to this study because the nickel started to act as an inert electrode with the absence of formation of a thin nickel oxide film. When the potential scan is limited between -0.8 V and -0.1 V at a scan rate ranging from 50 to 150 mVs^{-1}, the cathodic peak C2 in Figure 6.2b disappears. Since the potential scan already exists in a range post the oxidation peak A2 which corresponds to the oxidation of nickel wire, the reduction peak C2 disappears. The phenomenon thus confirms that the reduction peak C2 corresponds to the reduction of nickel oxide formed at A2.

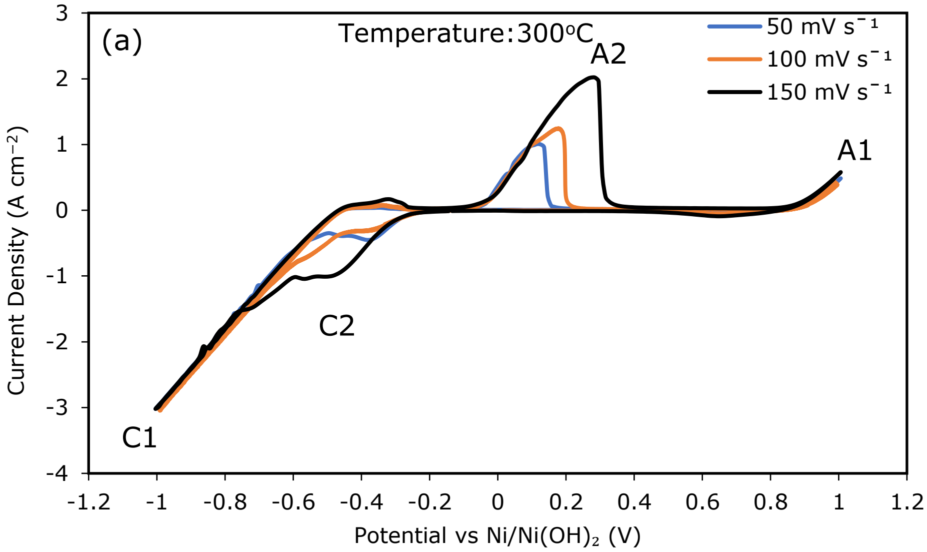

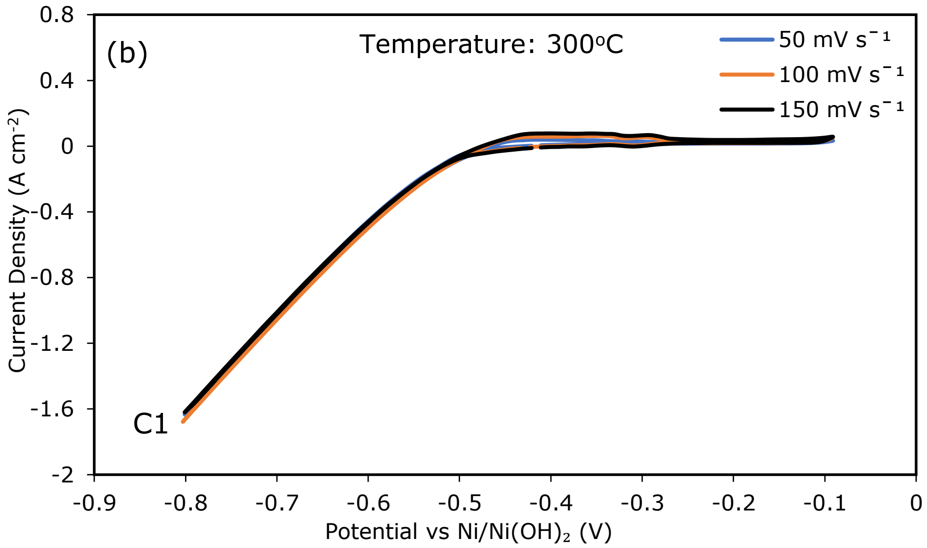

Figure 6.2 – Cyclic voltammograms of a 0.5 mm nickel wire in the eutectic molten hydroxide with different scan rate at 300°C. RE: $Ni/Ni(OH)_2$ in the mullite tube membrane; CE: 5 mm stainless steel rod; immersion depth: 14mm; an Ar gas atmosphere: 40cm^{3}min^{-1}. (a) Scans conducted negatively from -1.0 and 1.0 V, (b) Limiting the potential scan between -0.8 and -0.1 V.

6.2.1.2 Effect of changing (NaOH-KOH) temperature

The effect of changing the operating temperature of the eutectic molten hydroxide on the nickel electrode kinetics activity is shown in Figure 6.3a was also studied. The studied temperatures were 225 and 300°C respectively.

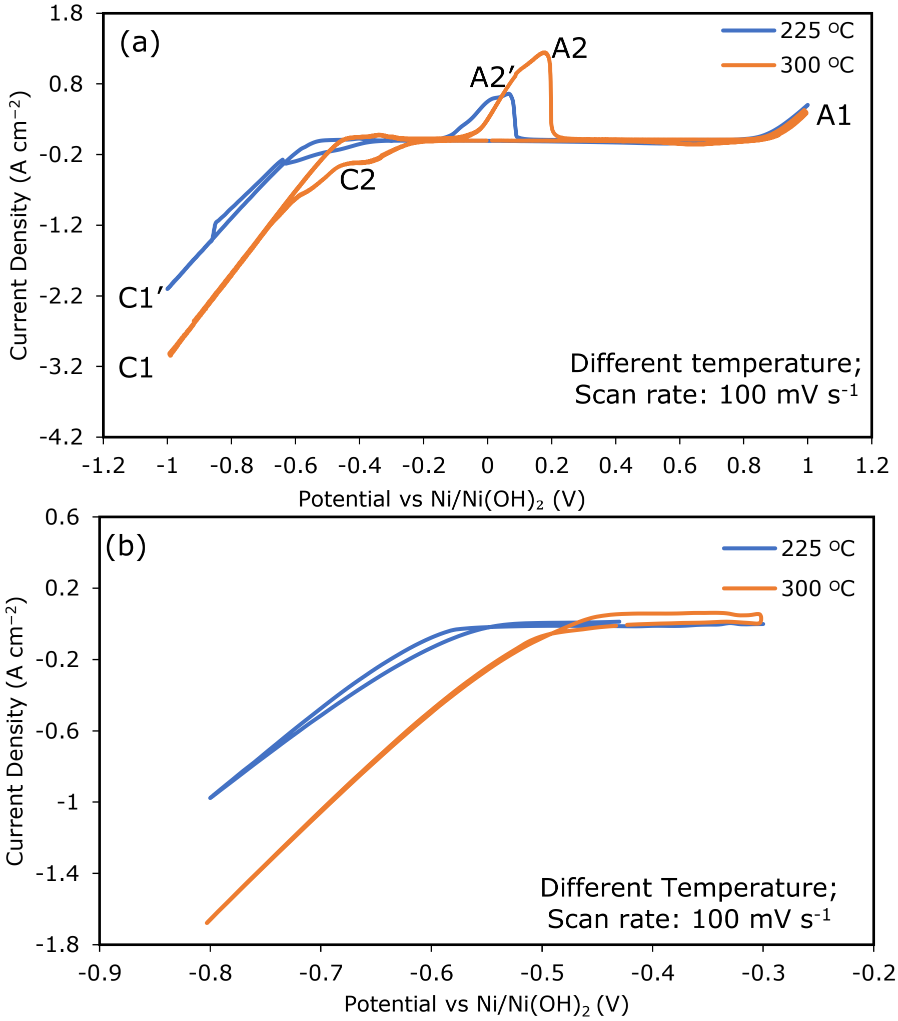

Figure 6.3 – Cyclic voltammograms of a 0.5 mm nickel wire in the eutectic molten hydroxide at a scan rate of 100 mV s^{-1} and different operating temperature. RE: $Ni/Ni(OH)_2$ in the mullite tube membrane; CE: 5 mm stainless steel rod; immersion depth: 14mm; an Ar gas atmosphere: 40$cm^3 min^{-1}$. (a) Potential scanned negatively between -1.0 and 1.0 V, (b) Limiting the potential scan between -0.8 and -0.3 V.

It is obvious from Figure 6.3a that the oxidation peak A2 shifts negatively to A2′ when the operating temperature decreases from 300 to 225^{o}C. This negative shift in the oxidation peak is followed by a negative shift in the reduction peak C2 and C1 respectively. Furthermore, the current density of the oxidation peak A2 decreases with a reduction in the operating temperature and this directly influences the kinetic activity of the nickel electrode activity which results in the formation of a nickel oxide thin film at A2. The cathodic potential limit C1 also shifts negatively to C1′ and its current density reduces with decreasing temperature. By limiting the potential scan between -0.8 and -0.3 V, it is easy to observe the effect of changing the operating temperature on the evolution of hydrogen gas at C1, as shown in Figure 6.3 b. It can be concluded that the evolution of hydrogen gas becomes more efficient and sees an increase with increasing temperature.

6.2.1.3 Effect of the presence of steam

Figure 6.4 shows the cyclic voltammetry of the nickel working electrode at a temperature of 300^{o}C and scan rate of 100 mV s^{-1} with and without the presence of steam in the eutectic molten hydroxide. It is clear that no significant change in the anodic peak A2 (oxidation of Ni) is observed with the presence of steam inside the eutectic molten hydroxide as shown in Figure 6.4a. The current density of the cathodic limit increases from -1.6 A cm^{-2} to -2.09 A cm^{-2} with the presence of steam. In order to exhibit the effect of the presence of steam in increasing the evolution of hydrogen gas, the potential scan is limited between -0.8 and -0.3 V as shown in Figure 6.4b. It is obvious from the figure that the reduction potential for the evolution of hydrogen gas is the same with and without steam.

However, the effect of steam can be recognised by increasing the current density limit for the evolution of hydrogen gas. The increase in the current density represents the amount of steam that exists inside the eutectic molten hydroxide and contributed to an increase in the yield of the hydrogen gas.

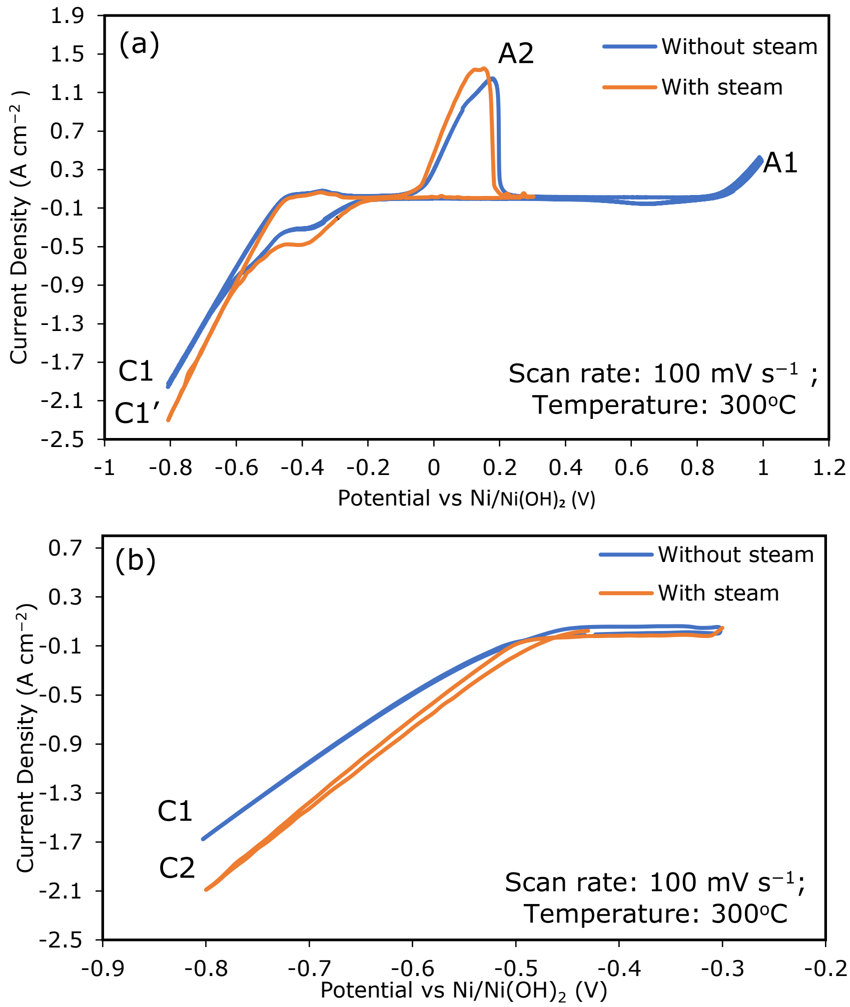

Figure 6.4 – Cyclic voltammograms of a 0.5 mm nickel wire in the eutectic molten hydroxide with 100 mV s^{-1} of scan rate at temperature of 300°C. RE: Ni/Ni(OH)$_2$ in the mullite tube membrane; CE: 5 mm stainless steel rod; immersion depth: 14mm; an Ar gas atmosphere: 40 cm^{3}min^{-1}. (a) Scan negatively from -0.8 to 1.0 V without steam, (b) Limiting the potential scan between -0.8 and -0.3 V.

6.2.2 Cyclic voltammetry investigation of a platinum working electrode

Most electrochemical studies use platinum as a working electrode in molten hydroxides to achieve reliable results because of its relatively high chemical stability (Ge et al., 2015). Figure 6.5a shows the cyclic voltammetry of the platinum working electrode in the eutectic molten hydroxide at a temperature of 300°C and scan rate of 100 mV s^{-1}.

It can be observed from Figure 6.5a that the anodic limit A1 of the system is due to oxidation of the eutectic molten hydroxides (Híveš et al., 2006) as in reaction (6.5).

$$2OH^- \rightarrow \tfrac{1}{2}O_2(g) + H_2O + 2\,e^- \qquad \textbf{(6.5)}$$

While the reduction of the water, formed at the anode, derives the cathodic limit C1 (Híveš et al., 2006) as in reaction (6.6).

$$H_2O + e^- \rightarrow \tfrac{1}{2}H_2(g) + OH^- \qquad \textbf{(6.6)}$$

Therefore the corresponding potential for hydrogen gas evolution at C2 is -0.44 V. The potential scan is limited between -0.8 and -0.3 V to focus the scan on the cathodic limit as shown in Figure 6.5b. When the potential scan range is limited, the scan is still stable but the reduction potential shifts negatively to a value about 0.04 V smaller than the full scan. Furthermore, the potential scan rate varies for the purposes of testing the platinum working electrode in the eutectic molten hydroxide at a temperature of 300°C.

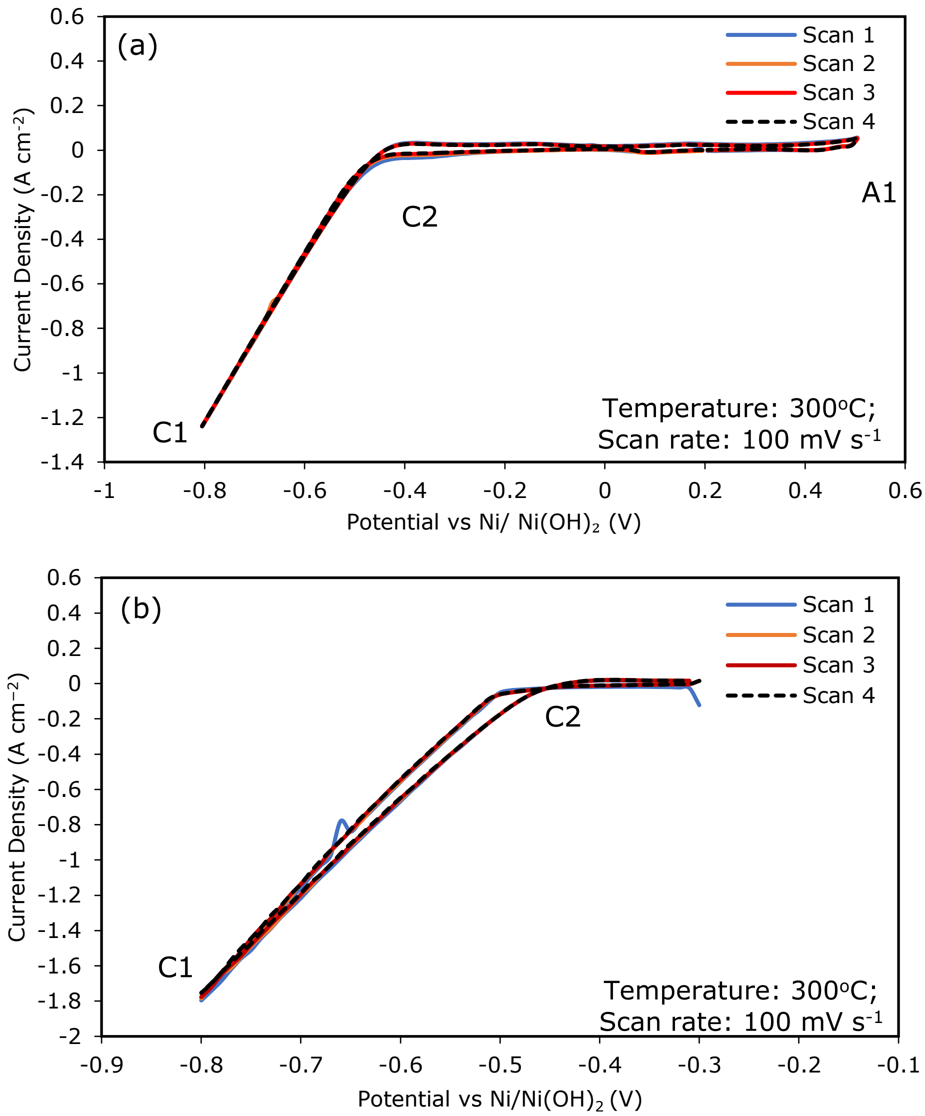

Figure 6.5 – Cyclic voltammograms of a 0.5 mm Platinum working electrode in the eutectic molten hydroxide at a temperature of 300°C. RE: $Ni/Ni(OH)_2$; CE: 5 mm SS rod; an Ar gas atmosphere at 40cm^{3}min^{-1}; the immersion depth: 14mm; Scan rate: 100 mV s^{-1}.

The range of the scan rate speed is fixed between 50 and 150 mV s^{-1} to test its electrostability in the eutectic molten hydroxide as shown in Figure6.6. Although the scan rate speed is altered, no significant change can be observed from the plot. This confirms the notion that the platinum acts as an inert electrode irrespective of the scan rate being slow or fast.

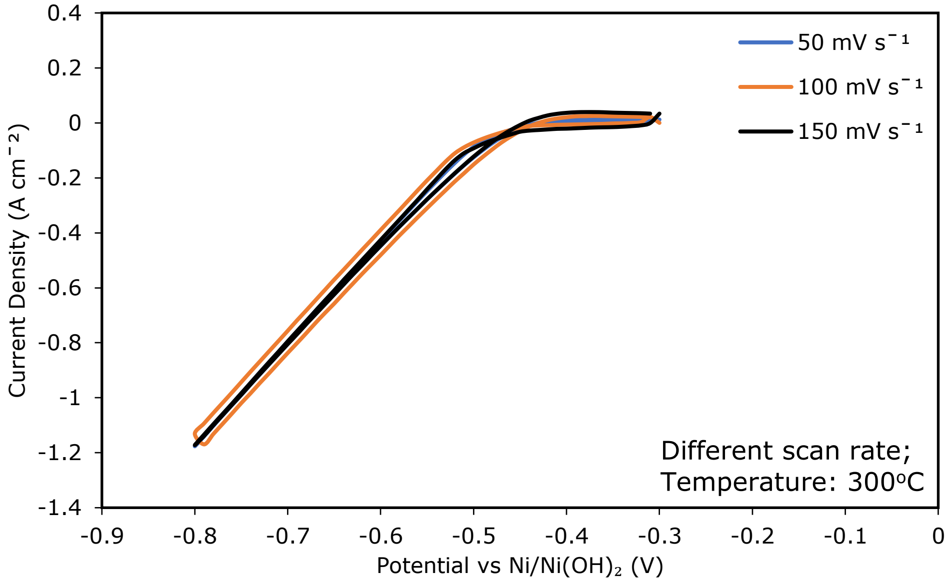

Figure 6.6 – Cyclic voltammograms of a 0.5 mm Platinum working electrode in the eutectic molten hydroxide with different scan rate, the potential scanned negatively between -0.8 and -0.3 V at 300°C. RE: Ni/Ni(OH)$_2$ in the mullite tube membrane; CE: 5 mm stainless steel rod; immersion depth: 14mm; an Ar gas atmosphere: 40cm^{3}min^{-1}.

The cyclic voltammetry of the platinum working electrode in the eutectic molten hydroxide was also performed at a temperature of 225°C and a scan rate of 100 mV s^{-1}. The obtained scan is compared with the scan at a temperature of 300°C as shown in Figure 6.7a.

At low temperature, a small reduction in the peak C2' appears around 0.38V. This reduction peak corresponds to the reduction of PtO$_x$ film formed during the anodic potential scan on the platinum working electrode surface (Híveš et al., 2006). However, this reduction peak C2' does not appear at 300°C. At a temperature of 225°C, the cathodic limit C1' shifts negatively to -0.54 V. Furthermore, it can be observed from Figure 6.7a, that the current density at cathodic limit C1 decreases with a reduction in the operating temperature. This implies a lowering in the evolution of hydrogen.

In order to improve the clarity of the results, the cyclic voltammetry scan is fixed between -0.8 and -0.1 V at different operating temperature (225, 300°C) as shown in Figure 6.7b. It is noticeable that increasing the operating temperature results in positively shifting the reduction potential from -0.55 to -0.44 V and increasing the current density at C1 from 0.75 to 1.13 mA cm^{-2}.

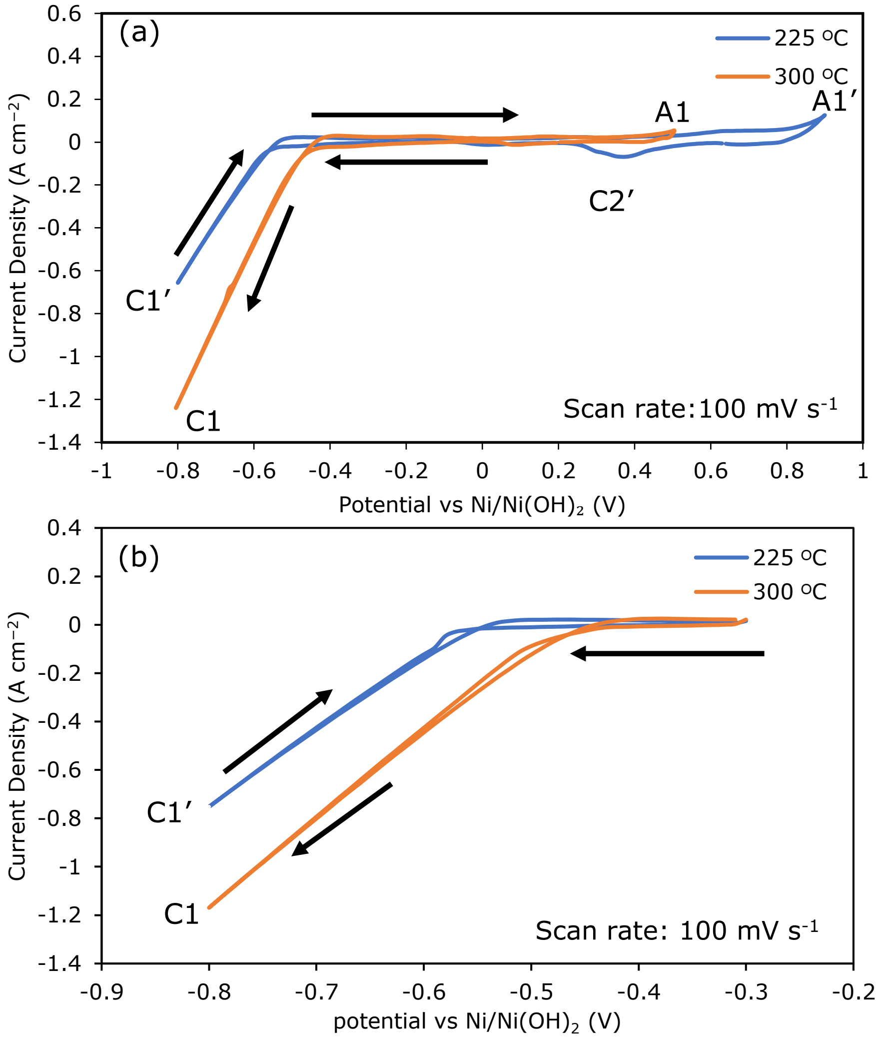

Figure 6.7 – Cyclic voltammograms of a 0.5 mm platinum working electrode in the eutectic molten hydroxide at a scan rate of 100mVs^{-1} and at a different operating temperature. RE: Ni/Ni$(OH)_2$ in the mullite tube membrane; CE: 5 mm stainless steel rod; immersion depth: 14 mm; an Ar gas atmosphere: 40 cm^3 min^{-1}. (a) Scan negatively from -0.8 to 0.9 V at 225°C and from -0.8 and -0.6 V at 300°C, (b) Limiting the scan between -0.8 and -0.3 V.

Furthermore to the above factors, it is imperative as well to study the effect of the presence of steam inside the eutectic molten hydroxide using platinum wire as the working electrode. The reason for investigating this factor is to understand its effect on the behaviour of the platinum working electrode. The cyclic voltammogram scan can translate this change to the behaviour of the electrode. Figure 6.8 shows the cyclic voltammogram scan in the eutectic molten hydroxide using platinum as a working electrode at 300^{o}C with and without the presence of steam inside the eutectic molten hydroxide. The cyclic voltammetry scan compares the influence of the presences of steam inside the eutectic molten hydroxide with the cyclic voltammetry scan without steam as shown in Figure 6.8a at a temperature of 300^{o}C and a scan rate of 100 mV s^{-1}. The presence of steam inside the eutectic molten hydroxide directly affects the obtained cyclic voltammetry scan by increasing the flow of current density at the cathodic limit from 1.16 mA cm^{-2} at C1 to 1.82 mA cm^{-2} at C1′. For more clarification, the cyclic voltammetry scans are limited between -0.8 to -0.3 V with and without presence steam in the eutectic molten hydroxide, as shown in Figure 6.8 b. There is no change in the cyclic voltammetry scan due to this limitation. The presence of steam merely influences the scan by increasing the current density limit of C1 to C1′ which represents the reaction of the evolution of hydrogen gas. Even though the platinum electrode is a stable metal in a eutectic molten hydroxide at high temperatures; it still has limited use in the industry because it is classified as a precious metal (Couper et al., 1990).

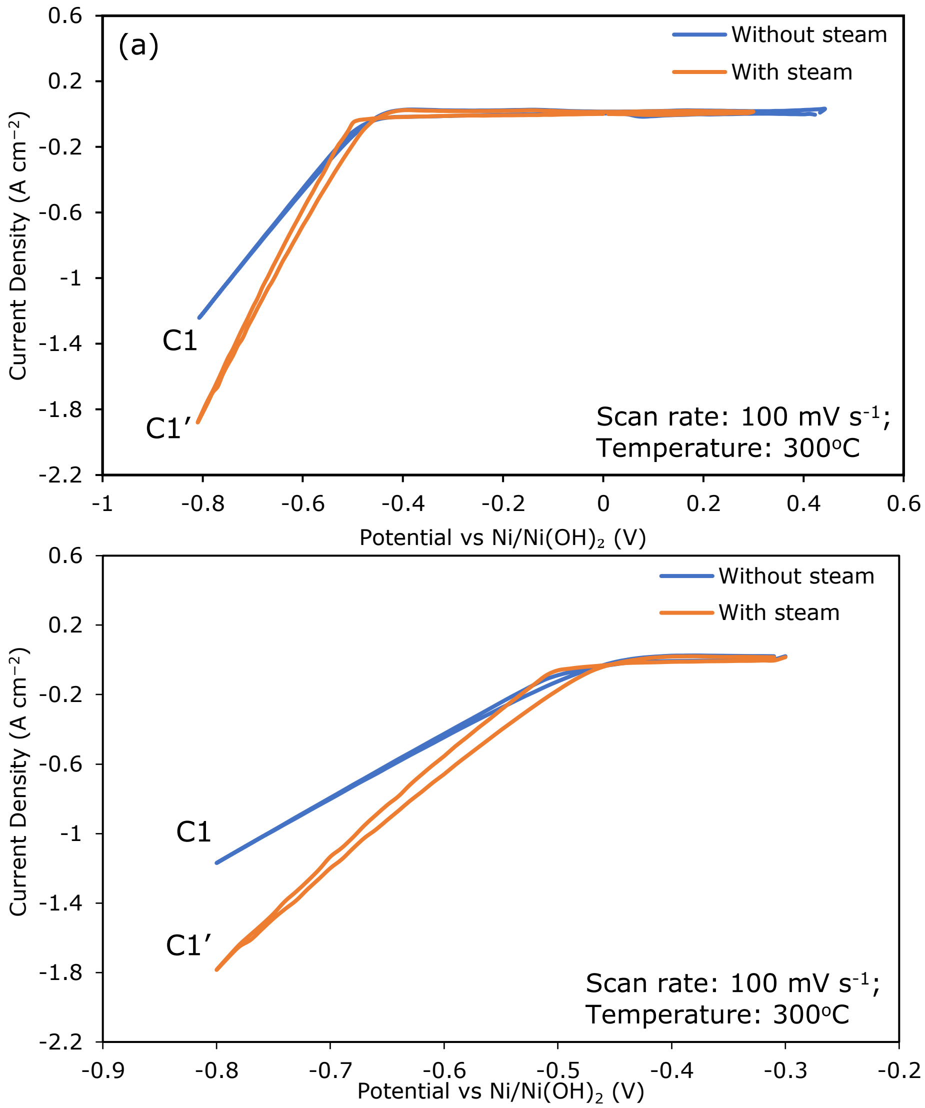

Figure 6.8 – Cyclic voltammograms of a 0.5mm platinum working electrode in the eutectic molten hydroxide at 100mVs^{-1} of scan rate and at an operating temperature of 300°C. RE: Ni/Ni(OH)$_2$ in the mullite tube membrane; CE: 5 mm stainless steel rod; immersion depth: 14mm; an Ar gas atmosphere: 40 cm^{3}min^{-1}. (a) Scan negatively between -0.8 and 0.5V with and without steam between -0.8 to 0.3V, (b) Limiting the scan between -0.8 and -0.3 V.

6.2.3 Cyclic voltammetry investigation of a silver working electrode

The blank cyclic voltammetry scan is also recorded for a silver working electrode in the eutectic molten hydroxide. It is performed in the eutectic molten hydroxide at an operating temperature of 300°C and scan rate of 100 mV s^{-1} as shown in Figure 6.9a.

Literature is scarce regarding the exact nature of the silver wire reaction in the hydroxide. For example, the study conducted by Miles (2003) reported that the reaction of the silver wire in the molten hydroxides may involve $Ag^{+} \rightarrow Ag$, $AgO_2 \rightarrow Ag + O_2$ or some other silver electrode reaction. Therefore, this study of the silver working electrode has been based on Miles (2003)'s findings.

The recorded cyclic voltammetry of the silver working electrode in the eutectic molten hydroxide shows a couple of redox peaks as displayed in Figure 6.10a. Therefore, the anodic peak A2 may be attributed to the oxidation of the silver wire surface which forms a thin film of silver oxide. Subsequently, the cathodic peak C2 is attributed to the reduction of the thin oxide film formed on the surface of the silver wire. In addition, the cathodically increased current of C1 at -0.52 V corresponds to the evolution of hydrogen gas (Cox and Fray, 2008) and the corresponding reaction is shown as reaction (6.7). Reaction (6.8) represents the generation of oxygen gas as appears in peak A1 of Figure 6.10a.

$$2\,H_2O + 2e^- \rightarrow H_2(g) + 2\,OH^- \qquad \textbf{(6.7)}$$

$$2\,OH^- \rightarrow \tfrac{1}{2}O_2(g) + H_2O + 2\,e^- \qquad \textbf{(6.8)}$$

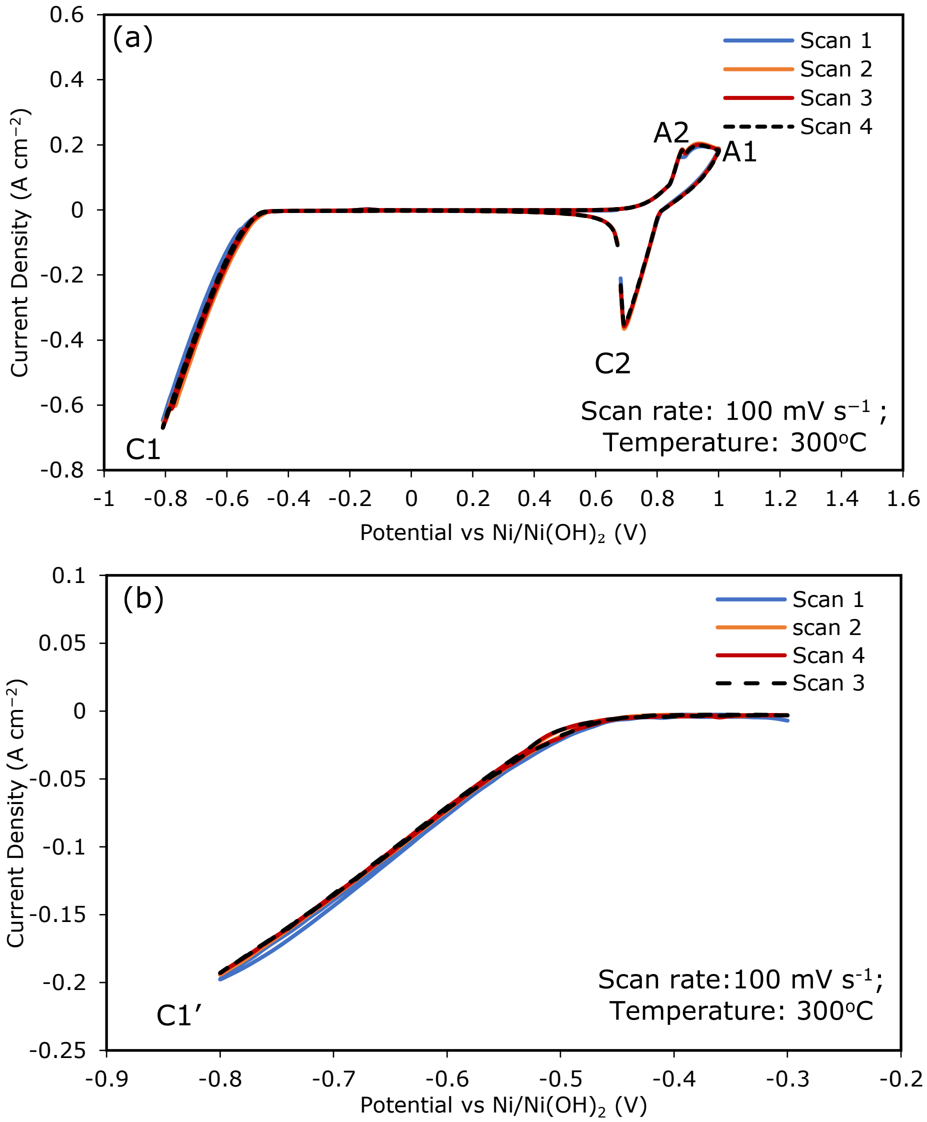

Figure 6.9 – Cyclic voltammograms of a 1.0 mm silver working electrode in the eutectic molten hydroxide at scan rate of 100mVs^{-1} and operating temperature of 300°C. RE: Ni/Ni(OH)$_2$; CE: 5 mm stainless steel rod; an Ar gas atmosphere of 40 cm^3 min^{-1}; the immersion depth: 14 mm; a) Scan negatively from -0.8 to 1.0 V, (b) Limiting the scan between -0.8 and -0.3 V.

Subsequently, the cyclic voltammetry scan is limited between -0.8 and -0.3V as shown in Figure 6.9b to emphasise on the cathodic limit of the evolution of hydrogen gas. It can be observed from the Figure 6.9b that during the period when the cyclic voltammetry scan is limited, there is no significant change in the starting point of the potential at the cathodic limit. It can also be observed that the current density at C1' decreased. The current density at the cathodic peak C1 (Figure 6.9a) is roughly about -0.61 A cm^{-2}, decreasing to approximately -0.18 A cm^{-2} at C1' (Figure 6.9b) when the potential scan is limited. The disappearance of the oxidation peak A2 and the reduction peak C2 when the potential scan is limited is because the scan starts at potential more negative than the oxidation potential of silver wire (or consequently, the reduction potential of silver oxide). If this is the case, the decrease in the current density of C1' should be proportional to the reduction of silver oxide to silver. Therefore, it should be mentioned that the silver oxide does not completely reduce at C2, but its reduction is completed at C1 simultaneously with the evolution of hydrogen reaction as seen in Figure 6.9a. This conclusion is based on a noticeable increase in the current density, which otherwise decreases when the potential scan is limited.

The influence of changing the potential scan rate speed on the silver working electrode in the eutectic molten hydroxide is shown in Figure 6.10. The cyclic voltammetry scans were conducted between -0.8 and -0.3 V at a temperature of 300^{o}C.

No significant change can be observed from the cyclic voltammetry scan of the silver working electrode with a change in the scan rate speed as shown in Figure 6.10. In contrast, stable scans are produced even though the speed of scan rates was varied. This inert behaviour of silver wire in the eutectic molten hydroxide takes place because the used potential range for the scan occurs after any reaction that can occur on the silver wire. The effect of changing the operating temperature of the eutectic molten hydroxide on the cyclic voltammetry scan of the silver working electrode is seen in Figure 6.11. The behaviour of the scan was studied at an operating temperature of 225 and 300°C and performed at a scan rate of 100mVs^{-1}.

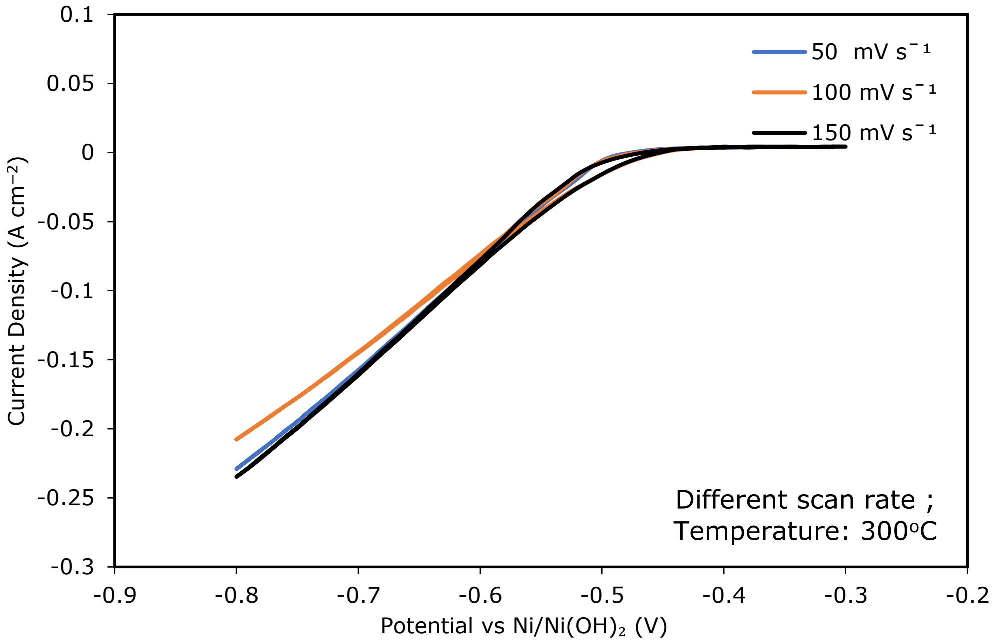

Figure 6.10 – Cyclic voltammograms of a 1.0 mm silver working electrode in the eutectic molten hydroxide at a different scan rate and a temperature of 300°C. RE: Ni/Ni(OH)$_2$; CE: 5 mm stainless steel rod, immersion depth: 14mm, an Ar gas atmosphere: 40cm^{3}min^{-1}.

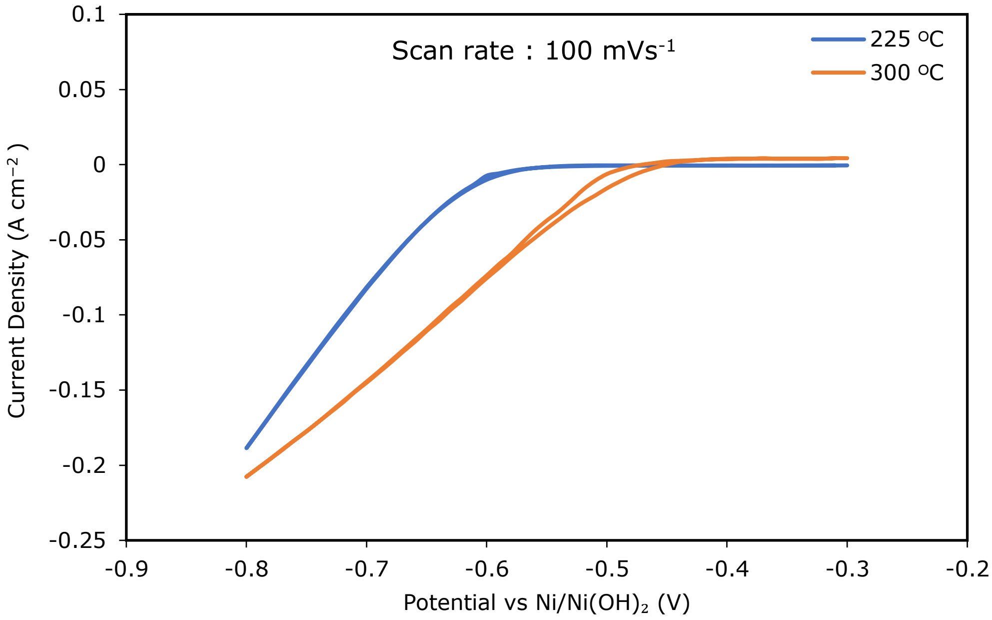

Figure 6.11 – Cyclic voltammograms of a 1.0mm silver working electrode in the eutectic molten hydroxide at a scan rate of 100mVs^{-1} and different operating temperature. RE: Ni/Ni$(OH)_2$; CE: 5 mm stainless steel rod; immersion depth: 14mm; an Ar gas atmosphere: 40cm^3 min^{-1}.

It is obvious from Figure 6.11 that the reaction encompassing the evolution of hydrogen gas at a high temperature happens at a faster rate than the low operating temperature of the eutectic molten hydroxide. Alternately, the reduction potential at cathodic limit shifts positively from -0.6 V at 225^{o}C to the -0.47 V at 300^{o}C (an approximate 0.13 V difference). This means that the electrocatalytic kinetics of the silver working electrode increases with increasing temperature.

Figure 6.12 shows the effect of Introducing steam inside the eutectic molten hydroxide at a temperature of 300^{o}C and a scan rate of 100 mV s^{-1} on the cathodic limit for the evolution of hydrogen gas reaction.

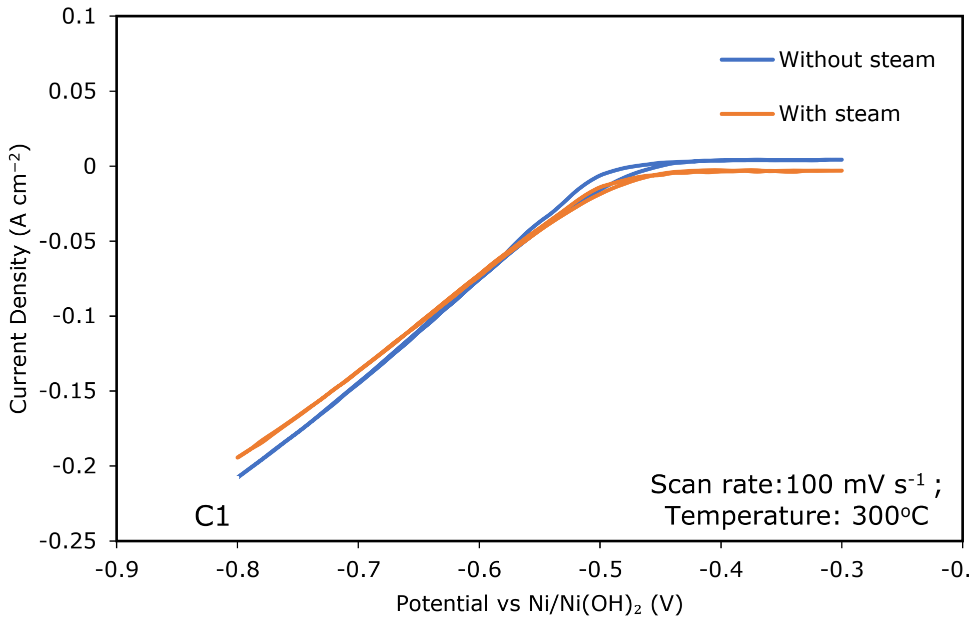

Figure 6.12 – Cyclic voltammograms of a 1.0 mm silver working electrode in the eutectic molten hydroxide at 100mVs^{-1} of a scan rate and temperature of 300^{o}C. RE: Ni/Ni(OH)$_2$; CE: 5 mm stainless steel rod; immersion depth: 14mm; an Ar gas atmosphere: 40cm^{3}min^{-1}. Scan negatively from -0.8 to -0.3 V with and without presence steam.

The presence of steam inside the eutectic molten hydroxide did not affect the reduction potential of the evolution hydrogen gas reaction as shown in Figure 6.12. Thus, the same scan was produced without steam as well. This stable behaviour of the scan can be attributed to how the silver working electrode in the eutectic molten hydroxide is stable.

6.2.4 Cyclic voltammetry investigation of a molybdenum working electrode

Molybdenum is one of the transition metals. It has good electrocatalytic capacity for enhancing the activity of other metals such as nickel (Jayalakshmi et al., 2008). Due to the electroactivity of the molybdenum, it was investigated as working electrode in this study. Figure 6.13a and b show the cyclic voltammetry of the molybdenum working electrode inside the eutectic molten hydroxide at 300^{o}C and a speed scan rate of 100mVs^{-1}.

It can be observed from Figure 6.13a, that the electrochemical stability window is between A and A′ (approximately 0.33 V). Cathodically, an increase in the current of C1 at -0.8 V should correspond to the evolution of hydrogen gas (Cox and Fray, 2008). The corresponding reaction is shown in reaction (6.9). While anodically, an increase in the current at A1 corresponds to the evolution of oxygen gas and the corresponding reaction is shown as reaction (6.10).

$$2\,\mathrm{H_2O} + 2\,\mathrm{e^-} \rightarrow \mathrm{H_2(g)} + 2\,\mathrm{OH^-} \qquad \textbf{(6.9)}$$

$$2\,\mathrm{OH^-} \rightarrow \tfrac{1}{2}\,\mathrm{O_2(g)} + \mathrm{H_2O} + 2\,\mathrm{e^-} \qquad \textbf{(6.10)}$$

The subsequent cyclic voltammetry scan is limited between -0.8 and -0.2V as shown in Figure 6.13b to focus on the evolution of the hydrogen gas reaction. Therefore, no change in the reduction peak can be noticed if the scan range is limited to the potential located after the potential of the oxidation peak A′ reaction takes place.

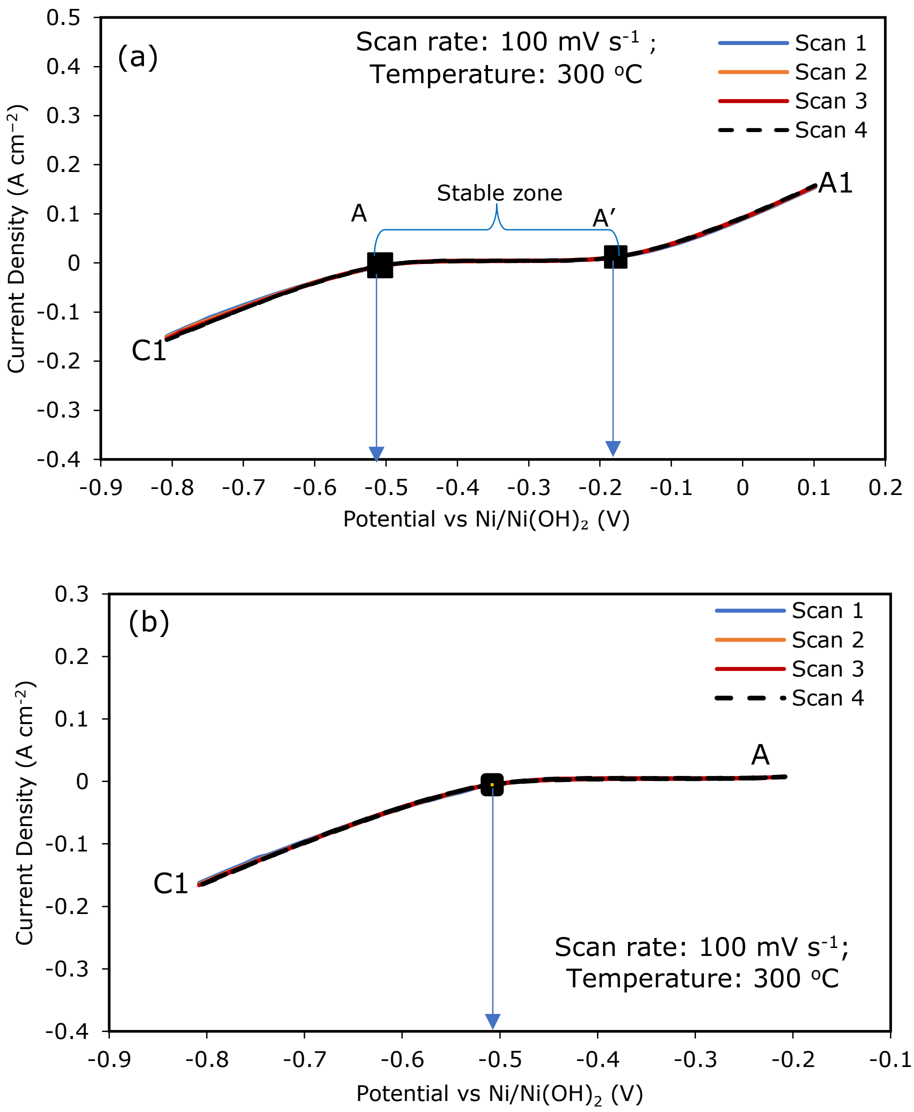

Figure 6.13 – Cyclic voltammograms of a 1.0 mm molybdenum working electrode in the eutectic molten hydroxide at a temperature of 300°C and a scan rate of 100 mV s^{-1}. RE: $Ni/Ni(OH)_2$; CE: 5mm stainless steel rod; an Ar gas atmosphere at 40$cm^3 min^{-1}$; the immersion depth: 14 mm; (a) Scan negatively from -0.8 to 0.1V, (b) Limiting the scan between -0.8 and -0.2 V.

Further insight into the electro-catalytic effect of the molybdenum working electrode reaction in the eutectic molten hydroxide can be observed by changing the potential scan rate speed. It is varied from 50 to 150 mV s^{-1} at an operating temperature of 300°C as shown in Figure 6.14. The electrocatalytic activity of the molybdenum working electrode is not affected by changing the speed of the potential scan rate. In contrast, the performed scans are stable in nature and the evolution of the hydrogen gas reaction happens at the same reduction potential even though the speed of scan rate changes as seen in Figure 6.14.

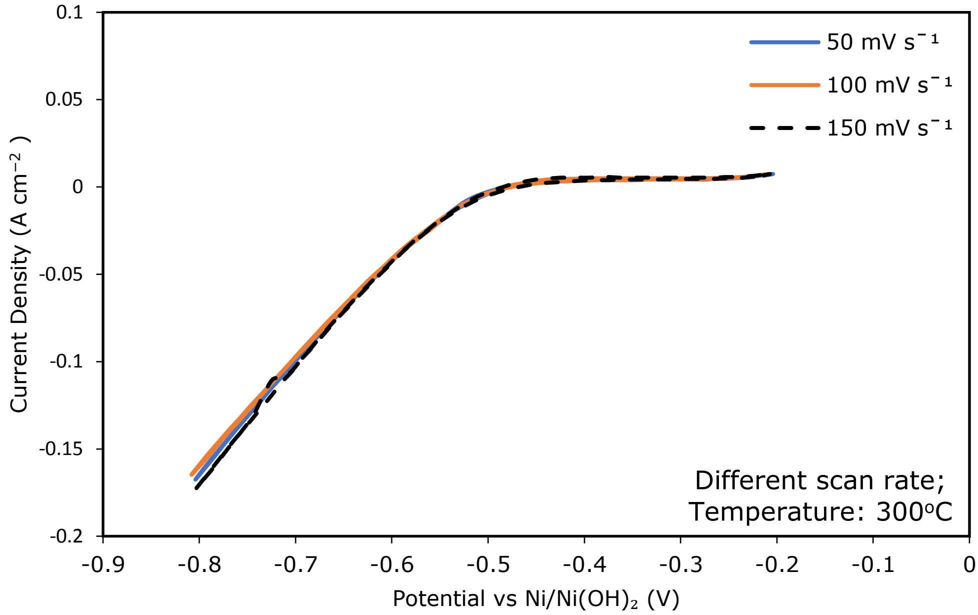

Figure 6.14 – Cyclic voltammograms of a 1.0 mm molybdenum working electrode in the eutectic molten hydroxide at a different scan rate and at a temperature of 300°C. RE: Ni/Ni(OH)$_2$; CE: 5mm stainless steel rod; immersion depth: 14mm; an Ar gas atmosphere: 40cm^{3}min^{-1}.

The effect of changing the operating temperature of the eutectic molten hydroxide on the molybdenum working electrode is shown in Figure 6.15a and b. At the anodic limit, there is no change that can be observed on the oxidation potential at -0.116 V as displayed in Figure 6.15a. Alternately, the current density of the evolution of the oxygen gas increases approximately from 0.156 A cm^{-2} at A1 to 0.635 A cm^{-2} at A1′. In contrast, the increase in the operating temperature of the eutectic molten hydroxide significantly affects the evolution of the hydrogen gas potential. The potential shifts positively with an increase in the temperature from -0.66V at 225°C to -0.49V at 300°C. In addition, this increase in the temperature not only influences the reduction potential but also contributes to increasing the current density of the evolution of hydrogen gas from -0.086 A cm^{-2} at C1' to 0.145 Acm^{-2} at C1. However, when the cyclic voltammetry scan range is limited to between -0.8 and -0.3 V as shown in Figure 6.15b, the observed current density at cathodic limits at C1 and C1' for the evolution of hydrogen gas reaction is similar at both low and high temperatures respectively. On the other hand, the reduction potential at the cathodic limit for the evolution hydrogen gas reaction does not change even when the scan is limited.

The effect of the presences of steam inside the eutectic molten hydroxide on the molybdenum working electrode electrocatalytic behaviour for increasing the hydrogen and oxygen gas evolution respectively, is also considered. Figure 6.16a, and b show the comparison of the cyclic voltammetry scans of the molybdenum working electrode with and without the presence of steam at an operating temperature of 300°C and scan rate of 100 mV s^{-1}.

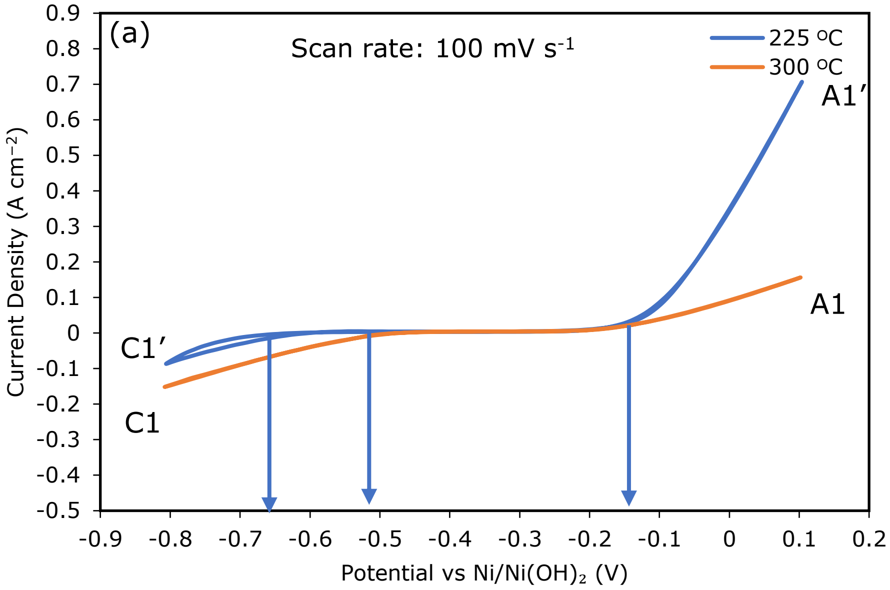

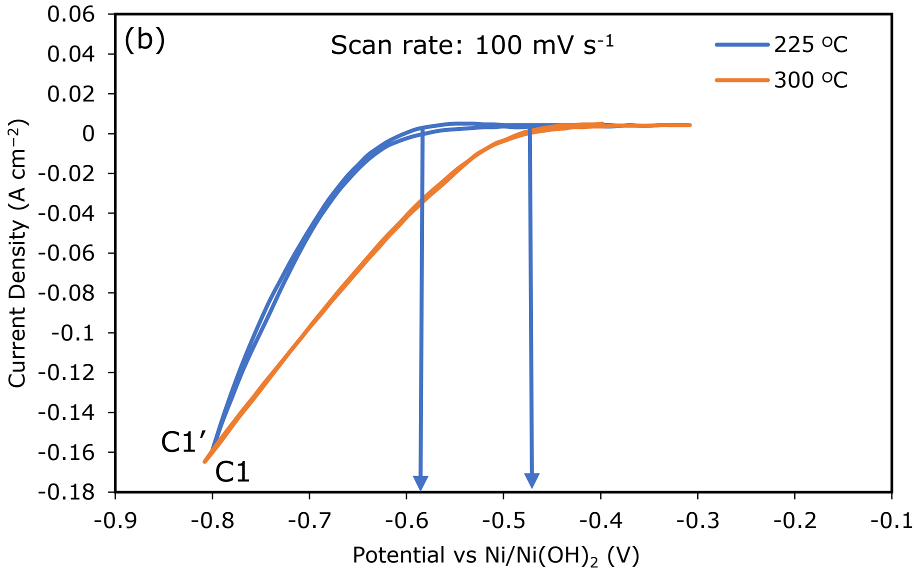

Figure 6.15 – Cyclic voltammograms of a 1.0 mm molybdenum working electrode in the eutectic molten hydroxide at a scan rate of 100mVs^{-1} and at different operating temperature. RE: Ni/Ni(OH)$_2$; CE: 5mm stainless steel rod; immersion depth: 14mm; an Ar gas atmosphere: 40 cm^{3}min^{-1}. (a) Scan between -0.8 and 0.1V (b) Limiting the scan between -0.8 and -0.3 V at 225 and 300^{o}C.

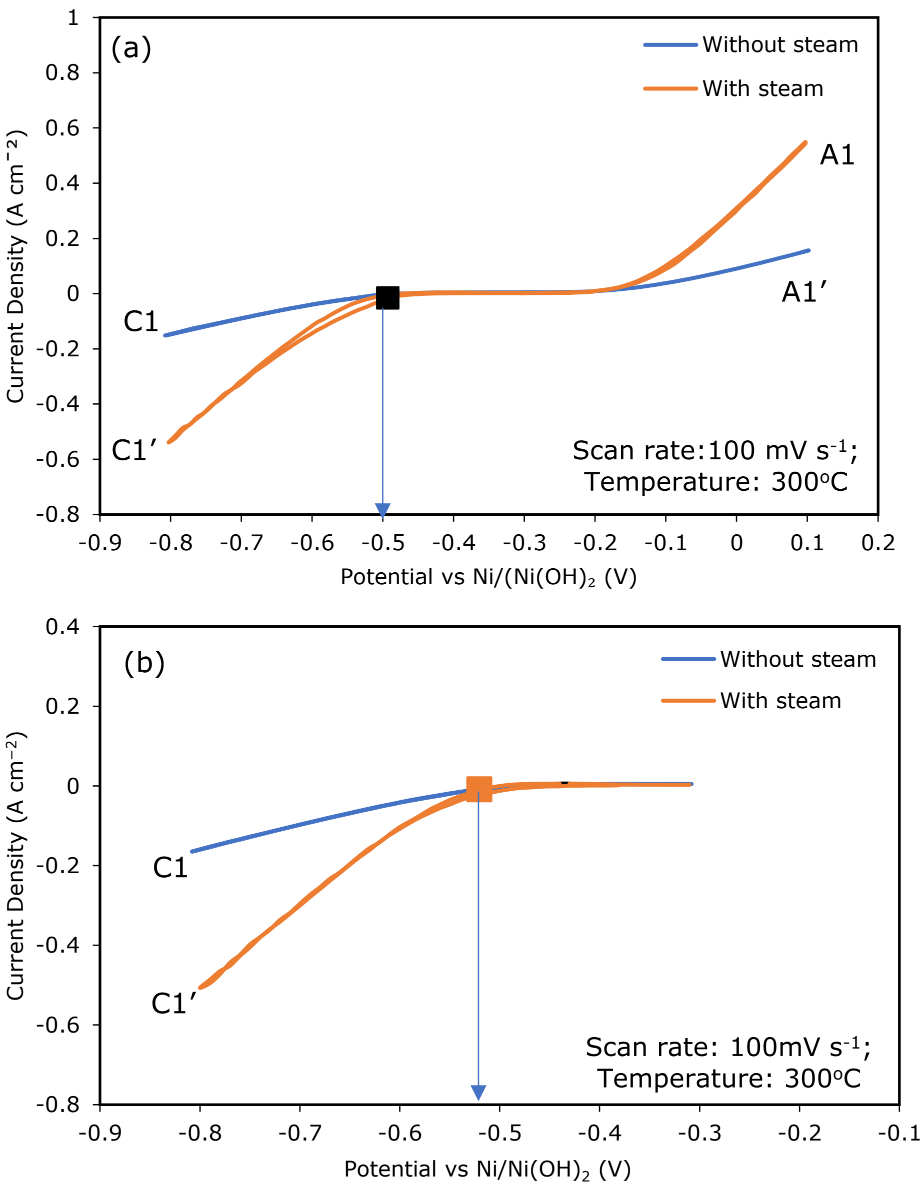

Figure 6.16 – Cyclic voltammograms of a 1 mm molybdenum working electrode in the eutectic molten hydroxide at a scan rate of 100 mV s^{-1} and a temperature of 300°C. RE: Ni/Ni(OH)$_2$; CE: 5mm stainless steel rod; immersion depth: 14mm; an Ar gas atmosphere: 40 cm^{3}min^{-1}. (a) Scan between -0.8 and 0.1 V, (b) Limiting the Scan between -0.8 and -0.3 V without steam and with steam.

It is obvious from Figure 6.16a that the effect of the presence of steam is apparent in increasing the current density of the evolution of hydrogen gas at the cathodic limit C1′, and the simultaneous evolution of oxygen gas at the anodic limit A1′. At the cathodic limit, the current density increases from -0.12 A cm^{-2} without the presence steam at point C1 to -0.49 A cm^{-2} with the presence of steam at point C1′. At the anodic limit, the current density increases from 0.14 A cm^{-2} without the presence of steam at point A1 to 0.465 A cm^{-2} with the presence of steam at point A1′. In order to clarify the effect of the presence of steam on increasing the current density of the evolution of hydrogen gas reaction, the cyclic voltammetry scan is limited between -0.8 and -0.3 V respectively as shown in Figure 6.16b. It is very clear from constraining the scan range that there is a considerable effect of the presence of steam in increasing the current density of the evolution of hydrogen gas reaction. It increases from -0.164Acm^{-2} at C1 to -0.51Acm^{-2} at C1′. This result is shown in Figure 6.16b through the increase of the molybdenum metal activity with the presence of steam inside the eutectic molten hydroxide and makes a significant change on the evolution of the hydrogen gas reaction.

6.2.5 Cyclic voltammetry investigation of a stainless steel working electrode

A stainless steel (302) is composed of iron, nickel, chromium, manganese, silicon, carbon, phosphorus and sulphur. It was used in this study as a working electrode to examine its stability and productivity in the eutectic molten hydroxide. Figure 6.17a shows a cyclic voltammetry scan at an operating temperature of 300^{o}C and a scan rate of 100 mV s^{-1}.

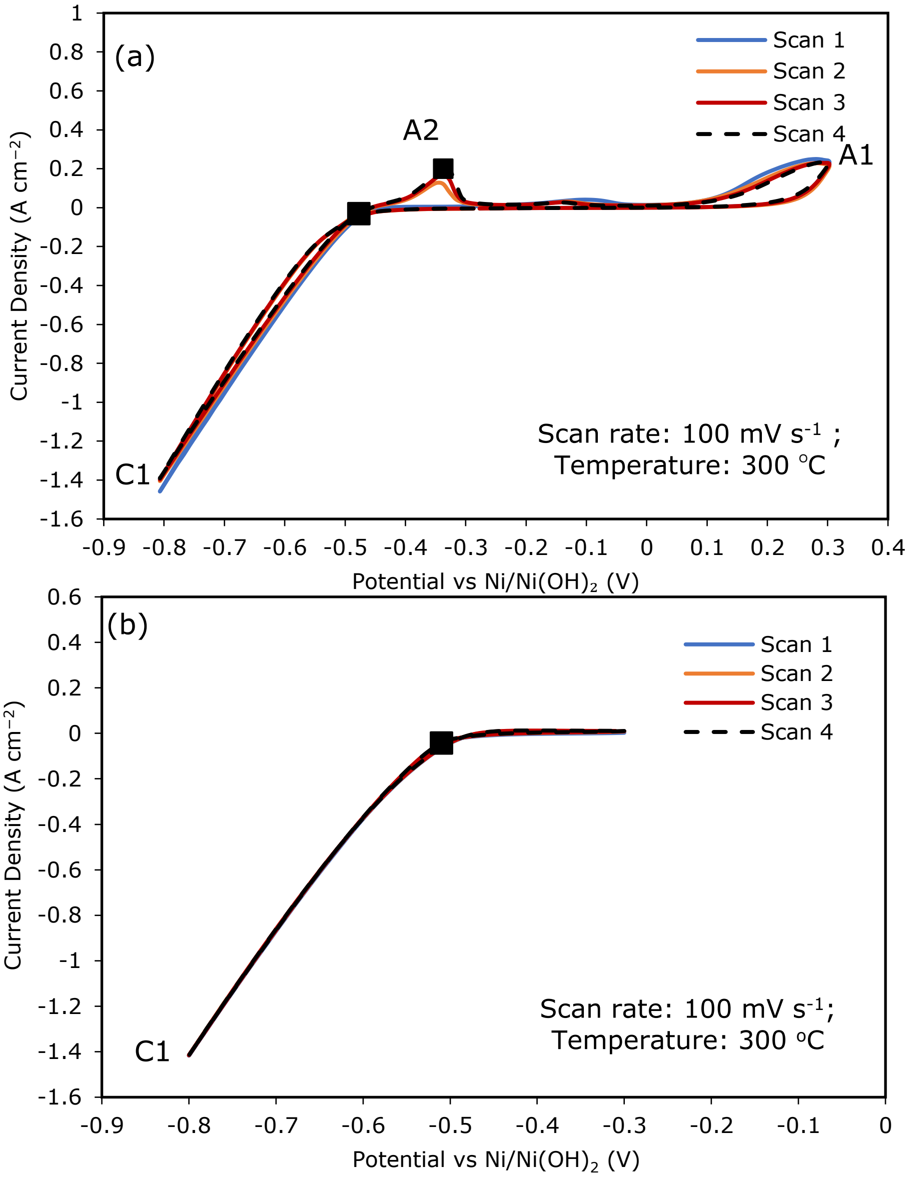

Figure 6.17 – Cyclic voltammograms of a 0.25 mm stainless steel working electrode in the eutectic molten hydroxide at a temperature of 300°C. RE: Ni/Ni(OH)$_2$; CE: 5 mm stainless steel rod; an atmosphere of Ar at 40cm^{3}min^{-1} ; the immersion depth:14mm; Scan rate: 100 mV s^{-1}, (a) Scan negatively from -0.8 to 0.3 V, (b) Limiting the scan between -0.8 and -0.3 V.

At the anodic limit A1, the corresponding peak is due to the oxidation of the melt (2 OH^- → 0.5 O_2 (g) + H_2O + 2 e^-) while the reduction of the water formed at the anodic limit is seen at the cathodic limit C1. The corresponding reaction of the reduction water becomes:

$$H_2O + e^- \rightarrow \frac{1}{2} H_2(g) + OH^- \quad \textbf{(6.11)}$$

In the case of the oxidation peak A2, it corresponds to the oxidation occurring on the surface of the stainless steel working electrode and the potential of oxidation observed at -0.33 V. Subsequently, the CV scan is limited to a range between -0.8 V and -0.3 V in order to focus the scan on the cathodic limit for the hydrogen evolution reaction as shown in Figure6.17b. No change in the reduction potential which starts at -0.5 V, and the current at the cathodic limit C1 which approximately equals -1.4 A cm^{-2}; is discernible. The oxidation peak A2 disappears when the CV scan is limited, even though the potential of the return scan is positive prior to A2 peak. Cyclic voltammetry scans were also recorded using the stainless steel working electrode at different scan rate speeds that range between 50 and 150 mV s^{-1} and at an operating temperature of 300^{o}C. The potential scan is fixed between -0.8 V to -0.3 V as shown in Figure 6.18. The performed CVs were stable even though the speed of the scan rate is changed as shown in Figure 6.18. This stable performed scan is attributed to the stable behaviour of the stainless steel working electrode in the eutectic molten hydroxide.

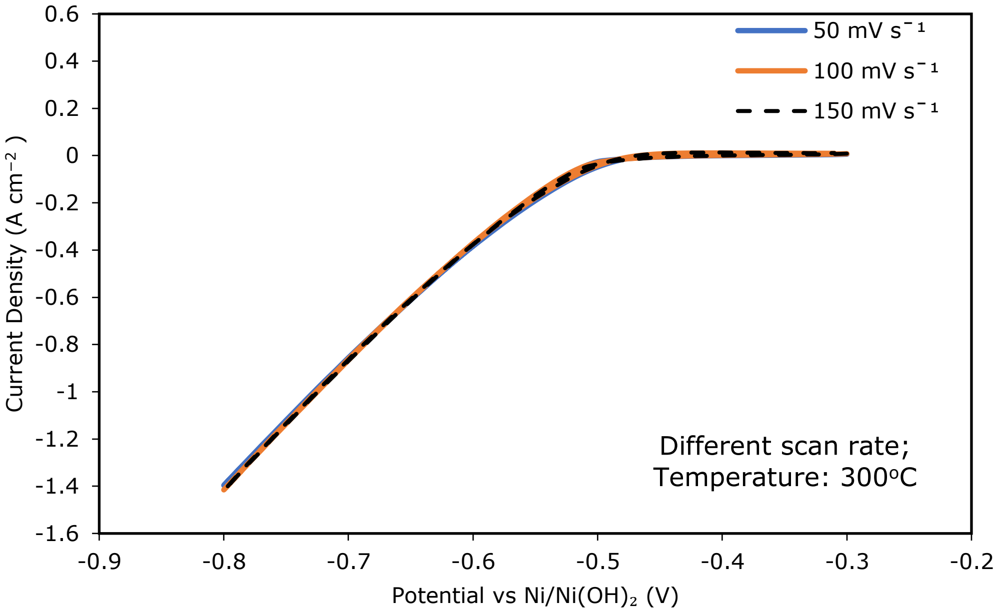

Figure 6.18 – Cyclic voltammograms of a 0.25 mm stainless steel working electrode in the eutectic molten hydroxide with different scan rate at 300°C. RE: Ni/Ni(OH)$_2$ in the mullite tube membrane; CE: 5 mm stainless steel rod; immersion depth: 14 mm; an Ar gas atmosphere: 40 cm^{3}min^{-1}.

However, when the operating temperature of the eutectic molten hydroxide was increased; a significant change can be observed from the cyclic voltammetry scan as displayed in Figure 6.19a. It can be observed from the Figure 6.19a that the reduction potential shifted positively by approximately 0.2 V when the operating temperature was increased by 75°C. The current density also increased from -0.33 A cm^{-2} at cathodic limit C1′ to -1.4 A cm^{-2} at the cathodic limit C1 with an increase in the operating temperature. The oxidation peak also increased and shifted positively from A2′ to A2 while no change can be observed at the anodic limit A1 with an increase in temperature. Cyclic voltammetry scan was limited between -0.8V and -0.3V even at a different operating temperature as shown in Figure 6.19b. The oxidation peak A2 at 300 °C disappeared when the scan was limited. Alternately, the oxidation peak A2′ at 225°C was still formed even when the scan was limited. The disappearance of the oxidation peak A2 at high temperatures happened because the potential scan range occurred before the oxidation peak reaction could begin.

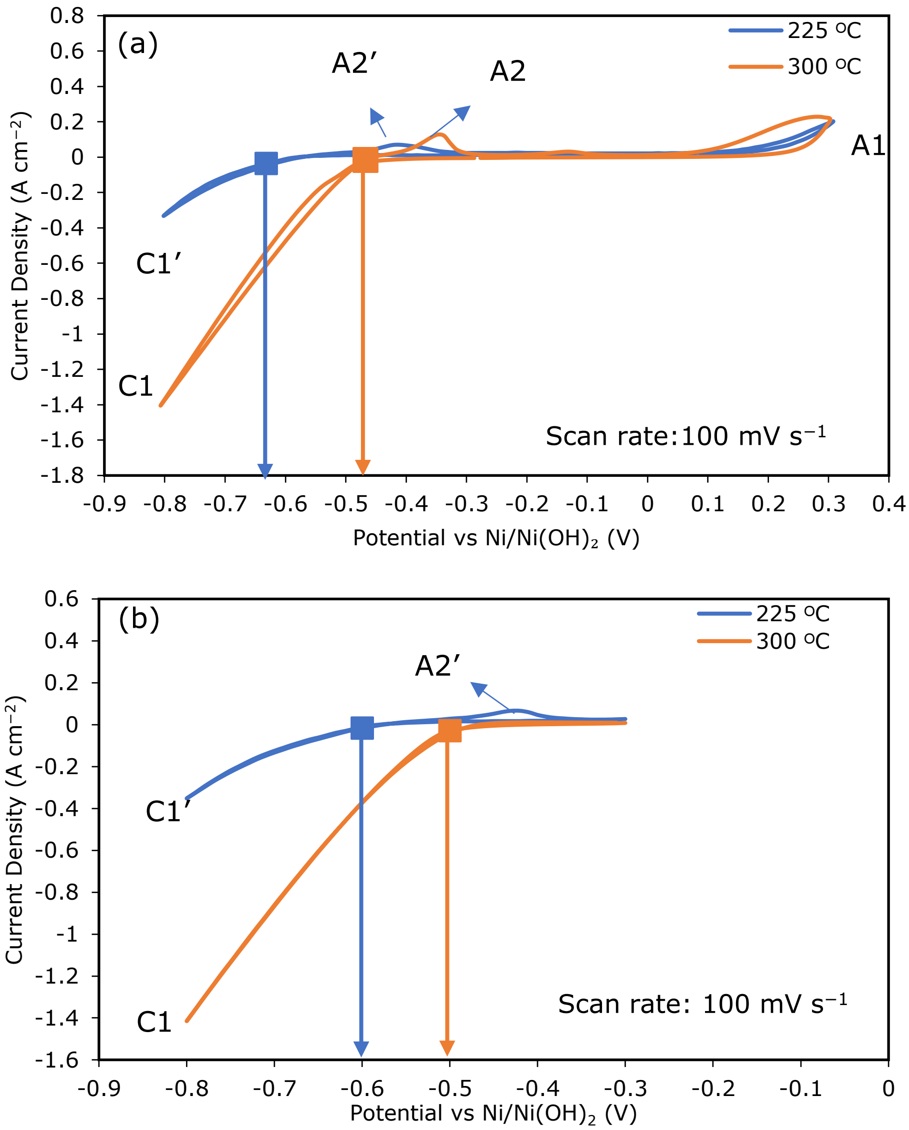

Figure 6.19 – Cyclic voltammograms of a 0.25 mm stainless steel working electrode in the eutectic molten hydroxide at a scan rate of 100 mV s^{-1} and different temperature. RE: Ni/Ni(OH)$_2$; CE: 5mm stainless steel rod; immersion depth: 14mm; an Ar gas atmosphere: 40cm^{3}min^{-1}. (a) Scan negatively between -0.8 and 0.3V, (b) Limiting the scan between -0.8 V and -0.3 V.

Figure 6.20 shows the cyclic voltammetry of the stainless steel with and without the presence of steam inside the eutectic molten hydroxide at an operating temperature of 300°C and scan rate of 100 mV s^{-1}. No significant change can be observed from the figure regarding the presence the steam inside the eutectic molten hydroxide at the cathodic limit C1 for the evolution of hydrogen reaction as shown in Figure 6.20. At the oxidation peak, the current density increased from 0.12 A cm^{-2} without the presence steam (A2′) to 0.23 A cm^{-2} with the presence of steam (A2). This increase in the current density from A2′ to A2 is responsible for increasing the surface area of the oxide metal.

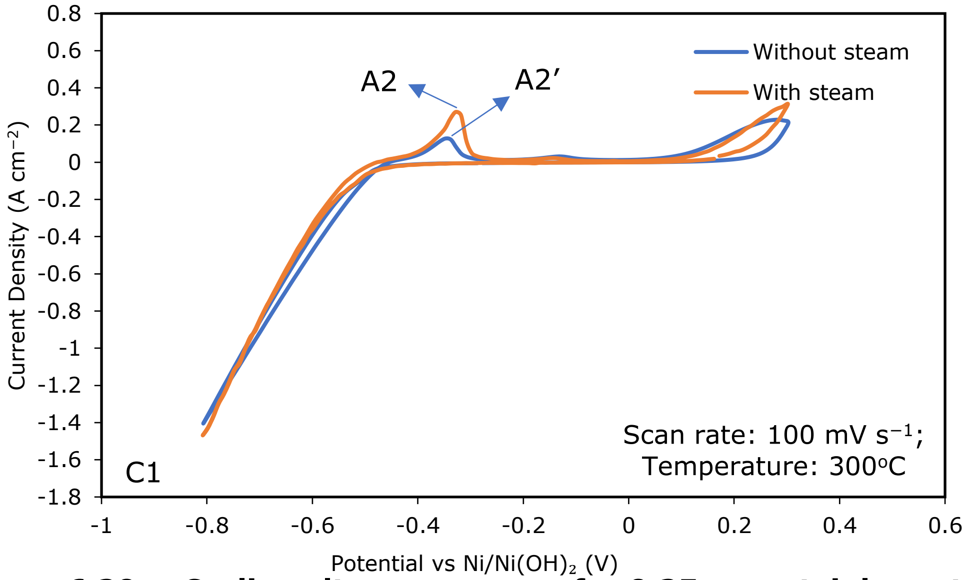

Figure 6.20 – Cyclic voltammograms of a 0.25 mm stainless steel working electrode in the eutectic molten hydroxide at a scan rate of 100 mV s^{-1} and different operating temperatures. RE: Ni/Ni$(OH)_2$; CE: 5 mm stainless steel rod; immersion depth: 14 mm; an Ar gas atmosphere: 40 cm^3 min^{-1}.

6.3 Cyclic Voltammetric Comparison between Different Working Electrodes

After studying the kinetic reaction of each working electrode separately in the eutectic molten hydroxide at different operating conditions respectively; it is imperative to compare their performance. This is essential for discerning which electrode provides more affordable, durable, stable kinetics; and also a fast catalytic response for the hydrogen evolution reaction. The comparison focuses mainly on the cathodic limit of the hydrogen evolution reaction. Cyclic voltammetry scans of the different working electrodes (i.e. Ni, Pt, Ag, Mo, SS) are compared in the eutectic molten hydroxide at a temperature of 300°C, a potential scan rate of $100 mVs^{-1}$ and an argon gas atmosphere as shown in Figure 6.21.

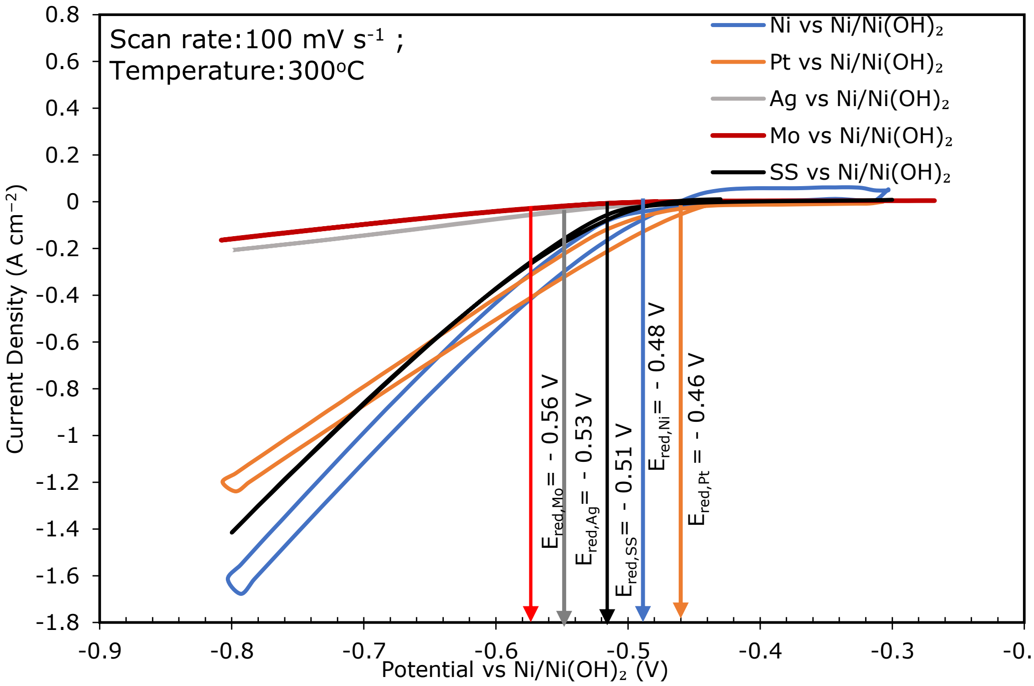

Figure 6.21 – Comparison of cyclic voltammograms of Ni, Pt, Ag, Mo, SS working electrode in the eutectic molten hydroxide at a temperature of 300°C and scan rate of 100 mV s^{-1}. RE: 0.5 mm of $Ni/Ni(OH)_2$ and CE: 5 mm of stainless steel; immersion depth: 14mm, an Ar gas atmosphere: 40 $cm^3 min^{-1}$.

It is obvious from the Figure 6.21 that each working electrode has a unique reduction potential value. It can therefore be observed from the above figure that the platinum working electrode had more positive reduction potential value (approximately -0.46 V) followed by the reduction potential of the nickel working electrode (approximately -0.48 V) and then the reduction potential of the stainless steel working electrode at -0.51 V. The reduction potential values of the silver and molybdenum working electrodes occurred at the lower end of the comparison at -0.53 V and -0.56 V respectively. The current density at the cathodic limit is the highest for the nickel working electrode followed by the stainless steel and platinum working electrodes respectively. However, silver and molybdenum have the lowest current density respectively. Table 6.1 displays the reduction potential and the current density at the cathodic limit as observed from the above figure for different working electrodes.

Table 6.1 – The reduction potential and the current limit at the cathodic limit for a different working electrode in the eutectic molten hydroxide at an operating temperature of 300°C and the scan rate of 100 mV s^{-1} at argon gas atmosphere of 40cm^3min^{-1}.

Working electrode	Temperature (°C)	Reduction potential E_{red} (V)	Current density j (A cm^{-2})
Ni	300	-0.49	-1.67
Pt	300	-0.47	-1.23
Ag	300	-0.53	-0.20
Mo	300	-0.55	-0.16
SS	300	-0.51	-1.41

A high current density measured at the cathodic limit means a high hydrogen evolution reaction. This high hydrogen evolution reaction is influenced directly by the catalytic activity of the working electrode inside the eutectic molten hydroxide. As mentioned and tabulated in Table 6.1, the highest hydrogen evolution reaction that can be achieved at the cathodic limit is done by using the nickel working electrode followed by stainless steel, platinum, silver and finally molybdenum. Therefore, the nickel wire had a higher electrode activity in comparison to the other working electrodes. This behaviour reinforces nickel as a popular choice in electrochemical processes as cathode material for the hydrogen gas evolution reaction. However, some studies such as (Abouatallah et al., 2002) have revealed that nickel can be deactivated during hydrogen evolution in alkaline water electrolysis and the metal requires the addition of a soluble to the electrolyte to cause reactivation.

These observed results were repeatedly for three times for all working electrodes, no change on the observed results. The comparison of different working electrodes was also performed at a different operating temperature of the eutectic molten hydroxide and with and without steam as presented in Appendix A, Figure A.1, Figure A.2, Figure A.3 and Table A.1.

6.4 Hydrogen Evolution Reaction (HER)

Figure 6.22 shows the obtained current-time chronoamperometry at constant potential of all tested working electrodes in the eutectic molten hydroxide during a 10 minutes' period of the hydrogen evolution reaction. This test was performed at operating temperature of $300^{o}C$ and at $40cm^{3}min^{-1}$ argon atmosphere.

These chronoamperometric curves show that the electrodes change during the first stages of hydrogen evolution reaction (HER), accomplishing a near stationary state. Their reactivity is maintained along the observed period, with platinum followed by nickel being by far, the best of the tested materials and showing the highest current density values in comparison to stainless steel, silver and molybdenum. This result confirms that the blank metal of platinum and nickel working electrodes in the eutectic molten hydroxide respectively, have a better performance for splitting steam to produce hydrogen gas. The stainless steel working electrode is third in order for hydrogen gas production.

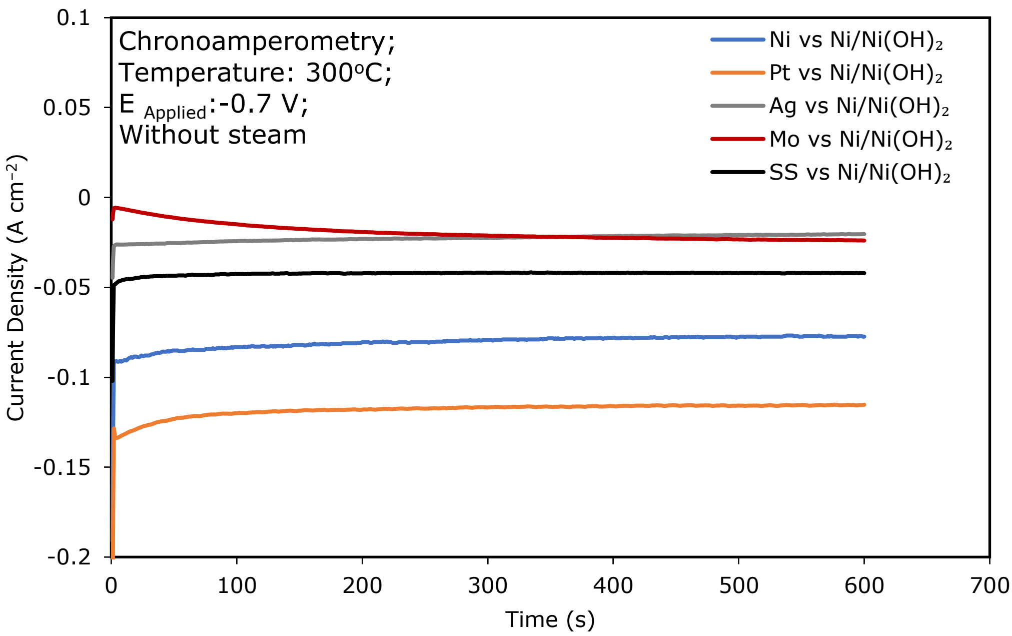

Figure 6.22 – Chronoamperograms of the hydrogen evolution reaction for all working electrodes (Ni, Pt, Ag, Mo, SS) in the eutectic molten hydroxide at a temperature of 300°C, and at an applied potential of -0.7 V during 10 min. Without steam and argon gas atmosphere at 40 cm^3min^{-1}.

The performance of the different working electrodes was also tested with the presence of steam inside the eutectic molten hydroxide and at an operating temperature of 300 °C, as shown in Figure 6.23.

It is obvious from the figure that the attained current density value of different working electrodes (without steam) slightly increased with the presence of steam inside the eutectic molten hydroxide. It can also be observed from the above figure that a significant increase in the current density of stainless steel as the working electrode, occurs in the presence of steam. This increase indicates that the electro-catalytic activity of stainless steel under these condition mirrors the value of nickel metal. On the other hand, platinum still ranks as the most electro-active for the hydrogen evolution reaction. Despite this, its use was generally limited in history because it is classified as a precious metal in comparison to the others.

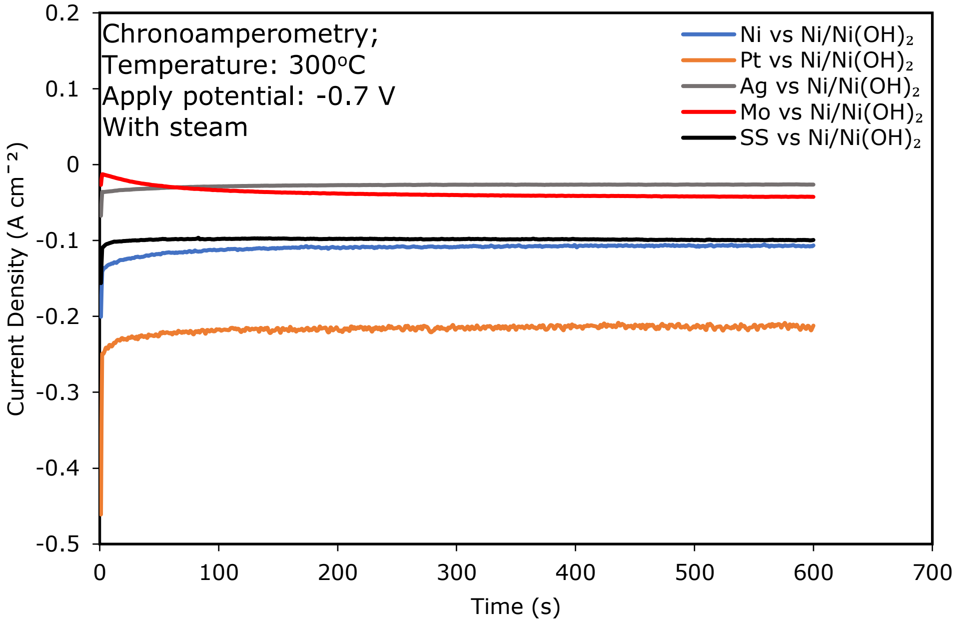

Figure 6.23 – Chronoamperograms of the hydrogen evolution reaction for all working electrodes (Ni, Pt, Ag, Mo, SS) in the eutectic molten hydroxide at a temperature of 300°C, and at an applied potential of -0.7 V during 10 min. With steam and argon gas atmosphere at 40 cm^{3}min^{-1}.

6.5 Summary

The findings in this chapter can be summarised as follows:

- The most important finding that can be drawn from the results presented in this chapter is that the reduction potential of the hydrogen evolution reaction using different working electrodes was in order of (more positive to negative reduction potential): Pt > Ni > SS > Ag > Mo. The performance of each working electrode for the hydrogen evolution reaction was confirmed through chronoamperometry tests at a constant potential of -0.7 V. These tests confirm the stability and productivity of each working electrode. The produced chronoamperograms found that the platinum had the highest current density followed by nickel, stainless steel, silver then molybdenum at the constant potential of -0.7 V.
- It was also found from the cyclic voltammograms that the presence of steam inside the eutectic molten hydroxide is apparent in increasing the current density at the cathodic limit for the hydrogen evolution reaction. However, the starting point of reduction potential for the hydrogen evolution reaction was still approximately the same with and without the presence of steam inside the eutectic molten hydroxide. These achieved results were applicable for all tested working electrodes throughout this chapter.
- Chronoamperometry was used to confirm the effect of the presence of steam inside the eutectic molten hydroxide in increasing the current density at the constant applied potential of -0.7 V for different working electrodes. It was found that the platinum had the highest current density followed by nickel, stainless steel, silver and molybdenum.

- The effect of increasing the operating temperature of the eutectic molten hydroxide influenced the performed cyclic voltammetry scans. This effect appeared to clearly shift the reduction potential in a positive direction at high temperatures. This positive shift was applicable for all tested working electrodes. The shift in the reduction potential with an increase in the operating temperature was approximately 0.1 V for all tested working electrodes. This was despite the fact that each one had a different reduction potential for the hydrogen evolution reaction.
- Limiting the cyclic voltammetry scan range to focus on the cathodic limit at a potential scan rate range between 50-150 mV s^{-1} was also done in order to focus on the hydrogen gas evolution reaction. It was found that the stability of the produced scans in the eutectic molten hydroxide for these different working electrodes was stable even though the scan rate speed varied.

CHAPTER 7

THE ELECTROCHEMICAL PROCESS AND CELL EFFICIENCY

7.1 Introduction

Chapter 6 focused on the process of finding an efficient electrocatalytic working electrode that can be used to increase the hydrogen gas production rate in eutectic molten hydroxide. This chapter focuses on the techniques of using different working cathodes to increase the output of the hydrogen evolution reaction during the electrochemical process. The most successful electrodes tested were nickel, platinum and stainless steel. A comparative study undertaken in this chapter was based on finding the most efficient electrochemical cell that increased the efficiency of steam splitting through electrolysis of eutectic molten hydroxide. This was primarily done since steam splitting is a key aspect of increasing the production rate of hydrogen gas. Another aspect of focus is ensuring that the present efficiency of the electrochemical process is increased.

There were limited studies that have been conducted on how the electrochemical process occurs through the splitting of steam via molten hydroxide salt for hydrogen gas production. The most recent electrochemical study that focused on molten hydroxides for water splitting to generate hydrogen fuel, was demonstrated by (Licht et al., 2016). The study investigated a wide range of pure and mixed alkali hydroxides as electrolytes such as LiOH, NaOH, KOH, $Ba(OH)_2$ at temperatures between

200 and 700°C. The applied voltage range was maintained between 1.1 and 2.3 V using a nickel and platinum plate as an anode and a nickel plate as a cathode, respectively. The investigation of Nagai et al. (2003) focused on the effect of generated bubbles between electrodes and on the efficiency of hydrogen production by water electrolysis using 10 wt% of KOH aqueous solution under atmospheric pressure and Ni-Cr-Fe alloy as the cathode material. The study of Licht et al. (2014) presented an electrochemical pathway for producing ammonia from air and steam via an equimolar ratio of molten NaOH-KOH with suspended nano-Fe_2O_3 particles using nickel electrodes at a temperature of 200°C and an applied voltage of 2 V. Ganley (2009) described experimental work involving the direct electrolysis of 18 M of KOH at a temperature of 400°C and at steam partial pressure of 8.7 MPa. Monel alloy was fixed as the cathode while different metals (i.e. nickel, monel alloy, lithiated nickel, cobalt-plated nickel) were used as the anode in different experiments. At temperatures as low as 80°C, the study of Anani et al. (1990) discovered a technique to produce high purity hydrogen gas at the cathode while maintaining high current efficiency during the electrolysis of hydrogen sulphide. The intermediary solution resulting in the generation of the latter contained an equimolar concentration of NaOH and NaHS at the experimental temperature.

The two-electrode electrolysis process has been used in this chapter to apply a voltage to the cathode and anode to split steam through eutectic molten hydroxide. Subsequently, hydrogen and oxygen gas was collected from the cathode and anode compartment respectively. Hydrogen gas was detected by using a hydrogen gas tube and hydrogen gas sensor whereas the actual rate of hydrogen gas production was measured using the pneumatic trough method. This chapter aims to record an increase in the efficiency of hydrogen gas production by optimising several operating conditions such as temperature and applied voltage; or by changing the material used for cathode or anode construction in the electrochemical cell.

7.2 Electrochemical Investigation of Different Cathode Metals

The overall electrical energy required to split water at 25°C is 1.23 V which is also the minimum voltage required to produce hydrogen gas. The overall reaction of water splitting can be represented in equation (7.1) as:

$$H_2O + 2\,e^- \leftrightarrow H_2 + \tfrac{1}{2}O_2 \qquad \textbf{(7.1)}$$

In practice, the electrochemical cell voltage needs to be larger than the required cell voltage in order to kick-start the reaction due to the activation energy barrier, low reaction rate and the bubble formation. Therefore in this study, the cell voltages used were kept above the minimum cell voltage of 1.23V even though it needs to be lower than this minimum value at high operating temperatures. The higher applied voltages between 1.5V and 2.5V to split water were arranged in such an order to overcome any barrier for the electrolysis process and ensure continuous hydrogen gas production. The electrolysis process was operated in a temperature range between 225°C and 300°C.

7.2.1 An electrochemical investigation using a nickel cathode

The nickel electrode has been evaluated as one of the best working electrodes for the hydrogen evolution reaction to use in eutectic molten hydroxide as seen from the previous chapter. Figure 7.1a, b, and c show the current−time responses at different operating temperatures (225, 250, 300^{o}C) respectively. At each operating temperature, a different voltage was applied (1.5, 2.0 and 2.5 V respectively). It should be noted here that the steam and argon mixture was bubbled inside the eutectic molten hydroxide for an approximate duration of 600-900 s before the electrolysis process was started.

From these plots obtained during electrolysis, the current flow observed was with some level of noise at most conditions. This noise observed is shown in Figure 7.1, and is quite typical during electrolysis of steam via eutectic molten hydroxide and during the formation of hydrogen gas bubbles around the cathode.

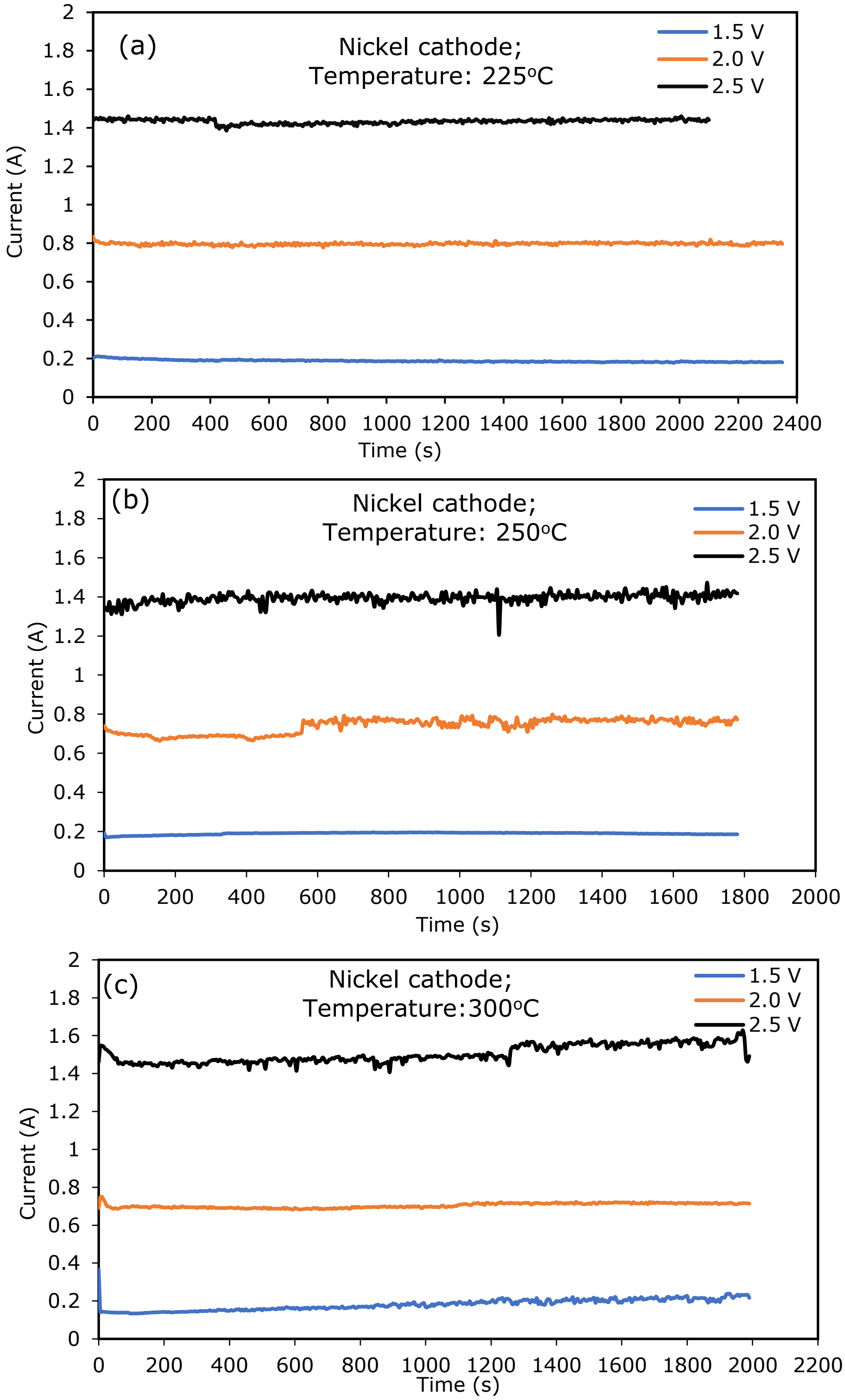

Figure 7.1 – Current-time plots recorded from 1800-2400 s electrolysis in eutectic molten hydroxide at (a) 225°C, (b) 250°C, and (c) 300°C; 1.5, 2.0, 2.5 V cell voltages; Ni cathode (D:5 mm, immersion depth: 1.5 cm); SS anode D: 5 mm; at atmosphere of argon gas of 40 $cm^3 min^{-1}$ and with steam.

When hydrogen molecules are formed, they migrate away from the cathode in order to allow other steam molecules to be split into forming new hydrogen molecules. This transfer of the hydrogen and steam molecules to and from the nickel cathode surface during the electrolysis process can be listed as the reason for the noise noticed in the current-time plot. It is significant to mention here that the nickel cathode is highly stable for molten hydroxide water splitting as stated by (Licht et al., 2016); and corroborates our findings. The increase in electrolysis voltage generally leads to an increase in the rate of hydrogen gas production and this is reflected in Figure 7.1a, b, and c. The effect of increasing the operating temperature of the eutectic molten hydroxide with regards to current flow at different applied voltages was slightly increased at the same applied voltages; and this directly influenced the production rate of hydrogen gas which was increased, as is explored in later sections.

Stainless steel was employed as the anode material in the electrolysis process. Therefore it should be mentioned that when it was employed at high temperatures in the eutectic molten hydroxide, it had a passivate type behaviour even though it was used in a corrosive environment (Bozzini et al., 2012). Even though the stainless steel anode undergoes passivation with the creation of an outer layer shield, there is no influence on the response of the current-time plot which is directly reflected in the rate of hydrogen gas formation.

These results were repeatedly obtained for four times over, and thus noises were not caused by experimental errors. The noise, as mentioned earlier, was due to steam splitting and the formation of hydrogen gas bubbles on the surface near the nickel cathode.

7.2.2 Platinum cathode

Platinum metal was also selected as one of the best working electrodes for the hydrogen evolution in the eutectic molten hydroxide. The recorded current–time plots are shown in Figure 7.2a, and b at different applied voltages and operating temperatures, respectively. As mentioned previously, platinum is a precious metal and this prevents it from large-scale industrial use, limiting its usage for laboratory scale investigations. In this study, a platinum wire of 0.5 mm diameter was used. Since the diameter of the used platinum is very small, it was necessary to increase the surface area that was exposed to the electrolyte to be approximately the same as the nickel electrode surface area. This was done to ensure a smooth comparison of current flow and production rate of hydrogen gas at the same operating conditions. Therefore, in order to achieve a surface area of 2.55 cm^2, it was simply rolled into a spiral shape with15 cm of the wire length. This increase in the surface area significantly contributed to increasing the current flow value at different applied voltages.

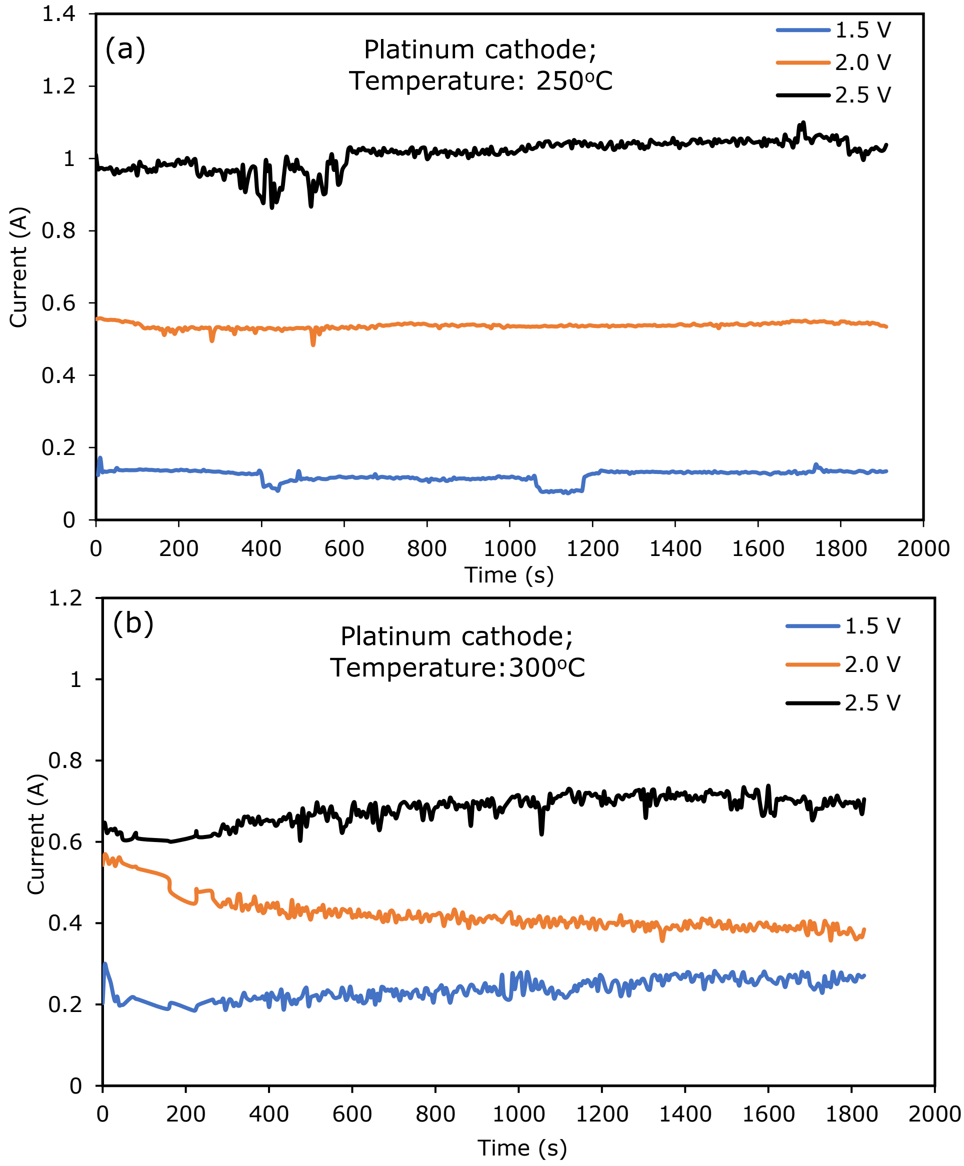

Figure 7.2 – Current-time plots recorded for 1800 s electrolysis in eutectic molten hydroxide at (a) 250°C, (b) 300°C; 1.5, 2.0, 2.5 V cell voltages; Pt cathode (D: 0.5mm, immersion depth: 1.5cm×15); SS anode (D:5 mm); at atmosphere of argon gas of 40 cm^{3}min^{-1} and with steam.

It can be observed from Figure 7.2a and Figure 7.2b that current flow increases with an increase in the applied voltage at different operating temperatures. The efficiency of the rate of hydrogen gas production will be explored in a later section. After electrolysis, no change can be observed on the surface of the platinum electrode. The reason for there being no change in the surface area of the electrode is because platinum is an inert metal and does not inhibit the reaction occurring at its surface. It simply acts as a means to transfer electric charge from the power supply to the electrolyte without undergoing any change. Platinum can also be classified as a corrosion resistance metal to specifically withstand sodium hydroxide melt under suitable conditions (Smith, 1956).

7.2.3 Stainless steel cathode

Stainless steel metal was also used as a cathode in the eutectic molten hydroxide to compare with other tested materials at the same operating conditions. The current-time response is recorded at different applied voltages and operating temperatures respectively, as shown in Figure 7.5.

It can be observed from Figure 7.3a, b, and c that the current increases with an increase in the applied voltage. At 225^{o}C, the current response is stable and the current increases approximately with an increment of 0.2 A for every 0.5 V increase in the applied voltage as seen in Figure 7.3a. This observed phenomena of the current at 225^{o}C is not applicable when the temperature is increased to 300^{o}C. However, when the temperature increases, the current response curve starts to appear noisy, especially at higher applied voltages. The increase in the production of hydrogen gas molecules around the cathode is mainly responsible for this noisy response of the current-time plot as clearly seen in Figure 7.3b and 7.3c.

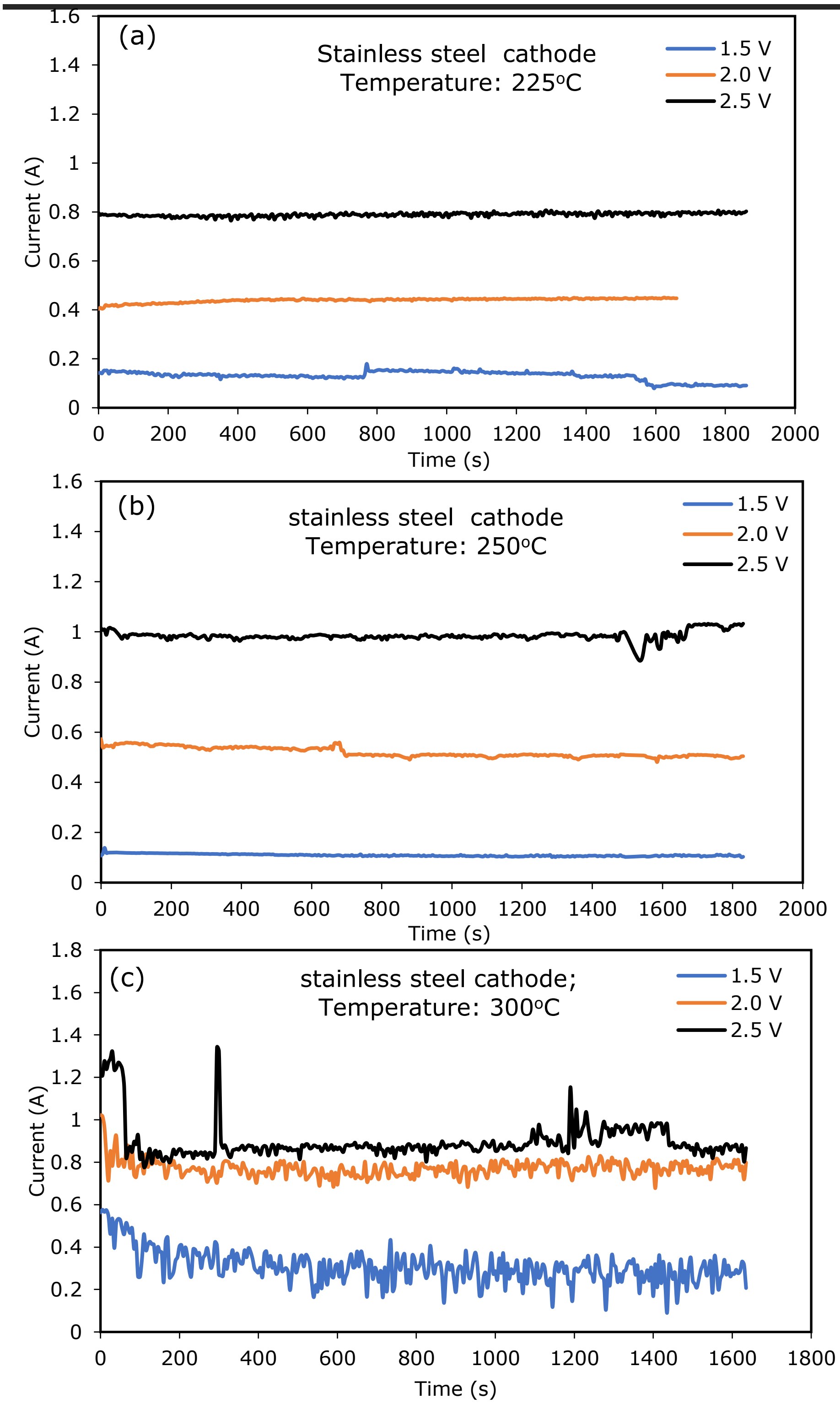

Figure 7.3 – Current-time plots recorded for 1800 s electrolysis in the eutectic molten hydroxide at (a) 225°C, (b) 250°C, and (c)300°C; 1.5, 2.0, 2.5 V cell voltages; SS as anode and cathode (D:5mm, immersion depths: 1.5 cm); an atmosphere of argon gas of 40cm^{3}min^{-1} and with steam.

7.3 Comparison of Different Cathode Materials and the Rate of Hydrogen Gas Production

The above-tested cathode materials (Ni, Pt, and SS) were compared at different operating temperatures (225, 250, 300^{o}C) and at different applied voltages (1.5, 2.0, 2.5 V). This comparison is shown in Figure 7.4a, b, and c; Figure 7.5a, b, and c; and Figure 7.6a, b, and c respectively. These electrolysis processes were carried out as mentioned previously, under a steady argon gas flow rate 40cm^{3}min^{-1} and a fixed steam flow 7.23cm^{3}min^{-1}. The anode material that was used throughout these electrolysis processes is stainless steel electrode. The reason for this comparison is to find out the most efficient cathode material during the electrochemical process for a higher rate of hydrogen gas production. The important point that can be observed from Figure 7.4a, b, and c; Figure7.5a, b, and c; and Figure 7.6a, b, and c is that the recorded current is the highest when using the nickel as cathode material during electrolysis inside the eutectic molten hydroxide. These observed results are consistent for the nickel electrode at different applied voltages and different operating temperatures. Furthermore, for the nickel electrode, when the applied voltage increases from 1.5 V to 2.5 V, the current increased accordingly as seen in Figure 7.4a, b, and c; Figure 7.5a, b, and c; and Figure 7.6 a, b, and c. For instance, at 225^{o}C the current increases from 0.2 A at an applied voltage of 1.5 V to 1.6 A at an applied voltage of 2.5 V. For stainless steel and platinum electrodes, the recorded current-time plots show that their current responses are approximately the same at different applied voltages and at different operating temperatures.

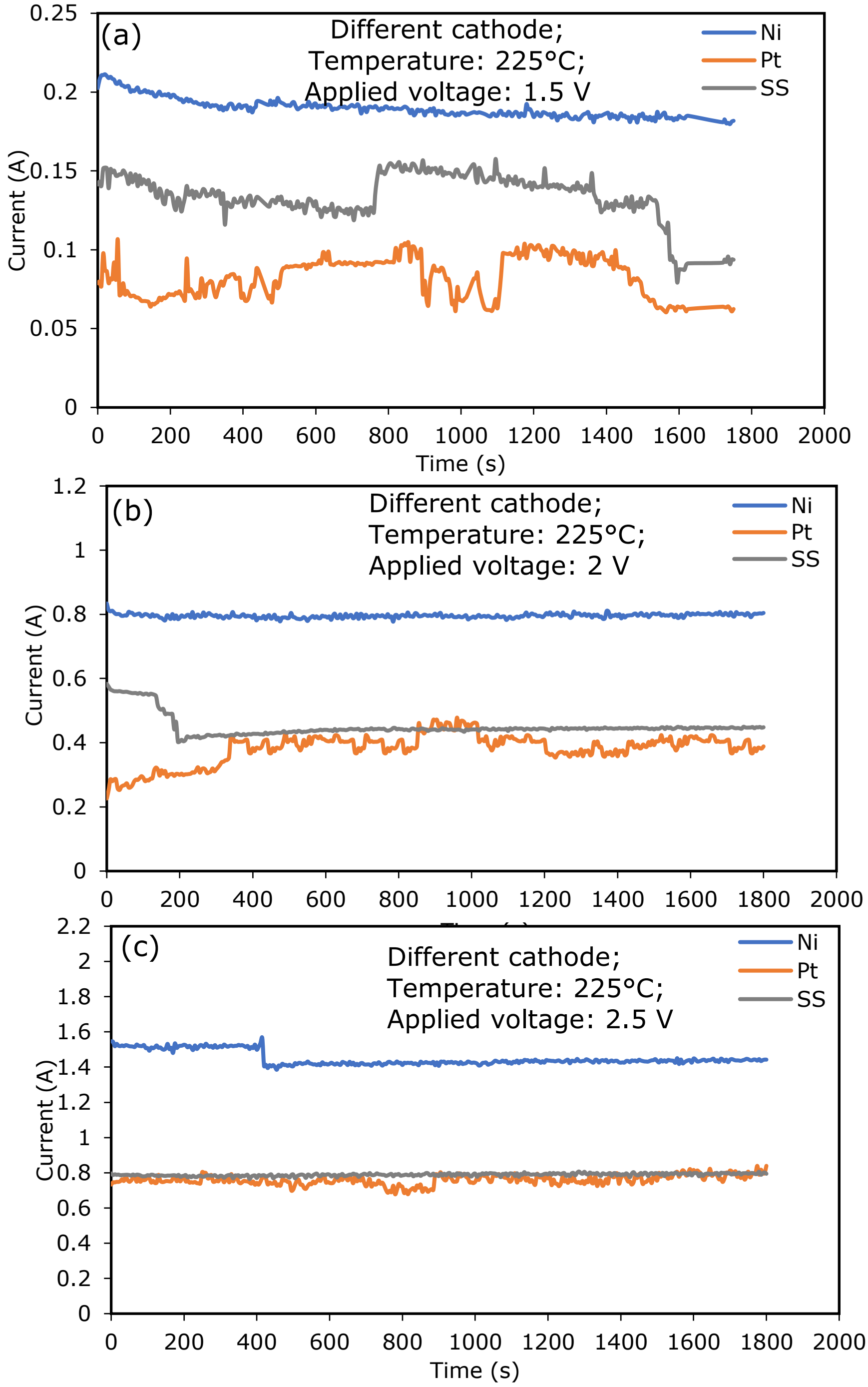

Figure 7.4 – Current-time plots recorded for 1800 s electrolysis in the eutectic molten hydroxide at temperature of 225°C and at applied voltages of 1.5, 2.0, 2.5V respectively; cathode: (Ni D: 5mm; SS D:5 mm; immersion depths: 1.5cm), (Pt D: 0.5 mm, immersion depth: 16 cm); SS anode: 5mm. An atmosphere steam and argon gas of 7.23 and 40 cm^3min^{-1} respectively.

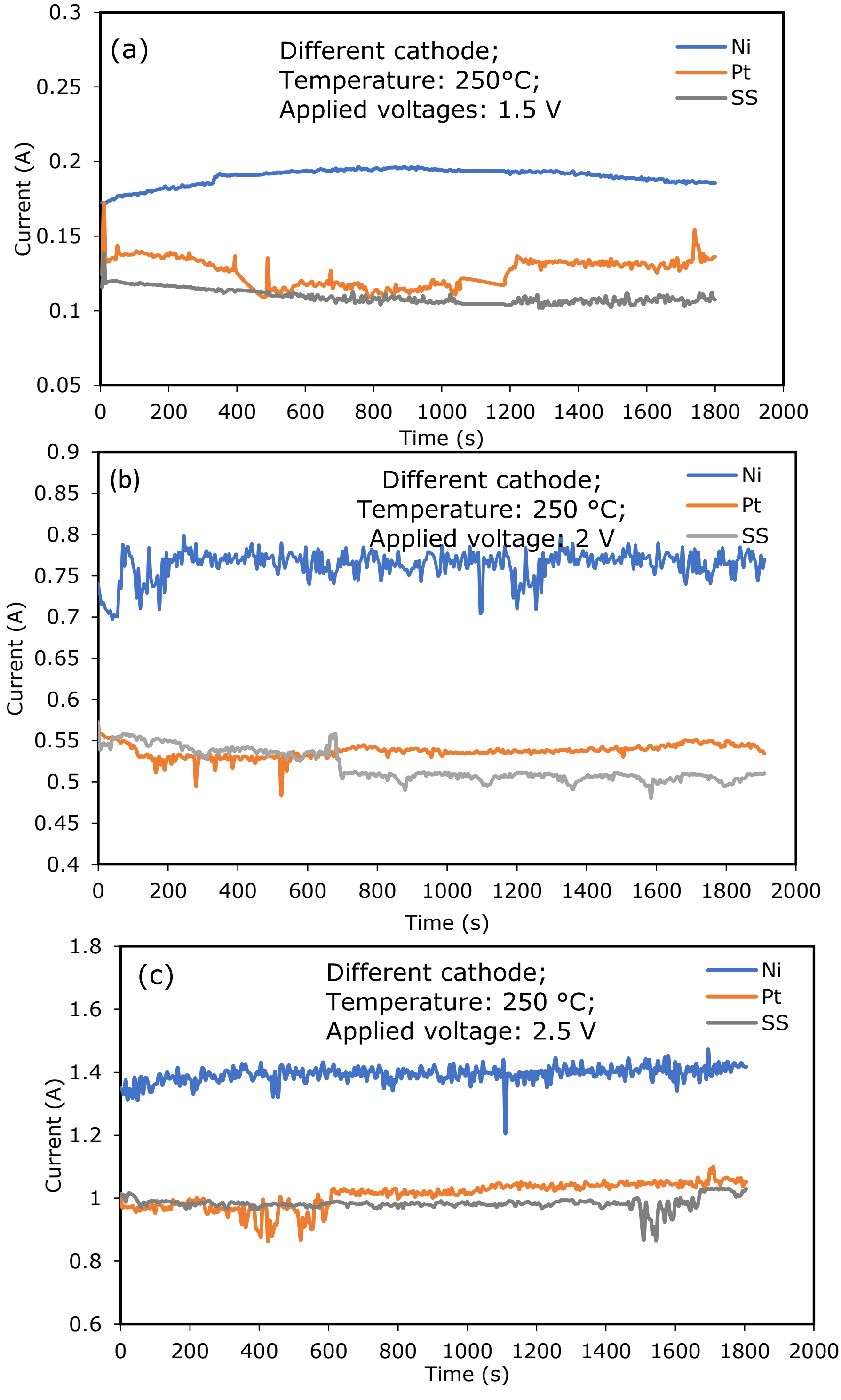

Figure 7.5 – Current-time plots recorded for 1800 s electrolysis in the eutectic molten hydroxide at temperature of 250°C and at applied voltages of 1.5, 2.0, 2.5 V respectively; cathode: (Ni D:5mm; SS D:5 mm; immersion depths: 1.5 cm), (Pt D: 0.5 mm, immersion depth: 16cm); anode: SS: 5 mm. An atmosphere steam and argon gas of 7.23 and 40cm^{3}min^{-1} respectively.

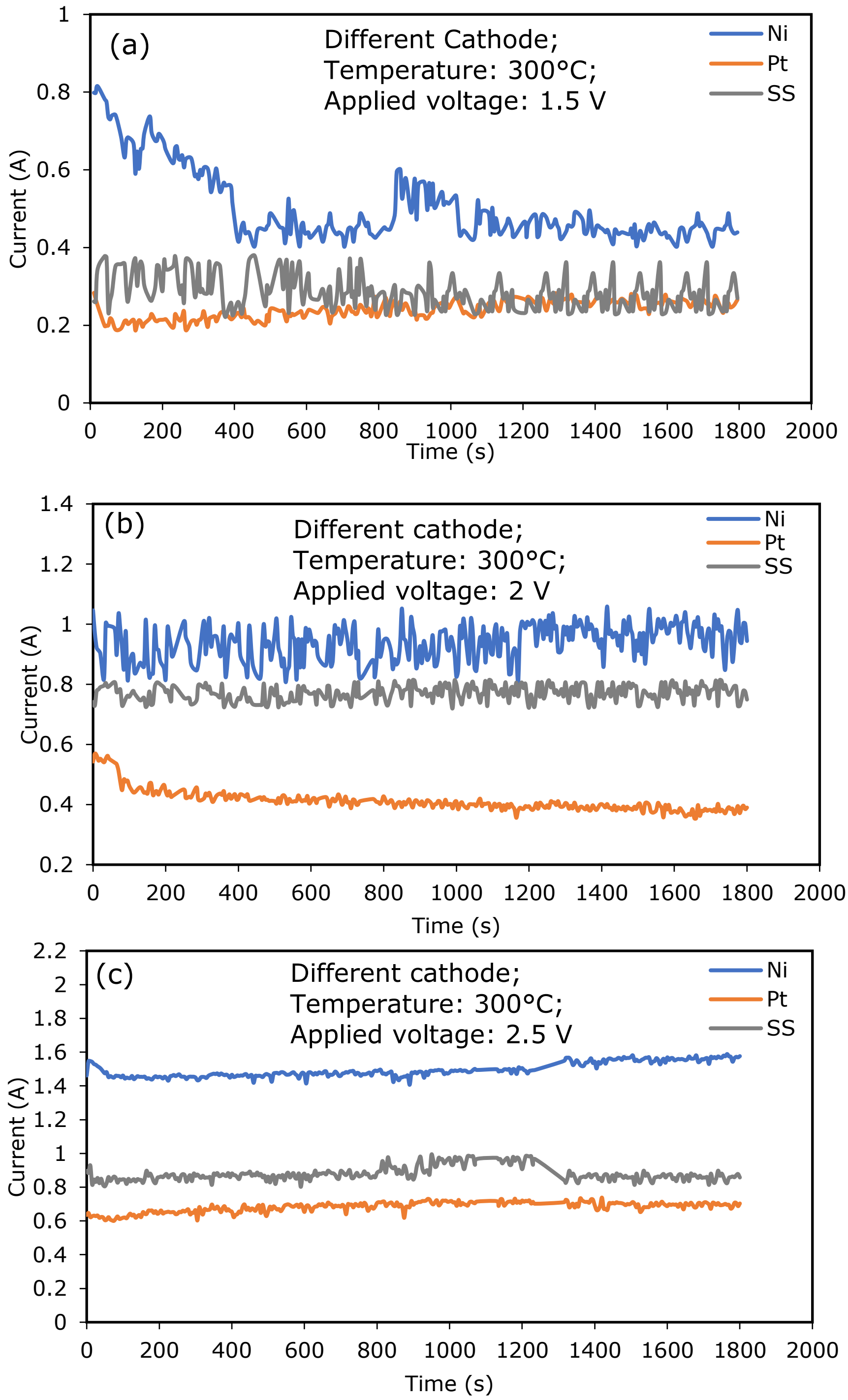

Figure 7.6 – Current-time plots recorded for 1800 s electrolysis in the eutectic molten hydroxide at temperature of 300°C and at applied voltages of 1.5, 2.0, 2.5 V respectively; cathode: (Ni D:5mm; SS D:5 mm; immersion depths: 1.5 cm), (Pt D: 0.5 mm, immersion depth: 15 cm); SS anode: 5 mm. An atmosphere steam and argon gas of 7.23 and 40cm^{3}min^{-1} respectively.

During electrolysis, hydrogen gas was produced at the cathode while oxygen gas was produced at anode. The produced gases originated from the splitting of steam that was present inside the eutectic molten hydroxide. The H_2 gas produced at the cathode was analysed using a gastec hydrogen gas detector tube which measures the percentage of hydrogen gas up to 2.0%. The detector tube confirmed that the hydrogen gas produced was more than 2.0% as shown in Figure 7.7.

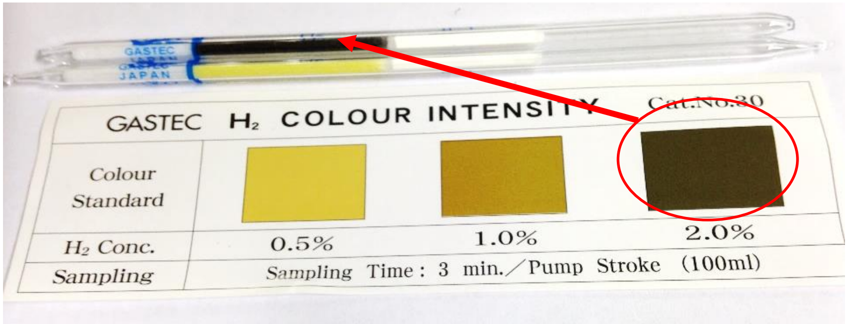

Figure 7.7 – Photo of the used hydrogen gas detector to examine the produced gas at the cathode compartment.

The second method used to confirm that hydrogen was the released gas at the cathode involves the use of a hydrogen gas sensor (PRO-GASBADGE). This sensor monitored the hydrogen gas produced up to 2000 PPM. The hydrogen gas sensor detected the hydrogen gas between 655 to 705 PPM at an applied voltage of 1.5 V to the electrolysis cell and at more than 2000PPM at an applied voltage of 2 V. This confirmed that the only gas produced at the cathode is hydrogen. To quantify the amount of hydrogen gas produced at the cathode, the gas flow was collected in a measuring cylinder using the water displacement method. The hydrogen gas was collected and measured over a period of 10 minutes intervals. The process was repeated four times and the production rate remained approximately constant. Table 7.1 shows the rate of hydrogen gas production at different cathodes (Ni, Pt, and SS) at different operating temperatures and at different applied voltages respectively.

Table 7.1 – The rate of the hydrogen gas production at different cathode at the different applied voltages and operating temperatures respectively, during electrolysis.

Metal	Temperature (°C)	H_2 production rate ($cm^3\ min^{-1}$)		
		1.5 V	2.0 V	2.5 V
Ni	225	0.5–1.0	4.0–5.0	9.0–9.5
	250	1.0–1.5	4.5–5.0	9.5–10.0
	300	1.3–1.5	4.5–5.5	10.7–11.3
Pt	225	0.5–1.5	1.5–2.0	4.0–5.5
	250	0.7–1.0	3.0	6.0
	300	1.4–1.6	1.8–2.0	4.5
SS	225	0.5	3.0	5.0–5.5
	250	0.7–1.0	3.3–3.5	7.0–7.5
	300	1.0–2.0	3.5–4.0	7.0

It is clear from Table 7.1 that a steady increase in the hydrogen gas production rate at the cathode can be noticed when an increase in the operating temperature and applied voltage respectively, is enforced. This trend is valid for all examined cathode materials. Furthermore, the flow rate of hydrogen gas using a nickel electrode recorded the highest value in comparison to the other two used cathode materials i.e. stainless steel and platinum in this order respectively. For example, the hydrogen gas flow rate at 250°C and at applied voltage of 2 V using a nickel, stainless steel and platinum cathode was 5.0, 3.5, 3.0 $cm^3 min^{-1}$ respectively. These results indicate that nickel has an enhanced level of catalytic activity in the current eutectic molten hydroxide, contributing towards splitting the steam with a higher efficiency.

Hydrogen gas production rates calculated from equation 7.2:

$$\text{Production Rate} = \frac{\text{Mass of H}_2\text{ produced}}{\text{Immersed area of cathode}\times\text{Duration of H}_2\text{ production}} \times 100 \quad \textbf{(7.2)}$$

The production rates are plotted against different applied voltages and operating temperatures respectively, as shown in Figure 7.8a, b, and c.

Two major trends in the hydrogen gas production rate can be observed from Figure 7.8a, b, and c. Firstly, the hydrogen gas production rate increases with an increase in the applied voltage. Consequently, an increase in the current value would be expected. In other words, a higher voltage applied during steam electrolysis for hydrogen production, results in a larger current and as a consequence, a larger hydrogen gas production rate. Secondly, it would appear that the hydrogen gas production rate attained was generally higher at higher temperatures. Comparing the hydrogen gas production rates obtained for each of the three cathode materials at different operating temperatures, it would appear that the nickel electrode had the highest production rates; whilst the stainless steel and platinum electrodes had fairly similar hydrogen production rates.

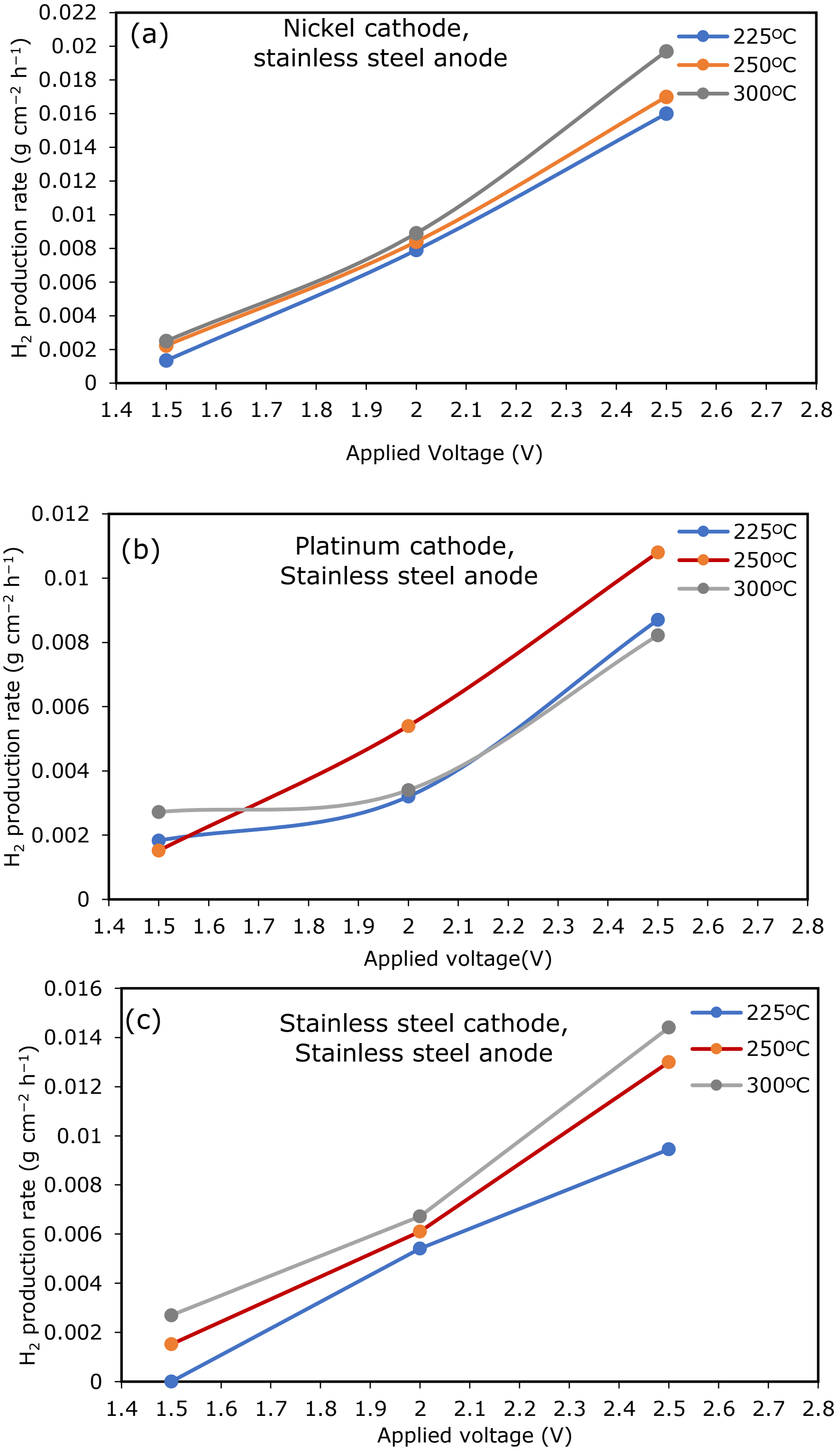

Figure 7.8 – Hydrogen gas production rate versus the applied voltages at different operating temperatures (225, 250, 300°C); the cathode material: Ni, Pt, and SS. The anode is stainless steel.

The calculated current efficiency of the hydrogen gas using equation 7.3 as follows:

$$\text{Current Efficiency} = \frac{\text{Charge needed to produce hydrogen in theory}}{\text{Charge passed during electrolysis}} \times 100 \qquad \textbf{(7.3)}$$

This value is presented in Table 7.2 using different cathode materials and at different operating temperatures and applied voltages respectively.

Table 7.2 – Current efficiency of the electrochemical cell for hydrogen gas production at different applied voltages and different operating temperatures. The anode is made from stainless steel.

Cathode metal	Temperature (^oC)	Current Efficiency Range (%)	Average Current Efficiency (%)
Ni	225	47.9 to 78.6	63.2
	250	81.1 to 85.9	83.5
	300	87.1 to 94.0	90.5
Pt	225	59.0 to 156.0	107.5
	250	69.0 to 83.6	76.3
	300	55.0 to 82.2	68.6
SS	225	48.1 to 81.6	64.8
	250	82.6 to 97.8	90.2
	300	59.4 to 100.6	80.0

It is obvious from the above table that the current efficiency of the hydrogen gas production rate using a nickel cathode reached up to 90.5 % at 300^oC. This achieved value of efficiency shows that the value of the current in practical was approximately close to the value of the current in theory. Alternately, when platinum was used as a cathode, the current efficiency of the hydrogen gas production rate decreased with an increase in the temperature. This implies that the platinum catalytic activity decreased to allow the reaction to occur with increasing temperature. It was clear from the above table that the achieve current efficiency at 225^oC was about 107.5%. The reason for being the value of the current efficiency above 100% was due to the experimental error or other side reactions happened. Using stainless steel as cathode also shows an increase in the current efficiency at 300^oC up to 100.6% as presented in Table 7.2. The reason of being the value of the current efficiency above 100% was attributed to the experimental error while the data collected.

When interpreting the hydrogen gas production rate and current efficiencies, different factors that need to be taken into account are the ionic transfer and gas bubble behaviour in the electrolyte. These factors in turn influence the current during electrolysis. Ionic transfer is determined from viscosity and the flow field of the electrolyte. As the steam is consumed during electrolysis, the concentration of the electrolyte increases, resulting in an increase in the viscosity. Therefore, steam is continuously added to the system in order to maintain a constant electrolyte concentration and subsequently, the viscosity. However, better mass transfer does not mean more hydrogen production. It is true that mass transport leads to greater reaction rates, but the large number of gas bubbles formed, resulting from the increased reaction rate, can adversely hinder contact between the electrodes and the electrolyte. For future work, the recirculation of electrolyte can be mechanically applied to accelerate the departure of the bubbles and remove them from the respective electrode compartment.

7.4 Effect of Using Graphite Anode Material on the Electrolysis Cell Performance

Further electrochemical investigation undertaken in the eutectic molten hydroxide uses graphite as the material for the anode and alternates between nickel, platinum and stainless steel as the cathode. The reason for using graphite in place of stainless steel in this study is to compare the effect of changing the anode material on the electrolysis cell performance. Specifically, it must be investigated whether it has a direct effect on the hydrogen gas production rate and the current efficiency. This cell performance was tested at different operating temperatures and different applied voltages. The current-time plots are shown in Figure 7.9a,b, and c; Figure 7.10a, b, and c; and Figure 7.11a, b, and c respectively. These electrolysis processes were performed for 1800s under an argon gas atmosphere.

It is obvious from Figure 7.9a, b, and c; and Figure 7.10a, b, and c that the current response using nickel and stainless steel electrodes is approximately similar at operating temperatures of 225^{o}C and 250^{o}C and applied voltages of 1.5, 2.0, 2.5 V, respectively. Alternately, when the operating temperature of the eutectic molten hydroxide is raised to 300^{o}C, the current response using a nickel cathode becomes higher than for the stainless steel cathode. This difference between the former and latter is approximately 0.2 A and 0.4 A at 2.0 V and 2.5 V respectively as shown in Figure 7.11b and c. On the other hand, the current response using a platinum cathode is recorded as the lowest among the three different materials at different operating temperatures and applied voltages respectively.

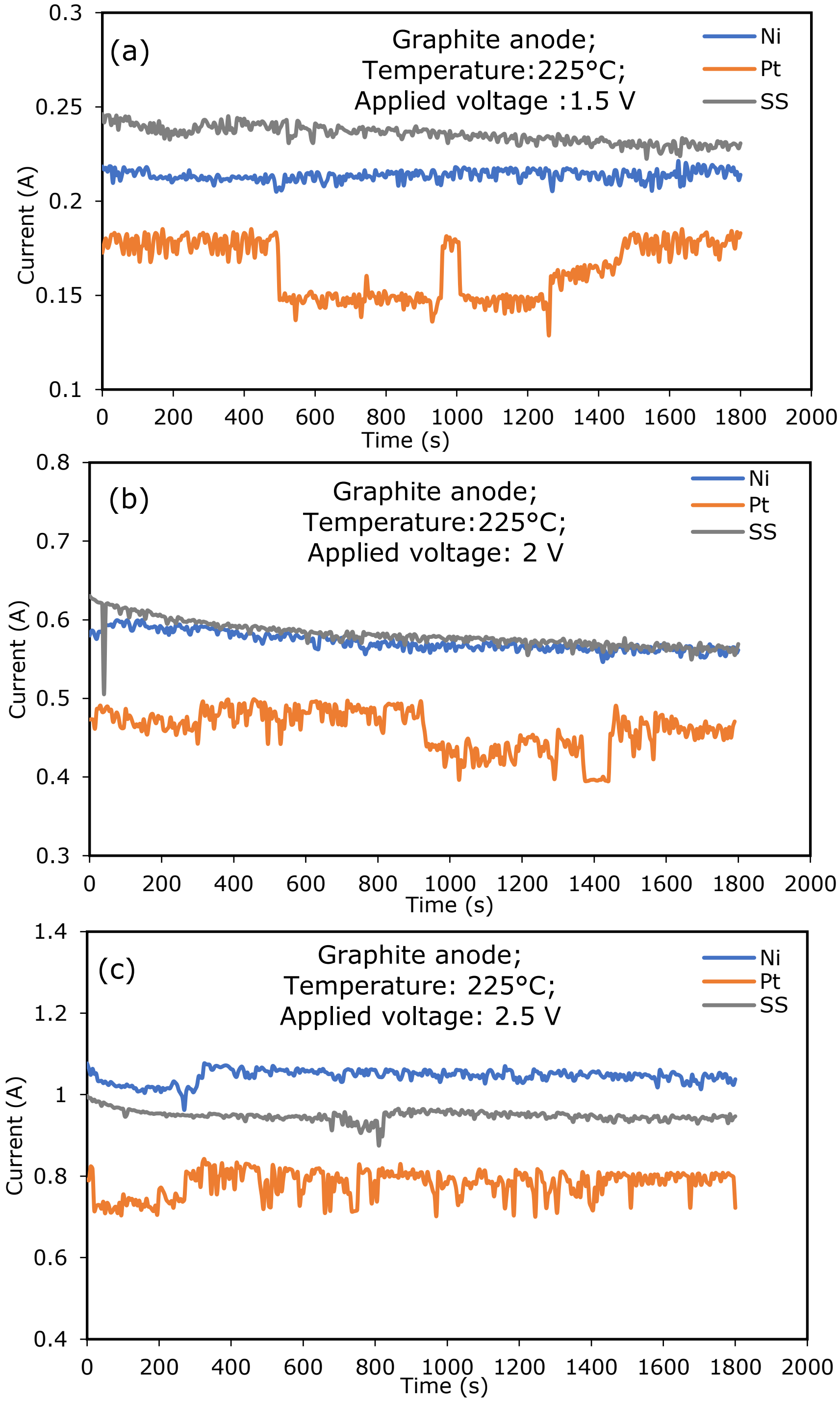

Figure 7.9 – Current-time plots recorded for 1800 s electrolysis in the eutectic molten hydroxide at a temperature of 225°C and at applied voltages of 1.5, 2.0, 2.5 V respectively; cathode: (Ni D:5mm; SS D:5 mm; immersion depths: 1.5 cm), (Pt D: 0.5 mm, immersion depth: 16 cm); anode: graphite: 10 mm. An atmosphere steam and argon gas of 40 cm^{3}min^{-1}.

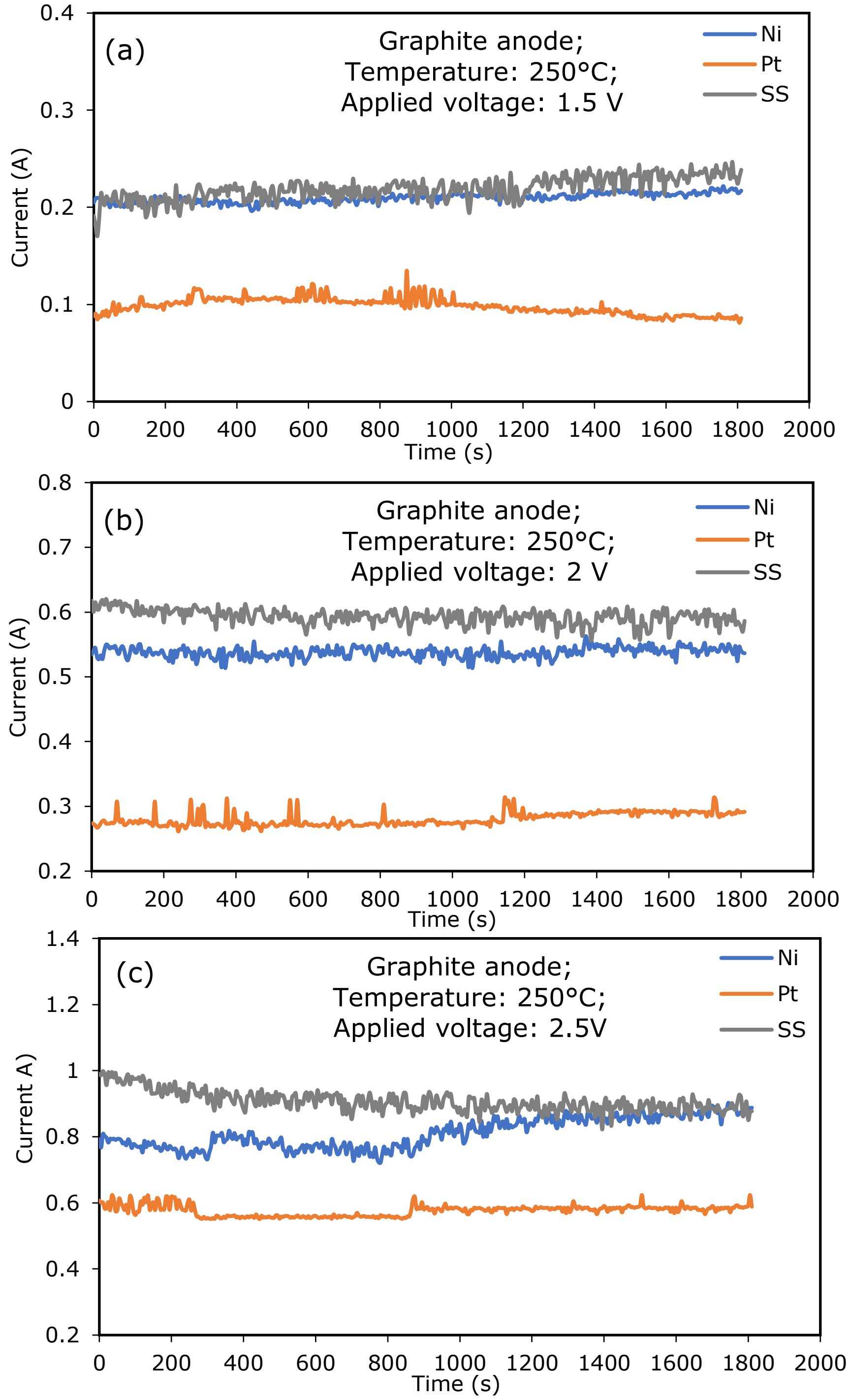

Figure 7.10 – Current-time plots recorded for 1800 s electrolysis in the eutectic molten hydroxide at a temperature of 250°C and at applied voltages of 1.5, 2.0, 2.5 V respectively; cathode: (Ni D:5mm; SS D:5 mm; immersion depths: 1.5 cm), (Pt D: 0.5 mm, immersion depth: 16 cm); anode: graphite: 10 mm. An atmosphere steam and argon gas of 40cm^{3}min^{-1}.

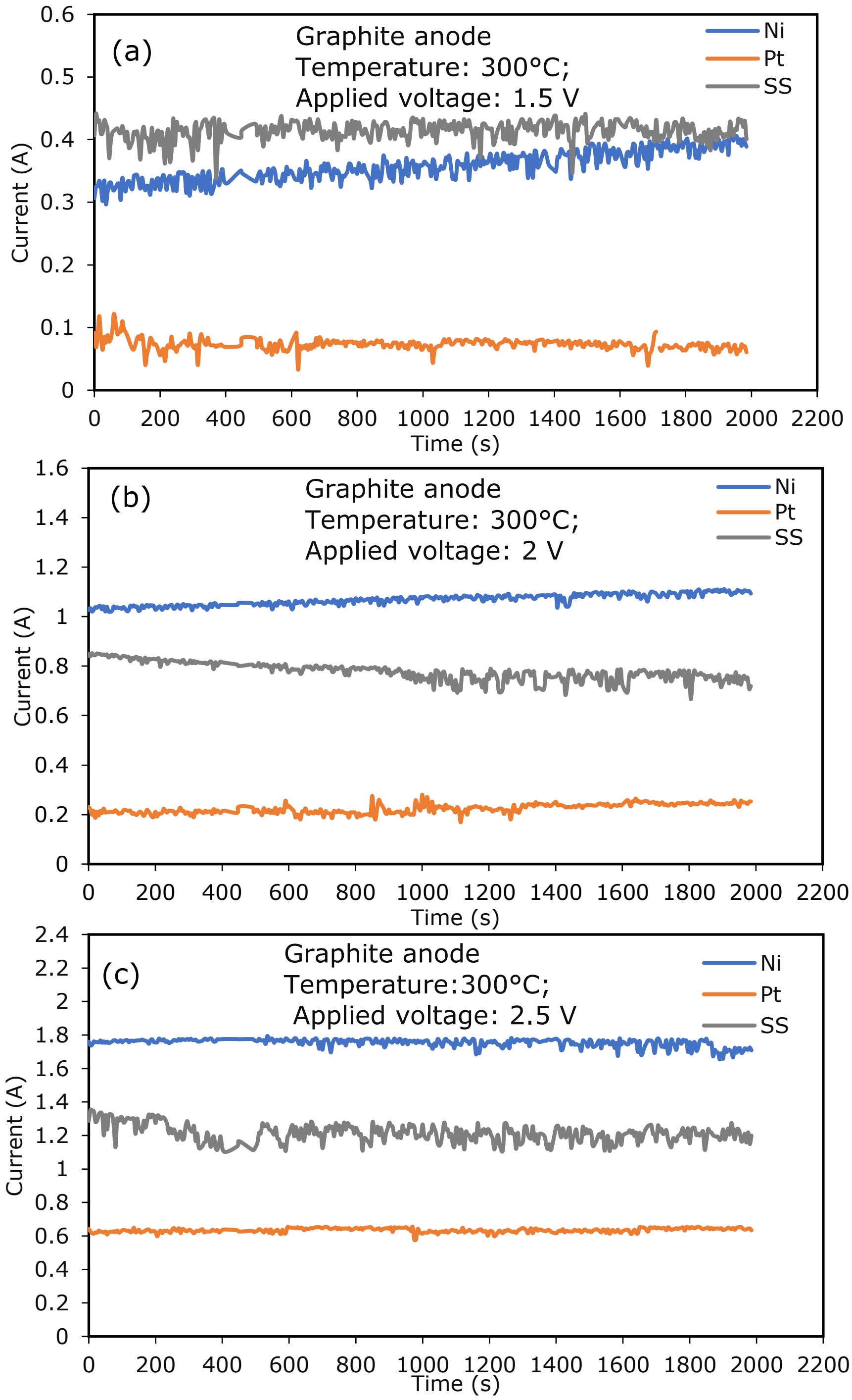

Figure 7.11 – Current-time plots recorded for 1800 s electrolysis in the eutectic molten hydroxide at a temperature of 300°C and at applied voltages of 1.5, 2.0, 2.5 V respectively; cathode: (Ni D:5mm; SS D:5 mm; immersion depths: 1.5 cm), (Pt D: 0.5 mm, immersion depth: 16 cm); anode: graphite: 10 mm. An atmosphere steam and argon gas of 40 cm^{3}min^{-1}.

The electro-activity of the nickel cathode increased during electrolysis with increasing temperature. Platinum however saw no change in its electro-activity even when the operating temperature of the eutectic molten hydroxide or the applied voltages was increased respectively. This finding can be considered as a promising finding for potentially novel, green technology aiming at producing hydrogen gas using cheap, untreated metal instead of precious platinum metal.

Table 7.3 shows the hydrogen gas flow rate produced at the cathode at different operating temperatures in the eutectic molten hydroxide and at different applied voltages. The collection of the gas using water displacement method was carried out for 10 minutes and repeated twice to confirm the accuracy of gas production rate.

Table 7.3 – The rate of hydrogen gas flow rate from the cathode compartment at different operating temperatures and applied voltages. The anode material is graphite.

Metal	Temperature (°C)	H_2 gas rate (cm^3min^{-1})		
		1.5 V	2.0 V	2.5 V
Ni	225	0.5	3-3.5	7.5
	250	0.5-1.0	1.5-3.5	6.0-6.5
	300	1.0-1.5	8.0-8.5	13.0
Pt	225	0.5-1.0	2.5-3.5	5.5-6.5
	250	0.5-1.0	1.5	3.5-4.0
	300	-	1.0-1.5	3.5-4.5
SS	225	1.5-2.5	4.0-4.5	7.0-7.5
	250	1.5-2.0	4.0-5.5	6.5-7.0
	300	2.5	4.0-5.5	9.0

The hydrogen gas flow rate increases with an increase in the operating temperatures of the eutectic molten hydroxide and when the applied voltage increases during electrolysis, as seen in Table 7.3. For the nickel cathode, the hydrogen gas flow rate produced during electrolysis at 300°C and at an applied voltage of 2.5 V, records the highest flow rate followed by stainless steel and platinum under the same operating conditions. Alternately, the nickel electrode electro-activity for producing hydrogen gas reduces at a low temperature of 225°C and at applied voltage of 1.5 V to be lower than the stainless steel electrode gas flow rate at the same operating conditions, as seen in Table 7.3.

When comparing the hydrogen gas flow rate for both the anodes made of stainless steel and graphite respectively; and using different cathode metals, no significant change can be observed in the gas flow rate as seen in Table 7.1 and Table 7.3. It is still imperative in this regards to mention that when graphite is used as an anode, the reduction process can possibly be obstructed by carbon particles blocking the pores of the oxide. This can prevent electrolyte contact to the oxide and significantly hamper the overall electrolytic process as mentioned by (Cox and Fray, 2008). Therefore, it is important to take care when using graphite repeatedly to avoid contaminating the electrolyte and contributing to unfavourable side reactions.

Figure 7.12a, b, and c show the production rates of hydrogen gas for three different cathode materials (Ni, Pt, SS) in the eutectic molten hydroxide at different applied voltages and operating temperatures respectively. Graphite was used as an anode for all of the tests recorded in the figures. The production rate for each electrode was calculated using equation 7.2.

The production rate for hydrogen gas increases with an increase in the operating temperature of the eutectic molten hydroxide. The platinum cathode did not exhibit this behaviour because its production rate decreases with increasing temperature as shown in Figure 7.12b. This behaviour was seen even when stainless steel was used as an anode. The production rate of hydrogen gas decreases when the temperature increases to 300^{o}C as shown in Figure 7.8b. This result leads to conclusion that the electro-activity of platinum metal inside the eutectic molten hydroxide decreases with increasing operating temperature.

Alternately, the hydrogen gas production rate increases with an increase the applied voltage for all used cathode material as seen in Figure 7.12a, b, and c. This increase in the production rate of hydrogen gas is due to an increase in the current passing through the eutectic molten hydroxide during electrolysis; thereby splitting steam and producing hydrogen gas.

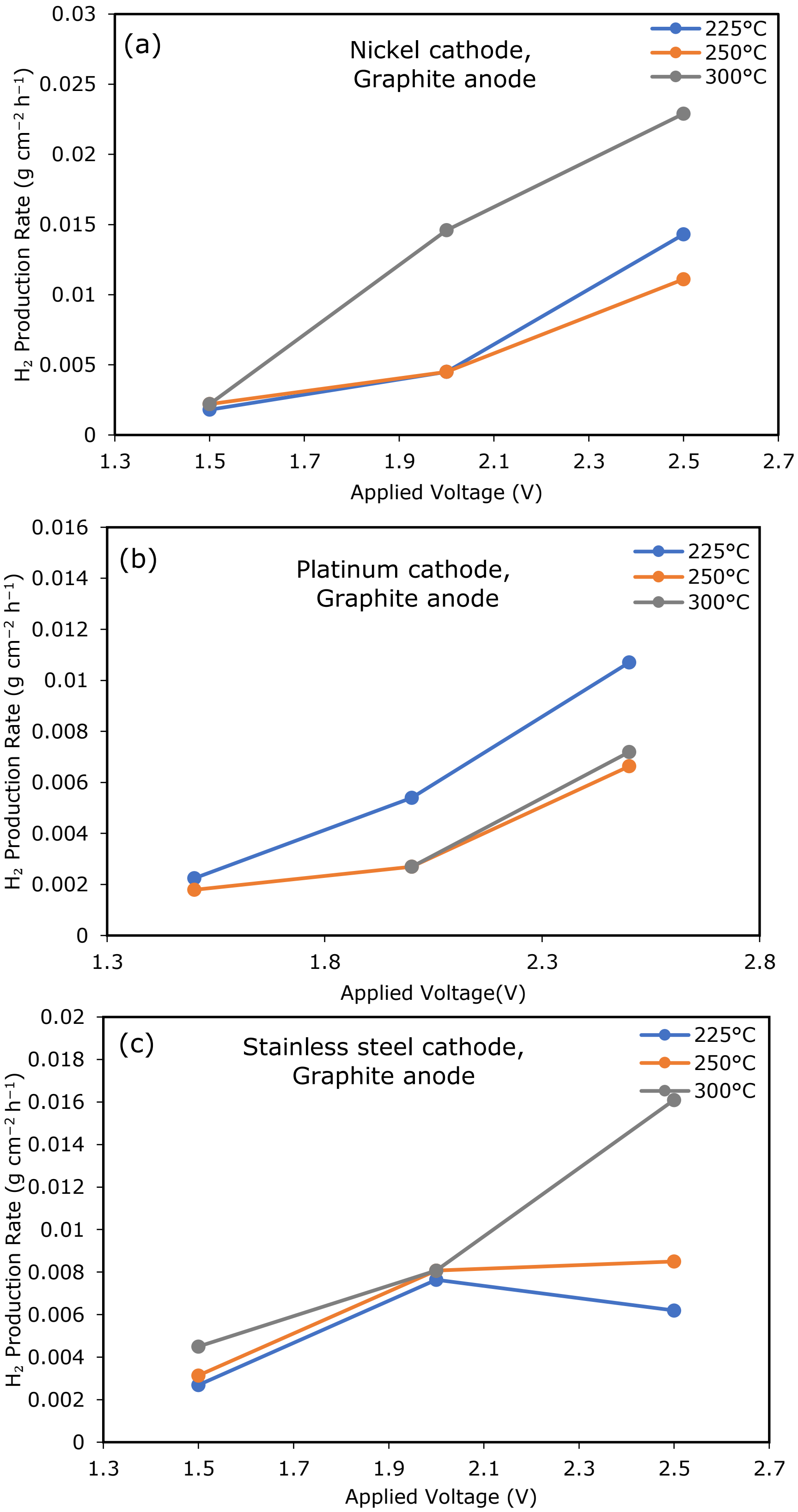

Figure 7.12 – The hydrogen gas production rate versus the applied voltages at different operating temperatures (225, 250, 300^{o}C); the cathode material: Ni, Pt, and SS. The anode is graphite.

Table 7.4 presents the range and the average calculated values of current efficiency for the electrochemical cell using different cathode materials and at different operating temperatures.

Table 7.4 – Current efficiency of the electrochemical cell for hydrogen gas production at applied voltages ranging between 1.5 and 2.5 V; and different operating temperatures. The anode is graphite.

Cathode metal	Temperature (°C)	Current Efficiency Range (%)	Average Current Efficiency (%)
Ni	225	81.0 to 122.2	101.6
	250	61.8 to 93.6	77.7
	300	42.0 to 94.0	68.0
Pt	225	89.3 to 115.4	102.3
	250	65.9 to 124.0	94.9
	300	77.6 to 80.8	79.2
SS	225	76.4 to 155.3	115.8
	250	64.1 to 97.1	80.6
	300	74.2 to 91.4	82.8

As observed from Table 7.4, the current efficiency of hydrogen gas production decreases with an increase in the operating temperature of the eutectic molten hydroxide. For example, as temperature increases from 225°C to 250°C and finally to 300°C, the current efficiency decreases respectively by 101.6%, 77.7%, to 68.0% using nickel metal as the cathode and graphite as the anode. The reason for being the current efficiency about 101.6% at 225°C using nickel cathode as seen in Table 7.4 can be explained as an experimental error. For use stainless steel and platinum cathodes, the current efficiencies were 115.3% and 102.3 % respectively at 225^{o}C as presented in Table 7.4. The reason for being the current efficiency of them more than 100% are explained as an experimental error happened at this specific operating temperature.

The reason for the decrease in current efficiency for hydrogen generation with an increase temperature of the eutectic molten hydroxide, is because the formation of superoxide O_2^- reduction increases and subsequently competes with the hydrogen formation reaction (Licht et al., 2016) as seen in equation (7.4) and equation (7.5):

$$\text{Anode:} \quad 4OH^- \rightarrow O_2^- + 2H_2O + 3e^- \quad \mathbf{(7.4)}$$

$$\text{Cathode:} \quad O_2^- + 2H_2O + 3e^- \rightarrow 4OH^- \quad \mathbf{(7.5)}$$

This finding relating to the decrease in current efficiency with increasing temperature and applied voltage respectively; and is not in agreement with the current efficiency findings for hydrogen gas production using stainless steel as an anode. The only exception to this rule was using platinum as the cathode. In conclusion, the current efficiency increases with an increase in the operating temperature of the eutectic molten hydroxide (for all cathode materials) and increasing the applied voltages in case of using either nickel or stainless steel as the cathode during electrolysis.

7.5 Summary

The findings in this chapter can be summarised as follows:

- This study finds that steam splitting assisted the eutectic molten hydroxide electrolysis at high operating temperatures for hydrogen gas production, and is the way forward to reduce applied voltages.
- For all tested cathode materials (Ni, Pt, SS), the current passing through the electrolyte increased with an increase in the operating temperature of the eutectic molten hydroxide from 225 to 300^oC and subsequent increase in the applied voltages from 1.5 to 2.5 V respectively.
- For the nickel cathode, the increase in the current directly affected the hydrogen gas flow rate at the cathode. The current increased with an increase in the operating temperature and applied voltage. When the applied voltages increased from 1.5 to 2.5 V at 300^oC, the flow rate of hydrogen gas increased from 1.5 to 11.3 cm^3 min^{-1}. In addition, the production rate also increased with an increase in the operating temperature and the applied voltage. For example, at 300^oC, the production rate increased from 0.002 to 0.02 g cm^{-2} h^{-1} when the applied voltage increased from 1.5 to 2.5 V. The achieved current efficiency increased from 63.2% to 90.5% with an increase in the operating temperature from 225 to 300^oC respectively.
- For the platinum cathode, the flow rate of hydrogen gas production increased from 1.6 to 4.5 $cm^3 min^{-1}$ with an increase in the applied voltage from 1.5 to 2.5 V at 300^oC. The production rate of hydrogen gas production decreased with an increase in the operating temperature. The decreasing in the production rate directly influenced the current efficiency

which decreased from 107.5% to 68.6% with an increase in the operating temperature from 225 to 300°C.

- For the stainless steel cathode, the hydrogen gas flow rate also increased from 2 to 7 $cm^3\ min^{-1}$ with an increase in the applied voltage from 1.5 to 2.0 V at 300°C. The production rate for hydrogen gas also increased with an increase in the operating temperature and the applied voltage. This increase in the production rate also directly influenced the current efficiency which increased from 64.85% to 80% with an increase in the operating temperature from 225 to 300°C.
- For the anode material, when stainless steel was used in the electrolysis process, no change in the response of the current-time plot was observed even though stainless steel has a passivation-type behaviour in eutectic molten hydroxide. Consequently, the formation of this shield had no influence on the electrolysis process. The production rate of hydrogen gas increased with increasing temperature and applied voltage respectively.
- However, when the graphite anode was used during electrolysis, the response of the current increased with an increase in the operating temperature. The subsequent production rate also increased, but the current efficiency decreased with an increase in the operating temperature for all three cathode materials. This behaviour can be attributed to the carbon particles that obstruct the reduction process by blocking the pore of the oxide and preventing the oxide from coming in contact with the electrolyte. The achieved current efficiency for this electrolysis process using nickel, platinum, and stainless steel cathode at 300°C was 68.0%, 79.2%, and 82.8% respectively. This current efficiency was lower than that achieved using stainless steel as anode at the same operating conditions.

CHAPTER 8

CONCLUSIONS AND FUTURE WORK

8.1 Conclusions

The research presented in this thesis covers a range of fundamental areas concerning the development of producing hydrogen gas from steam through eutectic molten hydroxide electrolysis. The work has covered investigations of using cyclic voltammetry and amperometry techniques to predict the electrolysis reactions and also the correlation between the efficiency of the process and different experimental parameters. In addition, hydrogen gas has been produced using a direct electrolysis process of steam through eutectic molten hydroxide. The hydrogen gas produced has been examined using a variety of different analysis techniques including a hydrogen gas tube detector and a hydrogen gas sensor, whereas quantifying the hydrogen produced was done using the water displacement technique. The most important conclusions that can be drawn from the preceding chapters are reiterated in the following paragraphs.

Firstly, a comprehensive cyclic voltammetry investigation was carried out to find a suitable ionic membrane to contain the nickel reference electrode. A mullite membrane that covers the $Ni/Ni(OH)_2$ electrode was found to have more stable behaviour in comparison to the alumina membrane for the eutectic molten hydroxide in question. The reason of this stable performance was attributed to that the OH^- can penetrate through the mullite tube membrane and made stable ion channel between the outside electrolyte and inner electrolyte mixture. Furthermore, it was found that the mullite membrane covered reference electrode can be used for up to 9 days inside the eutectic molten hydroxide to obtain reliable results in comparison to 3 days for the alumina membrane nickel reference electrode.

The fabricated nickel reference electrode covered with a mullite membrane was compared with the platinum and silver wire quasi-reference electrodes inside the eutectic molten hydroxide to control the working electrode kinetics of Platinum. The cyclic voltammetry results found that the $Ni/Ni(OH)_2$ covered with a mullite membrane reference electrode has shown to be very stable in controlling effectively the potential of the examined platinum working electrode which thus leads to a high cathodic product (hydrogen gas). This stable behaviour of the prepared nickel reference electrode inside the eutectic molten hydroxide inspired to use it to examine various working electrodes behaviour effectively. This finding of stable reference electrode considered as novel finding in this research because of the previous research unable to find a suitable reference electrode to use it in the molten hydroxide.

The nickel reference electrode covered with a mullite membrane was also used to examine the kinetic reactions of various working electrodes (including Ni, Pt, Ag, Mo and SS). The cyclic voltammetry results for the examine working electrodes found that the reduction potential of the hydrogen evolution reaction using different working electrodes was in the order of (more positive potential to negative): Pt > Ni > SS > Ag > Mo. The observed performance of each working electrode for the hydrogen evolution reaction was confirmed through chronoamperometry at a constant potential of -0.7 V. Furthermore, the presence of steam inside the electrolyte contributed towards increasing the observed current density of the hydrogen evolution reaction for all used working electrodes even though the reduction potential remained approximately unchanged. When the scan range was magnified to focus into the reduction peak for the hydrogen evolution reaction at a different scan rate ranging between 50-150 mV s^{-1}, it was found that a very stable cyclic voltammetry scan was produced even though the scan speed varied.

The direct electrolysis process was performed to split steam in the eutectic molten hydroxide using the three most efficient and electrocatalytic working electrodes (nickel, platinum, and stainless steel). These materials were individually used as a cathode and stainless steel was used as the anode in all cases. The selectivity of these cathode materials depends on the electroactivity of the individual electrode in terms of speeding up the reduction reaction of splitting water and increasing the hydrogen evolution reaction. It was determined that the passed current for all tested materials increased with an increase in the operating temperature of the eutectic molten hydroxide and with an increase in the applied voltages. The achieved current efficiency for the electrolysis cell at 300°C using nickel, platinum and stainless steel cathodes and stainless steel anode was 90.5%, 68.6% and 80.0% respectively. Furthermore, the use of a graphite anode instead of stainless steel did not improve the production rate of hydrogen and in contrast, the current efficiency decreased for nickel, platinum and stainless steel cathode with an increase in the temperature from 225 to 300°C. The achieved current efficiency for nickel, platinum, stainless steel cathodes when using a graphite anode at 300°C was 68.0%, 79.2%, and 84.8% respectively. It should be mentioned that the using of graphite anode not preferred because even though the production rate of hydrogen gas increased with increasing the temperature and applied voltage, the current efficiency was decreased. This behaviour can be attributed to the carbon particles that obstruct the reduction process by blocking the pore of the oxide and preventing the oxide form coming in contact with the electrolyte. Therefore, the using the stainless as anode considered more effective for this process compared to the graphite anode. Furthermore, the nickel cathode most efficient cathode electrode to use in the eutectic molten hydroxide for hydrogen gas production.

8.2 Future Work

The work has produced many lines of enquiry which need to be further investigated before the process can be optimized. Below are some recommendations that can be followed in the development of the process.

- Integrating the electrochemical cell for hydrogen production with renewable energy sources such as solar energy to perform electrolysis process to overcome greenhouse gas emissions.
- The possibility of investigating different eutectic molten hydroxide mixtures such as LiOH-KOH, LiOH-NaOH, or ternary molten hydroxides such as LiOH-KOH-NaOH can be pursued.
- Further Investigation into finding more suitable electro-catalytic cathodic metals using nickel as a base material with the addition of other elements such as Co, Mo, Cu or Cr can be pursued. This can eventually lead to a further increase in the electrode kinetics for increasing the hydrogen evolution reaction.

- Studying the effect of the distance between the cathode and anode towards increasing the hydrogen gas production rate.
- Studying the "bubble phenomena" and the effect of formation of bubbles on the surface of the cathode or anode towards increasing the electrical resistance. These bubbles can be reduced by using suitable additives to the electrolyte that can reduce the surface tension on the electrode surface.

REFERENCES

ABOUATALLAH, R., KIRK, D. and GRAYDON, J. 2002. Impedance Study of Nickel Cathode Reactivation by Vanadium During Hydrogen Evolution in Alkaline Water. *Electrochemical and solid-state letters,* 5**,** E9-E12.

ABOUATALLAH, R., KIRK, D., THORPE, S. and GRAYDON, J. 2001. Reactivation of Nickel Cathodes by Dissolved Vanadium Species During Hydrogen Evolution in Alkaline Media. *Electrochimica acta,* 47**,** 613-621.

ANANI, A., MAO, Z., WHITE, R. E., SRINIVASAN, S. and APPLEBY, A. 1990. Electrochemical Production of Hydrogen and Sulfur by Low-Temperature Decomposition of Hydrogen Sulfide in an Aqueous Alkaline Solution. *Journal of the Electrochemical Society,* 137**,** 2703-2709.

BALAT, M. 2008. Potential Importance of Hydrogen as a Future Solution to Environmental and Transportation Problems. *International Journal of Hydrogen Energy,* 33**,** 4013-4029.

BARD, A. J. and FAULKNER, L. R. 2001. *Fundamentals and Applications,* New York, John Wiley & Sons Inc.

BELMONT, C. and GIRAULT, H. 1994. Coplanar Interdigitated Band Electrodes for Synthesis Part I: Ohmic Loss Evaluation. *Journal of applied electrochemistry,* 24**,** 475-480.

BIRD, R. B., STEWART, W. E. and LIGHTFOOT, E. N. 2007. *Transport Phenomena*, John Wiley & Sons.

BLOOM, H. and GUTMANN, F. 1977. *Electrochemistry: The Past Thirty and the Next Thirty Years,* New York, Plenum Press.

BOCKRIS, J., CONWAY, B. and YEAGER, E. 1980. *Comprehensive Treatise of Electrochemistry*, Springer.

BOCKRIS, J., CONWAY, B., YEAGER, E. and WHITE, R. 1981. *Comprehensive Treatise of Electrochemistry,* Boston, Springer US.

BORUP, R., MEYERS, J., PIVOVAR, B., KIM, Y. S., MUKUNDAN, R., GARLAND, N., MYERS, D., WILSON, M., GARZON, F., WOOD, D., ZELENAY, P., MORE, K., STROH, K., ZAWODZINSKI, T., BONCELLA, J., MCGRATH, J. E., INABA, M., MIYATAKE, K., HORI, M., OTA, K., OGUMI, Z., MIYATA, S., NISHIKATA, A., SIROMA, Z., UCHIMOTO, Y., YASUDA, K., KIMIJIMA, K.-I. and IWASHITA, N. 2007. Scientific Aspects of Polymer Electrolyte Fuel Cell Durability and Degradation. *Chemical Reviews,* 107**,** 3904-3951.

BOZZINI, B., BARELLA, S., BOGANI, F., GIOVANNELLI, G., NATALI, S., SCARSELLI, G. and BONIARDI, M. 2012. Corrosion of Stainless Steel Qrades in Molten NaOH/KOH Eutectic at 250 °C: AISI304 Austenitic and 2205 Duplex. *Materials and Corrosion,* 63**,** 967-978.

CORPORATION., G. 2016. *Gastec Hydrogen Detector Tubes* [Online]. Available: https://www.gastec.co.jp/en/product/detector_tube/type/#short [Accessed october 2017].

COUPER, A. M., PLETCHER, D. and WALSH, F. C. 1990. Electrode Materials for Electrosynthesis. *Chemical Reviews,* 90**,** 837-865.

COX, A. and FRAY, D. J. 2008. Mechanistic Investigation into the Electrolytic Formation of Iron from Iron (III) Oxide in Molten Sodium Hydroxide. *Journal of Applied Electrochemistry,* 38**,** 1401-1407.

CZERNIK, S., FRENCH, R., FEIK, C. and CHORNET, E. 2002. Production of Hydrogen from Biomass by Pyrolysis/Steam Reforming. *In:* GRÉGOIRE PADRÓ, C. E. & LAU, F. (eds.) *Advances in Hydrogen Energy.* Boston, MA: Springer US.

DABO, P., MENARD, H. and BROSSARD, L. 1997. Electrochemical Characterization of Graphite Composite-Coated Electrodes for Hydrogen Evolution Reaction. *International journal of hydrogen energy,* 22**,** 763-770.

DELL, R. M. and RAND, D. A. J. 2004. *Clean Energy,* Cambridge, The Royal Society of Chemistry.

DELL, R. M. and RAND, D. A. J. 2008. *Hydrogen Energy: Challenges and Prospects,* Cambridge, UK, The Royal Society of Chemistry.

DIÉGUEZ, P. M., URSÚA, A., SANCHIS, P., SOPENA, C., GUELBENZU, E. and GANDÍA, L. M. 2008. Thermal Performance of a Commercial Alkaline Water Electrolyzer: Experimental Study and Mathematical Modeling. *International Journal of Hydrogen Energy,* 33**,** 7338-7354.

DIVISEK, J., MERGEL, J. and NIESSEN, H. F. 1980. Production of Hydrogen by the Electrolytic Decomposition of Water in Fused Sodium Hydroxide. *International Journal of Hydrogen Energy,* 5**,** 151-164.

DIVISEK, J., MERGEL, J. and SCHMITZ, H. 1982. Improvements of Water Electrolysis in Alkaline Media at Intermediate Temperatures. *International Journal of Hydrogen Energy,* 7**,** 695-701.

DÖNER, A., KARCı, İ. and KARDAŞ, G. 2012. Effect of C-felt Supported Ni, Co and NiCo Catalysts to Produce Hydrogen. *International Journal of Hydrogen Energy,* 37**,** 9470-9476.

FERREIRA, A., GONZALEZ, E., TICIANELLI, E., AVACA, L. and MATVIENKO, B. 1988. The Effect of Temperature on the Water Electrolysis Reactions on Nickel and Nickel-Based Co-deposits. *Journal of applied electrochemistry,* 18**,** 894-898.

FISCHER, A. 1996. *Electrode Dynamics*, Oxford University. Press.

FUJISHIMA, A. and HONDA, K. 1972. Electrochemical Photolysis of Water at a Semiconductor Electrode. *Nature,* 238**,** 37.

FUNK, J. E. 2001. Thermochemical Hydrogen Production: Past and Present. *International Journal of Hydrogen Energy,* 26**,** 185-190.

GANLEY, J. C. 2008. An Intermediate-Temperature Direct Ammonia Fuel Cell with a Molten Alkaline Hydroxide Electrolyte. *Journal of Power Sources,* 178**,** 44-47.

GANLEY, J. C. 2009. High Temperature and Pressure Alkaline Electrolysis. *International Journal of Hydrogen Energy,* 34**,** 3604-3611.

GAO, P., JIN, X., WANG, D., HU, X. and CHEN, G. Z. 2005. A Quartz Sealed Ag/AgCl Reference Electrode for $CaCl_2$ Based Molten Salts. *Journal of Electroanalytical Chemistry,* 579**,** 321-328.

GAYER, K. H. and GARRETT, A. 1949. The Equilibria of Nickel Hydroxide, Ni $(OH)_2$, in Solutions of Hydrochloric Acid and Sodium Hydroxide at 25^{O}C. *Journal of the American Chemical Society,* 71**,** 2973-2975.

GE, J., ZHANG, F., JIAO, H. and JIAO, S. 2015. Metallic Nickel Preparation by Electro-Deoxidation in Molten Sodium Hydroxide. *Journal of The Electrochemical Society,* 162**,** E185-E189.

GEISSLER, K., NEWSON, E., VOGEL, F., TRUONG, T.-B., HOTTINGER, P. and WOKAUN, A. 2001. Autothermal Methanol Reforming for Hydrogen Production in Fuel Cell Applications. *Physical Chemistry Chemical Physics,* 3**,** 289-293.

GÖNDEREN B ZAMAN. 2013. *How Does Hydrogen Power Work?* [Online]. Available: http://hydrogenenergy11b.blogspot.co.uk/ [Accessed October 2013].

GORET, J. and TREMILLON, B. 1966. *bulletin de la societe chimique***,** 0037-8796.

GUO, L., CALO, J. M., DICOCCO, E. and BAIN, E. J. 2013. Development of a Low Temperature, Molten Hydroxide Direct Carbon Fuel Cell. *Energy & Fuels,* 27**,** 1712-1719.

GUPTA, R. B. 2008. *Hydrogen Fuel: Production, Transport, and Storage*, Crc Press.

HEINZE, J. 1984. Cyclic Voltammetry “Electrochemical Spectroscopy”. New Analytical Methods *Angewandte Chemie International Edition in English,* 23**,** 831-847.

HÍVEŠ, J., BENOVÁ, M., BOUZEK, K. and SHARMA, V. K. 2006. Electrochemical Formation of Ferrate (VI) in a Molten NaOH-KOH System. *Electrochemistry Communications,* 8**,** 1737-1740.

HÍVEŠ, J., BENOVA, M., BOUZEK, K., SITEK, J. and SHARMA, V. 2008. The Cyclic Voltammetric Study of Ferrate (VI) Formation in a Molten Na/K Hydroxide Mixture. *Electrochimica Acta,* 54**,** 203-208.

HOLLADAY, J. D., HU, J., KING, D. L. and WANG, Y. 2009. An Overview of Hydrogen Production Technologies. *Catalysis Today,* 139**,** 244-260.

JANJUA, M. and LE ROY, R. 1985. Electrocatalyst Performance in Industrial Water Electrolysers. *International Journal of Hydrogen Energy,* 10**,** 11-19.

JAYALAKSHMI, M., KIM, W.-Y., JUNG, K.-D. and JOO, O.-S. 2008. Electrochemical Characterization of Ni-Mo-Fe Composite Film in Alkali Solution. *Int. J. Electrochem. Sci,* 3**,** 908-917.

JEWELL, D. 2009. *Novel Electrochemical Engineering for the Intelligent Extraction of Titanium.* PhD Thesis, University of Nottingham.

KAPDAN, I. K. and KARGI, F. 2006. Bio-hydrogen Production from Waste Materials. *Enzyme and Microbial Technology,* 38**,** 569-582.

KIM, S., KORATKAR, N., KARABACAK, T. and LU, T.-M. 2006. Water Electrolysis Activated by Ru Nanorod Array Electrodes. *Applied physics letters,* 88**,** 263106.

KINOSHITA, K. 1992. *Electrochemical Oxygen Technology*, John Wiley & Sons.

KISSINGER, P. T. and HEINEMAN, W. R. 1983. Cyclic Voltammetry. *Journal of Chemical Education,* 60**,** 702.

KLEBANOFF, L. and KELLER, J. 2012. Final Report for the DOE Metal HydrideCenter of Excellence. New Mexico, California: Sandia National Laboratories

KOTHARI, R., BUDDHI, D. and SAWHNEY, R. L. 2008. Comparison of Environmental and Economic Aspects of Various Hydrogen Production Methods. *Renewable and Sustainable Energy Reviews,* 12**,** 553-563.

KUBO, S., NAKAJIMA, H., KASAHARA, S., HIGASHI, S., MASAKI, T., ABE, H. and ONUKI, K. 2004. A Demonstration Study on a Closed-cycle Hydrogen Production by the Thermochemical Water-Splitting Iodine–sulfur Process. *Nuclear Engineering and Design,* 233**,** 347-354.

KUMAR, S. 2015. *Clean Hydrogen Production Methods,* New York Dordrecht London, Springer.

LABRIE, R. J. and LAMB, V. A. 1959. A Porcelain Reference Electrode Conductive to Sodium Ions for Use in Molten Salt Systems. *Journal of The Electrochemical Society,* 106**,** 895-899.

LAWRENCE, R. 2013. *Carbon From Carbon Dioxide via Molten Carbonate Electrolysis: Fundamental Investigation.* PhD Thesis, The University of Nottingham.

LEROY, R. 1983. Industrial Water Electrolysis: Present and Future. *International Journal of Hydrogen Energy,* 8**,** 401-417.

LEROY, R. L., BOWEN, C. T. and LEROY, D. J. 1980. The Thermodynamics of Aqueous Water Electrolysis. *Journal of the Electrochemical Society,* 127**,** 1954-1962.

LEVIN, D. B., PITT, L. and LOVE, M. 2004. Biohydrogen Production: Prospects and Limitations to Practical Application. *International Journal of Hydrogen Energy,* 29**,** 173-185.

LEWERENZ, H. J., LAURENCE, P. and 2013. *Photoelectrochemical Water Splitting: Materials, Processes and Architectures,* Cambridge, UK, The royal society of chemistry.

LICHT, S., CUI, B., WANG, B., LI, F.-F., LAU, J. and LIU, S. 2014. Ammonia Synthesis by N_2 and Steam Electrolysis in Molten Hydroxide Suspensions of Nanoscale Fe_2O_3. *Science,* 345**,** 637-640.

LICHT, S., LIU, S., CUI, B., LAU, J., HU, L., STUART, J., WANG, B., EL-GHAZAWI, O. and LI, F.-F. 2016. Comparison of Alternative Molten Electrolytes for Water Splitting to Generate Hydrogen Fuel. *Journal of The Electrochemical Society,* 163**,** F1162-F1168.

LLOPIS, J., COLOM, F. and BARD, A. 1976. Encyclopedia of Electrochemistry of the Elements. *Vol. VI*.

LUCIA H., MIROSLAV G.L, KAMIL K. and HÍVEŠ J. 2013. The Influence of Anode Composition on the Electrochemical Ferrate (VI) Production in Molten KOH. *international Journal of Electrochemical Science,* 8**,** 7768-7778.

MARSHALL, A. T., SUNDE, S., TSYPKIN, M. and TUNOLD, R. 2007. Performance of a PEM Water Electrolysis Cell Using $Ir_xRu_yTa_zO_2$ Electrocatalysts for the Oxygen Evolution Electrode. *International Journal of Hydrogen Energy,* 32**,** 2320-2324.

MARTIN, A., POIGNET, J., FOULETIER, J., ALLIBERT, M., LAMBERTIN, D. and BOURGÈS, G. 2010. Yttria-Stabilized Zirconia as Membrane Material for Electrolytic Deoxidation of $CaO–CaCl_2$ Melts. *Journal of applied electrochemistry,* 40**,** 533-542.

MILES, M., KISSEL, G., LU, P. and SRINIVASAN, S. 1976. Effect of Temperature on Electrode Kinetic Parameters for Hydrogen and Oxygen Evolution Reactions on Nickel Electrodes in Alkaline Solutions. *Journal of the Electrochemical Society,* 123**,** 332-336.

MILES, M. H. 2003. Exploration of Molten Hydroxide Electrochemistry for Thermal Battery Applications. *Journal of Applied Electrochemistry,* 33**,** 1011-1016.

MOMIRLAN, M. and VEZIROĞLU, T. 1999. Recent Directions of World Hydrogen Production. *Renewable and Sustainable Energy Reviews,* 3**,** 219-231.

NAGAI, N., TAKEUCHI, M., KIMURA, T. and OKA, T. 2003. Existence of Optimum Space Between Electrodes on Hydrogen Production by Water Electrolysis. *International Journal of Hydrogen Energy,* 28**,** 35-41.

NEWMAN, J. 1991. *Electrochemical Systems,* New Jersey, Wiley.

NI, M., LEUNG, D. Y. C., LEUNG, M. K. H. and SUMATHY, K. 2006. An Overview of Hydrogen Production from Biomass. *Fuel Processing Technology,* 87**,** 461-472.

OLDHAM, K. and MYLAND, J. 1993. *Fundamentals of Electrochemical Science*, Elsevier.

ONDA, K., KYAKUNO, T., HATTORI, K. and ITO, K. 2004. Prediction of Production Power for High-pressure Hydrogen by High-pressure Water Electrolysis. *Journal of Power Sources,* 132**,** 64-70.

OTTO, H. W. and SEWARD, R. P. 1964. Phase Equilibria in the Potassium Hydroxide-Sodium Hydroxide System. *Journal of Chemical & Engineering Data,* 9**,** 507-508.

PAL, R., ANANTHASIVAN, K., ANTHONYSAMY, S. and GANESAN, V. 2011. Development and Electrochemistry of a Novel Ag/AgCl Reference Electrode Suitable for Mixed Chloride–fluoride Melts. *Electrochimica Acta,* 56**,** 4276-4280.

PANT, K. and GUPTA, R. B. 2009. Fundamentals and Use of Hydrogen as a Fuel. *Hydrogen fuel: Production, Transport, and Storage***,** 3-32.

PICKETT, D. J. 1979. *Electrochemical Reactor Design,* Amsterdam, Elsevier Scientific.

POTVIN, E. and BROSSARD, L. 1992. Electrocatalytic Activity of Ni-Fe Anodes for Alkaline Water Electrolysis. *Materials Chemistry and Physics,* 31**,** 311-318.

POWERS, W. D. and BLABOCK, G. C. 1954. Energy Comm *Rept. ONRL***,** 1653.

QUANDT, K. H. and STREICHER, R. 1986. Concept and Design of a 3.5 MW Pilot Plant for High-temperature Electrolysis of Water Vapor. *International Journal of Hydrogen Energy,* 11**,** 309-315.

RIEGER, P. 1987. Electrochemistry. Prentice-Hall, Englewood Cliffs, NJ.

ROCHELEAU, R. E., MILLER, E. L. and MISRA, A. 1998. High-Efficiency Photoelectrochemical Hydrogen Production Using Multijunction Amorphous Silicon Photoelectrodes. *Energy & Fuels,* 12**,** 3-10.

ROSSINI, F. D., WAGMAN, D. D., EVANS, W. H., LEVINE, S. and JAFFE, I. 1952. *Selected Values of Chemical Thermodynamic Properties*, US Government Printing Office Washington, DC.

ROSSMEISL, J., LOGADOTTIR, A. and NØRSKOV, J. K. 2005. Electrolysis of Water on (Oxidized) Metal Surfaces. *Chemical Physics,* 319**,** 178-184.

SAKAMURA, Y. 2004. Zirconium Behavior in Molten LiCl-KCl Eutectic. *Journal of the Electrochemical Society,* 151**,** C187-C193.

SANTOS, D. M., SEQUEIRA, C. A. and FIGUEIREDO, J. L. 2013. Hydrogen Production by Alkaline Water Electrolysis. *Química Nova,* 36**,** 1176-1193.

SCHIAVON, G., ZECCHIN, S. and BOMBI, G. G. 1972. Copper (I)-Copper Reference Electrode in Molten Hydroxides. *Journal of Electroanalytical Chemistry and Interfacial Electrochemistry,* 38**,** 473-475.

SMITH, G. 1956. Corrosion of Materials in Fused Hydroxides. Oak Ridge National Lab., Tenn.

SØRENSEN, B. 2005a. Chapter 1 - Introduction. *Hydrogen and Fuel Cells.* Burlington: Academic Press.

SØRENSEN, B. 2005b. Chapter 2 - Hydrogen. *Hydrogen and Fuel Cells.* Burlington: Academic Press.

STEINFELD, A. 2005. Solar Thermochemical Production of Hydrogen–a Review. *Solar Energy,* 78**,** 603-615.

STEVENSON, A. 2017. *Development of a Novel Electrochemical Pyroprocessing Methodology for Spent Nuclear Fuels.* PhD thesis, University of Nottingham.

THERMOCHEMISTRY, C. F. R. I. C. 2016. *Data from FT salt-FACT salt databasees* [Online]. Available: http://www.crct.polymtl.ca/fact/documentation/ [Accessed February 2016].

TRASATTI, S. 1971. Work Function, Electronegativity, and Electrochemical Behaviour of Metals: II. Potentials of Zero Charge and "Electrochemical" Work Functions. *Journal of Electroanalytical Chemistry and Interfacial Electrochemistry,* 33**,** 351-378.

URSUA, A., GANDIA, L. M. and SANCHIS, P. 2012. Hydrogen Production From Water Electrolysis: Current Status and Future Trends. *Proceedings of the IEEE,* 100**,** 410-426.

VISWANATH, R. 2004. A Patent for Generation of Electrolytic Hydrogen by a Cost Effective and Cheaper Route. *International journal of hydrogen energy,* 29**,** 1191-1194.

WANG, H., SIAMBUN, N. J., YU, L. and CHEN, G. Z. 2012. A Robust Alumina Membrane Reference Electrode for High Temperature Molten Salts. *Journal of The Electrochemical Society,* 159**,** H740-H746.

WENDT, H. and KREYSA, G. 1999. *Electrochemical Engineering: Science and Technology in Chemical and other Industries*, Springer Science & Business Media.

WHITE, R., BOCKRIS, J., CONWAY, B. and YEAGER, E. 1984. *Comprehensive Treatise of Electrochemistry* New York, Plenum.

WU, T., XIAO, W., JIN, X., LIU, C., WANG, D. and CHEN, G. Z. 2008. Computer-aided Control of Electrolysis of Solid Nb_2O_5 in molten $CaCl_2$. *Physical Chemistry Chemical Physics,* 10**,** 1809-1818.

YANG, J., MUROYAMA, H., MATSUI, T. and EGUCHI, K. 2014. Development of a Direct Ammonia-fueled Molten Hydroxide Fuel Cell. *Journal of Power Sources,* 245**,** 277-282.

ZAAFARANY, I. and BOLLER, H. 2009. Electrochemical Behavior of Copper Electrode in Sodium Hydroxide Solutions. *Current World Environment,* 4**,** 277-284.

ZABINSKI, P., NEMOTO, H., MEGURO, S., ASAMI, K. and HASHIMOTO, K. 2003. Electrodeposited Co-Mo-C Cathodes for Hydrogen Evolution in a Hot

Concentrated NaOH Solution. *Journal of The Electrochemical Society,* 150**,** C717-C722.

ZECEVIC, S., PATTON, E. M. and PARHAMI, P. 2004. Carbon–air Fuel Cell without a Reforming Process. *Carbon,* 42**,** 1983-1993.

ZENG, K. and ZHANG, D. 2010. Recent Progress in Alkaline Water Electrolysis for Hydrogen Production and Applications. *Progress in Energy and Combustion Science,* 36**,** 307-326.

ZOULIAS, E., VARKARAKI, E., LYMBEROPOULOS, N., CHRISTODOULOU, C. N. and KARAGIORGIS, G. N. 2004. A Review on Water Electrolysis. *TCJST,* 4**,** 41-71.

APPENDIX A

A.1 Cyclic Voltammetry of Different Working Electrodes with and without Steam

The cyclic voltammetry of different working electrodes at different operating temperatures of with and without steam as presented in table A.1.

Table A.1 – The reduction potential and the current limit at -0.8 V† for different working electrodes with and without steam at a different temperature.

	Temperature (°C)	Without steam		With steam	
		E_{red} (V)	j (A cm^{-2})	E_{red} (V)	j (A cm^{-2})
Ni	225	-0.56	-0.97	-0.56	-1.00
	300	-0.49	-1.67	-0.47	-2.10
Pt	225	-0.55	-0.75	-0.53	-0.92
	300	-0.47	-1.23	-0.47	-1.78
Ag	225	-0.61	-0.16	-0.59	-0.03
	300	-0.53	-0.20	-0.53	-0.20
Mo	225	-0.61	-0.151	-0.59	-0.03
	300	-0.55	-0.164	-0.53	-0.48
SS	225	-0.59	-0.32	-0.59	-0.43
	300	-0.51†	-0.86†	-0.49†	-0.96†

† The current limit of the reduction potential at Ss is -0.7 V at 300 °C.

Figure A.1 shows the performed cyclic voltammetry scans of different working electrodes at 300°C with the presence of steam.

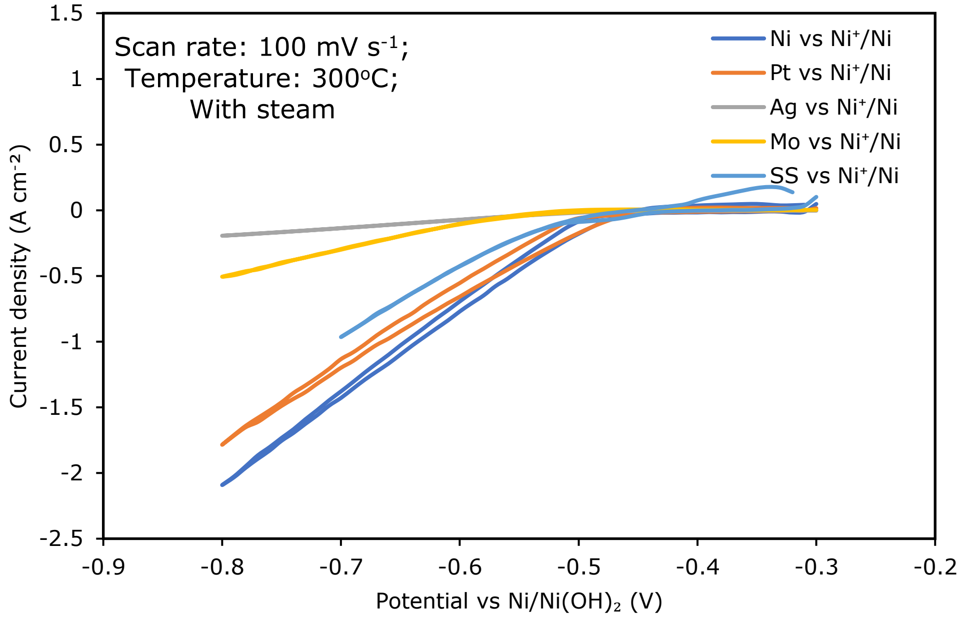

Figure A.1 – Cyclic voltammograms comparison of Ni, Pt, Ag, Mo, SS working electrodes in the eutectic molten hydroxide at 300°C and 100 mV s^{-1} scan rate with steam. RE: 0.5 mm of Pt wire and CE:5mm of stainless steel. Immersion depth: 14mm, atmosphere: 40cm^3min^{-1} of Ar gas.

Figure A.2 shows the performed cyclic voltammetry of different working electrodes at temperature of 225°C without steam.

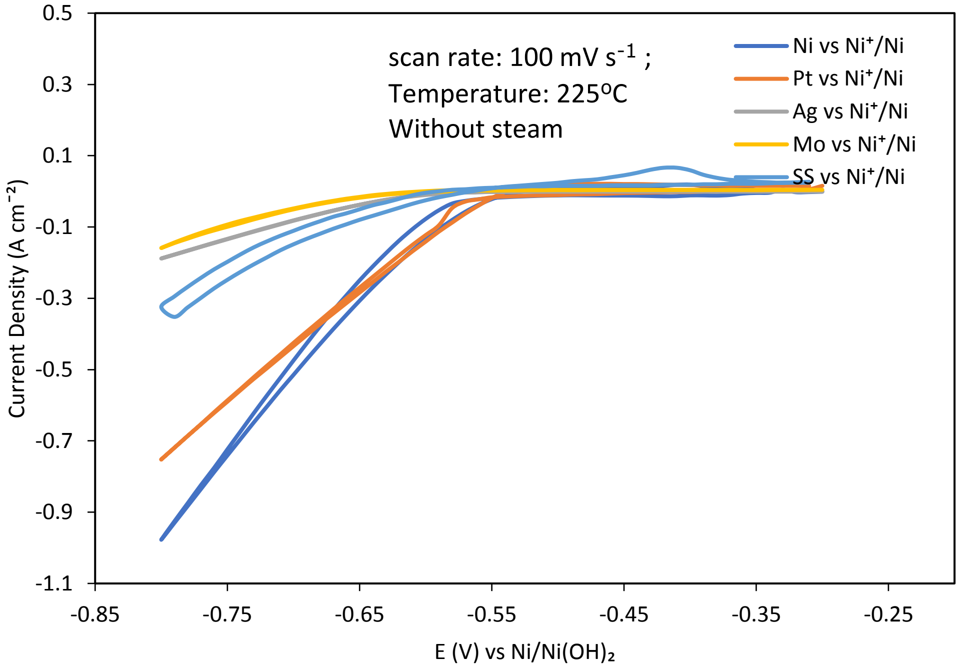

Figure A.2 – Cyclic voltammograms comparison of Ni, Pt, Ag, Mo, SS working electrodes in the eutectic molten hydroxide at 225°C and 100 mV s^{-1} scan rate without steam. RE: 0.5 mm of Pt wire and CE: 5mm of stainless steel. Immersion depth: 14mm, atmosphere: 40 cm^3min^{-1} of Ar gas.

Figure A.3 shows the preformed cyclic voltammetry of different working electrode with steam at 225 ℃.

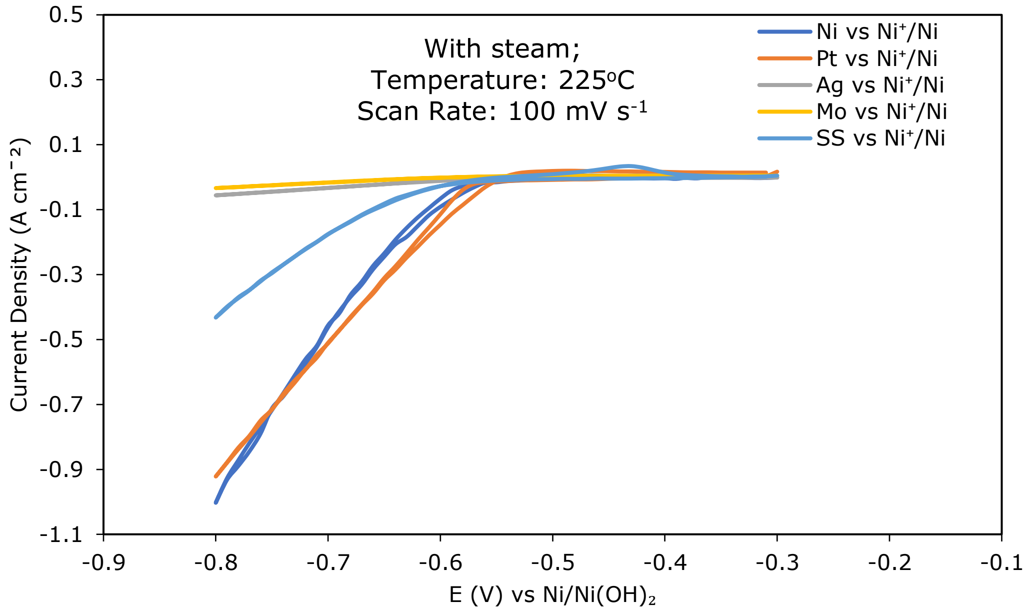

Figure A.3 – Cyclic voltammograms Comparison of Ni, Pt, Ag, Mo, SS working electrodes in the eutectic molten hydroxide at 225°C and 100 mV s^{-1} scan rate with steam. RE: 0.5 mm of Pt wire and CE: 5 mm of stainless steel. Immersion depth: 14 mm, atmosphere: 40 $cm^3 min^{-1}$ of Ar gas.

A.2 Steam Electrolysis in Molten Hydroxide (NaOH-KOH; 49-51 mol%)

Figure A.4 shows the current-time plot of silver cathode electrolysis in the eutectic molten hydroxide at different operating temperatures.

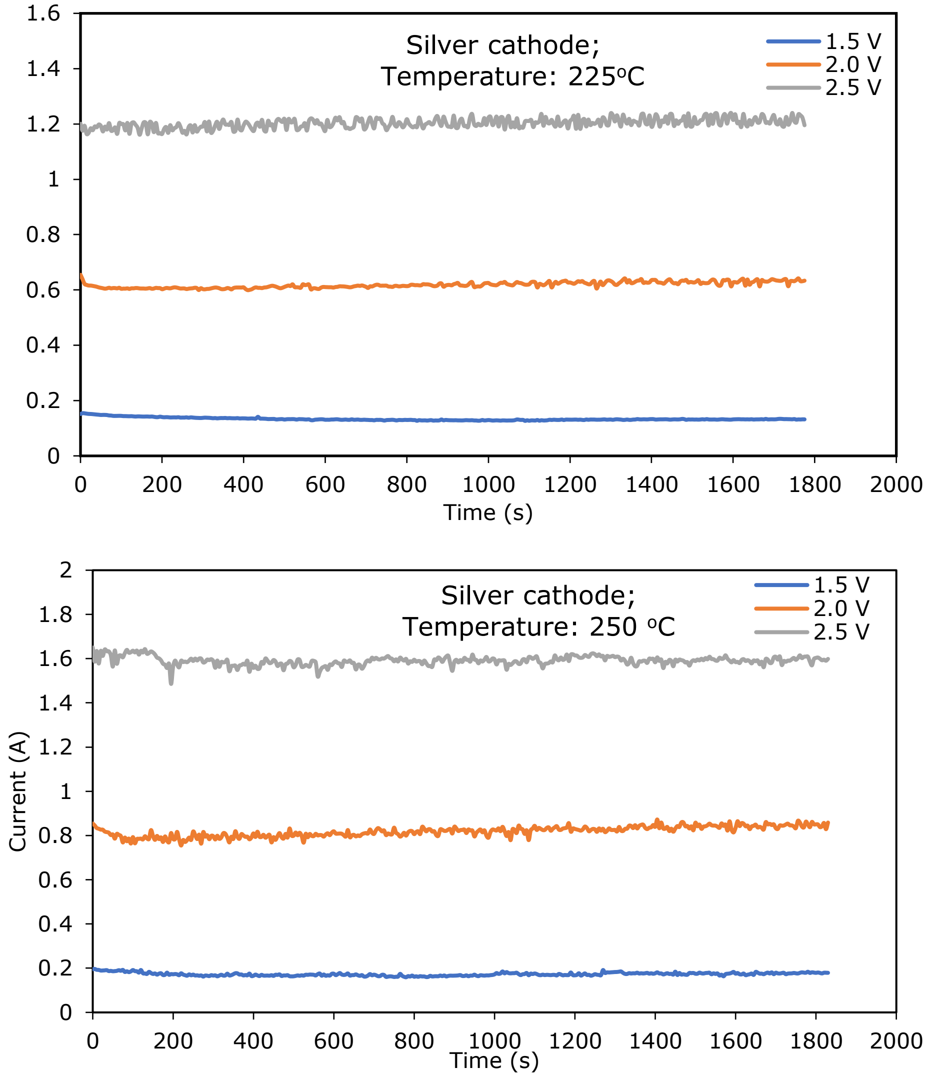

Figure A.4 – Current-time plots recorded for less than 1.0 h electrolysis in molten hydroxide at (a) 225°C, (b) 250°C; (1.5, 2.0, 2.5V) cell voltages; 1 mm diameter silver cathode (immersion depths: 9 cm); 5 mm stainless steel anode and with steam and argon gas of 40 cm^3min^{-1} atmosphere.

A.3 Electrolysis with a Molybdenum Cathode in the Eutectic Molten Hydroxide

Molybdenum metal is another cathode metal that was used throughout this study. It was considered by (Jayalakshmi et al., 2008) as one of the best electrocatalytic metals in an alkali solution for hydrogen production. Electrolysis was carried out in the eutectic molten hydroxide (NaOH-KOH;49-51 mol%) and the recorded current time plots are given in FigureA.5. The anode electrode that was used during the electrolysis was stainless steel metal. The noticeable aspect from the figure is that there is a slight increase in current observed with increasing temperature.

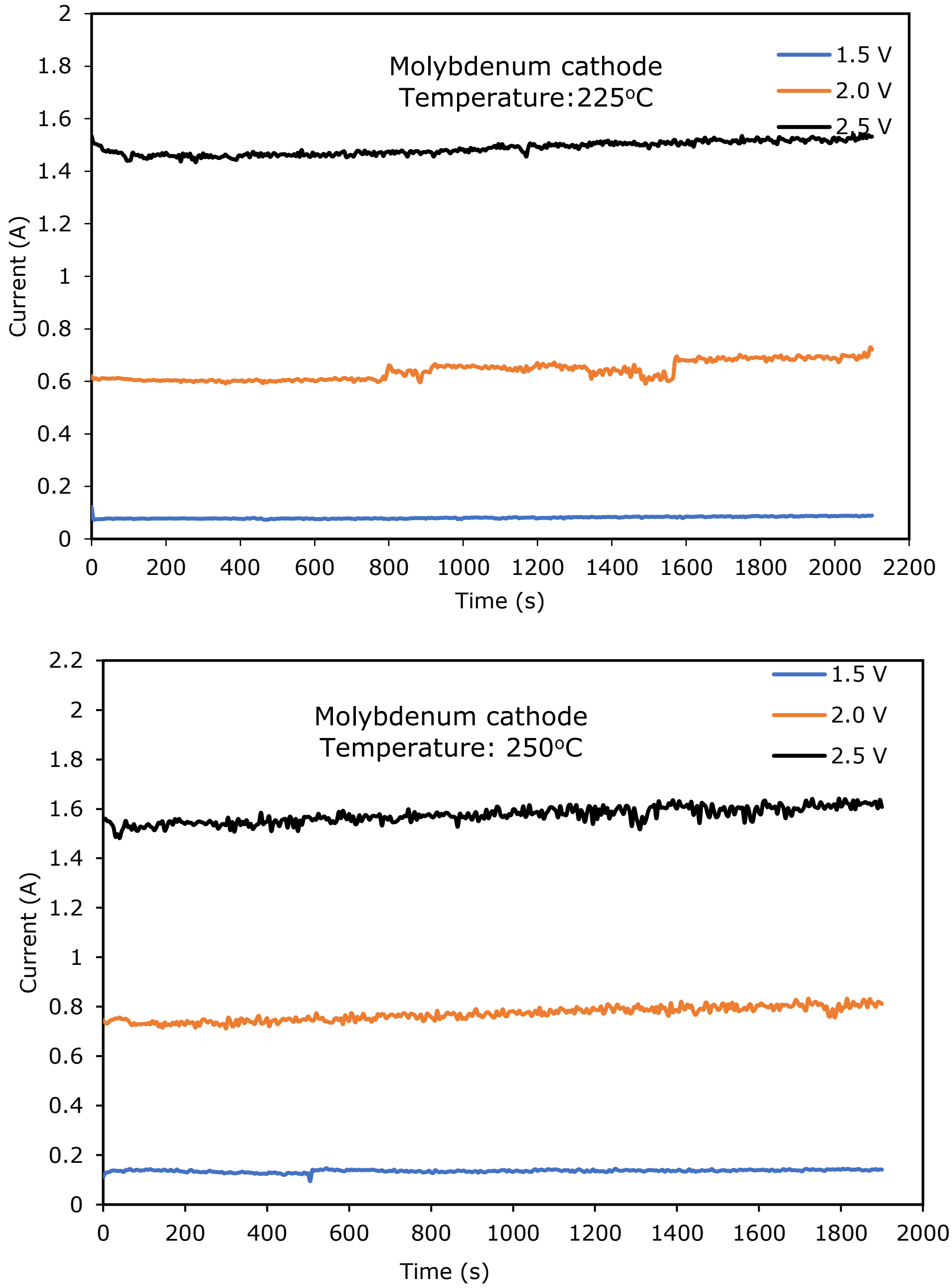

Figure A.5 – Current-time plots recorded for less 1.0 h electrolysis in eutectic molten hydroxide at (a) 225°C, (b) 250°C; 1.5, 2.0, 2.5 V cell voltages; 3 mm diameter molybdenum cathode (immersion depths: 1.5 cm); 5 mm stainless steel anode and with steam and argon gas of 40 cm^3min^{-1} atmosphere.